Durham E-Theses

The magnetic properties of plastically deformed steels.

Thompson, Sarah M.

The Magnetic Properties of Plastically Deformed Steels

by

Sarah M. Thompson

A Thesis submitted in partial fulfilment of the requirements for the degree of Doctor of Philosophy

Physics

The University of Durham
1990

1 7 OCT 1991

Declaration

The work contained in this thesis was carried out by the author between 1987 and 1990 in the Physics Department at the University of Durham, any collaborations are appropriately acknowledged. None of this work has been submitted in candidature for any other degree.

Abstract

This study concentrates on low carbon pearlitic steels. Two sets of experiments are carried out, the first on a section of semi-killed gas pipe and the second on specially prepared alloys of iron and carbon with pearlite fractions varying from 0.19% to 100%. Their magnetic properties are studied both in the as received state and after tensile plastic deformation. In addition, four different heat treatments are applied to the low carbon steel.

Standard magnetisation and fluxmeter techniques are used to determine the bulk magnetic properties, with further use of a vibrating sample magnetometer for coercivity measurements. The Barkhausen noise of the samples is also recorded and High Voltage Lorentz Electron Microscopy used to directly observe the domain configurations and the interaction of the domain walls with dislocation tangles.

The changes in the magnetic properties after tensile deformation are similar to those due to elastic compressive stress, with an additional increase in the coercivity. For the initial magnetisation curve initial permeability (μ_i) and maximum relative permeability both decrease, while the field at which the latter occurs (Hm) increases. The hysteresis curve shears over reducing the maximum differential permeability and the remanence and also increasing the coercivity. These results and the change in the shape of the hysteresis curve, most noticeable in the low carbon steels, are explained in terms of the reduction in easy domain wall movement due to the dislocation tangles, as observed under the electron microscope, and to the magnetostrictive effect of the compressive residual stress.

Inter-relationships are found between coercivity and both μ_i and Hm. The coercivity is also found to vary linearly with both Vickers Hardness and Yield Stress. The Kneppo formula for the initial magnetisation curve is found to hold better for the higher carbon content steels with the fit deteriorating with increasing plastic deformation.

Acknowledgements

List of Publications

Birkett A.J., Corner W.D., Tanner B.K. and Thompson S.M. *Influence of Plastic Deformation on Barkhausen Power Spectra in Steels* J. Phys. D: Appl. Phys. **22**, 1240 (1989)

Thompson S.M., Tanner B.K. *The Magnetic Properties of Plastically Deformed Steels* J. Magn. Mag. Mat. **83**, 221 (1990)

Thompson S.M., Allen P.J. and Tanner B.K. *Magnetic Properties of Welds in High-Strength Pearlitic Steels* IEEE Trans. Mag. **26**, No.5, 1984 (1990)

Table of Contents

ix

<center>Chapter I</center>

<center>Introduction to Magnetism.</center>

The subject of Magnetism has a wide audience and applications in many branches of Science from Biology to Astrophysics; it is used in numerous Engineering situations from electronics to its non-destructive testing applications on oil rigs, gas pipes and aircraft. Despite its ancient recognition satisfactory explanations for the phenomenon required the advent of quantum mechanics and the subject is still growing with increased uses in recording technology and the study of new magnetic interactions in magnetic multilayers. Much of the standard literature dates from the 1960's and an excellent background in the subject can be gained by studying the texts of Bates (1963), Brailsford (1966), Chikazumi (1964) and Morrish (1965), whereas ferromagnetism is treated by Bozorth (1951) and Craik et al (1965). More recently good introductory texts have been written by Crangle (1977) and Jakubovics (1987), but the most relevant book is that of Cullity (1972). In addition many solid-state texts such as Kittel (1976) discuss the theory of magnetism. A summary is provided here of the origins of magnetism paying particular attention to the discussion of magnetic domains and their detection as a method of determining the magnetic properties of a material.

1.1 Basic Magnetic Properties.

The magnetic force applied to a material is given the symbol H and units of ampères per metre (Am^{-1}) as it is derived from the magnetic field that arises from a current flowing in a wire. The magnetic induction B measured in webers per square metre (Wb m^{-2}) or tesla (T) is the magnetisation induced in the medium, and depends on the susceptibility of the material to be magnetised. In free space B is directly proportional to H and the constant of proportionality is called the permeability of free space μ_o which has the value $4\pi \times 10^{-7}$ henries per metre (Hm^{-1}). The induction in free space, B_o is therefore given by :-

$$\mathbf{B_o} = \mu_o \mathbf{H} \ldots (1.01)$$

<center>1</center>

and in any other medium :-

$$B = \mu_o(H + M) \ldots (1.02)$$

which can also be written as:-

$$B = B_o + \mu_o M \ldots (1.03)$$

M, the magnetisation per unit volume, measured either in ampères per metre (Am^{-1}) or joules per tesla per cubic metre $(JT^{-1}m^{-3})$ is the magnetic dipole moment per unit volume. The maximum value of M is the saturation magnetisation M_s and is an intrinsic property of the material. A parameter often used to describe a material's response to an applied magnetic field is susceptibility χ_v per unit volume and χ_m per unit mass defined as:-

$$\chi_v = \frac{M}{H} \quad \chi_m = \frac{M}{\rho H} \ldots (1.04)$$

where ρ is the density of the material. However it is often more practical to rewrite equation 1.02 as :-

$$B = \mu_o \mu_r H \ldots (1.05)$$

and measure μ_r, the relative permeability, derived as :-

$$\mu_r = 1 + \frac{M}{H} \ldots (1.06)$$

1.2 The Origins of Magnetism.

Analogous to the magnetic dipole moment that originates from a current flowing in a loop, the electron orbit of an atom results in a magnetic dipole moment proportional to its angular momentum. In addition the electron itself has an intrinsic angular momentum due to its spin and the total magnetic dipole moment of the atom is given by the vector sum of these two quantities.

When atoms are confined to a bound state in a molecule or an ionic system they usually combine such that no net dipole moment exists in the absence of an

2

applied field. When placed in a magnetic field the electrons acquire an additional precessional motion according to Larmor's Theorem and this additional angular momentum results in a non-zero magnetic moment. However this moment, according to Lenz's law, is antiparallel to the applied field and if there is no other source of magnetic moment then the material has a negative, temperature and field independent, susceptibility and is said to be **diamagnetic**. All materials display diamagnetism, but the negative susceptibilities involved are very small ($\chi_v \sim 10^{-5}$) and are usually masked by any additional moments present.

Materials whose bound states do result in a net atomic, molecular or ionic magnetic moment, but whose moments are randomly orientated in a zero magnetic field are said to be **paramagnetic**. As a field is applied the moments align resulting in positive susceptibilities of $\chi_v \sim 10^{-3}$ and a temperature dependence determined by the Curie-Weiss Law:-

$$\chi_v = \frac{C}{T - T_c} \ldots (1.07)$$

Where C is the Curie constant, T the absolute temperature and T_c the Curie temperature (a characteristic constant for a particular material and usually zero for paramagnetic materials).

Some materials, notably the transition metals and hence also steel, exhibit magnetic ordering even in the absence of an applied field, the mechanisms responsible will now be discussed under the general term **ferromagnetism**.

1.2.1 Ferromagnetism.

At absolute zero the magnetic moments in the three classes of ordered magnetic materials, ferro-, antiferro- and ferri- magnetics, are perfectly aligned. Increasing the thermal energy introduces disorder into the system so that above some critical temperature, the Curie temperature for a ferromagnet, the material reverts to paramagnetism and the Curie-Weiss Law as defined above is obeyed. Iron has a Curie temperature of 1043K and is therefore ferromagnetic at room temperature.

The first explanation for magnetic ordering was given by Weiss (1907) who developed a theory based on an internal field, the 'Weiss molecular field', which

3

would align the moments in a similar manner to an external field. The theory satisfactorily explained the temperature dependence of the saturation magnetisation but the internal field necessary, supposed to arise from molecular interactions, was enormous ($\sim 10^3$ tesla) and no mechanism could be found that could provide this.

Magnetic ordering was discovered to be a quantum mechanical effect and Heisenberg in 1928 considered the Pauli exclusion principle to be responsible for an exchange interaction between the unpaired spins of electrons in adjacent atoms. This resulted in mutual repulsion between parallel spins and mutual attraction between antiparallel ones. The electrostatic exchange energy is described by the Heisenberg Hamiltonian H_{ex} which sums the interaction between neighbouring atoms i and j over all N atoms in the solid. The interaction is characterised by J_{ij} the exchange constant derived by considering the spatial wavefunctions of the electrons from the two atoms.

$$H_{ex} = -2 \sum_{\substack{i=1 \\ i\neq j}}^{N} \sum_{\substack{j=1 \\ j\neq i}}^{N} J_{ij} \mathbf{S_i}.\mathbf{S_j} \ldots (1.08)$$

Where $\mathbf{S_i}$ and $\mathbf{S_j}$ are the spin quantum numbers of the two neighbouring atoms i and j respectively. If J_{ij} is positive then the exchange energy will be a minimum when the spins are parallel resulting in a net magnetic moment and **ferromagnetic** ordering. Minimum exchange energy for negative J_{ij} therefore occurs for antiparallel spins. In this case, if the adjacent opposing magnetic dipole vectors are of equal magnitude then there will be no net magnetic moment and the material is **antiferromagnetic**, if however they are not equal then a net moment will exist and **ferrimagnetism** occurs. A large ratio of interatomic distance to orbital radii is conducive to a positive exchange interaction (as there is mutual repulsion between the parallel spins) as is the case for iron, cobalt and nickel.

This **direct exchange** interaction describes the simplest situation and different mechanisms are actually responsible for the ordering in many cases: **superexchange** occurs in ferrimagnetic materials such as ferrites where the intermediate non-magnetic atom or ion mediates the exchange between the magnetic ones; in rare earth metals the interaction between the f-shell electrons occurs by **indirect exchange** via the conduction electrons. In metals, including the transition metals the non-localised nature of the conduction band 3d electrons resulted in the

4

development of Stoner and Slater's collective electron or band model of **itinerant exchange**.

1.3 Magnetic Domains.

The theory of exchange mechanism can explain the very large magnetisations achieved in ferromagnets, but cannot describe their magnetic properties which include the ability to have zero magnetisation both with and without an applied field and to display magnetic hysteresis. Weiss postulated in 1907 that the material was divided up into small domains within which the magnetic moments were aligned, random orientation of these domains would result in zero overall magnetisation. The subsequent application of a field to the material causes the rearrangement of these domains; involving either the growth of preferentially orientated domains and hence the movement of the domain walls separating them or the alignment of the magnetisation directions of the individual domains in the direction of the external applied field. A study of the magnetisation process in a ferromagnet must therefore deal with the energy considerations for the formation and movement of these domains. The minimisation of these energies determines the domain configuration in the sample and the positions of the domain walls. In an imperfect polycrystalline sample the effects of grain boundaries, inclusions, dislocations and stress on these energies and hence domain configuration and wall movement must also be considered.

1.3.1 Magnetocrystalline Anisotropy.

The energy associated with the magnetisation of a ferromagnetic crystal depends on the direction of magnetisation with respect to the crystal orientation leading to easy and hard directions of magnetisation. The actual exchange interaction between electronic spins is isotropic and cannot therefore provide an explanation for crystal anisotropy. A weak coupling exists between the spin moments and the lattice via the spin-orbit coupling as the orbit is in turn strongly coupled to the lattice. Hence when an external field attempts to reorientate the spins the coupling will attempt to distort the lattice which will resist the reorientation until the spin-orbit energy can be overcome.

In body centered cubic (b.c.c.) crystals of iron the cube edge directions $\langle 100 \rangle$ are the easiest directions of magnetisation, and the $\langle 111 \rangle$ cube diagonal the hardest. The resulting magnetocrystalline energy can be written as a series expansion as follows:-

$$E_k = K_o + K_1(\alpha_1^2\alpha_2^2 + \alpha_1^2\alpha_3^2 + \alpha_2^2\alpha_3^2) + K_2(\alpha_1^2\alpha_2^2\alpha_3^2)\ldots(1.09)$$

Where the K_n are the magnetocrystalline anisotropy constants and the α_i the direction cosines between the magnetisation direction and the cubic axes. An approximation to the anisotropy is often given using the first anisotropy constant K_1 which is $4.7 \times 10^4 Jm^{-3}$ for iron.

Where there is a more direct coupling between the spin moments and the crystal lattice such as in the rare earth metals the crystal anisotropies are very large.

1.3.2 Magnetostriction.

Closely related to the magnetocrystalline anisotropy is the magnetoelastic strain anisotropy. In an attempt to minimise the magnetocrystalline energy the crystal suffers a small deformation when magnetised, introducing an additional strain into the system. The resulting strain is dependent on the crystal symmetry and the direction of magnetisation such that magnetostriction constants λ_{100} and λ_{111} along the $\langle 100 \rangle$ and $\langle 111 \rangle$ directions respectively can be defined. In iron a tensile strain develops in the $\langle 100 \rangle$ easy directions and the previously b.c.c. structure becomes tetragonal with $\frac{\delta l}{l} \sim 10^{-5}$. For polycrystalline specimens the constituent crystals are assumed to be randomly orientated so that $\lambda_{100} \simeq \lambda_{111} = \lambda_s$ and the resulting magnetostriction at an angle θ to the direction of magnetisation is found by :-

$$\frac{\delta}{l} = \frac{3}{2}\lambda_s\{cos^2\theta - \frac{1}{3}\}\ldots(1.10)$$

However, this assumes the individual grains to be magnetically isotropic and does not account for any preferred orientation within the sample.

The inverse effect to a strain resulting from the application of a magnetic field is the affect on the magnetisation due to the application of elastic stress. This inverse

magnetostriction effect can be expressed in terms of a magnetoelastic energy which depends on the product of the magnetostriction constant and the applied stress σ hence the polarity of the energy can be reversed by the sign of either of these two quantities. At an angle θ to the magnetisation, the magnetoelastic energy is given by :-

$$E_{me} = \frac{3}{2}\lambda_s \sigma cos^2\theta \ldots (1.11)$$

For iron, with a positive magnetostrictive constant, the magnetoelastic energy will be minimised for a tensile stress applied parallel to the magnetisation.

1.3.3 Magnetostatic Energy.

The magnetostatic energy arises from a discontinuity in the magnetisation either at the specimen surface or within the sample itself. To counteract the discontinuity a demagnetising field develops antiparallel to the direction of magnetisation. On a macroscopic scale the demagnetising field of the sample can be expressed in terms of a demagnetising factor D which is determined by the sample geometry:-

$$(\mathbf{B_o})_D = -D\mu_o\mathbf{M} \ldots (1.12)$$

and the magnetostatic energy density by :-

$$E_{ms} = \frac{1}{2}D\mu_o M^2 \ldots (1.13)$$

The demagnetising factor can only be found exactly for perfect ellipsoids, but very often can be successfully approximated (Brailsford 1966). This shape anisotropy can be a very significant factor in determining the direction of magnetisation particularly for particles with elongated axes, and in determining the domain configuration within a sample.

1.3.4 Domain Walls

Whilst the domains in a sample may preferentially lie along easy axes of magnetisation or parallel to the direction of applied field, in order to reduce magnetostatic energy usually more than one domain will be present. The region, or wall, between adjacent domains is a region of changing magnetisation direction and some

energy is therefore required to create it. This energy must be offset against the reduction in energy that results from the multiple domain configuration.

Domain walls are often classified as either 180°walls separating regions of antiparallel magnetisation or 90°walls which separate regions whose magnetisations are approximately perpendicular.

The first type of wall to be discussed is the Bloch wall (figure 1.01) in which the magnetisation vector, the spin direction for a transition metal, rotates about an axis normal to the boundary. The exchange energy between adjacent spins is a minimum if they are parallel encouraging a gradual rotation of spins through the wall, but as the spins rotate out of the easy direction extra magnetocrystalline energy is incurred. Hence the final width of the wall is determined by minimising the sum of these two energies.

From equation 1.08 the extra exchange energy incurred by rotating a spin away from its parallel neighbour by an angle ϕ is given by $J_{ex}S^2\phi^2$. For a 180°wall on a $\{100\}$ surface of a cubic crystal, lattice constant a, N atoms thick $\phi = \frac{\pi}{N}$ the extra exchange energy per unit area of wall is found by:-

$$\gamma_{ex} = \frac{J_{ex}S^2\pi^2}{Na^2} \ldots (1.14)$$

The quantity $A = \frac{2J_{ex}S^2}{a}$ is often used to characterise the material so that the exchange energy becomes:-

$$\gamma_{ex} = \frac{A\pi^2}{2Na} \ldots (1.15)$$

The anisotropy energy per unit area can be approximated using the first anisotropy constant K_1 :-

$$\gamma_a = NaK_1 \ldots (1.16)$$

The wall energy γ_w is found by the sum of γ_{ex} and γ_a and the optimum wall thickness N_oa is the value of N at minimum wall energy when $\frac{d\gamma_w}{dN} = 0$:-

$$N_o = \frac{\pi}{a}\sqrt{\frac{A}{2K_1}} \quad \text{therefore} \quad \delta_w = \pi\sqrt{\frac{A}{2K_1}} \ldots (1.17)$$

8
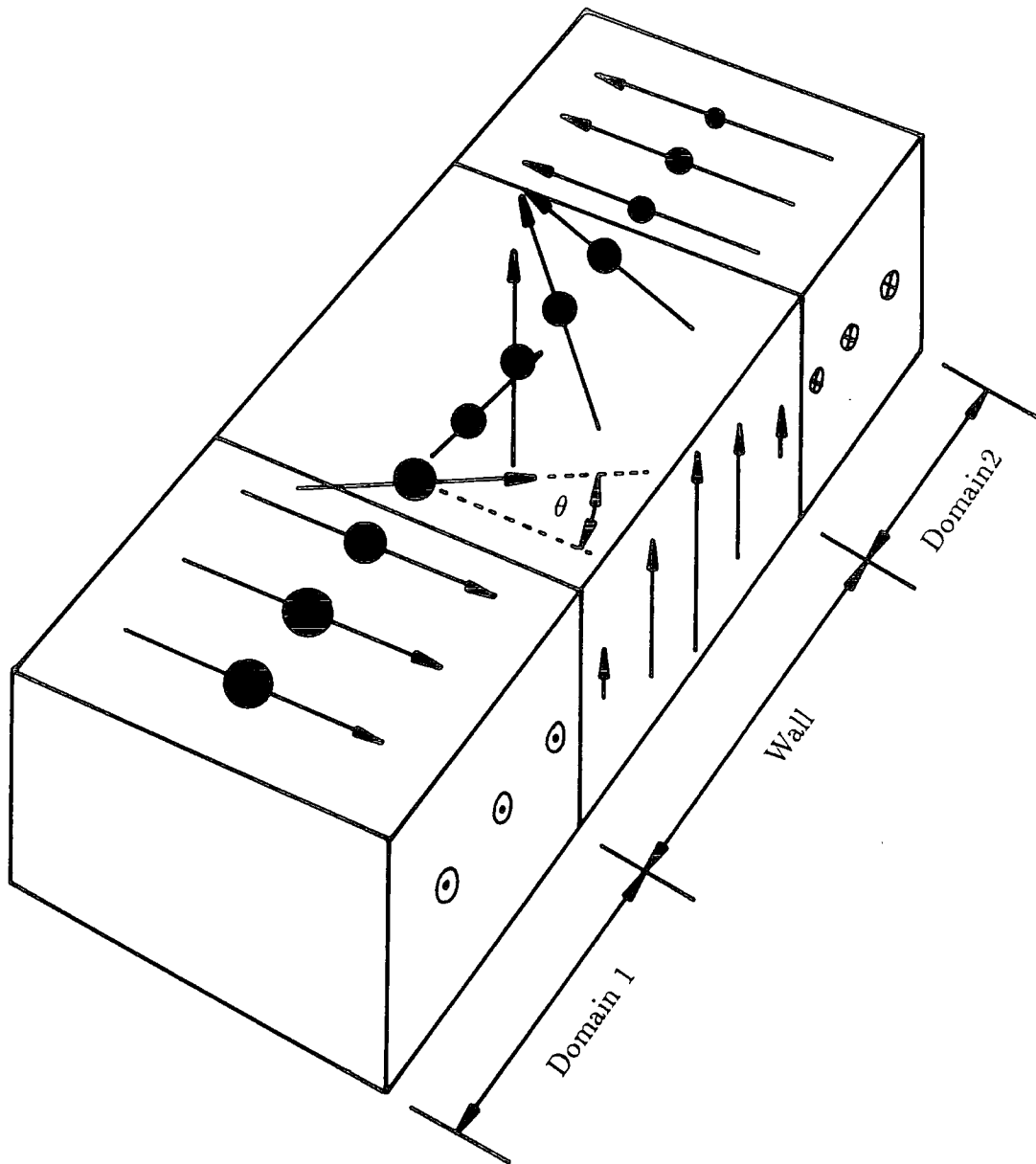
Figure 1.01 Schematic Diagram of a 180°Bloch Domain Wall. The Arrows Represent the Magnetisation Vectors.

9

Hence the minimum wall energy can also be written as:-

$$\gamma_w = \pi\sqrt{\frac{AK_1}{2}} + \pi\sqrt{\frac{AK_1}{2}} \ldots (1.18)$$

therefore $\quad \gamma_w = 2\pi\sqrt{\frac{AK_1}{2}} \ldots (1.19)$

and $\ldots \gamma_w = 2\delta_w K_1 \ldots (1.20)$

So the minimum wall energy occurs for equal increases in exchange and anisotropy energy.

Substituting values for iron : $K_1 = 4.7 \times 10^4 Jm^{-3}$, $a = 2.86 \times 10^{-10}m$, $S = 1$, $T_c = 1043K$. Using $J \simeq \frac{kT_c}{5}$, where $k = 1.38 \times 10^{-23}$ is the Boltzman constant, $J = 2.9 \times 10^{-21}J$ and hence $A \simeq 2.0 \times 10^{-11} Jm^{-1}$. This gives values for iron of:-

$$\delta_w \simeq 4.6 \times 10^{-8}m \quad i.e. \quad N_o \simeq 160 atoms$$

$$\gamma_w \simeq 4.3 \times 10^{-3} Jm^{-2}$$

These values should be compared with those of $\sim 0.4 Jm^{-2}$ for grain boundary energy densities. Despite the fact that these values do give reasonable agreement with those determined experimentally they are necessarily approximate due to the Ising approximation which assumes a 1 dimensional model for calculating the exchange energy, the approximation of a simple cubic lattice for iron and the assumption of uniform rotation through the wall. It can be shown that the local exchange energy is everywhere equal to the local anisotropy energy and that the angle between the spin direction and the x-axis ,θ, follows the relation :-

$$cos\theta = tanh\left[z\sqrt{\frac{K_1}{A}}\right] \ldots (1.21)$$

where z is the distance from the centre of wall.

In the case of deposited thin films, or thinned foils the thickness of the sample is reduced to the same order as the wall thickness itself. The increase in the
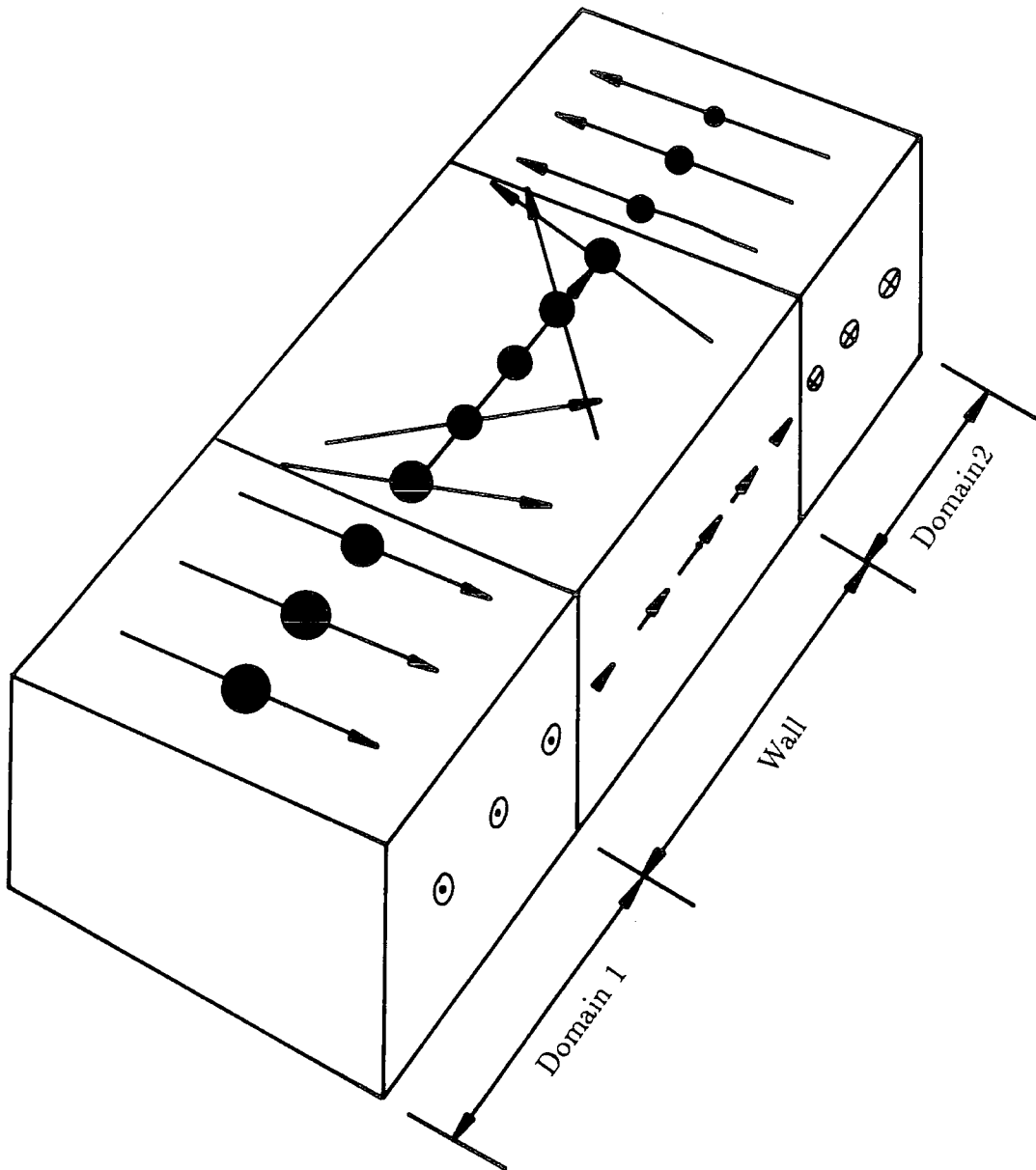
Figure 1.02 Schematic Diagram of a 180°Neél Domain Wall. The Arrows Represent the Magnetisation Vectors.

11

demagnetising factor causes the magnetostatic component of the wall energy to become large compared to the anisotropy and exchange components. This eventually results in the Bloch wall becoming unstable in preference to a Néel wall.

In a Néel wall (figure 1.02) the magnetisation vector rotates in the plane of the film creating free poles on the wall surface, but none on the film surface itself. Due to these free poles the effect of a Néel wall can be felt over a greater distance than that of a Bloch wall.

The type of wall present is also affected by the angle between the magnetisations of the adjacent domains and becomes particularly important at the transition thickness between Bloch and Néel walls. If the angle is less than the critical angle, which increases as the film thickness decreases, pure Néel walls will form, and if it is 180°pure Bloch walls will form. At intermediate angles transition walls can exist which consist of both Bloch and Néel components. These transition walls are often unstable and low energy partition walls are preferentially formed. Here a Bloch wall is subdivided into sections of alternate perpendicular magnetisation vectors by Néel lines and a Néel wall divided into alternating segments by Bloch lines. The latter is called a cross-tie wall and is illustrated in figure 1.03. Where the magnetisation in the wall rotates such that the flux closure lines are parallel with the adjacent domains the rotation is smooth, but in alternate sections a rapid change occurs known as the cross-tie.

The wall structure is affected by inhomogeneities such as periodic variations in the anisotropy. This results in a ripple wall structure where lines develop perpendicular to the wall and the magnetisation.

The two main categories of wall illustrate the processes involved in wall formation, but as in the case of partition walls many domain walls have a more complex structure. They may form asymmetric Bloch walls, asymmetric Néel walls or vary in width along their length.

1.3.5 Domain Configurations.

In a uniaxial crystal, magnetised along the easy direction, the magnetostatic energy is reduced by increasing the number of parallel stripe domains until it

12

Ms
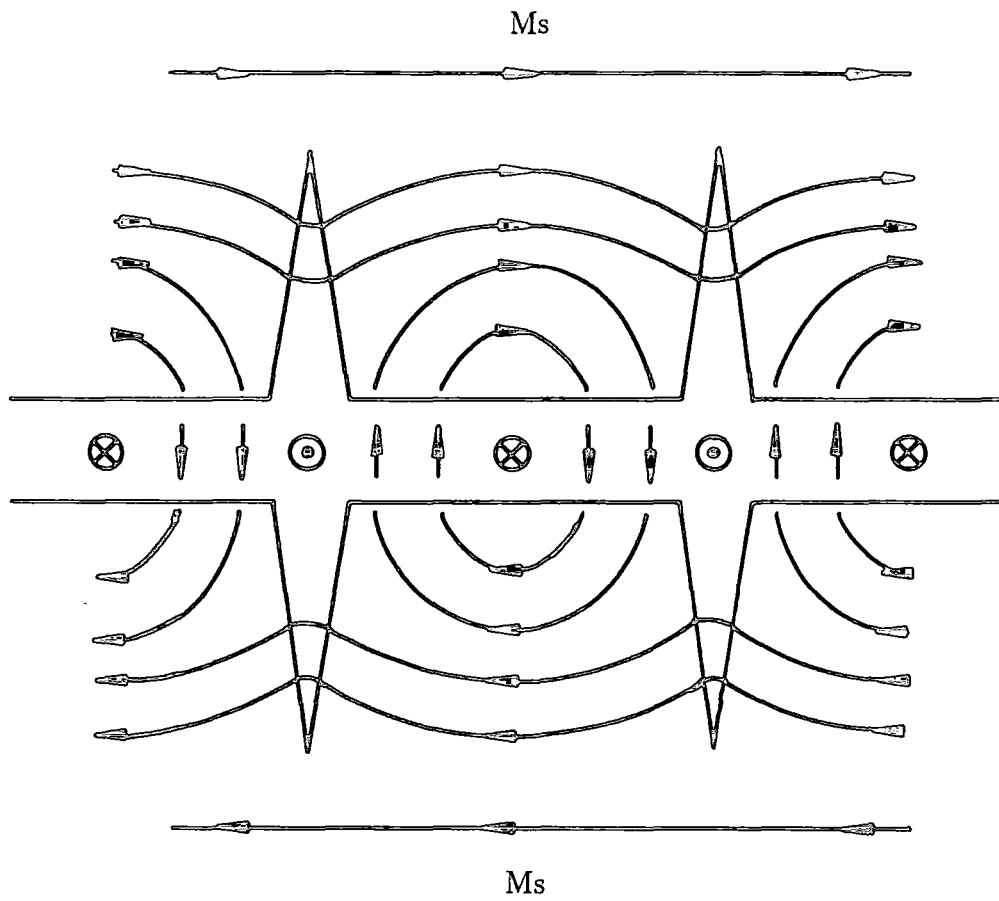
Figure 1.03 The Magnetisation Distribution Surrounding a Cross-tie Wall. (After Craik and Tebble 1965)

13
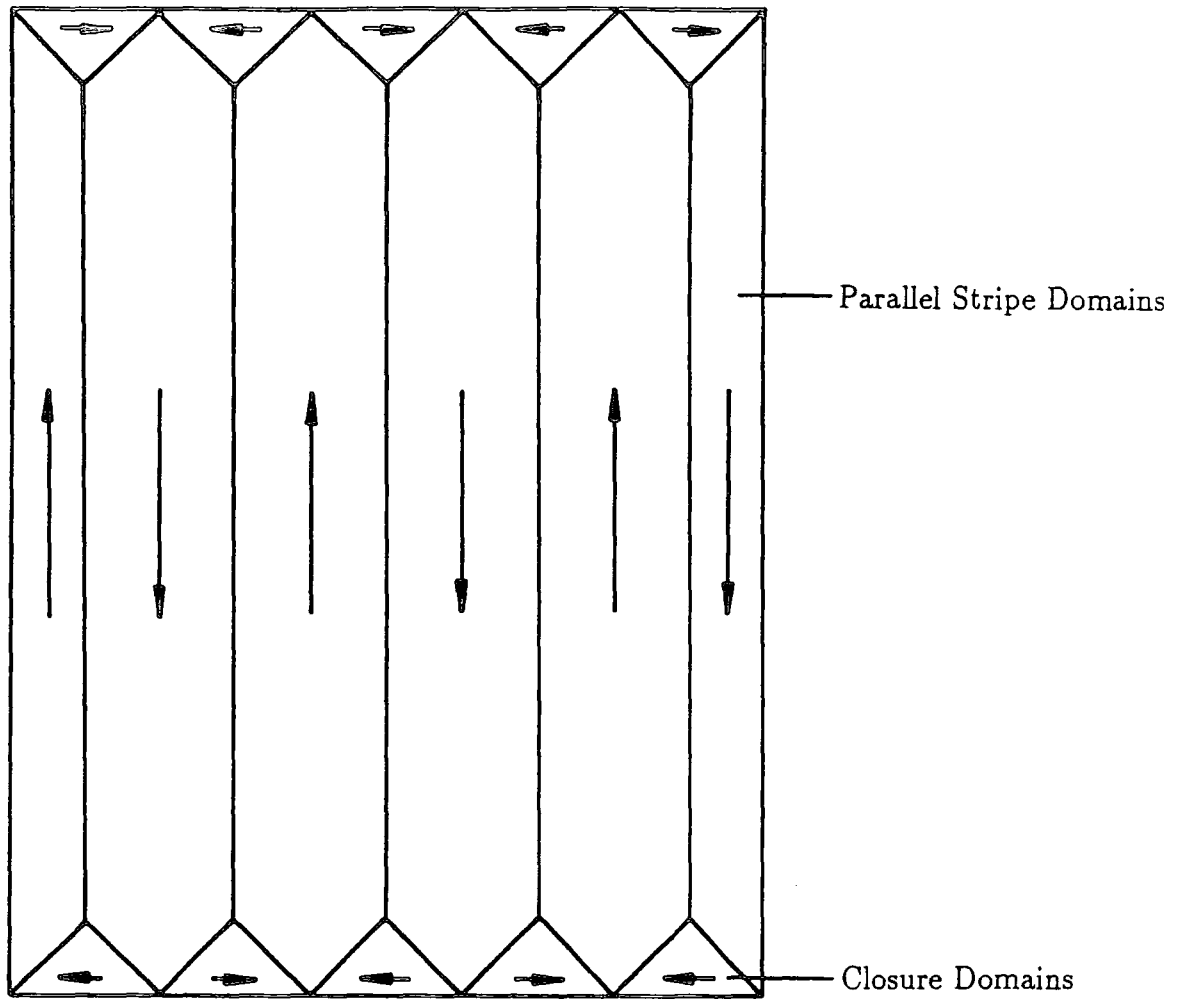
Figure 1.04 Hypothetical Domain Configuration in a Cubic Crystal Showing the Formation of Closure Domains.

14

is balanced by the wall energy. Further reduction in the surface magnetostatic energy can also be made by the creation of small, pointed spike domains of reverse magnetisation which do not require much wall energy, but result in the creation of some interior poles. In a cubic crystal with more than one easy axis more complex structures can evolve in order to reduce the magnetostatic energy. One very common arrangement is that of closure domains (figure 1.04) perpendicular to the main stripe domains, which complete the flux path. These domains will however incur some magnetoelastic energy (equation 1.11); this is proportional to their volume and can be minimised by increasing the number of the stripe domains. If the closure domains are to completely close the flux path, then the angle the domain wall makes with the stripe domains must be 45°.

The situation is more complex in a polycrystalline material where the grain surfaces do not usually lie exactly along an easy direction and the domains are interrupted by grain boundaries, inclusions, regions of microstress and dislocations. All these inhomogeneities alter the energy of the system and hence the domain structure, but the problem of free poles forming at grain boundaries and at inclusions is often the dominant factor resulting in the formation of closure, spike or multiple stripe domains to reduce the magnetostatic energy of the system.

Where a domain wall bisects an inclusion closure domains tend to form around it to reduce the magnetostatic energy. Within the domain itself the energy is reduced by the formation of spike domains, as illustrated in figure 1.05, the spike magnetisation is at an angle with the main domain that is as close to 45°as possible.

1.3.6 Domain Wall Motion and Hysteresis.

When a magnetic field is applied to a demagnetised ferromagnetic material such as iron the magnetisation initially increases by the growth of preferentially orientated domains by reversible domain wall motion. This is followed by irreversible domain wall motion and finally by domain rotation until all the domains are aligned. Plotting the resulting induction against the applied field produces the initial magnetisation curve as illustrated in figure 1.06 which also indicates the values used to parameterise the curve: the initial permeability μ_i, maximum relative permeability μ_{max} and saturation induction Bs. As the saturating magnetic field is reduced to zero the direction of magnetisation within each domain returns to

Spike Domain

Inclusion

Closure Domain

a)

b)
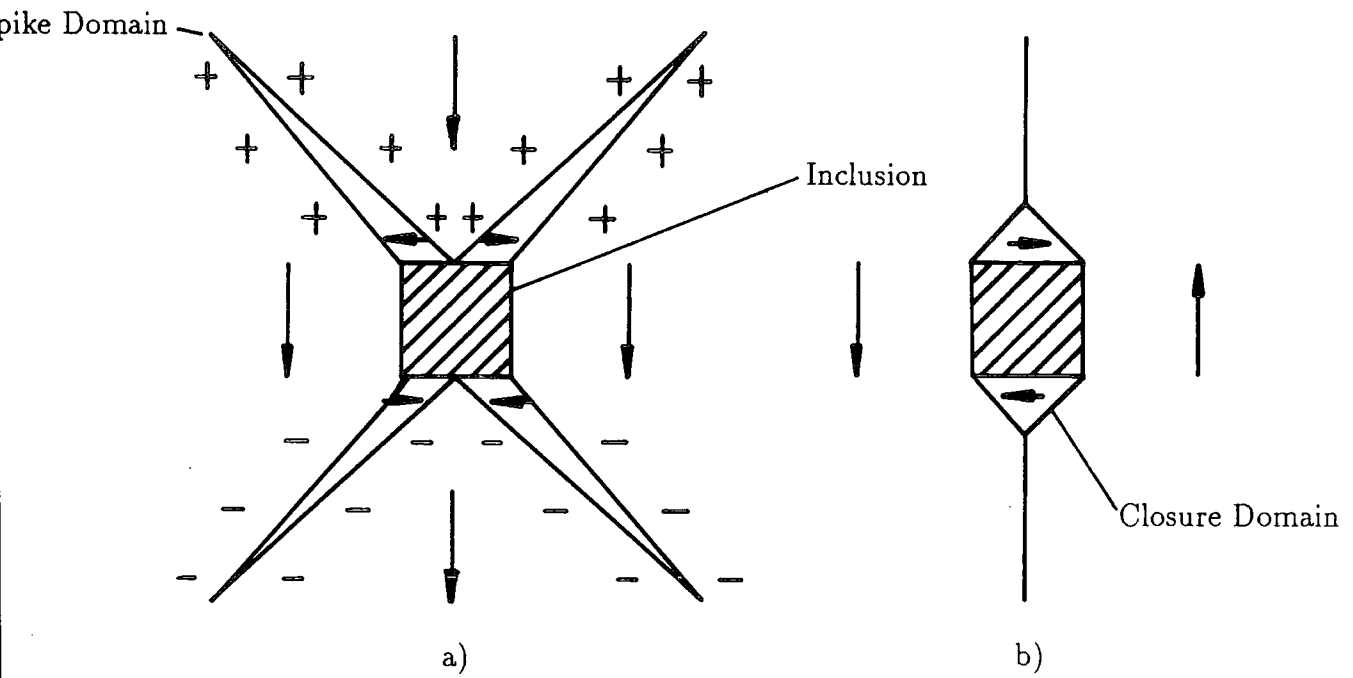
Figure 1.05 The Formation of Spike Domains on an Inclusion Bisected by a Domain Wall. (Reproduced from Cullity 1972)

16
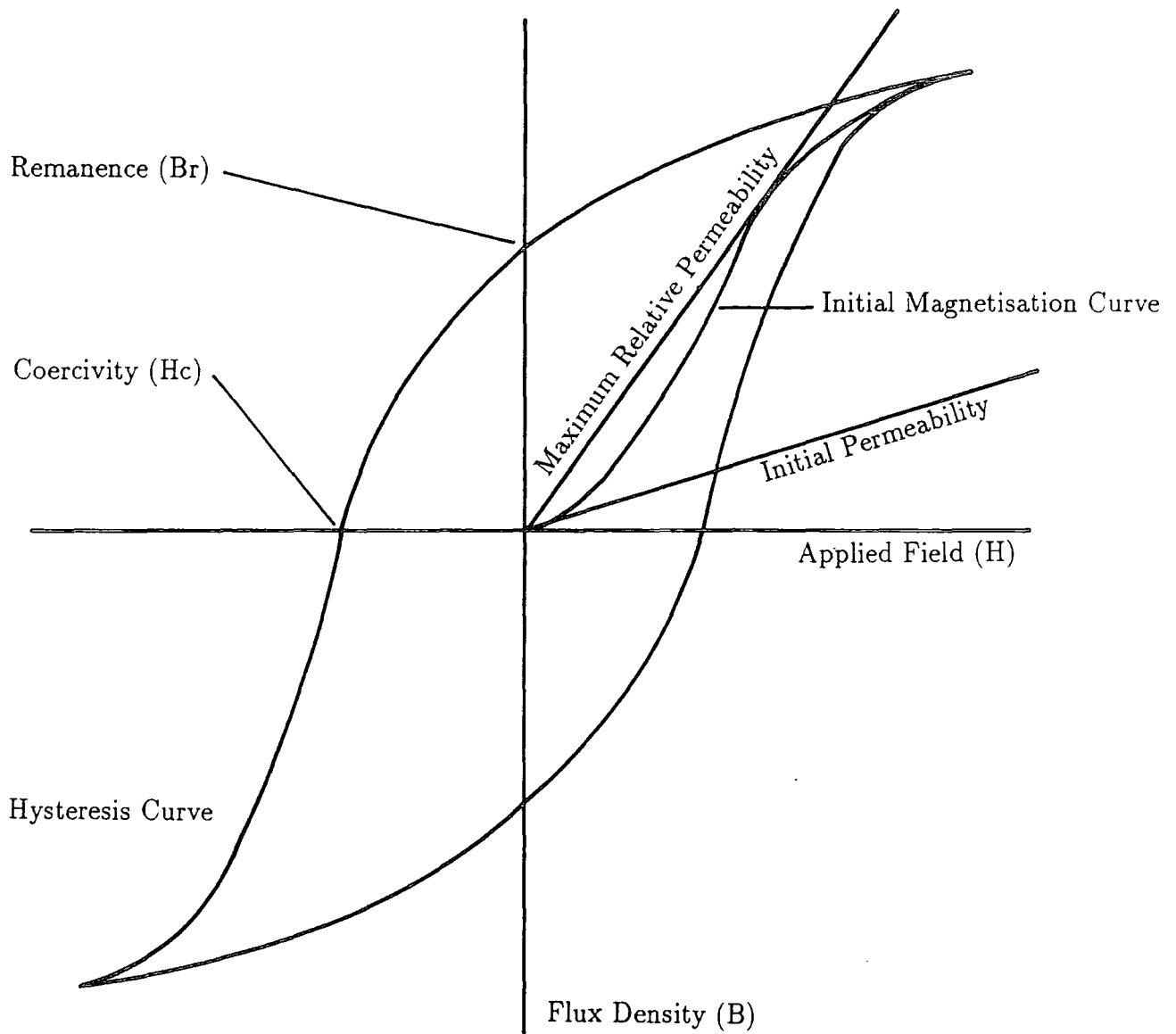
Figure 1.06 Example Initial Magnetisation and Hysteresis Curves for a Ferromagnet.

its easy direction and some easy domain wall movement occurs reducing the magnetisation to remanence. The subsequent application of the reverse magnetic field allows the more difficult domain wall motion to occur and reduce the induction to zero at the coercive point. Subsequently increasing the field causes further domain wall movement and rotation to bring the material to negative saturation. The loop that the magnetisation of the sample traverses as the applied field is alternated between positive and negative saturation values is called the hysteresis loop and is also illustrated in figure 1.06. The magnetic induction B has been plotted as this is the quantity which is often measured experimentally. Marked on the curve are some of the properties used to characterise the curve : the remanent field B_r and coercive field H_c required to reduce the magnetisation of the sample to zero from the remanent point. The irreversible motion of domain walls results in work being done to complete the hysteresis cycle, this hysteresis loss corresponds to the area under the curve. Measuring the parameters defined above for the initial magnetisation and hysteresis curve of a material yields much information about its magnetic properties and this method is often used to characterise a magnetic material.

Domain growth requires the movement of domain walls and their passage through the material will be impeded by any inhomogeneities encountered such as regions of microstress or inclusions. Any region with a spontaneous magnetisation that differs from the bulk can be considered an inclusion in this situation, and hence in steel they may take the form of cementite particles, other impurities, dislocations or grain boundaries.

To illustrate the mechanism by which a domain wall may pass through an inclusion, the motion of a wall through a hypothetical, nonmagnetic inclusion will be considered, the theoretical domain structure is illustrated in figure 1.07. As the field parallel to the left-hand domain is increased this domain grows and the wall tries to move to the right. As it moves, the closure domains are extended to form tube domains and this reversible motion continues until in 1.07 d) the increased wall energy of the tube domains becomes too high and the wall is released leaving two spike domains around the inclusion to reduce its magnetostatic energy. Until the wall is released the wall movement is irreversible as reducing the applied field would cause the the walls to revert back to their original configuration, however

18
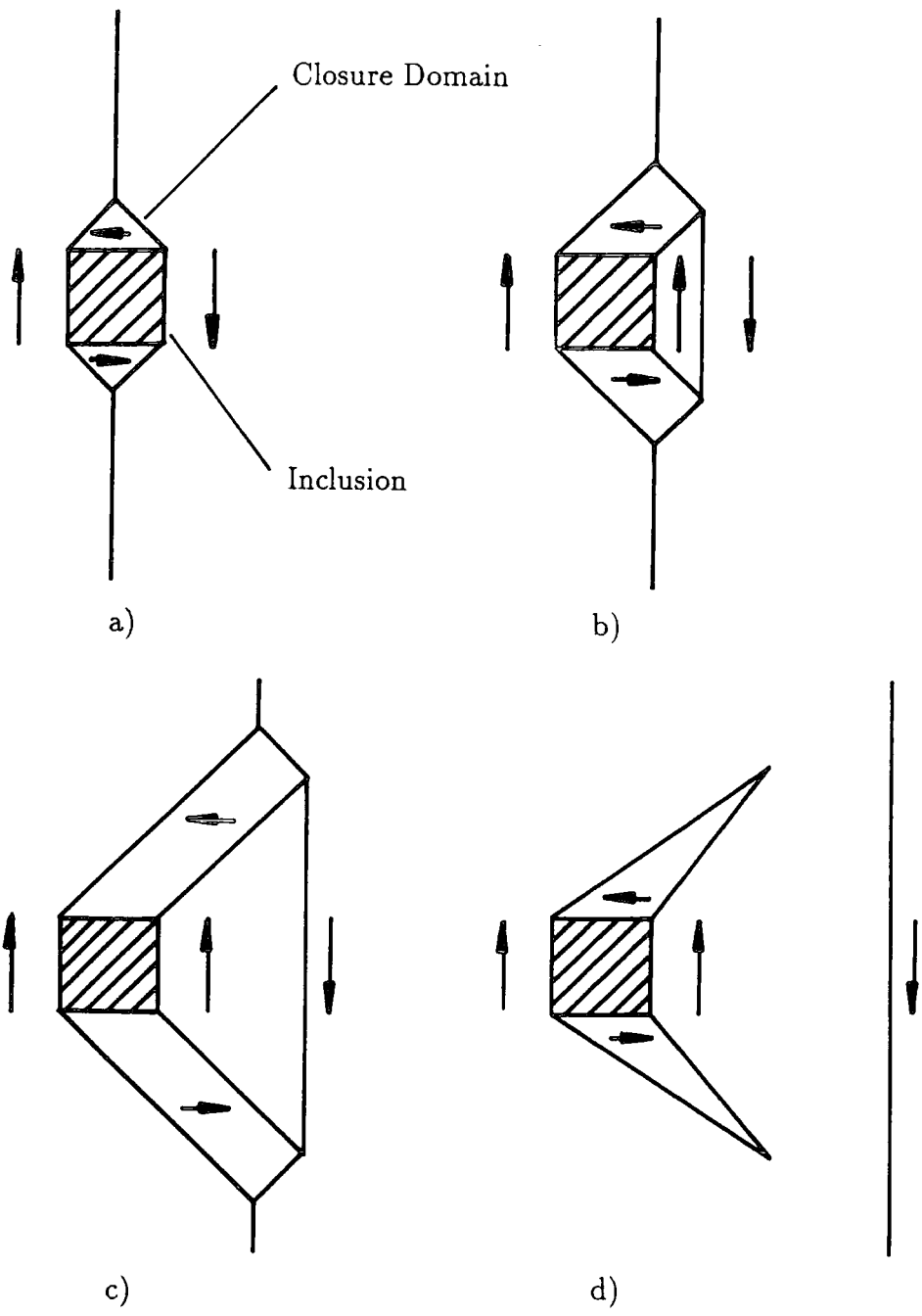
Figure 1.07 The Passsage of a Domain Wall through an Inclusion. (Reproduced from Cullity 1972)

once the wall has been released and the field reduced, the returning wall will encounter a completely different situation. A single irreversible movement of a domain wall is known as a Barkhausen jump.

In general an inclusion smaller than the width of a domain wall has little magnetostatic energy and hence its presence in the wall reduces the wall energy, therefore requiring more energy for the wall to leave its position bisecting the inclusion. A larger inclusion bounded by closure domains will pin the domain wall due to its subsidiary domains as outlined in the above situation. Inclusions approximately the same size as the wall width are the most effective at pinning the wall.

Regions of residual microstress in a domain will affect the domain and wall energy due to their magnetoelastic energy. Plastic deformation involves the creation of many dislocations and very quickly large concentrations of dislocations called dislocation tangles resulting in a very complex distribution of microstress. Each dislocation is surrounded by a strain field, which decreases approximately with the inverse square of the distance from the dislocation, and associated magnetoelastic energy. The affect of the resulting microstress distribution on domain wall motion will depend not only on the direction and magnitude of the stress, but also on the magnetostriction constant of the material. The interaction of 180°and 90°walls with regions of stress is very different as no change in magnetoelastic energy is involved in the former so that only the energy of the wall is affected. The energies involved in the interaction of a single wall with a particular type of stress can be derived (Cullity 1972), but are of little value due to the complex situations found in practice. It is possible however to conclude that high stress gradients and magnetostriction are not conducive to easy domain wall motion. Where a wall is passing through a region of irregular microstress the wall will find the lowest energy point which balances the increased wall energy due to passing through a high stress region, and the increased magnetostatic energy which will result if the wall curves to avoid such regions.

The interaction of a domain wall with an inclusion or area of stress can be represented as in figure 1.08 by the energy variations in its path and the corresponding force required to move the wall represented by the differential of this curve. Ini-

20
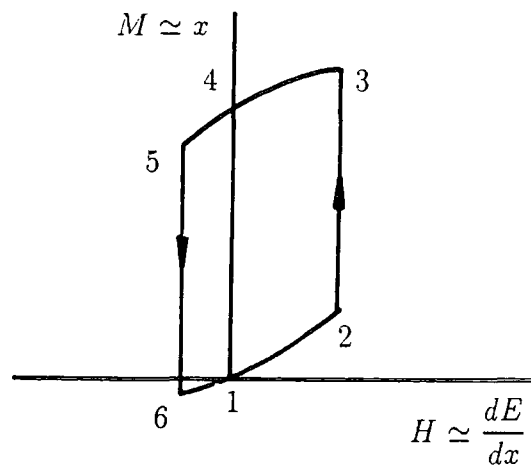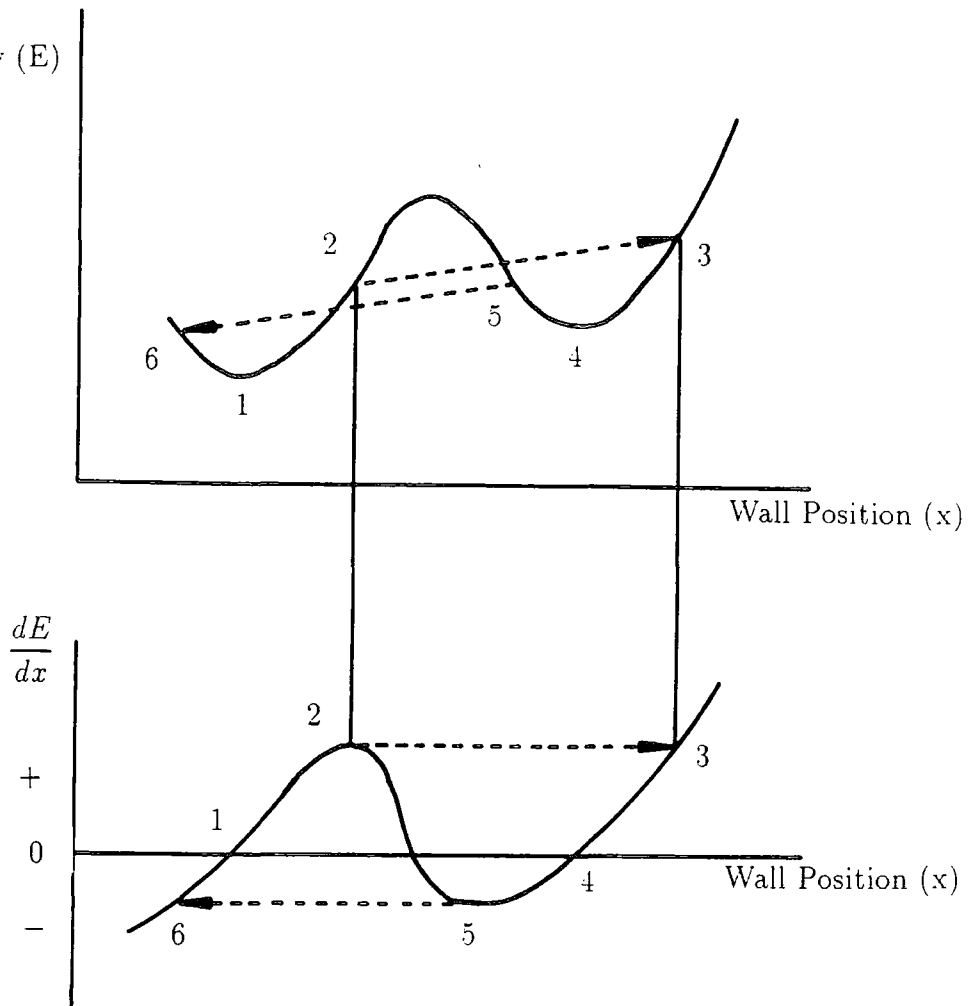
Figure 1.08 The Variation of Domain Wall Energy Along its Path. (Reproduced from Cullity 1972)

21

tially the wall is positioned at an energy minimum at **1**, increasing the field causes reversible movement until point **2** where any further increase in applied field results in an irreversible Barkhausen jump to point **3** on the curve which represents the same restoring force. Reducing the field from **3** now results in reversible movement to the local minimum at **4**. Further reduction in the field causes reversible movement until the wall reaches the point of inflection at **5** when another Barkhausen jump will occur to point **6**. Such consideration of the motion of a wall illustrates how a minor hysteresis loop can be traced out. The combination of the motion of all the walls in a real sample determines the final measured hysteresis curve.

1.3.7 Review of Domain Wall Imaging Techniques

Domains and domain walls are usually too small to be detected without magnification, a summary of the techniques available is given here followed by a more detailed description of the method used: Lorentz electron microscopy .

The oldest method, developed in 1931, is the Bitter or powder technique. Here a colloidal suspension of fine magnetic particles such as magnetite (Fe_3O_4) is applied to the surface of the sample, the particles are attracted to the field gradients which are most pronounced where domain walls intersect with the surface. It is very important that the surface of the specimen is carefully prepared so that the domain pattern that is delineated is representative of the material. This usually requires electropolishing as the final stage to remove the strains induced on the surface of the sample during mechanical polishing which influence the domain pattern. The orientation of the crystal with respect to the sample surface can also have a significant effect on the observed domain structure such as the complex "tree" pattern observed when a {100} surface is not parallel with the cut crystal surface belying the simple domain structure underneath. By applying a field to the specimen whilst it is under the optical microscope the movement of the domain walls can be observed although the technique is restricted by the inertia of the particles and so only very slow domain movement can be studied.

The plane of polarisation of polarised light undergoes a rotation when it encounters a magnetic medium. This magneto-optic effect is exploited for domain wall imaging using the Kerr effect for reflected light, and the Faraday effect for

transmitted light. In adjacent domains with different magnetisations the polarisation plane will be rotated in different directions hence, by using an analyser, contrast can be obtained between the different domains. As it is the component of magnetisation parallel to the direction of the light beam that determines the rotation then the technique is most effective on materials with magnetisations perpendicular to the surface. Normal incidence can then be used for transmission, and the polar Kerr effect for reflection measurements; otherwise oblique incidence and the longitudinal Kerr effect must be used. These methods are very well suited to the study of moving domain walls as they suffer no inertia and the image itself is not affected by the additional applied field.

The deflection of electrons by the Lorentz force in a magnetic field can be used in the transmission electron microscope to image both static and dynamic domains walls and domains. The technique of Lorentz microscopy in a transmission electron microscope (T.E.M.) can produce high resolution images that provide information on the structure of domain walls themselves and on their interaction with microstructural features such as grain boundaries and dislocation tangles. The study of magnetic domains in thin films has been reviewed by Chapman (1984).

The scanning electron microscope can also be used for the study of bulk samples using either Type I or Type II magnetic contrast, and its use has been reviewed by Jones (1978). Type I contrast relies on the presence of surface leakage fields and hence is most often used for uniaxial materials such as cobalt. The trajectories of the secondary electrons are deflected by the leakage fields above the specimen surface and hence in different directions from domains of different orientation. The ability of cubic materials such as iron to form closure domains precludes the formation of surface leakage fields and Type II magnetic contrast must be used which depends on the deflection of the primary electron beam by the internal magnetisation of the sample. The sample is tilted by about 55°towards the electron beam so that the Lorentz force in one domain causes the beam to be deflected further into the sample, and in the opposite domain the beam is deflected back towards the surface. This produces a variation in the backscattered electrons from the two domains allowing the domain structure to be imaged. Both methods require a high beam currents to obtain a satisfactory signal to noise ratio and a high standard of surface preparation.

1.4 Lorentz Electron Microscopy.

In the electron microscope electrons produced by a thermionic gun are accelerated down an evacuated column onto a specimen with focusing of the electron beam achieved by the use of magnetic lenses. A variety of elastic and inelastic scattering processes take place during interaction with the specimen before the reflected electrons in a scanning electon microscope (S.E.M.) are detected by a scintillator and the transmitted electrons in a transmission electron microscope (T.E.M.) imaged on a florescent screen. A useful introductory text to electron microscopy is that of Grundy et al (1976), and excellent works on thin film electron microscopy which also discuss Lorentz microscopy in detail are those of Hirsch et al (1965) and Reimar (1984).

Typical electron acceleration voltages in a T.E.M. are hundreds of kilovolts producing relativistic electron velocities. The de Broglie wavelength of an electron is given by :

$$\lambda = \frac{h}{p} \dots (1.22)$$

which non relavistically gives the wavelength of an electron accelerated through a potential V_e as:

$$\lambda = \frac{h}{\sqrt{2mV_e}} \dots (1.23)$$

Taking into account the relativistic velocity of the electron above $V_e \simeq 10^5 V$ introduces a correction of about 5%:

$$\lambda = \frac{h}{[2m_oV_e(1 + \frac{V_e}{2m_oc^2})]^{\frac{1}{2}}} \dots (1.24)$$

where m_o is the rest mass of the electron and h is Planck's constant so that:

$$\lambda = \frac{12.26}{[V_e(1 + 0.9788 \times 10^{-6}V_e)]^{\frac{1}{2}}} \text{Å} \dots (1.25)$$

At 1MV this gives an electron wavelength of 0.87pm.

In order to interpret the images formed in an electron microscope the theory behind the diffraction of the electron beam in the sample must be understood. In

24

the kinematical approximation of diffraction theory it is assumed that the amplitude of the scattered wave is small compared to the incident wave, i.e that there is no multiple scattering. It is successful in providing qualitative explanations for most of the image contrast effects such as fringes produced by thickness variations and planar faults and dislocation contrast. For quantitative analysis the dynamical theory must be used which can also predict additional image effects.

However, the resolution obtained in this study was not sufficient for to analyse the electron micrographs in such detail and the kinematical approach provides sufficient information.

An electron in a magnetic field experiences a force, the Lorentz force, perpendicular to the direction of its velocity **v** and the direction of the field **B** :

$$\mathbf{F} = -e[\mathbf{v} \times \mathbf{B}] \dots (1.26)$$

Magnetic induction in the plane of the specimen will result in a deflection of the electrons from the vertical, z, direction in the xy plane given by :-

$$\phi_x = \frac{e\lambda t B_y}{h} \dots (1.27)$$

where λ is the electron wavelength, t the thickness of the specimen, h Planck's constant and B_y the y component of induction. At 900kV, $\lambda = 0.942$ pm and in a steel specimen 0.5μm thick saturated to 2 Tesla a deflection of 2.4×10^{-4}radians would result.

Early studies of magnetic domains by this technique were made by Fuller et al (1960 a and b), extensive studies have also been made by Grundy et al (1968) and Jakubovics (1975 and 1965). The two most commonly used methods of using this deflection to obtain magnetic contrast are described below.

1.4.1 Foucault Method.

Magnetic deflection results in the formation of a small angle diffraction pattern, known as the deflection pattern, in the back focal plane. By moving the objective aperture such that it absorbs one of these spots, the domains producing that deflection will appear dark, and the other domains bright (figure 1.09).

25

Incident Beam Direction

Specimen

Objective Lens

Ojective Aperture

Image
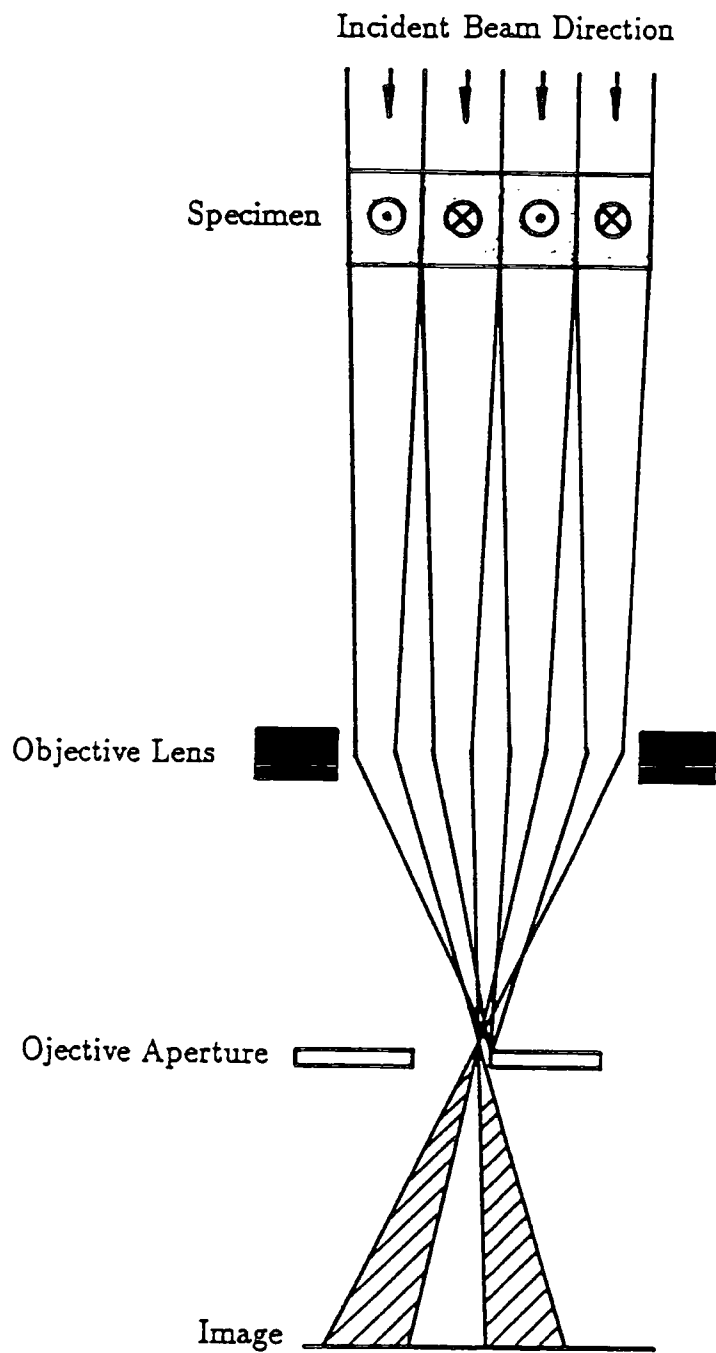
Figure 1.09 The Foucault Method of Domain Wall Imaging. (after Alcock 1985)

Blocking the other spot results in the opposite contrast. Due to scattering some contrast is still present in the dark regions and hence this technique allows infocus observation of microstructural regions and the domains. Although in principle it should be possible to conduct dynamic experiments in an applied field, in practice the positioning of the objective aperture is so sensitive that the image is often lost as the sample magnetisation and hence deflection is altered.

1.4.2 Fresnel Method.

Here the image of the specimen is defocused so that the deflections of the electrons in adjacent domains result in either a convergent or a divergent image in the region of the domain wall as (figure 1.10). The opposite contrast will be obtained for the opposite defocusing position enabling the walls to be studied in both the divergent and convergent situation. This method benefits from the greater structural detail that can be observed in the convergent walls at the expense of loss of simultaneous microstructural detail due to the defocusing. By magnetising the specimen insitu it is possible to observe the motion of domain walls and their interactions with such features as grain boundaries and dislocation tangles.

In the convergent wall image it is possible to use wave theory to consider the coherence effects and interference fringes produced by the two waves. It can be shown that the enclosed magnetic flux between two coherent waves traversing different paths from conjugate points (Δx apart) in the object and image introduces a phase shift between them of :-

$$\phi = \frac{2\pi e \Delta B \Delta x t}{\hbar} \ldots (1.28)$$

Equations can be derived for the fringe spacing and patterns determined for particular spin distributions that are sensitive to domain wall width. However the beam coherence necessary to resolve these fringes results in very low image intensities. In addition the wave-optical analysis is very sensitive to the exact experimental conditions. For these reasons the geometrical approach, valid at small defocusing distances, was used in this study. This technique has been used for studies of wall widths by Gong et al (1987).

Incident Beam Direction

Domain Wall

Domain Wall

Specimen

Image Plane

Deficient Intensity

Excess Intensity
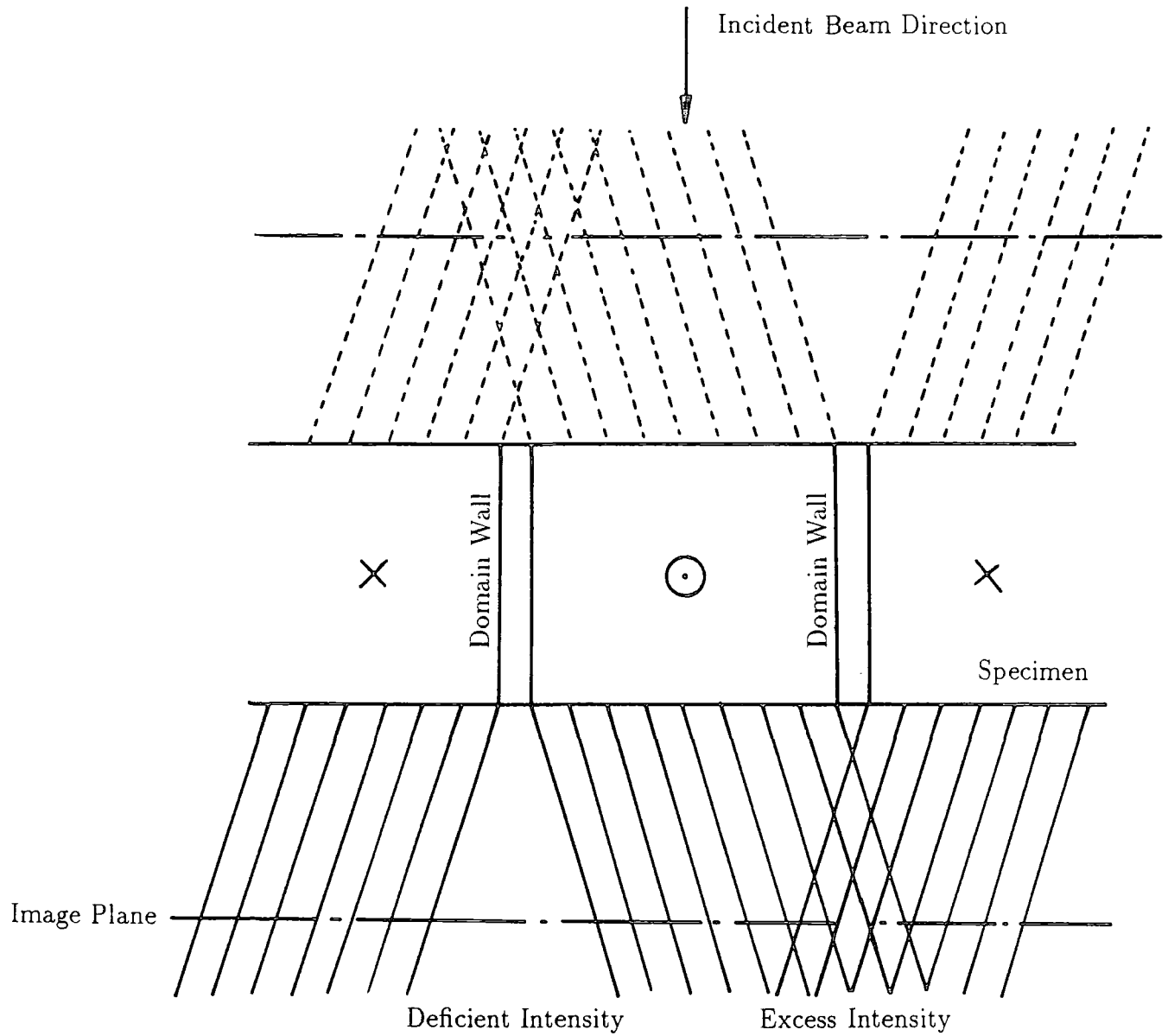
Figure 1.10 The Fresnel Method of Domain Wall Imaging. (After Hirsch et al 1965)

There are a number of advantages to using a High Voltage Electron Microscope (H.V.E.M.) for Lorentz microscopy. The amount of magnetic contrast increases with acceleration voltage until ~400kV, above this voltage the angular variation of the non-magnetic scattering decreases at a faster rate and the magnetic deflection is dependent only on the foil thickness. The higher the acceleration voltage the greater the penetration power of the electrons and the thicker the foils that can be imaged, $\simeq$ 700nm at 1MV. Using thicker foils also has the advantage that the observed domain structures are more likely to be representative of the bulk material and that fewer asymmetric walls will be observed. The defocusing limit for the geometrical theory also increases with increasing voltage. As the velocity of the accelerated electrons is increased the deflection of the electron beam by horizontal applied fields will be reduced. The increased electron velocity also improves the brightness of the image, reducing exposure times so that difficulties due to such problems as the instability of the microscope are reduced. Higher voltages also reduce chromatic aberration due to the energy spread of electrons and hence improve the resolution.

1.5 The Barkhausen Effect.

The discontinuous movement of domain walls is known as the Barkhausen effect. These irreversible jumps between positions of maximum wall energy gradient can be detected by the rate of change of flux through a search coil wound around or placed next to a sample being magnetised. Originally detected through a pair of loud speakers by Barkhausen in 1919, hence the term "Barkhausen Noise", it is the resulting voltage spikes that are usually recorded and analysed. Sources of noise in ferromagnetic materials have been reviewed by Bittel (1969).

While Lorentz electron microscopy enables direct observation of the movement of domain walls, it has the disadvantage that only very thin foils can be examined whose domain structures do not necessarily correlate with those in the bulk of the sample. Barkhausen noise can be detected from large samples and hence provides a means of studying the irreversible domain wall movement in the bulk. It is however only possible to detect the Barkhausen noise from the top few μm of the sample, a complementary study is that of magneto-acoustic emission which has a much greater penetration. An irreversible jump of a 90°wall causes an abrupt change in

29

elastic energy and the propagation of an elastic wave through the sample which can be detected by a piezo-electric transducer. A useful comparison can be made between Barkhausen signals due to both 180°and 90°walls and magneto-acoustic emissions sensitive only to the movement of 90°walls (Buttle et al. 1986). A detailed consideration of the magnetisation transitions that produce the Barkhausen noise is given by Tiitto (1977).

The magnetising coil can either contain the sample as described by Tiitto et al. (1976) or be wound on a small surface mounted coil as used by Säynäjäkangras (1974a); a triangular waveform is usually used to provide a constant rate of change of applied field. Many different arrangements of pick-up coils have been used to detect the noise and their geometry and characteristics are important as they can distort the shape of the Barkhausen pulses. Tebble et al (1950) treated the coil and a Barkhausen jump as a pair of coupled inductors and showed that provided the time constant of the coil is shorter than that of the jump no distortion of the pulse will occur.

Various methods have been used to record the noise and subsequently analyse it. Pulse height analysers have been used for analysis in the amplitude domain such as in the work of Säynäjäkangras (1974b). In this region parameters such as the Barkhausen amplitude (B.N.A.), peak heights and positions and median values are used to characterise the noise. Spectrum analysers are now commonly used (Tiitto et al 1986) for analysis in the frequency domain to calculate the power spectra (Mazzetti 1963).

Mazzetti and Montalenti (1964) and Mazzetti (1964) were the first to introduce the idea that individual Barkhausen jumps are not independent of each other, but are correlated over a particular volume of the material known as the correlation domain. Tiitto (1978) considered that the correlation could be due either to the short range magnetostatic coupling between neighbouring domains, or the long range indirect effect of other domain wall motions causing a change in the local field. The Correlations between domain reversals have led to the conclusion that any analysis of power spectra must take them into account (Manson 1972).

Celasco et al (1974a) considered the individual pulses to cluster together to form one discontinuity and that these discontinuities would be correlated within a

correlation domain. Using the distribution in time as:

$$P(t) = K_1 e^{-\mu_1 t} + K_2 e^{-\mu_2 t} \dots (1.29)$$

where K_1, K_2, μ_1 and μ_2 all depend on the physical properties of the material; they developed a new theory to describe the power spectra:

$$\Phi(\omega) = \phi(\omega)\left[1 + \frac{2\rho(1 - \nu\tau_o)^2}{1 + \omega^2 \rho^2 \tau_o{}^2 (1 - \nu\tau_o)^2}\right] \dots (1.30)$$

where $\phi(\omega)$ is the power spectra of the individual Barkhausen events without correlation; ρ is the number if individual events in a cluster; ν is the number of events per unit time and τ_o is the time between each event. This treatment is valid in the frequency range 0.001Hz to 1Hz. At low frequencies equation 1.30 can be approximated to:

$$\Phi(\omega) \simeq \phi(\omega)\frac{2\rho}{1 + \omega^2 \rho^2 \tau_o{}^2} \dots (1.31)$$

The power spectrum was found to vary with sample thickness and magnetising frequency (Tiitto et al 1975). Within the range 10^{-2}Hz to 10Hz they found evidence of clustering in the low frequency region (<20kHz) above which there was a region of random noise. They also considered the damping of the noise due to eddy currents deriving an expression for the damping function of the noise between frequencies f_1 and f_2:

$$D(x) = \frac{\int\limits_{f_1}^{f_2} g(f)e^{\sqrt{-Axf}}df}{\int\limits_{f_1}^{f_2} g(f)df} \dots (1.31)$$

where A is a constant and $g(f)$ is the noise function. The depth from which the noise can be detected increases for lower magnetising frequencies and for materials with low permeabilities and conductivities (Tiitto 1988).

The power spectrum was only found to be constant for infinitely thin samples and the surface to volume ratio important for thicknesses below 0.15mm. Celasco et al (1974b) recorded a drop in the low frequency part of the spectrum as they thinned their samples down from 0.4mm.

Chapter II

The Magnetic and Mechanical Properties of Steel.

Iron and its alloys are remarkable in the wide variation of both mechanical and magnetic properties that are obtainable by the addition of impurities and different heat treatments. Hence the use of steel in industry is extensive and there are many good texts to be found in the literature on its metallurgy; in particular the recent book devoted to steels by Honeycombe (1981) is especially comprehensive. Other metallurgy texts useful for this study include those of Bailey (1972), Higgins (1965), Johnson and Weeks (1964), Cottrell (1967) and Rollason (1964). The mechanical behaviour of steel and in particular plastic deformation is also well covered in the literature, again the text of Honeycombe (1970) was found to be particularly relevant. A more detailed treatment of dislocation theory can be found in Friedel (1964) and further discussions in Biggs (1965), Cottrell (1953) and Lubahn and Felgar (1961).

2.1 Plastic Deformation.

The concept of atomic crystal defects or dislocations was introduced independently by Orowan, Polanyi and Taylor (1934) to explain why experimental crystal strengths were orders of magnitude lower than the theoretical predictions made by Frenkel. A dislocation is a discontinuity between part of a crystal that has sheared, and part that has not. The deformation progresses through the crystal by the propagation of these dislocations along a slip plane. A dislocation can be defined by its **Burgers vector** which represents the amount and direction of slip which is produced when that dislocation has passed right through the crystal and is independent of the orientation of the dislocation itself. The Burgers circuit, figure 2.01a) and b), defines the Burgers vector more specifically. An atomic path of two perpendicular lattice directions is traversed and then repeated using vectors of the opposite sign. In a perfect crystal a closed rectangle will have been traced, but if the circuit encloses a dislocation then the vector required to complete the circuit is the Burgers vector. A perfect dislocation will have a Burgers vector that
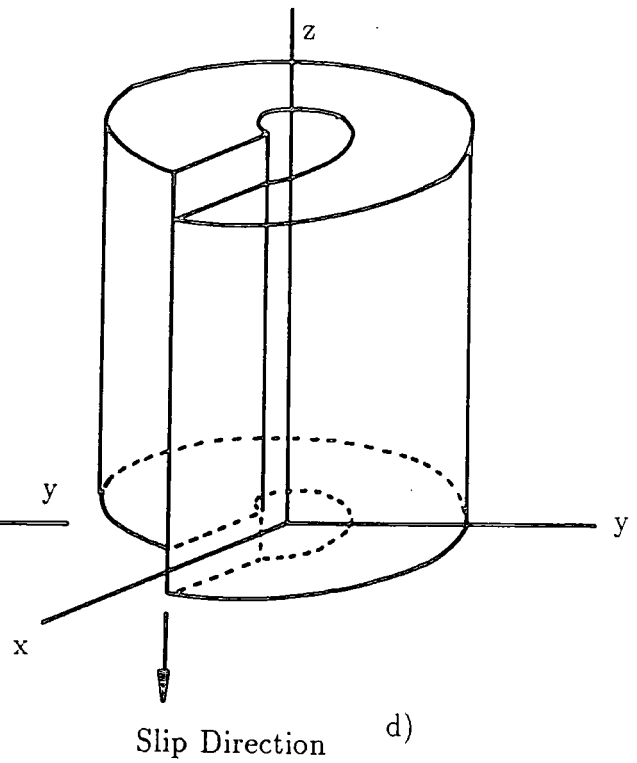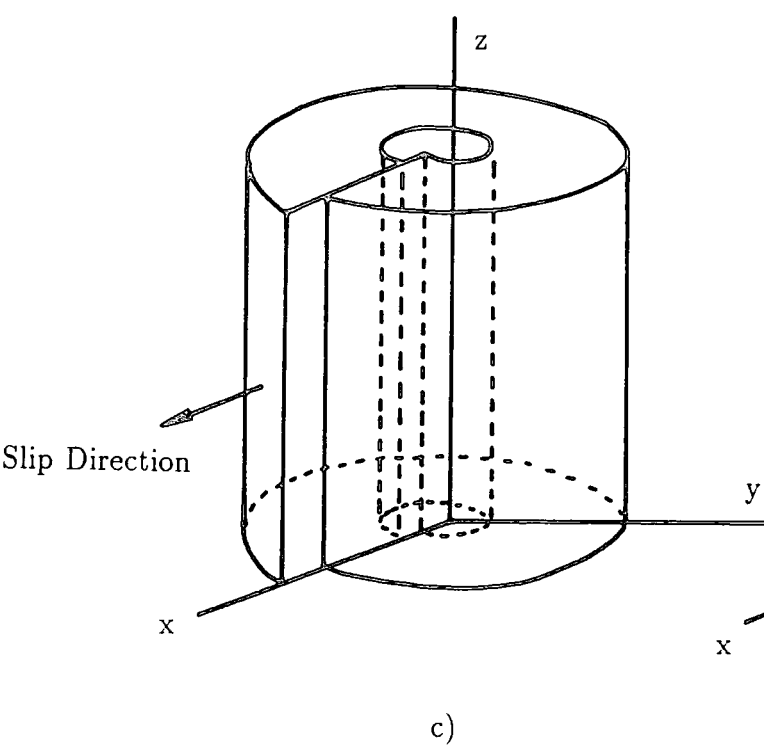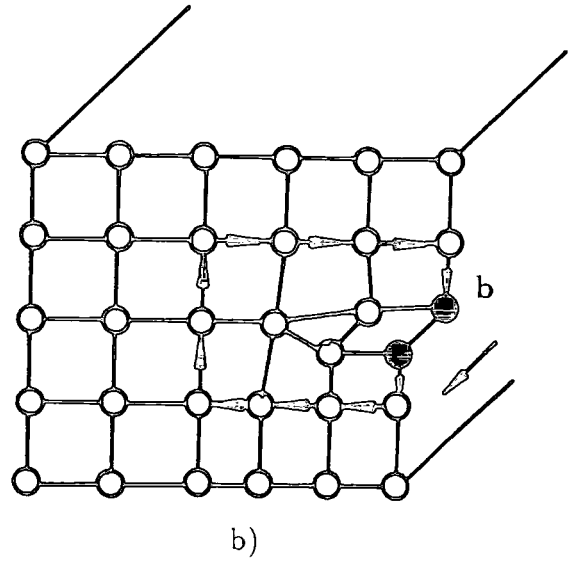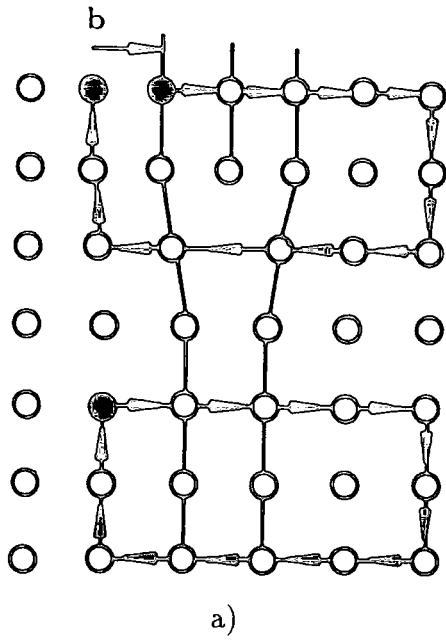
Figure 2.01 The Burgers Circuit in a) an Edge Dislocation and b) a Screw Dislocation (Reproduced from Friedel 1964); c) an Edge Dislocation and d) a Screw Dislocation. (Reproduced from Honeycombe 1970)

is a lattice translation; a partial dislocation for which the Burgers vector is not a simple lattice vector will result in a stacking fault.

2.1.1 The Edge Dislocation.

In a simple cubic lattice this can be characterized by the addition of an extra half plane of atoms inserted into the crystal as illustrated in figure 2.01c). Its Burgers vector lies in the slip plane and is perpendicular to the dislocation line. An edge dislocation lies at the centre of an internal stress field with the material above the slip plane in compression, and that below the slip plane in tension. The existence of dilational as well as shear stresses means that edge dislocations can act as sinks for impurity atoms, with atoms smaller than the host resting above the slip plane, and the larger impurity atoms being accommodated below the slip plane. Due to the extra half plane of atoms, the movement of an edge dislocation is non-conservative as atoms must diffuse either towards or away from the dislocation requiring thermal activation. If, however, vacancies migrate to the half plane at the dislocation, then the dislocation may be able to 'climb' out of its slip plane in a conservative glide.

2.1.2 The Screw Dislocation.

Here the slip direction is parallel to the dislocation line and coincides with the Burgers vector. It can be illustrated by shearing a cylinder of material along a line cut longitudinally as shown in figure 2.01d). The lattice is no longer a set of discrete planes , but a continuous helicoidal surface. As there is no extra half plane of atoms only shear stresses are involved and the movement of a screw dislocation is conservative rendering them more mobile and enabling movement between slip planes with common slip directions.

2.1.3 Dislocation Loops.

A region of deformation can be contained entirely within the crystal with no dislocations emerging on a crystal face. This is usually a combination of both edge and screw dislocations, the Burgers vector of this mixed dislocation lies at an arbitrary direction to the dislocation line but can be resolved into its screw and edge components.

2.1.4 Dislocation Dynamics.

The strain fields surrounding dislocations decrease as the inverse of the distance from the dislocation core, enabling dislocations to exert forces on each other and, if they are in opposite directions, to cancel out. The free surface is also able to exert an attractive force on the dislocation which may result in the loss of dislocations during thinning processes such as those used in preparing electron microscopy samples.

Applying external stress to a crystal results in a force acting on the dislocations. The force on the dislocation line, determined by Mott and Nabarro in 1948, is the product of the shear stress and the Burgers vector and acts along the slip plane normal to the dislocation. A critical stress, the Peierls' stress (Peierls 1940 and Nabarro 1947) is required to move a dislocation. Observed dislocation densities in metals are usually between $10^5 \mathrm{cm}^{-2}$ and $10^8 \mathrm{cm}^{-2}$ indicating that large numbers of dislocations must be generated within the crystals. The macroscopic yield point corresponds to the point at which this multiplication of dislocations begins to occur.

Figure 2.02a) illustrates the operation of the Frank-Read source which is a simple mechanism by which dislocations can be generated on a slip plane. The dislocation line is pinned at the points A and B causing the dislocation line to bow until it forms a perfect semicircle. At this point the stress required to operate the source is obtained and the dislocation loop begins expanding . As each point is acted on by the same stress, the line begins to spiral around the pinning points A and B which approach each other from opposite directions annihilating on contact. The closed dislocation loop is now free to expand continuously until an opposing stress or barrier is encountered. If an obstacle is encountered then the dislocations at this point will begin to pile up creating a stress concentration which exerts a back stress on the dislocation source.

2.1.5 The Stress-Strain Curve.

A schematic diagram of a stress-strain curve for steel is shown in figure 2.02b). The first part of the curve, up to the yield point 'A', is the region of elastic deformation. During a tensile test the strain rate is constant; immediately after
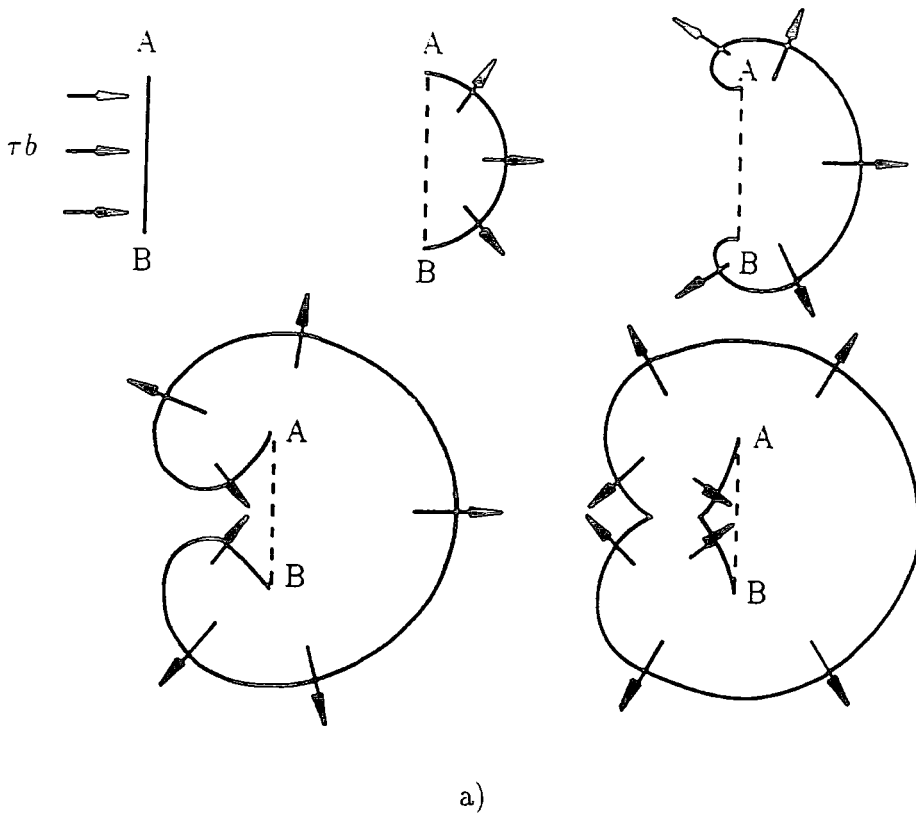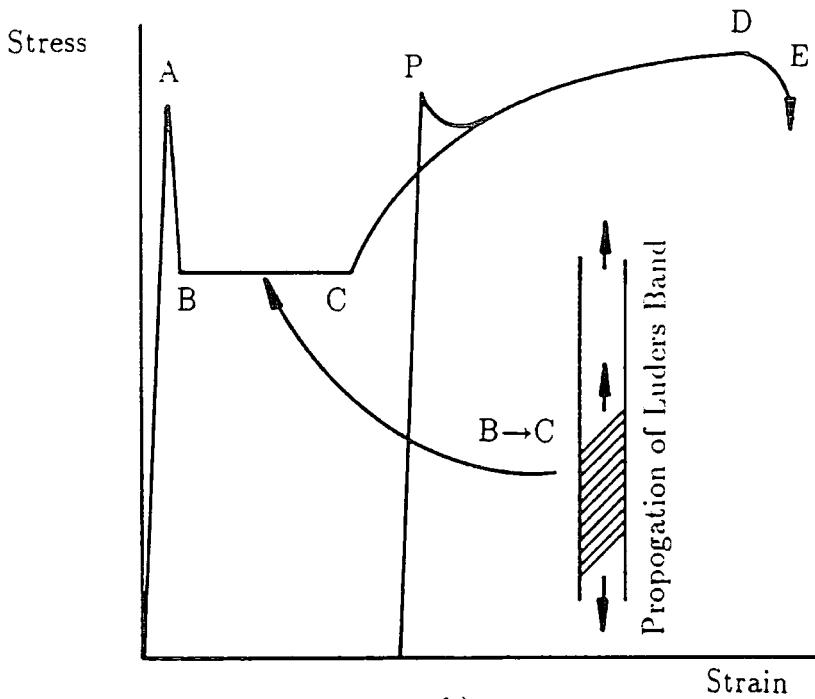
Figure 2.02 a)The Operation of a Frank-Read Source (Reproduced from Honeycombe 1970); b) Schematic Diagram of a Stress-Strain Curve for Steel. Inset: The Propagation of Luders Bands. (Reproduced from Honeycombe 1981)

the yield point 'A' the multiplication rate of dislocations is so high that the metal deforms faster than the driving yield mechanism and the drop in stress 'AB' results. After the lower yield point at 'B', the plastic deformation is propagated through the specimen observed by the movement of the Luders band (figure 2.02b inset). In the initial easy glide region 'BC' the work hardening rate is slow, the slip occurs on parallel planes and in an effort to minimise the force between them, the dislocations tend to line up under one another. A greater applied stress is then needed to push these dislocations past one another to continue the deformation. As the dislocations become more closely packed as the deformation proceeds this extra force also increases. It is also possible for dislocations on other slip planes to block the glide on the primary slip plane, these are called forest dislocations. During the second stage of linear hardening 'CD' the work hardening rate is more rapid due to the higher resistance to dislocation motion resulting in dislocation pile-ups at obstacles such as dislocation tangles cutting across the primary slip plane. This will also create difficulties for a dislocation on a parallel plane trying to pass the pile-up. As forest dislocations begin to multiply on other slip planes dislocations have to try and cut through them, a 'jog' forms which must move non-conservatively, requiring more energy. In the third and final stage 'DE' of parabolic hardening just before fracture, the stresses are large enough for cross-slipping to occur introducing new slip systems making deformation easier and reducing the hardening rate. Point 'P' represents the new yield point occurring on the reapplication of stress to a previously deformed specimen.

Fracture follows stage three when the increased stress due to the decrease in cross sectional area is no longer compensated for by the increase in work hardening. When significant plastic deformation occurs before fracture then it is referred to as a ductile fracture and otherwise as a brittle fracture. Brittle fracture is associated with cracks and occurs when the external stress is greater than the energy required to form the new, exposed faces. In some cases the crack tip hardens under the increased stress at its tip and plastic deformation can occur, but if the crack yields and opens up it causes catastrophic failure.

2.2 Steel–Metallurgy and Microstructure.

Steel is essentially an alloy of iron and carbon usually with small quantities of additional elements to obtain the desired mechanical characteristics. It is this ability to tailor the properties of steel and its relative cheapness that have resulted in its extensive use in industry. In order to understand how the properties of this complex series of alloys are affected by their chemistry and heat treatments it is necessary to study, in detail, the microstructure of iron and the iron-carbon equilibrium diagram.

2.2.1 The Microstructure of Iron

The multitude of properties of steels is due to the three possible phases of iron, an outline of these and their associated microstructure is given in table 2.01. There are two crystal forms of iron; the first, body-centered cubic (bcc) is present as α-iron, called ferrite, at temperatures up to the $\gamma - \alpha$ transformation at 910°C, and also as δ-iron at temperatures between 1390°C and the melting point at 1536°C; the second is a face-centered cubic (fcc) structure, γ-iron or austenite, present at the intervening temperatures (910°C-1390°C). Although the fcc austenite structure is closer packed than the bcc ferrite, it has larger interstitial holes and hence a greater solubility of carbon and nitrogen. Small additions of other elements have a marked affect on the properties of steel, as little as 0.1 wt% of carbon has a significant affect on the strength. Table 2.02 gives the atomic diameters for some of the common elements that are added to steel. In general the non-metallic elements have diameters small enough to enter interstitial sites, although evidently some lattice strain still occurs, whereas metallic elements form a substitutional solid-solution.

The difference in solubilities between the two structures (2.04 wt% C in γ-iron to 0.02 wt% in α-iron) and the higher rate of diffusion in the more loosely packed bcc ferrite have great consequences for heat treatment. The transformation between austenite and ferrite is a very rapid one, and its kinetics are very important in the formation of steel microstructure.

38

⇑1536 (mpt)	LIQUID
1390°C→1536°C	δ-iron, b.c.c.
910°C→1390°C	γ-iron, f.c.c. **Austenite** close packed structure large interstitial sites largest spheres fitting interstices: tetrahedral: 0.28Å octahedral: 0.51Å 2.04wt% solubility of C
910°C	RAPID TRANSFORMATION
⇓910°C	α-iron, b.c.c. **Ferrite** loose packed (1% volume increase from f.c.c.) faster diffusion small interstitial sites largest spheres fitting interstices tetrahedral: 0.36Å octahedral: 0.19Å 0.02wt% solubility of C ≤0.00005wt% at 20°C

Table 2.01 Summary of the Three Phases of Iron.

39

Element	Atomic radius r (Å)	$\frac{r}{r_{Fe}}$
α-Fe	1.28	1.00
B	0.94	0.73
C	0.77	0.60
N	0.72	0.57
O	0.60	0.47
H	0.46	0.36

Table 2.02 Atomic sizes of non-metallic elements in iron (Honeycombe 1981)

2.2.2 The Mechanical Properties of Iron and Steel.

A supersaturated solid-solution of 0.02wt% of carbon in α-iron, having been quenched from 700°C is not stable, and the carbon will be precipitated out as the close-packed hexagonal form of iron carbide (Fe_3C). The effect of the carbon diffusing through the ferrite is referred to as 'ageing'. Above 200°C the carbon is precipitated as orthorhombic cementite. A similar quenching affect is observed with nitrogen. Quench ageing causes a significant increase in the strength of the steel even at low carbon or nitrogen contents.

Carburizing and nitriding are hardening processes which take advantage of the rapid diffusivity of carbon and nitrogen in α-iron by heating to 500°C-1000°C in either a carbon, or nitrogen gaseous atmosphere.

The amount of stress required to yield the material (the yield stress) is a measure of its strength. A single crystal of pure iron has a yield stress as low as $10MNm^{-2}$ whereas the strength of steel can range from $200MNm^{-2}$ to $2000MNm^{-2}$. Many factors contribute to this range of strengths, and some of the main contributory mechanisms will now be considered.

The shortest translation vector in the bcc structure of ferrite is the close packed $\langle 111 \rangle$ direction resulting in a Burgers vector of $\frac{1}{2}\langle 111 \rangle$ and three possible slip planes: $\{110\}, \{112\}$ and $\{123\}$ (as illustrated in figure 2.3) . As cross slip can
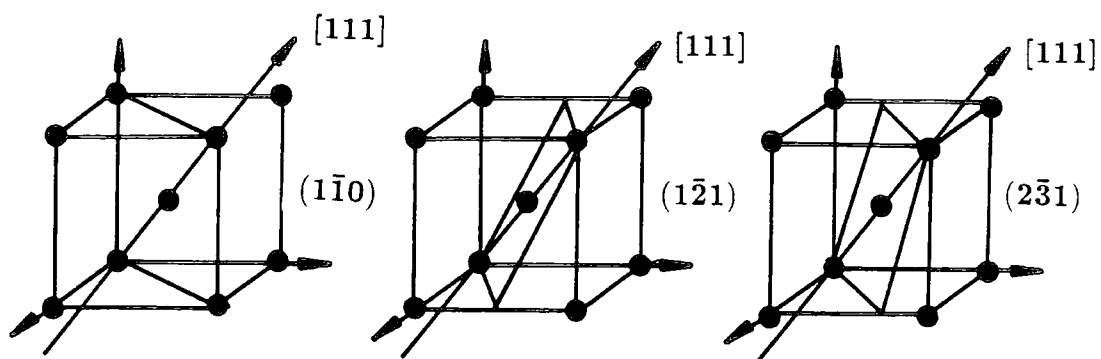
Figure 2.03 Slip Planes in b.c.c. Ferrite. (Reproduced from Honeycombe 1981)

occur between the different planes, then a deformed crystal displays wavy slip bands.

The shear stress, τ, necessary to produce further deformation is determined by the effective stress, τ^*, necessary to overcome short range obstacles such as isolated dislocations and the internal stress, τ_i, due to long range obstacles such as grain boundaries, arrays of dislocations, and cell walls :

$$\tau = \tau^* + \tau_i \ldots (2.01)$$

The ease of overcoming short range obstacles is increased by thermal activation and hence τ^* decreases with increasing temperature. This temperature dependence can be observed as a reduction in the yield stress as either the temperature or strain rate are increased, and is not affected by interstitial impurities in the iron.

Workhardening is a very effective method of strengthening without adding additional impurities, and is particularly useful for rods and wires. Work hardening increases the dislocation density of the material, increasing its internal stress (equation 2.01) which results in an increase in the yield stress independent of temperature.

The upper yield point, point 'A' in figure 2.02b, is reduced if carbon and nitrogen are removed by annealing in wet hydrogen, but re-emerges with only very small additions of interstial atoms (0.02 wt% C and 0.001 wt% N). Cottrell and Bilby explained this affect by considering the reduction in total strain energy due to the interaction of the strain fields associated with the interstial atoms and those associated with the dislocations. They showed that concentrations, or atmospheres of interstitial atoms developed near dislocations; lines of interstitial atoms forming at places of maximum dislocation density are referred to as condensed atmosphere. The dislocations are locked in position by the carbon atoms as the binding energy between the iron and carbon is approximately 0.5 eV. The yield-stress curve at elevated temperatures becomes serrated as the interstial atoms are able to diffuse more readily, destroying, and creating atmospheres. The very sharp yield point cannot be satisfactorily explained by the unpinning of dislocations once they have been locked in position, but by the sudden generation of large numbers of dislocations causing the specimen to yield (Gillman and Johnson).

The increased strength gained by the addition of substitutional elements such as vanadium and molybdenum is variable; generally the larger the difference in atomic size the greater the increment, but this is usually regarded as a subsidiary consequence of adding the element for other reasons.

The grain size however, is a very important parameter for altering the strength of steel. The relation of grain size, d, with yield stress σ_y is given by the Hall-Petch relationship:

$$\sigma_y = \sigma_o + k_y d^{-\frac{1}{2}} \ldots (2.02)$$

σ_o is the temperature dependent friction stress which corresponds to the yield stress of a single crystal. The constant k_y does not vary with temperature which further indicates that the yield point is not entirely due to an unpinning parameter such as that initially proposed by Cottrell.

The stresses in a grain build up as dislocations pile up in the adjacent grain, as they reach a critical value a new source is created in the grain. A greater build up of dislocations is possible in larger grains, resulting in a higher stress concentration and hence easier propagation of the strain through the material. Refining the grain size of the steel can therefore have a significant effect on its strength e.g. reducing the grain size from 0.25mm to 0.0025mm results in an increase in strength from $100 MNm^{-2}$ to $500 MNm^{-2}$.

The dispersion of other phases in the steel such as ferrite has a similar affect on the strength, in general the yield stress is inversely proportional to the spacing of the additional phases. For example in eutectoid pearlite the flow stress is inversely proportional to the square root of the uninterrupted mean free ferrite path.

In higher carbon steels rapid quenching from austenite can result in the formation of an acicular bcc distorted tetragonal structure called martensite. The resulting lattice distortion forms an effective barrier to dislocation motion forming an extremely hard and, without further treatment, very brittle material. The process of tempering or heating at a subcritical temperature encourages some of the carbon in solid solution to be released and form other less brittle carbides which disperse themselves through the α-iron matrix.

The ability of the steel to form martensite during the quenching process is called hardenability. This is increased by restriction of the transformation to ferrite and pearlite in steels with large grain sizes and metallic alloying.

2.2.3 Plain Carbon Steels.

The binary iron-carbon system is the basis of most steels and an insight into their behaviour can be gained from a study of the iron-carbon equilibrium diagram (figure 2.04). For more complex steels the effects of the alloying elements on the iron-carbon phases must be considered. There are four important temperatures to note on the diagram (A_1–A_4). The first, A_1 is the eutectoid temperature of 723°C. A_2 is the Curie point at 769°C for pure iron, but this has little structural significance. The transformation temperature between α-iron and γ-iron, A_3, occurs at 910°C for pure iron but is reduced as the carbon content is increased; while the temperature at which the transformation between γ-iron and δ-iron occurs, A_4, is increased from 1390°C as the carbon content is increased. The higher solubility of carbon in the fcc austenite is reflected by its dominance of the equilibrium diagram.

As a steel with less than the eutectoid composition of 0.87%C is cooled from the γ phase the austenite is transformed into hypo-eutectoid ferrite, enriching the remaining austenite that, containing 0.87%C at 723°C will transform into the lamellar mixture of ferrite and cementite (iron carbide Fe_3C) that is called pearlite. A hyper-eutectoid steel containing more than 0.8%C will form cementite on cooling, hence reducing the carbon content of the austenite to the eutectoid composition so that it too will transform to pearlite on reaching 723°C. A hyper-eutectoid alloy will therefore contain some free cementite as indicated by the large (γ+ Fe_3C) phase in the diagram.

The percentage of pearlite in the system can therefore be calculated from the percentage carbon content:

$$\%Pearlite = \frac{\%carbon \times 100}{0.87} \quad \ldots (2.03)$$

By cooling the steel at different rates the austenite-ferrite transformation can be forced to occur at different temperatures. The temperature at which the transformation occurs has a significant effect on the morphology of both the ferrite and

44

Figure 2.04 The Iron-Carbon Equilibrium Diagram. (Reproduced from Honeycombe 1981, after Hansen 1958, *Constitution of Binary Alloy* 2nd ed. McGraw Hill)

the cementite that form. Dubé classified four different morphologies, they apply to the formation of both ferrite and cementite, although each phase exhibits different crystallographic relations. At high transformation temperatures grain boundary allotriomorphs form. The crystals nucleate at austenite grain boundaries with which they have a crystallographic relation; the Kurdjumov-Sachs relation for ferrite:

$$\{111\}_{\gamma_1} \parallel \{110\}_{\alpha}$$

$$\langle 110 \rangle_{\gamma_1} \parallel \langle 111 \rangle_{\alpha}$$

and the more complex Pitsch relation for cementite:

$$(100)_c \parallel (5\bar{5}4)_{\gamma}$$

$$(010)_c \parallel (110)_{\gamma}$$

$$(001)_c \parallel (\bar{2}25)_{\gamma}$$

The growing crystals usually have a random orientation with the grain into which they are growing, with curved boundaries, but as the temperature is reduced facets begin to develop. As the mobility of the $\gamma - \alpha$ or γ-cementite boundary is reduced and more coherent interfaces begin to form then growth can occur into the Kurdjumov-Sachs or Pitsch grain. This horizontal growth along well defined matrix planes originating either from the grain-boundary or existing allotriomorphs is called Widmanstätten sideplates or laths and is the second classification. This sideways growth is more likely to occur in larger grains, and in steels with carbon contents greater than 0.4% the growth of pearlite restricts the ferrite. The third morphology consists of intragranular idiomorphs which are equiaxed crystals that can nucleate within austenite grains and can exhibit either curved boundaries or crystallographic characteristics. Intragranular plates that nucleate entirely within the grains form the final morphological classification at transformation temperatures of about 725°C.

The C-shaped time-temperature-transformation (TTT) curve for a eutectoid carbon steel is shown in figure 2.05. The transformation is driven by the degree of undercooling ($\Delta T = A_1 - T$) and the diffusivity. The transformation is therefore

46
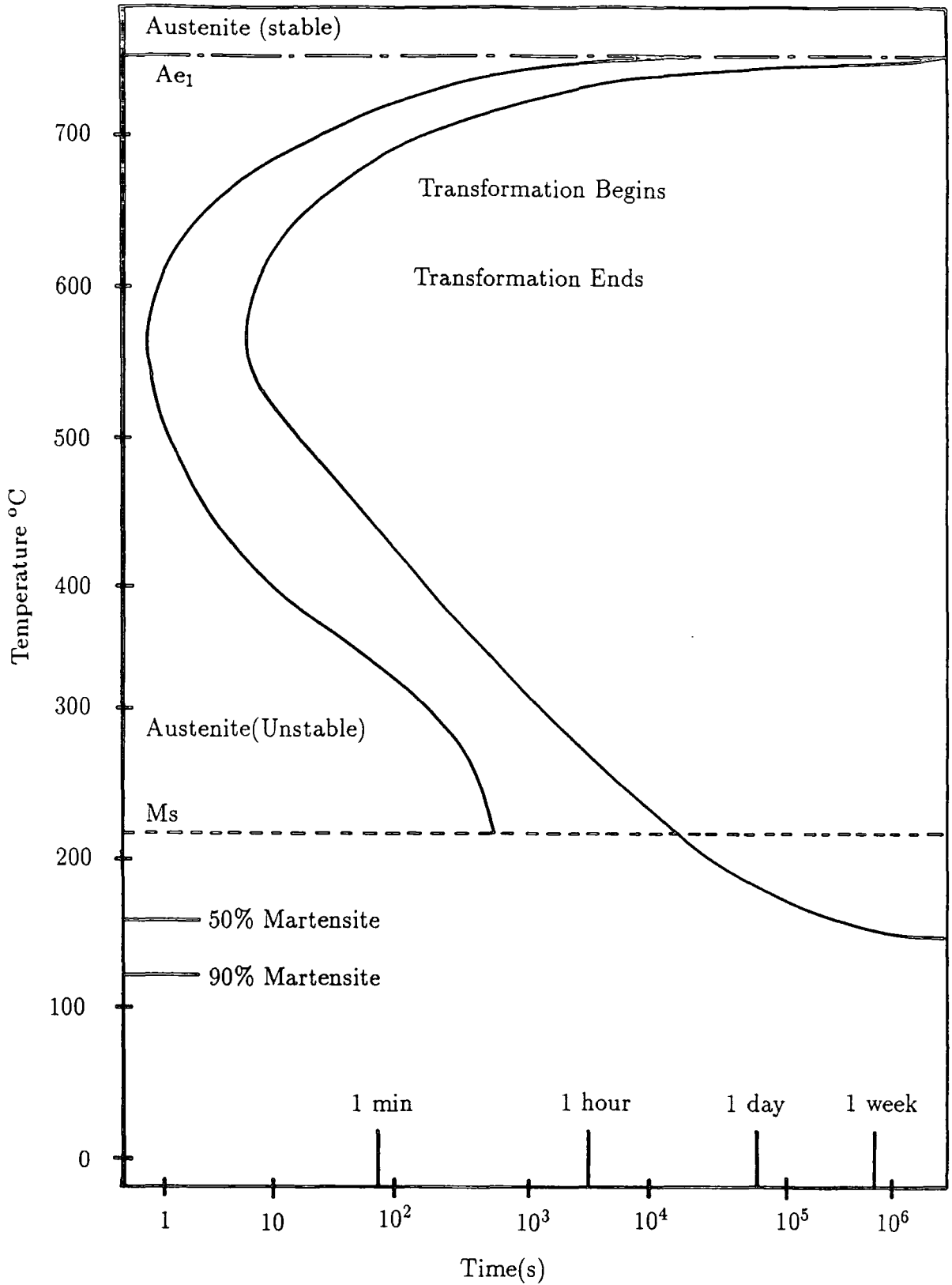
Figure 2.05 Time-Temperature-Transformation (TTT) Diagram for a 0.89% Carbon Steel. (Reproduced from Honeycombe 1981, after: U.S. Steel Co. *Atlas of Isothermal Diagrams.*)

47

slower at the higher temperatures where the degree of under cooling is low, and also at the lower temperatures where the diffusivity has been reduced.

The transformation from austenite to pearlite is primarily diffusion lead and the nucleation sites are determined by the composition of the steel; in a hypo-eutectoid steel ferrite will provide more sites than pearlite and vice versa for a hyper-eutectoid alloy. A schematic diagram of the growth of a hemi-spherical nodule of pearlite nucleated at an austenite grain boundary is given in figure 2.06a) and of the formation of pearlite colonies in figure 2.06b). A simple model of pearlite formation which neglects the strain energy and assumes that austenite and pearlite have the same specific heats produces the observed result that the higher the transformation temperature, the larger the spacing of the lamellae. This relation begins to break down at high degrees of under cooling.

$$\Delta H \left[\frac{T_e - T}{T_e} \right] \rho S_o = 2\gamma \ldots (2.04)$$

ΔH: Latent heat of transformation, T_e: Eutectoid temperature, ρ: density, S_o: Interlamella spacing and γ: interfacial energy per unit area. The fineness of the spacing is eventually limited by the available free energy. As we have seen, the strength of the alloy is inversely proportional to the square root of the interlamellar spacing and so a low transformation temperature will help produce a high strength alloy.

A pearlite nodule exhibits no relation with the austenite grain into which it is growing, but between the layers of ferrite and cementite within the nodule there exist two crystallographic relations;

the Pitsch-Petsch relation:-

$$(001)_{Fe_3C} \parallel (\bar{5}\bar{2}\bar{1})_\alpha$$

$$(010)_{Fe_3C} 2.6^o from [11\bar{3}]_\alpha$$

$$(100)_{Fe_3C} 2.6^o from [13\bar{1}]_\alpha$$

$$[001]_{Fe_3C} habit\ plane$$

Austenite Grain 1 (γ_1)

Cementite (Fe_3C)

Ferrite (α-iron)

Austenite Grain 2 (γ_2)
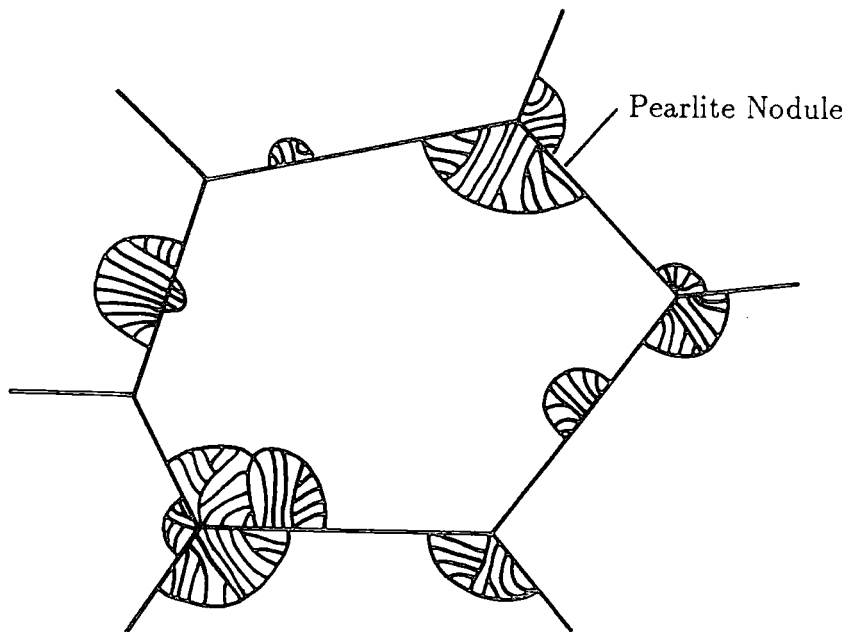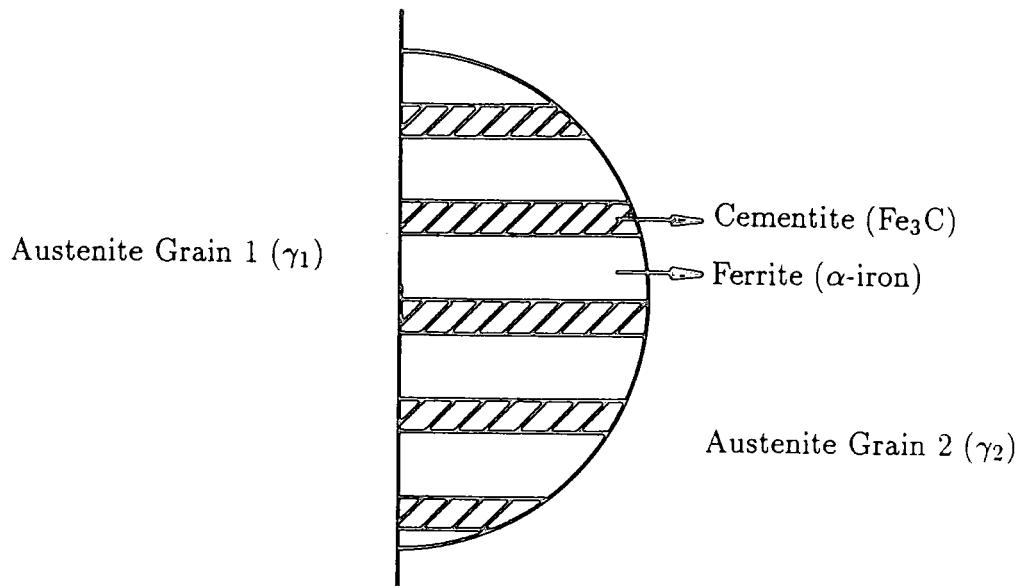
Pearlite Nodule

Figure 2.06 a) The Nucleation of a Pearlite Nodule on an Austenite Boundary (After Honeycombe 1981), b) the Growth of Nodules into Pearlite Colonies (After Kottrell (1967).

49

and the Bagaryatski relation:-

$$(100)_{\text{Fe}_3\text{C}} \parallel (0\bar{1}1)_\alpha$$

$$(010)_{\text{Fe}_3\text{C}} \parallel (1\bar{1}\bar{1})_\alpha$$

$$(001)_{\text{Fe}_3\text{C}} \parallel (211)_\alpha$$

$$[\bar{1}01]_{\text{Fe}_3\text{C}} \text{habit plane}$$

Where the subscripts 'Fe$_3$C' and α denote cementite and ferrite respectively. The Pitsch-Petch relation is usually found close to the eutectoid composition in nodules growing on clean austenite boundaries. The ferrite within the pearlite exhibits the Kurdjumov-Sachs relation and the pearlitic cementite the Pitsch relation with the γ_1 grain. The Bagaryatski relation is more often found in high carbon steels on cementite boundaries; here the grain boundary cementite shields the pearlitic ferrite from any crystallographic relations, but the pearlitic cementite is continuous with that from the grain it is growing.

2.2.4 Industrial Use of Ferrite-Pearlite Steels.

Although carbon is a very effective strengthening agent, it also reduces the ductility of the material causing machining problems, and potential cracking during welding. For these reasons it is often not desirable to increase the carbon content above 0.2 wt% and other methods need to be employed such as alloying and heat treatment to improve the properties of the steel further.

Alloying elements are added to the steel either to assist the manufacturing process during which some of the less desirable elements must be removed, or to import some particular characteristic to the steel such as corrosion resistance or added strength. These fall into two categories, γ stabilisers or α stabilisers.

Sulphur forms the brittle FeS compound, if manganese is added to the melt then MnS will preferentially form which is more ductile and can be deformed during a rolling process improving both the strength and the ductility. Manganese will also, in a similar way to carbon and nitrogen, increase the strength of the steel by interstitial solid solution. Silicon also acts as a deoxidant, but its additions must

be carefully controlled in high carbon steels to reduce the formation of free ferrite and graphite. Small amounts of elements such as aluminium, vanadium, titanium and niobium may be added as grain refiners, they form stable compounds with nitrogen in the case of aluminium or carbon which pin the grain boundaries and hence restrict grain growth. Phosphorus forms FeP which is another very brittle compound, and levels of phosphorus must be kept below 0.05%.

The steel can also be subjected to various forms of heat treatment to obtain particular microstructures:-

Normalising involves the heating of the steel to about $100^{\circ}C$ above the appropriate transformation temperature for that carbon content and air cooling to refine the austenite and ferrite grains.

The process of austenising at a high temperature followed by slow air cooling is referred to as annealing. The resulting transformation to pearlite at such high temperatures results in the formation of coarse grains which improve the steel's machinability. Coarse ferrite and pearlite can be formed by isothermal annealing where the steel is cooled to a subcritical temperature and isothermal transformation allowed to occur. If the steel is held below the transformation temperature then, the pearlite, in an effort to reduce the surface energy of the interfaces, begins to spheroidise : this treatment is called spheroidise annealing.

Steel with carbon contents less than 0.5 wt% is often used with no further treatment after hot rolling in structural applications such as buildings, and bridges, and the sheet form in fabrications where the surface finish is not important. Where greater strength and, or a better surface are required, cold rolling is used, sometimes followed by annealing to obtain an even higher quality sheet. In the same carbon content range the steel can also be cast and used in a wide range of applications. Steels with carbon contents from 0.2wt% to 0.5wt% are frequently used for closed die or drop forgings to manufacture such items as shafts and gears.

Closely controlling the application of heat and deformation during the rolling process is referred to as controlled rolling. This process, which encourages grain refinements results in the reliable attainment of the desired mechanical properties.

51

2.2.5 Steel Manufacture.

The raw material from which most steel is produced in a blast furnace is pig iron consisting of iron ore (such as magnetite, haematite, hydroxides such as limonite or carbonates such as siderite); limestone which combines with the non-metallic residue of the ore to form the bulk of the slag and coke which reduces the iron oxides.

The Basic Oxygen Furnace based on the Linz-Donawitz process is the most effective for low-carbon steels. The furnace consists of a lined steel shell in which the pig iron is melted, slag collects on the surface and can be poured away by tipping the furnace. The lining is usually of CaOMgO or magnesite to provide the lime to reduce the phosphorous content. A water-cooled oxygen lance feeds oxygen directly into the melt to oxidise the impurities, silicon and manganese first, followed by carbon and finally phosphorus forming phosphorous pentoxide. Carbon is then added to the required percentage , manganese to combine with the sulphur and also, along with silicon to de oxidise the melt. This deoxidation process is the process of 'killing' the steel. A semi-killed steel is left with sufficient oxygen to allow the gas evolution to offset the shrinkage of the ingot.

2.2.6 A Specific Example: High Pressure Gas Pipeline.

Steel used in British Gas high pressure pipe-lines must be able to withstand hoop stresses around the circumference of the pipe of up to 70 bar and they must therefore have good strength, ductility and weldability. Since 1963 when the first pipe-line was manufactured further requirements have been specified and the steel been modified accordingly.

Initially a semi-killed steel was used which was sufficient to satisfy the M.S.Y.S. (minimum yield stress required for 0.5% strain) value of $240MNm^{-2}$ for a 456mm (18$''$) pipe.

The increase in the volume of the transmitted gas led to the development of larger and more economic pipes, pipes of 1067mm diameter are not unusual with M.S.Y.S. values of $414MNm^{-2}$. The maximum M.S.Y.S. value attainable from the semi-killed steel was $386MNm^{-2}$ and so the increased yield stress was obtained

by using a fully-killed steel. Here the addition of excess manganese and silicon increase the strength by solid solution hardening, while the addition of vanadium and niobium strengthen by precipitation hardening through the formation of vanadium carbonitride and niobium carbide. Aluminium is added for grain refinement. The problem of crack propagation resulted in the assessment of the toughness of the steel and led to the Drop Weight Tear Test (D.W.T.T.) which required that the brittle-ductile transition be below 0°C. This was 10-30°C for the semi-killed steel, but was lowered to between -50°C and -10°C for the fully-killed material by concentrating on grain refinement as the strengthening process.

It was found that although this prevented brittle crack propagation the energy involved in the propagation could be greater than that absorbed by the steel, preventing the crack being arrested. A new criteria, the Charpy upper shelf energy (U.S.E.), was introduced to indicate the steel's ability to absorb crack energy. The manganese added in the killing process forms MnS in preference to the brittle FeS and this forms long ribbons during the rolling process which become weak planes along the length of the pipe. The weakness was reduced by adding rare-earth metals to form less deformable rare-earth metal sulphides. Charpy U.S.E. values are now in the region of 100-200 J compared to the earlier values of around 30J.

The weldability of the steel is defined by its carbon equivalent value (C.E.). The most significant factor in this equation is the carbon-content, this was subsequently reduced, with the result that further methods were then required to boost the strength up to the previous values. This was done by control rolling the steel to encourage grain refinement and by further addition of niobium.

All three types of steel: semi-killed, fully-killed and control-rolled are in operation in the British Gas high pressure pipe-line system .

Most of the pipes are manufactured by a U-ing and O-ing process from the rolled plate to a seam-welded pipe. Once the plate has been sheared to the correct size and the edges prepared for welding, the longitudinal edges are crimped to the right shape for the final diameter. The main deformation is carried out by the U-ing process and the circular shape then finished by a series of presses and dyes. The pipe is then seam-welded from both sides, and the weld checked by both radiographic and magnetic particle inspection techniques. The final shaping

53

of the pipe is done by high pressure hydraulic expansion during which process the weld can also be tested hydrostatically. The additional cold-working during this manufacturing process also improves the mechanical properties of the final pipeline.

2.3 Magnetic Properties.

In addition to the extensive use of iron and steel in industry for its mechanical properties, its magnetic properties are also exploited in a variety of applications. Pure iron is mechanically very soft and it also has a very high magnetic permeability, its magnetic properties can be manipulated by the addition of impurities and by altering its microstructure in a similar way to the mechanical ones. Alloys of iron that are very soft magnetically such as SiFe are used to manufacture such components as transformer cores, whereas iron also forms the base for alloys with extremely hard magnetic properties used as permanent magnets.

As the magnetic properties of steel are so sensitive to its microstructural characteristics, any change in the material's properties such as corrosion, cracking or straining can be detected by a corresponding change in its magnetic properties. These affects are exploited in a number of non-destructive evaluation techniques employed on the many structural engineering components that are manufactured from steel. There is a variety of such techniques available summarised in the review by Jiles (1988a) and for those methods designed to detect stress by Rudd (1982) and Theiner et al (1983).

A summary of the use of Barkhausen noise in non-destructive testing is given in Sundström et al (1979). Barkhausen noise has been successfully used for the detection of residual stress (Tiitto 1988) and this is being extended to the prediction of the imminence of fatigue (Tiitto 1989). Jiles (1990) is developing a "magnescope" which measures the flux density of components in situ and is investigating how measured properties such as coercivity and remanence change with cycled strain also in an attempt to predict fatigue. Buttle et al (1987) have used Barkhausen noise and magneto-acoustic emission to study the effects of neutron irradiation on α-iron. Langman (1987) has used the anisotropy that develops in the steel to detect applied stress and has compared his method with those using

54

the Barkhausen noise. Atherton et al (1982 and 1983) were able to detect stresses in buried gas pipelines by using a magnetometer above the ground.

Magnetic Particle Inspection (MPI) is extensively used for the detection of cracks especially in large engineering structures such as oil rigs. Magnetic particles either in the form of powder or in a suspension (forming a magnetic ink) are attracted by the flux leakage above the crack. The use of magnetic leakage fields is discussed by Förster (1983) and an analytical solution for this field by Edwards et al (1966). Recently work has been carried out in Durham on the magnetic inks used in this technique (McCoy 1988, McCoy et al 1989a) and b) and Tanner 1986).

British Gas uses both magnetic and ultrasonic techniques in its on-line inspection vehicles (or "intelligent PIGs") which are pushed through their high pressure gas pipelines by the gas pressure to detect and locate defects (by magnetic flux leakage) and cracks (using ultrasonics). Unlike ultrasonic techniques the changes in magnetic properties are large and the problems lie in analysing which change in the steel has produced the detected magnetic signal. In addition, as there is such a variety in the properties of the steels employed it cannot be assumed that their magnetic properties will all react in the same way. In order to successfully evaluate the data from the magnetic PIG to determine accurately defect size and position it was necessary to investigate the magnetic properties of the steels in use.

Some of this work was carried out in the Physics Department of Durham University (Willcock 1985, Morgan et al 1986, Willcock et al 1987). The volume fractions and grain sizes of ferrite and pearlite were found to have the greatest affect on the coercivity and correlations also found with tensile strength and less reliably with Vickers Hardness (Tanner et al 1988). The effect of the grain size was determined from observations of domain wall pinning by the cementite lamellae in pearlite grains using Lorentz electron microscopy (Hetherington et al 1987). Attempts were also made to apply harmonic analysis to the hysteresis loops and coercivity was found to vary linearly with the first and third even-order harmonic coefficients (Willcock et al 1986). This technique was also used to analyse the results of Anderson (1980) on plastically deformed 50D steel in which the monotonic decrease of the first harmonic component was found to be proportional to the increase in coercivity with plastic strain (Willcock et al 1983).

A series of studies on the magnetic properties of carbon steels has also been made by D.C. Jiles (1988b) in which a correlation was found between initial permeability and coercivity independent of carbon morphology; although the effect of the carbon morphology on the absolute values of coercivity was very marked. Spheroidised pearlite degraded the magnetic properties less than the lamellar pearlie and the harder martensitic steels had the hardest magnetic properties; further studies on the effects of different heat treatments on AISI 4130 steels were also made by Jiles et al 1988. For a particular type of heat treatment the magnetic properties were found to vary smoothly with carbon content.

The effect of plastic deformation on the magnetic properties of steel is important for two main reasons a) they may be used to detect unwanted plastic strain developing in an engineering component, in some cases this requires separating the effects of plastic and elastic strain; and b) plastic strain is inherent in many engineering components and its effects may mask or confuse measurements made to detect other properties. The results of previous studies on the effects of stress and strain on the magnetic properties of steel will be discussed in context with the analysis of this study in chapter six.

Chapter III

Equipment

The experimental methods and equipment used for the investigations in this thesis are described here, with new computer programs listed in Appendix C. The reader is referred to existing detailed descriptions, but any modifications are documented here.

3.1 Mechanical Properties.

Samples were prepared for optical microscopy using the Struers "Exotom" cutting wheel, the "Metaserve" mounting press and the Struers "Abraplan" and "Abramatic" automatic polishing wheels in the Metallography laboratory at the British Gas Engineering Research Station in Killingworth. The samples were polished down to $1\mu m$ and then the low carbon samples were etched (Petzow 1978) with "nital" (1–10 ml dilute nitric acid in 100 ml ethanol) and the higher pearlite content samples with "picral" (3 ml picric acid and 2 ml nitric acid in 100 ml ethanol). The specimens were then examined under the optical microscope at magnifications up to $\times 2000$. Vickers Hardness measurements were also carried out in the metallography laboratory with the 10kg mass (HV10).

The samples were plastically deformed on a 500kN Denison tensile testing machine in the School of Engineering and Applied Science at Durham University.

3.2 Measurement of Bulk Magnetic Properties.

A Vibrating Sample Magnetometer (V.S.M.) is a very sensitive and versatile instrument for magnetic measurements, but the large magnetic susceptibility of steel results in the demagnetising factor becoming dominant, making measurement of intrinsic permeability impractical. For this reason it was necessary to use other methods to determine the full hysteresis curves of the steel and reserve the V.S.M. for accurate measurements of coercivity, unaffected by the demagnetising factor as the magnetisation is zero at this point.

Both the toroid and permeameter methods are based on the magnetisation and fluxmeter technique, described in British Standard BS 6404 (1986), which rely on Faraday's law stating that the e.m.f. induced in a coil is proportional to the rate of change of flux passing through it. Where sufficient samples were available to allow the extraction of toroids this method was used to ensure complete flux closure. This was not feasible at every deformation stage in the second set of experiments and here a yoke permeameter was used.

3.2.1 Toroids

This method involves the magnetisation of a toroidal specimen by passing a current through a primary coil wound around the ring and the detection of the flux induced in secondary windings by an integrating fluxmeter (Cullity 1972).

The experimental apparatus is outlined in figure 3.01a). In order to provide a smooth primary magnetising current the Farnell power supply is set to less than one volt and amplified by the Amcron low noise power amplifier. The current through the coils is slowly varied by adjusting the output of the Amcron, and reversed at zero current using the reversing switch. Demagnetisation is achieved by driving the sample around decreasing hysteresis loops, the maximum current in each loop checked by the digital ammeter. A Hirst integrating fluxmeter, calibrated to N.P.L. standards is used to detect the flux induced in the secondary coils wound on the toroid. The voltage across the shunt resistor is supplied to the x-axis of the chart recorder and the output of the fluxmeter to the y-axis tracing out the hysteresis loop.

All the samples were mechanically extracted with extreme care by the Student Workshop at Durham University. An excess of coolant was applied during machining to prevent work hardening altering the magnetic properties of the steel. This method has been investigated in detail by Willcock (1985) and found to be acceptable. The details of the sample dimensions and windings can be seen in figure 3.01b). The rings were first wrappped in insulating tape to protect the insulation on the wire and a small wire attached to the metal so that any breakdown in this insulation could be detected. Nominally 100 turns were wound on each toroid for both the primary and secondary windings with s.w.g. 22 and s.w.g. 40 insulated copper wire respectively. BS6404 recommends that the cross-sectional
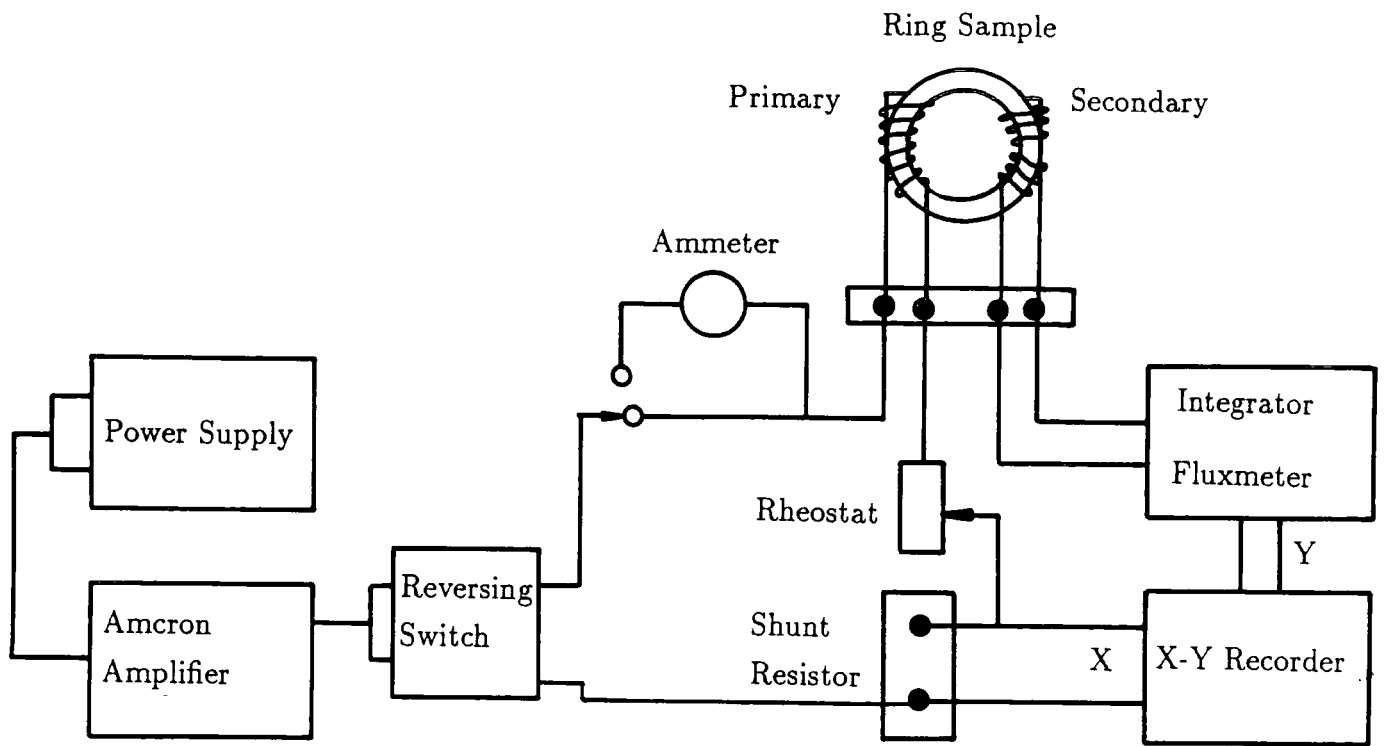
a)
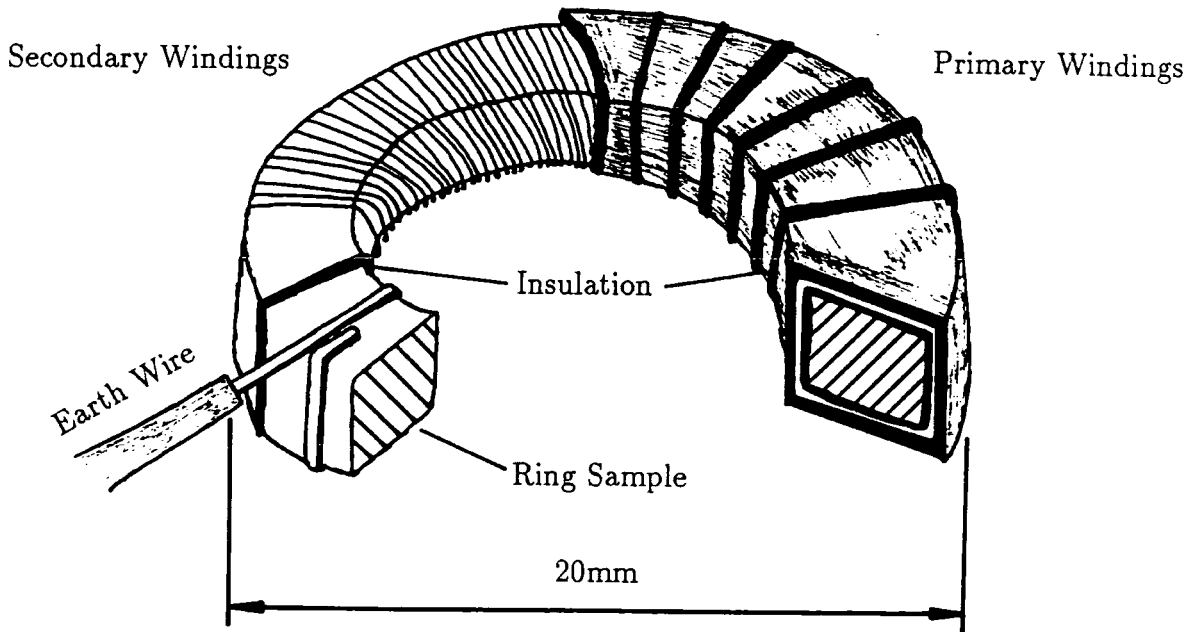
b)

Figure 3.01 a) Block Diagram of the Toroid Apparatus and b) Details of the
Toroid windings.

area of the samples be between 100mm² and 500mm² to reduce machining effects. The restrictions of the original sample dimensions rendered this impossible, but the recommended ratio of diameters was maintained.

$$D \leq 1.1d \ldots (3.01)$$

Where D is the outside diameter of the toroid, and d the inside diameter.

A comparison was made by Brown (1985) at the Welding Institute on two toroids cut from the same material, the first of similar dimensions to those used here, and the second within the recommended guidelines. It was found that the results for the two toroids differed by less than 4%, the smaller ring showing a higher magnetisation.

Equation (3.02) was used to calculate the magnetising field yielding a maximum field strength of 7kAm⁻¹ for a primary current of approximately 3 amps, and equation (3.03) to calculate the flux density in the ring.

$$\text{Applied field}: H = \frac{N_p I}{\pi L} \ldots (3.02)$$

$$\text{Flux density}: B = \frac{\phi}{N_s A} \ldots (3.03)$$

Where N_p and N_s are the number of primary and secondary turns respectively, L the mean toroid diameter, ϕ the induced flux, I the magnetising current, and A the cross-sectional area of the toroid.

3.2.2 The Yoke Permeameter

In the permeameter the flux path through the bar sample is completed by clamping a yoke onto it as illustrated in figure 3.02 b). The magnetising field is supplied by a coil that surrounds the sample and the flux induced in a search coil wrapped tightly around the sample measured by an integrating fluxmeter. The computer controlled compensated yoke permeameter at British Gas's Engineering Research Center, developed by M. Warnes according to BS5884 (1980), and calibrated with respect to National Physical Laboratory standards, was used to record the hysteresis curves of bar samples and is illustrated in figure 3.02.

60
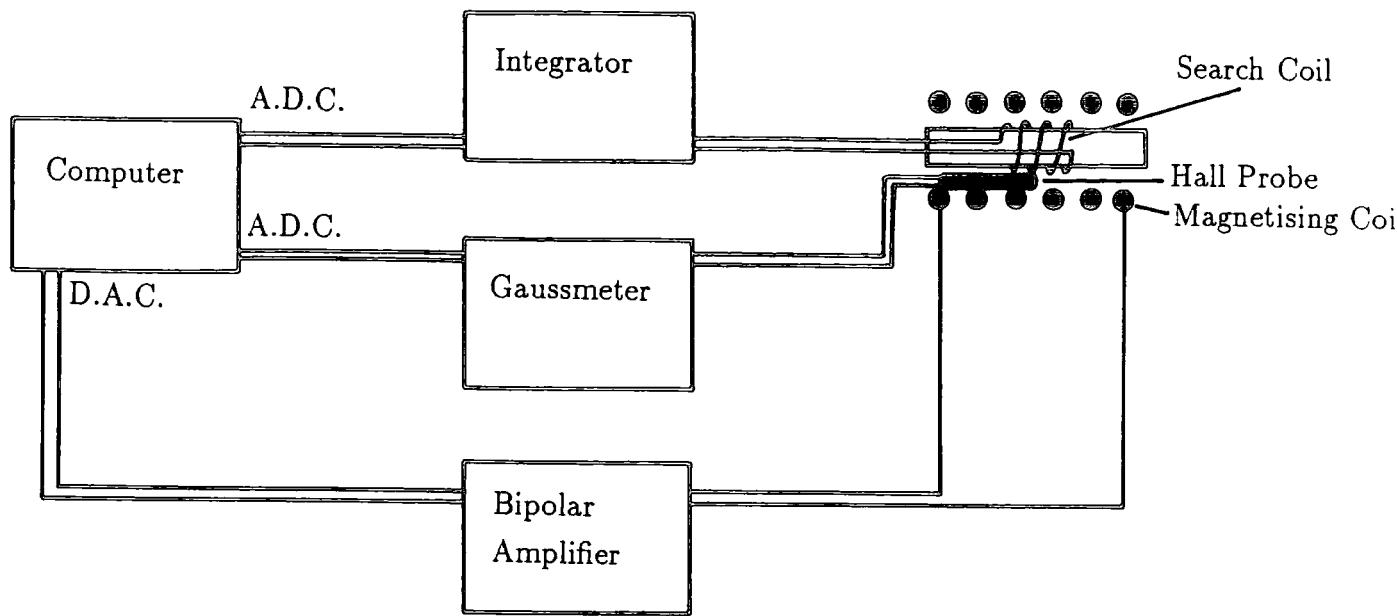
a)
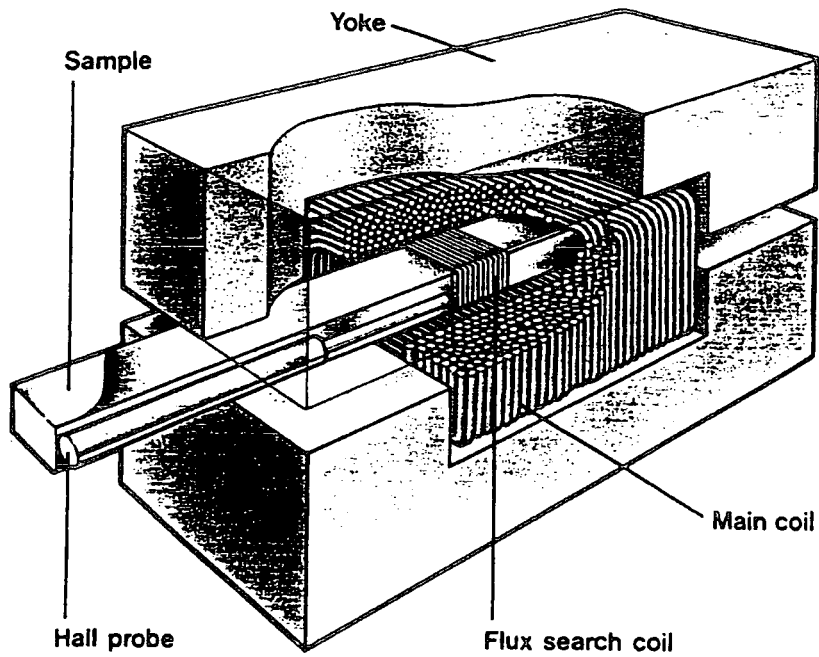
b)

Figure 3.02 Details of the British Gas Yoke Permeameter. (Diagram of windings courtesy of British Gas.)

The magnetising field is provided by both the main and auxiliary coils in order to achieve flux uniformity in the sample, and the magnetic circuit completed by a yoke. The current in the coils is controlled by the system's M.I.N.C. minicomputer whose ADC boards supply +/- 10V (for +/-2000 counts) to the bipolar Kepco amplifier. This is sufficient to produce an applied field in the sample of $100 \mathrm{Am}^{-1}$ to $40 \mathrm{kAm}^{-1}$. The field is measured by a Hall probe placed alongside the sample read by a computer controlled LDJ Gaussmeter. The output from a 50 turn search coil, wound onto the sample, is fed into an integrator and read by one of the M.I.N.C. ADC boards.

The sample is first demagnetised by driving it around decreasing hysteresis loops before an initial magnetisation curve is measured. This initial curve is measured by recording the maximum magnetisation occurring for a series of increasing minor loops. For every point three readings are taken at $+B_s$, $-B_s$ and then again at $+B_s$, the values compared, and repeated if not within predetermined tolerance limits. This helps to eliminate the inherent problems of integrator offset and drift, although does assume that the hysteresis curve is symmetrical. The programme pauses for 5 seconds before every reading to reduce the effects of eddy currents. After the first two points the computer attempts to predict the flux change in the sample in an attempt to achieve a set of readings equally spaced in B.

A full hysteresis curve can also be determined, this is completed by repeated cycling at the required maximum applied field with readings being taken at a different point on each cycle and with the same protocol as for the initial magnetisation curve.

An analysis program was written for the permeameter data once it was transferred to a P.C. (Appendix C). The program extracts values of initial permeability, maximum relative permeability and the field at which this occurs from the initial magnetisation curve and maximum differential permeability, coercivity and remanence from the full hysteresis curve. In addition the program allows plotting of both permeabilities as a function of applied field and testing of the Kneppo relation by plotting ln(flux density) against inverse applied field.

3.2.3 The Vibrating Sample Magnetometer.

The principle of the operation of a vibrating sample magnetometer (V.S.M.), as originally described by Foner (1956), is that if a sample is vibrated perpendicular to a magnetising field then an a.c. voltage will be induced in detection coils placed adjacent to the sample. This a.c. voltage will be proportional to both the frequency and amplitude of the vibration and the sample's magnetic moment. Hence if the amplitude and frequency of the vibration are kept constant then the signal will be proportional to the magnetic moment of the sample. Once the system has been calibrated with a known magnetic moment (such as a constant current coil or a sphere of high purity nickel), then the magnetisation of the sample can be measured as a function of the applied field. For a review of developments since Foner see Willcock (1985).

Both Durham's two 1.2T electromagnet double crank V.S.M.'s were built on the design of Hoon (1988 and 1983) and are described in detail there and in Willcock (1985), the differences incorporated during the construction of the second instrument being described by J.M.McCoy (1988). As a result only the outline of the systems will be described here, for a diagram of the instrument see figure 3.03. The first machine constructed by Hoon and Willcock will be referred to as "A" and the second one due to McCoy as "B" throughout. Both instruments were used for room temperature measurements of coercivity and only 'A' for low temperature work.

The double crank design of the sample vibration transducer provides a significant improvement on previous systems in amplitude and frequency stability, low vibrational noise and high inertial loading. A sine wave generator operating at approximately 60Hz, amplified by a transformer and Quad 50E amplifier to 240 V a.c., provides the power to the motor which drives the crank at half the supply frequency. A small permanent magnet is attached to an extension of the motor shaft and situated inside a small coil such that the signal induced in the coil will have the same frequency as the detection coil signal and can be used as the reference signal for the phase sensitive detector.

Both instruments use the Mallinson (1966) detection coil system which consists of two coils placed vertically above one another on each pole piece. A discussion of

63
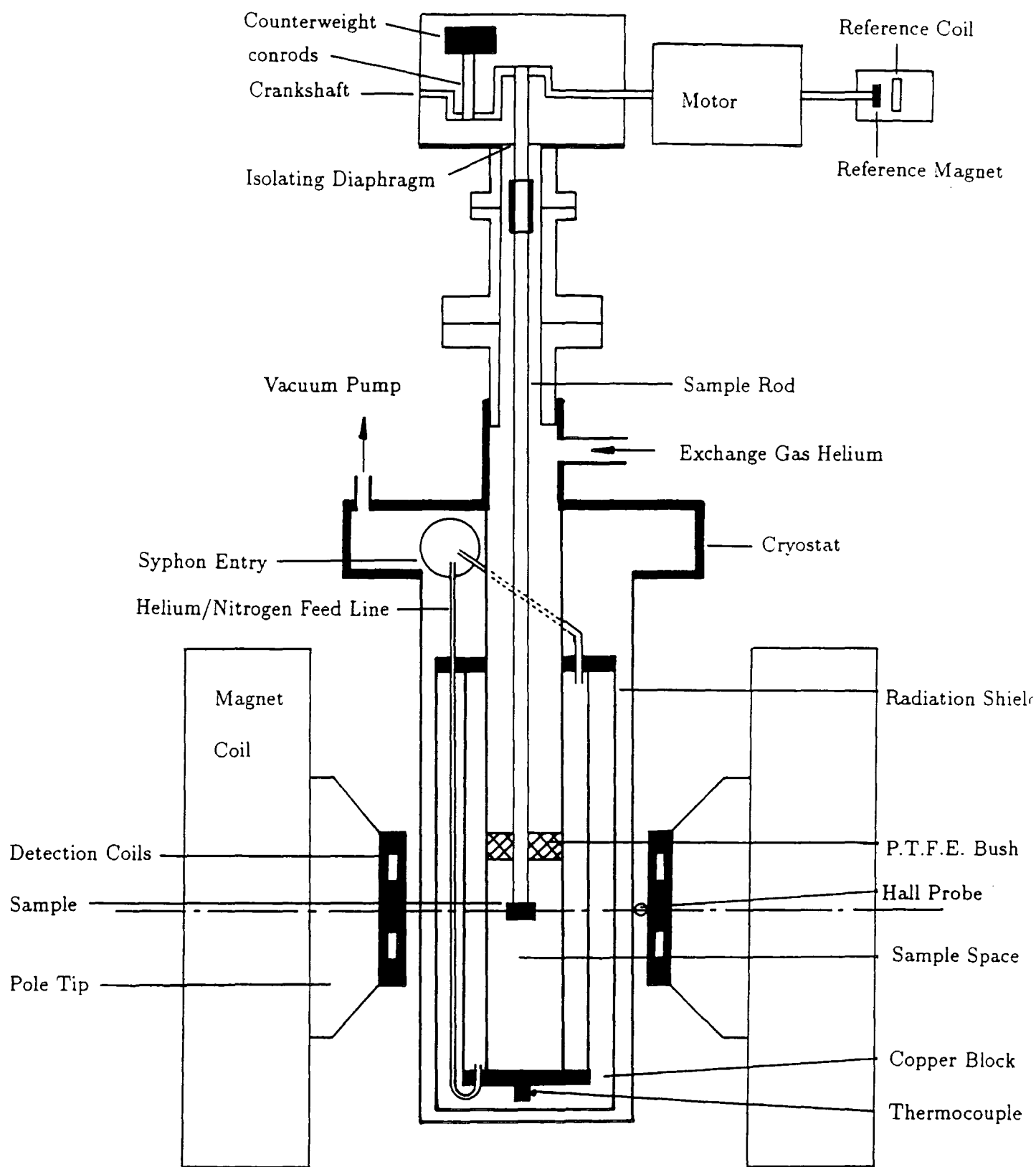
NOT TO SCALE

Figure 3.03 Schematic Diagram of the Durham Vibrating Sample Magnetometer and Cryostat.

other potentially suitable coil designs and the reasons for this choice are given by Willcock (1985). The detection coils are wound on tufnol formers mounted onto brass cheek plates and screened by copper covers fastened to the cheek plates. The coils for "B" are wound with 16000 turns compared to 4600 on "A", increasing the inductance of each coil by a factor of 15. The opposing signals from each set of coils are subtracted and fed into the lock-in amplifier.

The position of the sample between the polepieces can be altered in the x and y direction using the worm screws incorporated in the head supporting mechanism, and the whole head assembly raised or lowered in the z direction by altering the amount of air in the pneumatic support collar used to isolate the vibrations of the head from the detection system. It is important that the sample be mounted centrally as a 1% change in sensitivity can be detected for a displacement from the centre of as little as 1.5mm (McCoy 1988). This is facilitated for "A" where a P.T.F.E. bush automatically centralises the sample rod inside the cryostat. The variation in output as a function of position is shown in figure 3.04.

The power supply for the magnet in both cases is provided by a Newport Instruments C225 350V 30A control unit and generator with additional modifications designed by Willcock to provide a bipolar output and consequent current reversal. The current is controlled by a stepper–motor–controlled potentiometer and the applied field measured with a Hall effect probe placed adjacent to one of the pole pieces. The maximum working field used was 1.2 Tesla and this has been found to vary less than 0.38% (McCoy 1988) within a 10mm radius sphere of the sample.

Both systems are computer controlled, "A" by a Commodore PET via a Bede Scientific Instruments Minicam and the IEEE488 standard, and "B" by an Acorn BBC model B Microcomputer and 6502 second processor via both the IEEE488 standard and the BBC's RS432 interface. Both control and analysis programs, written in PET and BBC Basic for "A" and "B" respectively, are such that modification for individual requirements is straightforward. The recent introduction of an IBM compatible P.C. has led to new analysis and control programs being written.

Both programs allow the operator to carry out the necessary setting up of the lock-in amplifier, gaussmeter and sample positioning, and to specify field re-
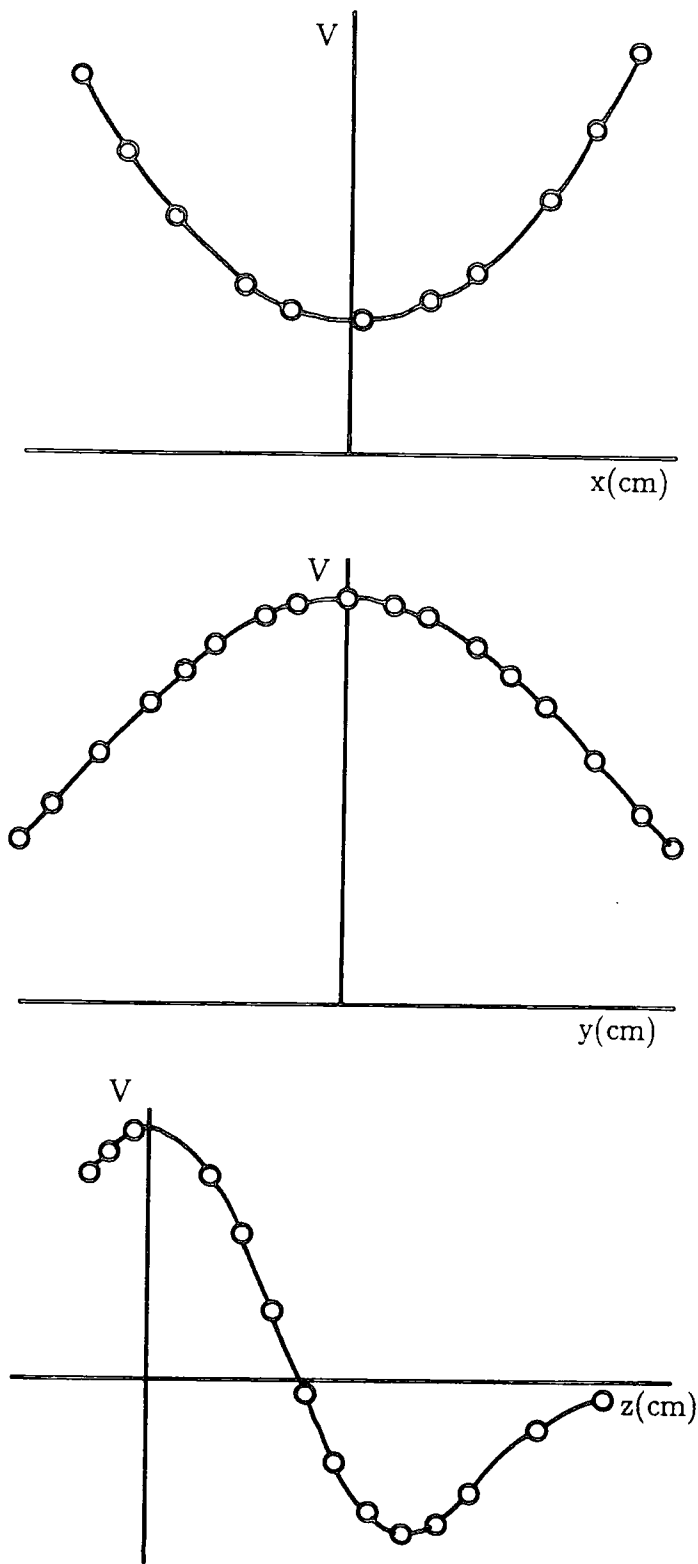
Figure 3.04 The Sensitivity of the Detection Coil System as a Function of Position. (After McCoy 1988)

quirements and the number and density of points required before taking complete control. Ten readings are taken at each point, a standard deviation calculated, repeating the reading if the deviation is too high. The measurement of coercivity is carried out within the remanent field of the magnet ($\simeq 150$ Gauss), with approximately 100 readings taken in this linear region for both positive and negative applied field. A least squares fit is then applied to the data with the x intercept yielding the coercive force. As the magnetisation at the coercive point is zero no calibration of the system or demagnetising corrections are necessary and hence the system can be used even for soft magnetic materials such as steel.

For weaker samples the magnetic moment of the sample rod and holder must be corrected for and a least-squares fit of the residual noise is subtracted from the raw sample data. A demagnetising factor (Brailsford 1966) for the sample must also be calculated and used in conjunction with the nickel calibration to determine the true magnetisation of the sample.

"A" is fitted with an Oxford instruments CF1200 helium gas flow cryostat, modified to fit between the pole pieces of the electromagnet. This enables measurements to be made in the temperature range 4.2K to 500K. The temperature is measured with a gold–0.07 iron-chromel thermocouple attached to the heater block at the base of the sample space and controlled by an Oxford Instruments 3120 temperature controller. The helium exchange gas in the sample space is isolated from the atmosphere by flexible coupling between the sample space and the vibrating head Willcock (1985). A useful text for low temperature work was found in Richardson and Smith (1988).

3.3 Barkhausen Noise Detection.

The Barkhausen noise detection system used was essentially that developed by A.J.Birkett (1988) but with the Commodore PET computer replaced by a P.C. for the second set of experiments accompanied by new control and analysis programs (Appendix C).

The system (after Rulka 1975) consists of a magnetising coil which surrounds the sample and a small pick-up coil placed, with its axis perpendicular to the magnetising direction, close to the sample. The small voltages induced in this coil
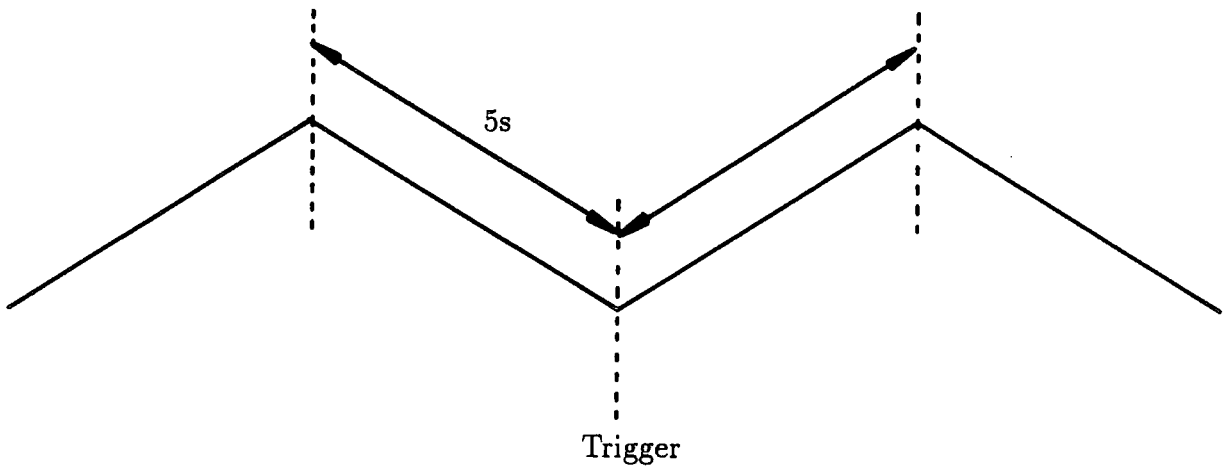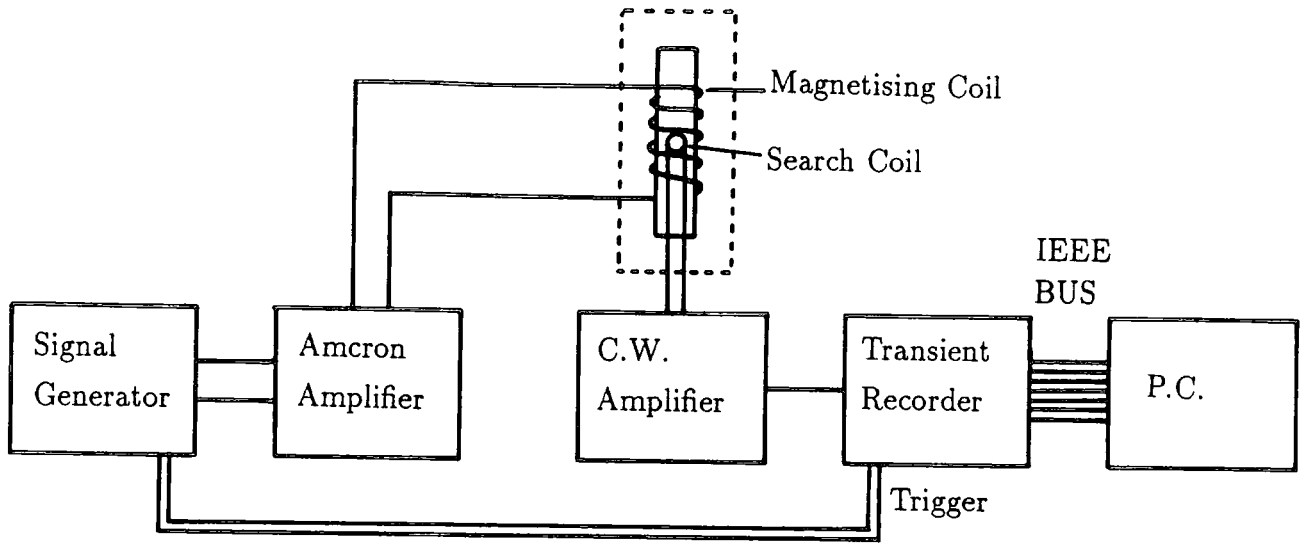
Figure 3.05 a) Outline of The Barkhausen Apparatus, b) the Triangular Magnetising Waveform.
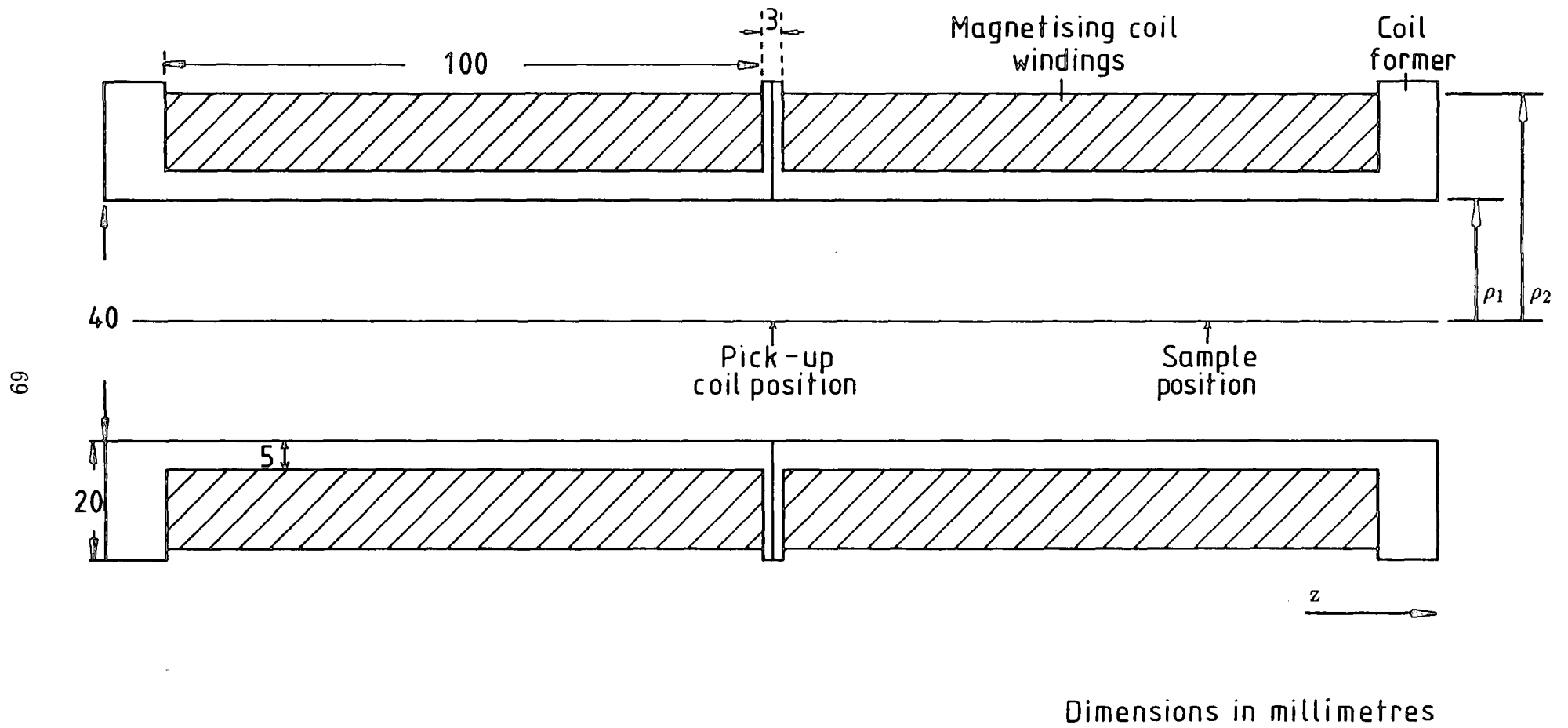
Figure 3.06 Details of the Barkhausen Magnetising Coil. Windings. (Courtesy of Dr. A.J. Birkett)

as the sample is magnetised are amplified and recorded by a transient recorder. An outline of the system and the details of the coil system are shown in figures 3.05 and 3.06 respectively.

The magnetising coil is wound in two sections on tufnol formers, each nominally of 900 turns of 0.8mm diameter wire. The method of Zijlstra (1967) is used to calculate the magnetising field generated by the coils along the axis for a current density of 1 Amp:

$$H_z = \frac{\tau}{2}\rho_1 \beta ln\left[\frac{\alpha + \sqrt{(\alpha^2 + \beta^2)}}{1 + \sqrt{(1 + \beta^2)}}\right] \ldots (3.04)$$

Where $\rho_2 = \alpha\rho_1$, the length of the coil runs from $z_o = 0$ to $\beta\rho_1$ and τ is the current density. As the magnetising field is proportional to the current density, the field can be calculated at any point in the magnetisation cycle.

A Mullard 4B1 ferrite core, diameter 1.5mm, length 12mm wound with 804 turns of 0.1mm wire is used as the pick-up coil. This is supported in the centre of the magnetising coil by a tufnol holder which also supports the bar sample. The Barkhausen signal of between 0.01mV and 10mV induced in the coil is amplified 1000 times by a low noise amplifier designed by C.D.H. Williams and then input to a Thorn EMI Waveform Analyser SE2550. The whole coil assembly is enviromentally shielded in a steel box constructed from 1/4 inch thick steel.

A triangular waveform of frequency 0.1Hz is used to provide a uniform magnetisation rate. The transient recorder is triggered at the peak of the waveform and the delay set on the transient recorder to determine the section of the cycle to be analysed, figure 3.05. The region around the coercive force, found to be the area of most activity can then be divided up into a convenient number of sections for recording. The data is then transferred to the NUMAC Amdahl mainframe computer where the data can be analysed and where desired the power spectra calculated.

3.4 Lorentz Electron Microscopy.

All the electron microscopy was conducted on the A.E.I. EM7 1MV High Voltage Electron Microscope in the Department of Materials Science at the University

of Oxford. The main features of the microscope are outlined in figure 3.07. The condenser lenses focus the electron beam onto the specimen inside the Faraday cage which aligns the beam. The objective lens forms the specimen image which is magnified by the projector lenses P1, P2, and P3 onto a tilted flourescent screen which can be rotated vertical to allow the image to be projected onto the camera for the taking of photographs. Dynamic images such as the movement of domain walls whilst operating the magnetising coils can be viewed instead on a television screen and recorded onto a Sony U-matic video recorder using the sound-track to record the applied field.

A specially designed magnetising stage for Lorentz microscopy (R.A. Taylor 1980) was fitted to the microscope for all this work making both Fresnel and Foucault imaging possible. The stage is situated in the top entry port where the axial field is only 10 Oe and where sufficient space is available to site the magnetising coils. A diagram of the magnetising stage showing the position of the specimen is shown in figure 3.08a). The field profile along the microscope axis of the coil windings is shown in figure 3.08b), the field variation across the specimen has been calculated to be within 10% Taylor (1980). With the specimen situated in its usual position in the plane of the bottom set of coils a maximum magnification of 40K is available and a 4μm shift of the image is suffered for a 100Oe change of field. The coils provide a maximum field variation of 12 kAm^{-1}and the field vector can be rotated through 360°to within 5°.

With the sample raised above the objective lens, the available magnification is severely reduced, calibration was done on a 2.3mm grid with 2160 lines mm^{-1}. The monographs of Edington (1974 and 1975) and (Chescoe et al 1984) were found to be of good practical use in operating the microscope.

3.4.1 Sample Preparation

The 2.3mm diameter, 1mm thick discs were initially mechanically polished to approximately 100μm,in the case of the pipe steel by hand, and for the pure steel samples on the Struers polishing wheels at British Gas. Electropolishing to remove the surface strains was done in 5% perchloric acid in acetic acid (Goodhew 1984, Hetherington 1985) in a Struers Tenupol electropolishing unit at Oxford.

71

This method produces a dish shaped sample with the area around the central hole sufficiently thin for study under the EM7 High Voltage Electron Microscope.

ACCELERATOR   **GENERATOR**

Intersystem Valve

C1 Lens

C2 Lens

Condensor Aperture

Specimen Chamber
Objective Aperture

Objective Lens
Diffraction Aperture

P1 Lens

P2 Lens

P3 Lens

Window

C1 Aperture

Faraday Cage

Condensor Stigmator

Dark Field Stigmator
Objective Alignment

Specimen Holder

Objective Stigmator

Diffraction Alignment
P1 Stigmator

Shutter

Beam Stop

Screen

Camera
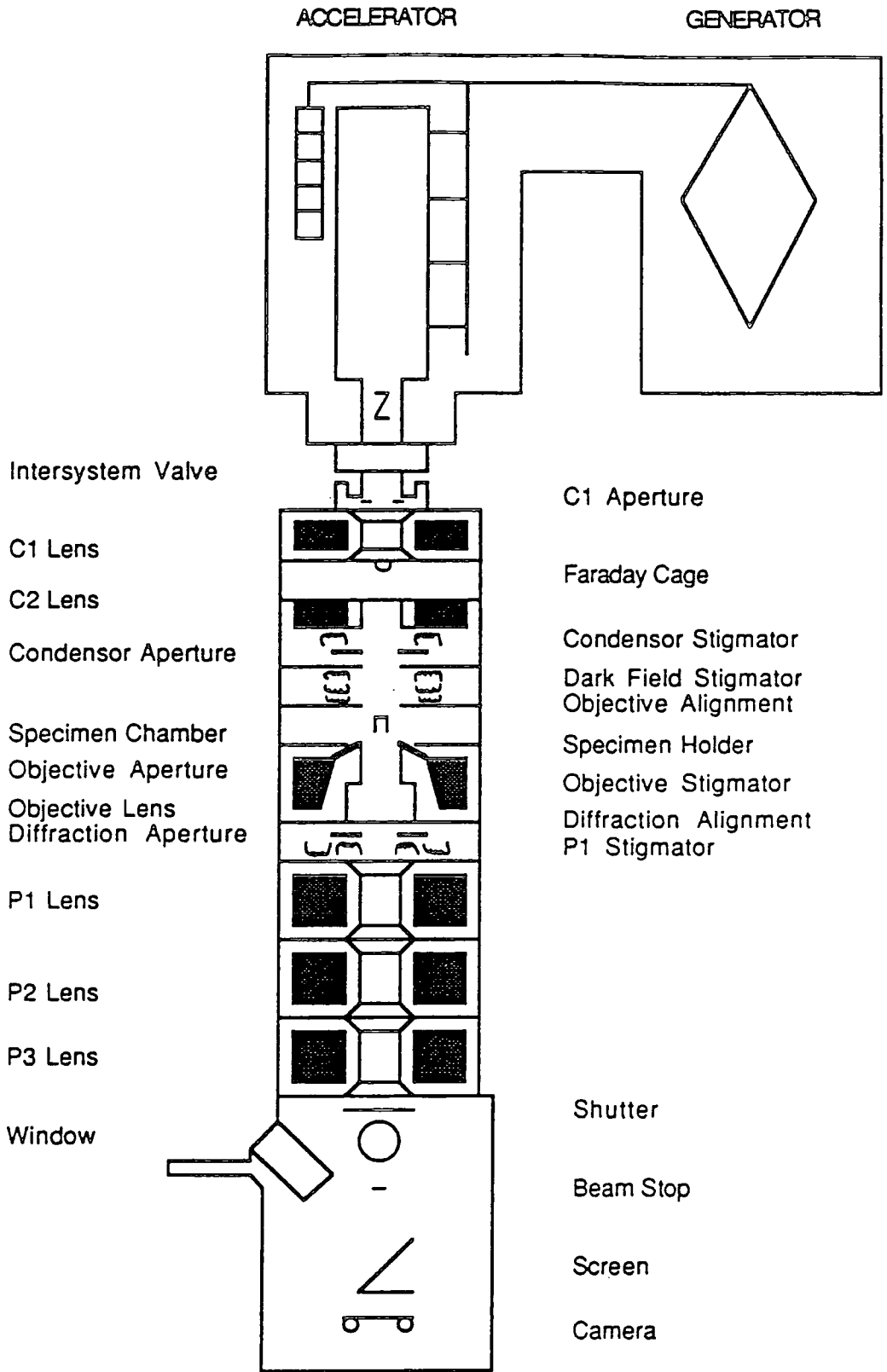
Figure 3.07 Details of the A.E.I. EM7 High Voltage Electron Microscope. (After Alcock 1985)

a)

Windings

Core

Distance (mm)

16　　　　　　0　　　8

Transverse Field kAm^{-1}

b)
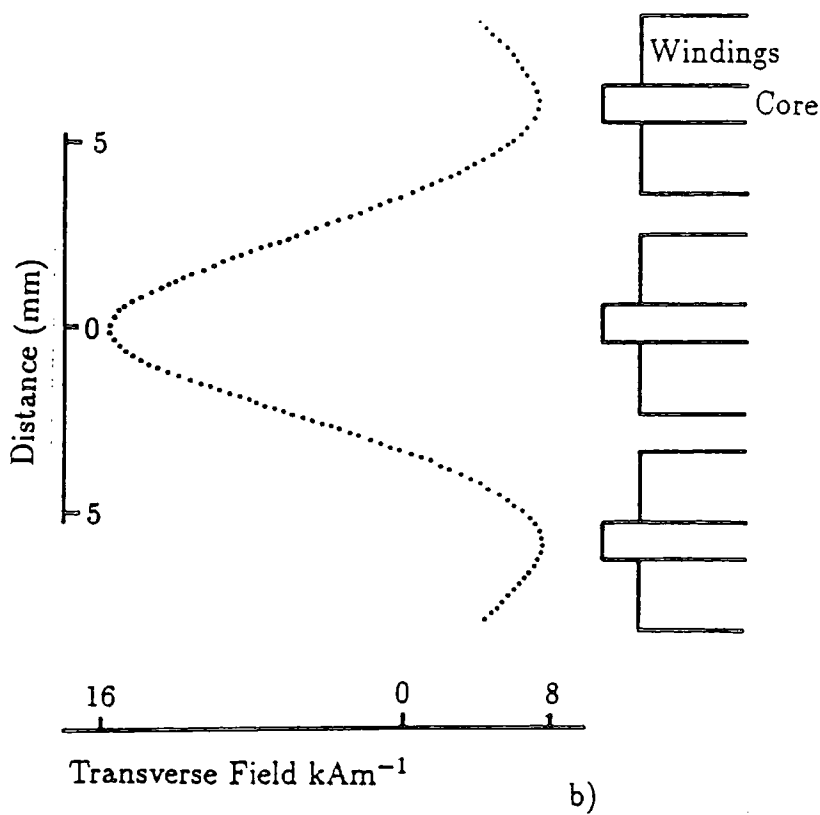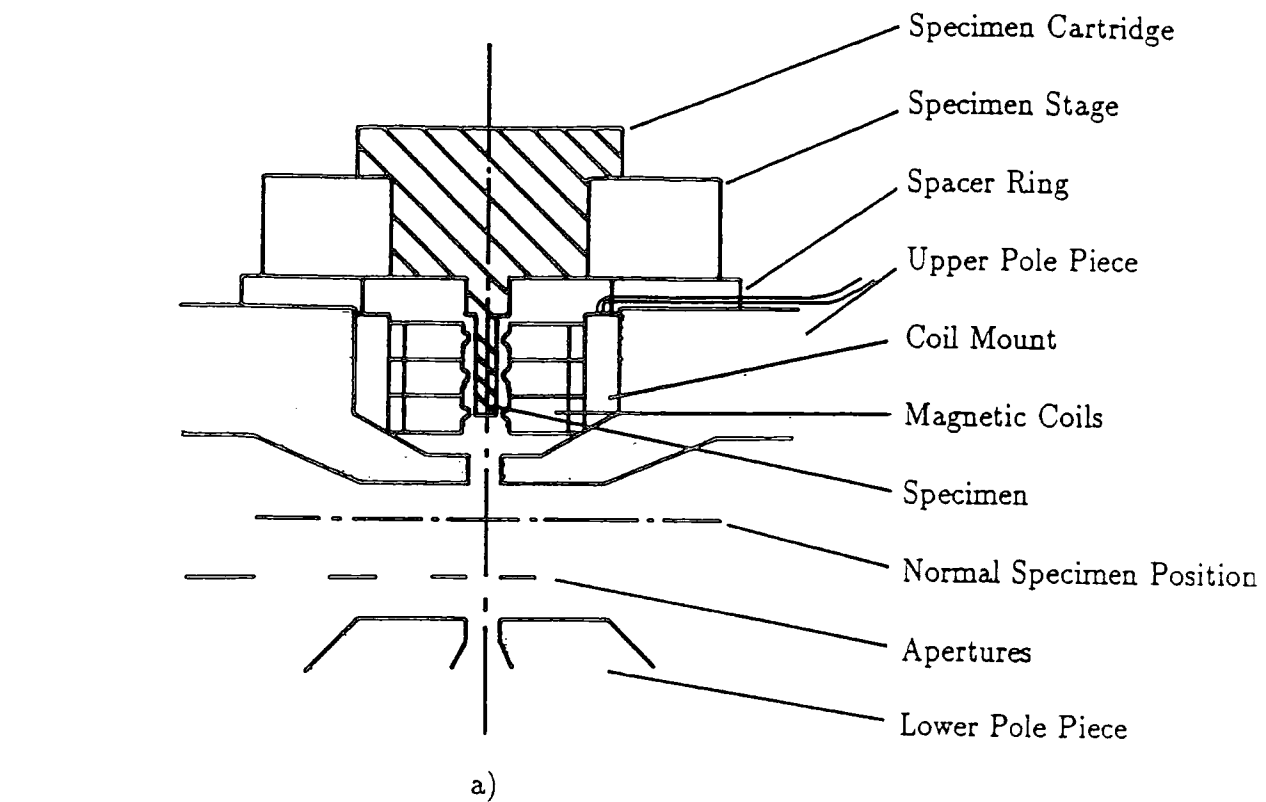
Figure 3.08 a) The Magnetising Stage for Lorentz Microscopy in the Oxford
A.E.I. EM7 Microscope, b) the Field Profile of the Magnetising Coils.
(After Taylor 1980)

74

Chapter IV

Initial Experiments on Pipe Steel.

4.1 Introduction and Sample Details.

A section of typical British Gas pipeline manufactured from 2401 semi-killed steel (pearlite content 17%) was used for the initial experiments; a summary of its chemical composition , mechanical and magnetic properties as determined by Willcock (1985) is given in Appendix A. Ten bar samples with central dimensions of 50 x 22 x 6 mm were extracted from this section as indicated in figure 4.01.

The microstructure of the steel was studied under an optical microscope and micrographs of the undeformed material are displayed in figures 4.02a) and b) and of a 20% deformed sample in figures 4.02c) and d). The rolling and also deformation direction is horizontal and the elongation of the grains in this direction can be seen in all the micrographs. The individual grains of pearlite and ferrite are clearly defined with the finely spaced pearlite lamellae ($\sim 0.7\mu m$) visible in the ×1000 micrographs. The microstructure is not noticeably affected by the plastic deformation at these magnifications.

Using a 500kN Denison tensile testing machine nine of these bars were plastically deformed to residual strains ranging from 2.4 to 20.4%. Two example stress-strain curves are shown in figure 4.03 and figure 4.04 plots the gradient of the stress-strain curve as the load is removed against the residual strain achieved indicating the degree of work-hardening of the sample. The Barkhausen noise from all these bars was recorded before samples were extracted from them (figure 4.01) for use in the experiments described below. The samples were toroids of diameter 20 mm and discs of dimension 2.3 x 1 mm (type A parallel, and type B perpendicular to the rolling and hence deformation direction). All the experimental methods used to determine the results presented here have been described in the previous chapter.

75
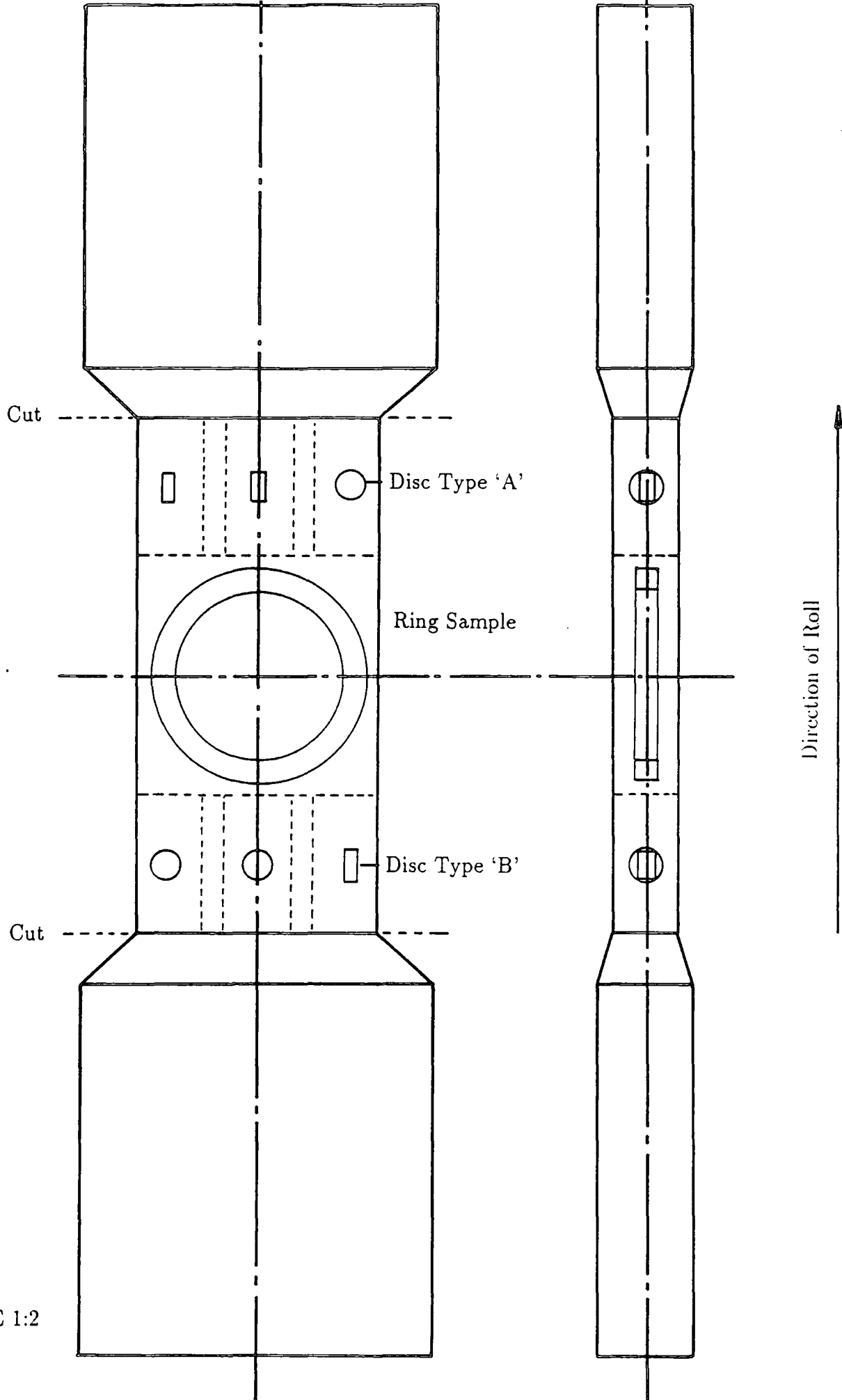
Figure 4.01 Details of the Test Samples Removed From the Section of 2401 Pipesteel.

Cut

Cut

Disc Type 'A'

Ring Sample

Disc Type 'B'

Direction of Roll

SCALE 1:2
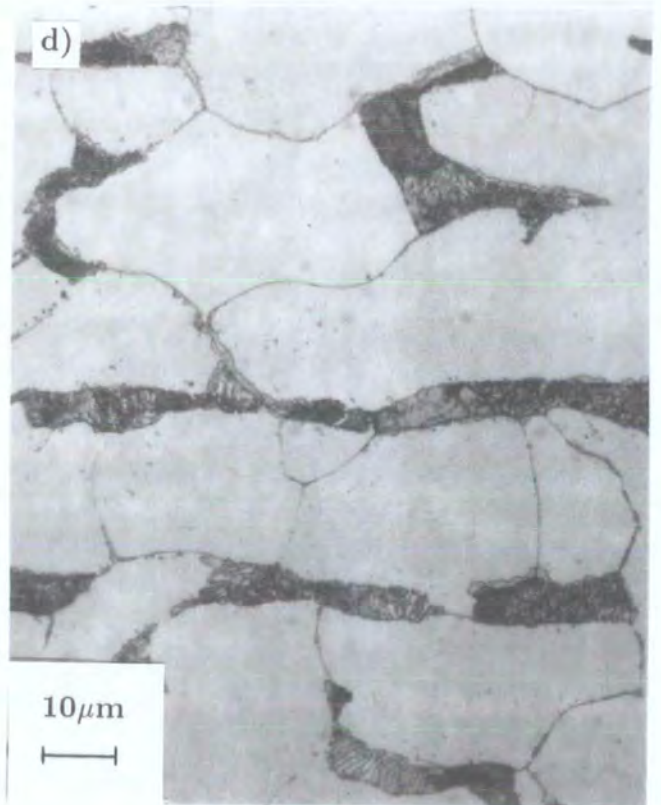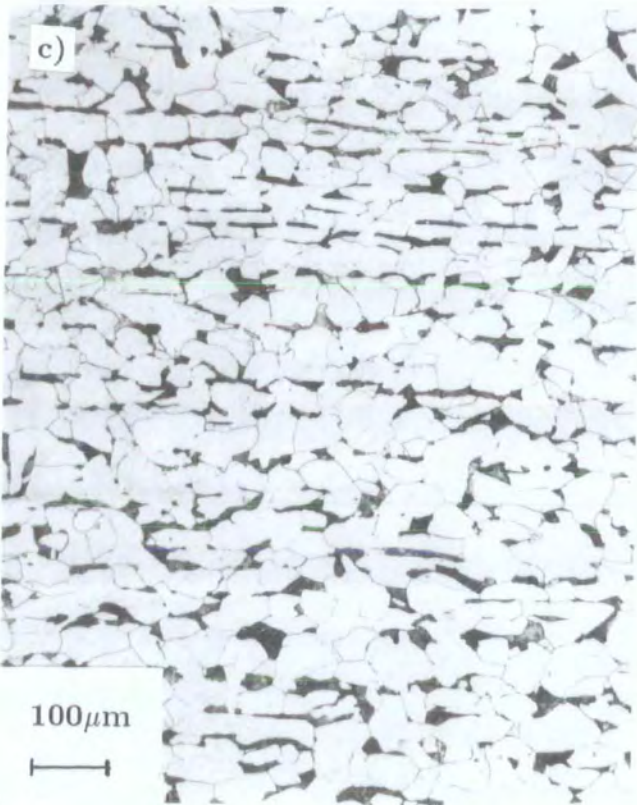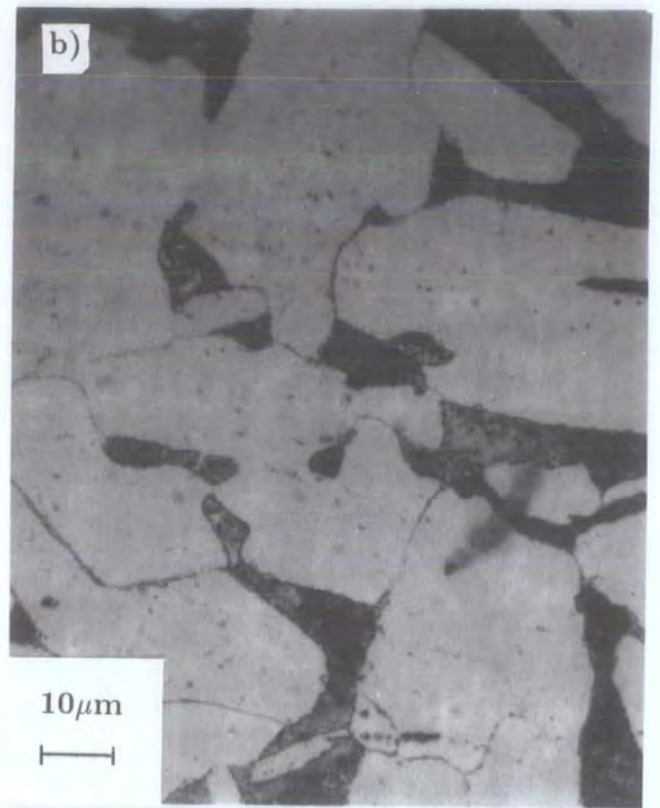
Figure 4.02 Optical micrographs of 2401 pipe steel a) ×100 undeformed; b) ×1000 undeformed; c) ×200 20% deformed; d) ×1000 20% deformed.
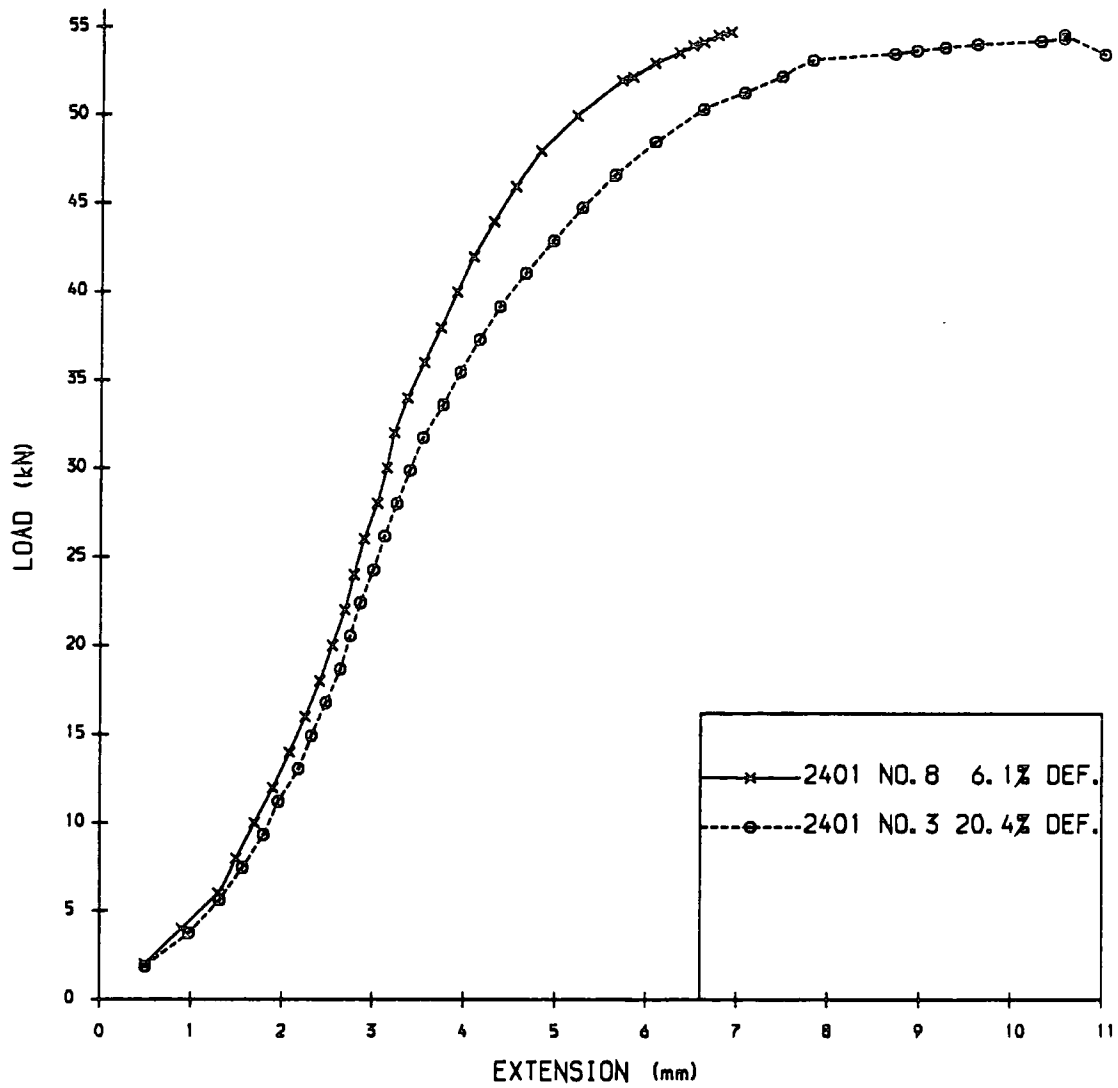
Figure 4.03 Load vs. Extension curves for two of the Pipesteel samples Strained to 6.1% and 20.4% Plastic Deformation.
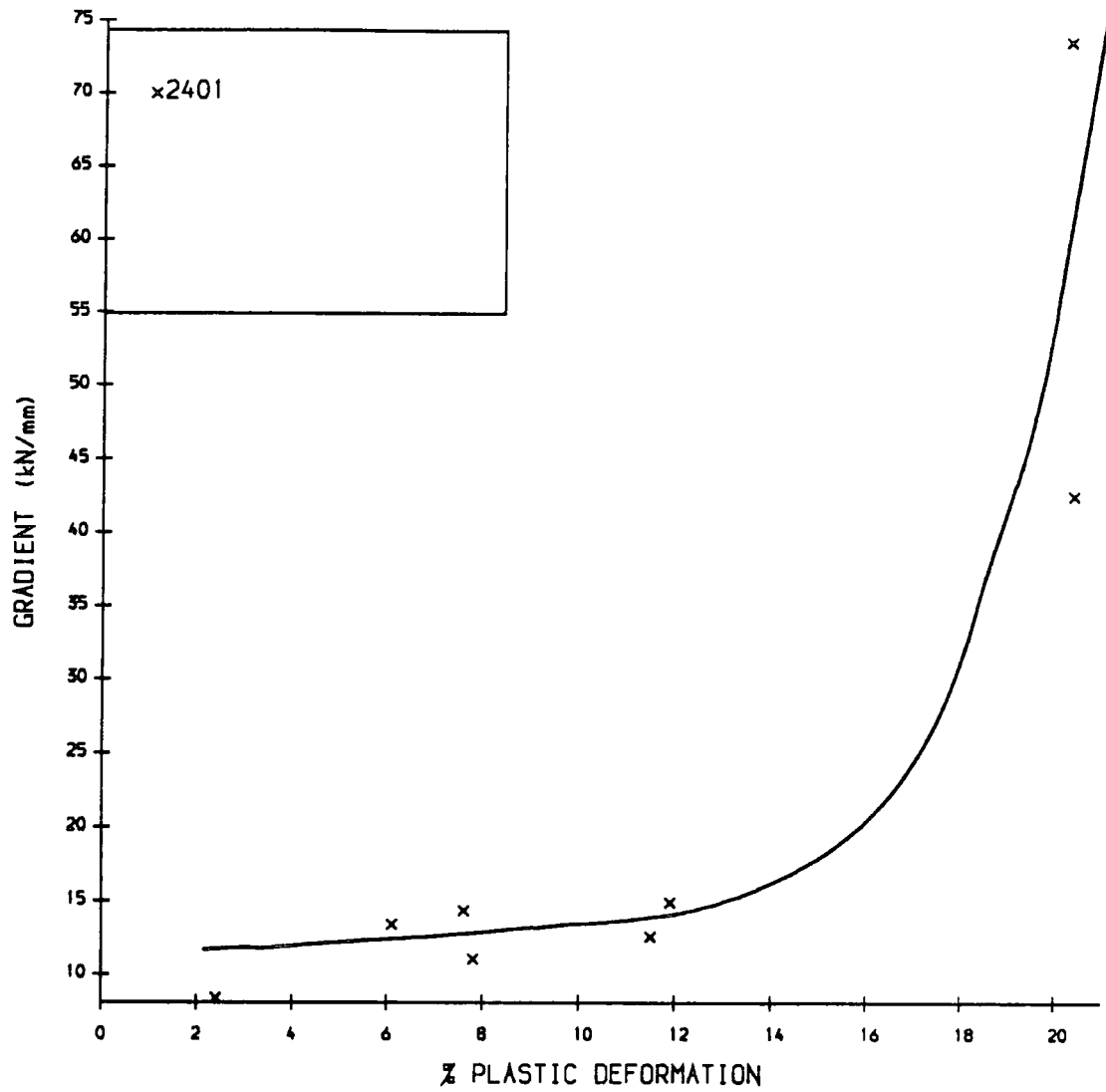
Figure 4.04 Gradient of the Stress-Strain Curve as the Load is Removed.

79

4.2 Bulk Magnetic Properties (Room Temperature).

To determine the bulk magnetic properties of the pipesteel and investigate their variation with plastic deformation initial magnetisation and hysteresis curves were recorded for all the samples. These were determined manually from the toroids using the standard magnetisation and fluxmeter technique demagnetising the samples first and then saturating in an applied field of $14kAm^{-1}$. A summary of the factors by which the various properties changed with plastic deformation is given in table 4.01 and a detailed record of the results in Appendix B. From the curves traced on the x-y plotter values of maximum relative permeability μ_{max} on the initial curve, maximum differential permeability μ'_{max} (measured at the coercive point), remanence Br and coercivity Hc were obtained. Figure 4.05 shows example curves for an undeformed and a 20% deformed sample. The reduction over the 20% deformation range of μ_{max} and the increase in the field at which μ_{max} occurs Hm are plotted in figure 4.06 and the increase in μ'_{max} with the decrease in Br in in figure 4.07.

More accurate coercivity measurements were made using the vibrating sample magnetometers; the coercivities both parallel and perpendicular to the direction of strain (also the rolling direction) were measured, saturating the samples in 1.2T and the results plotted in figure 4.08. The coercivities parallel to the direction of strain correlated with those from the toroid measurements and increased with plastic strain, while the coercivity perpendicular to the strain remained, within experimental error, constant. At 0% strain the coercivity is higher perpendicular to the rolling direction corresponding to the direction in which the rolled steel is deformed during the process of pipe manufacture.

Steel	%Carbon	Maximum %Deformation	μ_{max}	Hm	Hc $//^l$	Br	μ'_{max}
2401	0.15	20.4	⇓2.6	⇑4.2	⇑1.8	⇓1.5	⇓3.1

Table 4.01 FACTORS by which the magnetic properties 2401 pipe steel changed over the maximum range of plastic deformation.
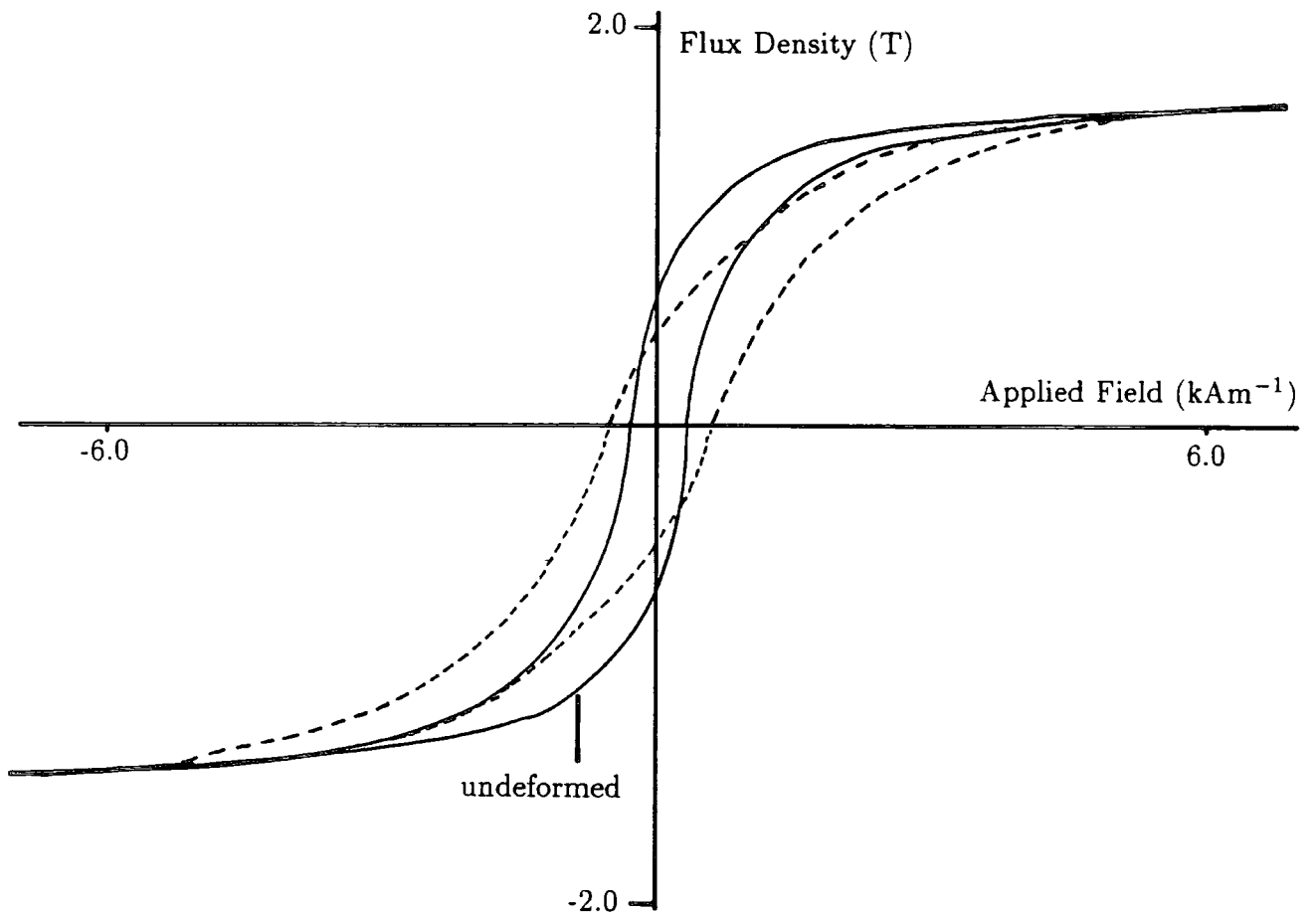
Figure 4.05 Example Hysteresis Curves for 0% and 20% Plastically Deformed Samples of 2401 pipesteel.

81
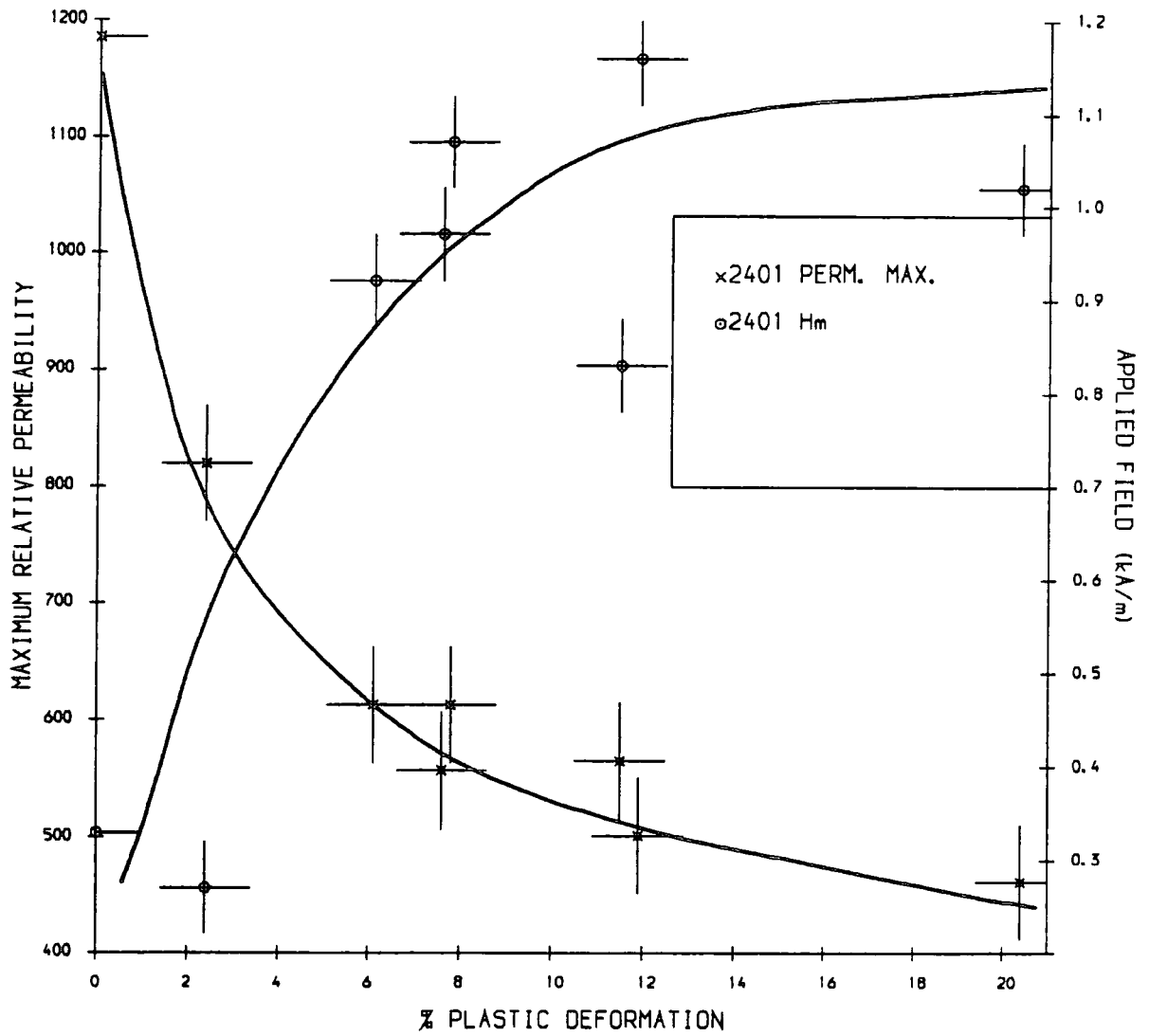
Figure 4.06 The Variation of Maximum Relative Permeability and the Field at which this occurrs with Plastic Deformation.

82
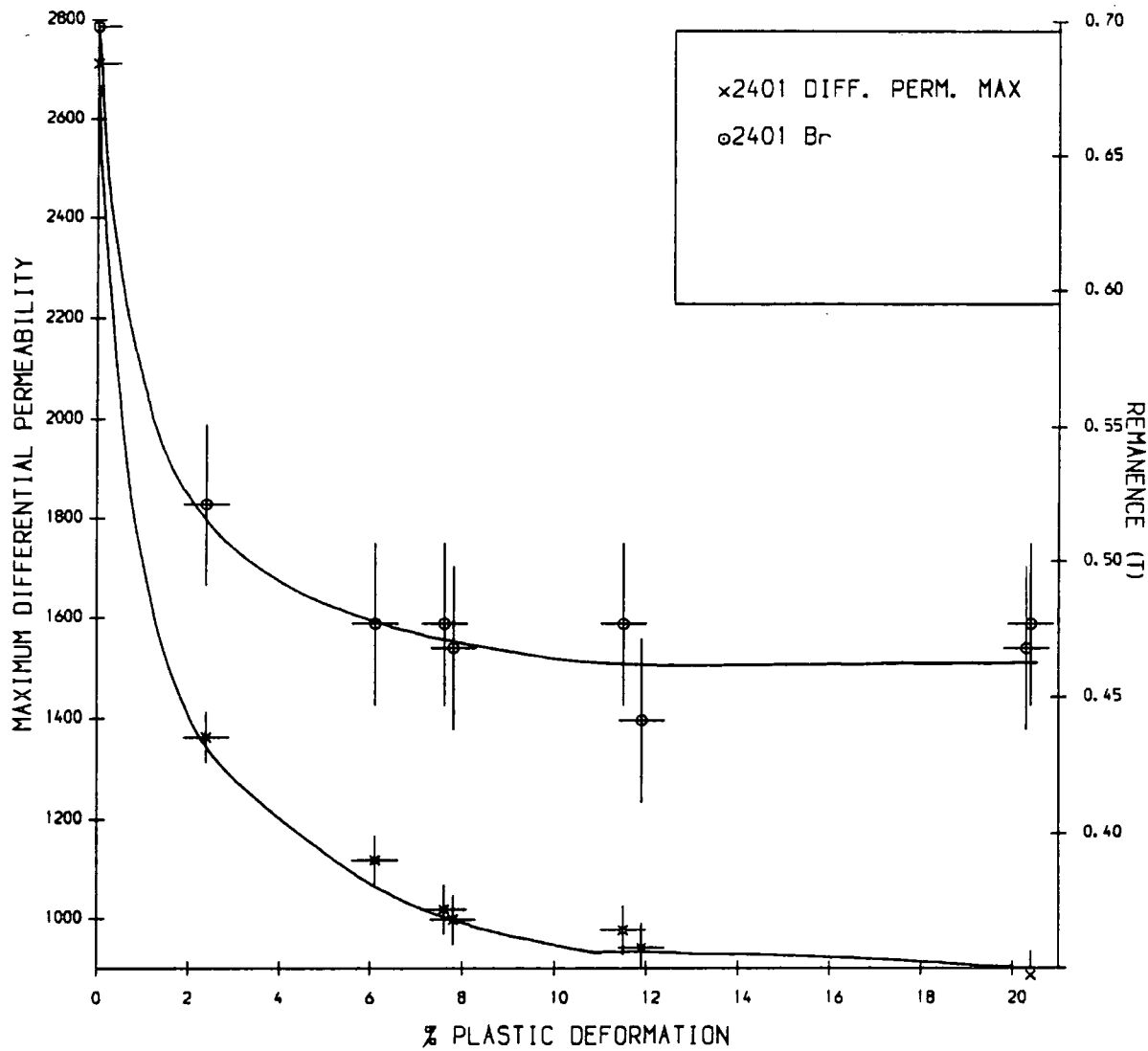
Figure 4.07 The Variation of Maximum Differential Permeability and Remanence with Plastic Deformation.

83
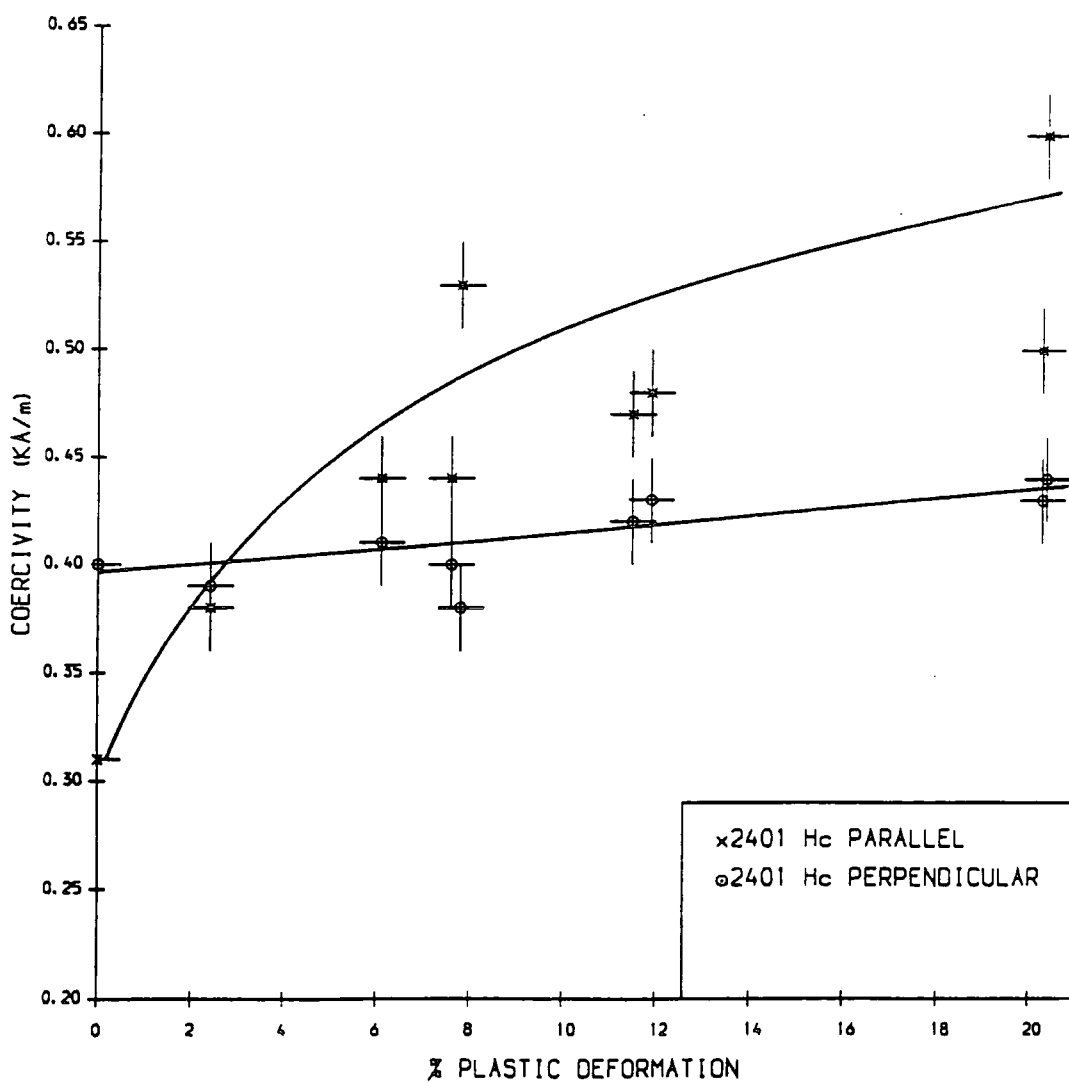
4.08 The Variation of Coercivity with Plastic Deformation Both Parallel and Perpendicular to the direction of Strain.

4.3 Coercivity as a Function of Temperature.

In order to investigate whether the contribution to the coercivity due to the plastic deformation was temperature dependent, the variation of coercivity with temperature in the range 4.2K to 300K was measured using the vibrating sample magnetometer for three samples with different strain values of : 0%, 7.8% and 20%. The decrease in coercivity with increasing temperature was found to be constant for all three deformation values, figure 4.09.

4.4 Minor Loops

The rate of change of remanence and coercivity as the maximum applied field is increased or decreased gives an indication of the energy distribution of the pinning sites. To determine how this energy distribution changes as the steel is plastically deformed a series of D.C. Demagnetising (D.C.D.M.) curves and Irreversible Magnetising (I.R.M.) curves were taken for an undeformed and a 20% strained sample using the manual toroid apparatus. The D.C.D.M. curve was taken by saturating in a negative field of about $10kAm^{-1}$, removing the applied field to reach the remanent point and then repeating the process for decreasing fields. The I.R.M. curve follows the same procedure but starting with a very low applied field applied to the demagnetised state. As it was found that the same results were obtained in both the first and the third quadrants the curves were subsequently taken for series of full minor loops the I.R.M. curve following on immediately after the D.C.D.M.. The low field portions of these curves are shown for the two samples in figures 4.10a) and 4.10b). Values of Br were then measured and plotted against applied field in figures 4.11 to 4.14, the results for the I.R.M. and D.C.D.M. curves were found to be identical for each sample. A similar method is often used with fine particle systems Dr. K. O'Grady (private communication), plotting two remanence curves against each other to determine the time dependence of the system. The differentials of these curves were then calculated and plotted using the mathematical package Matlab, figures 4.15 to 4.18.
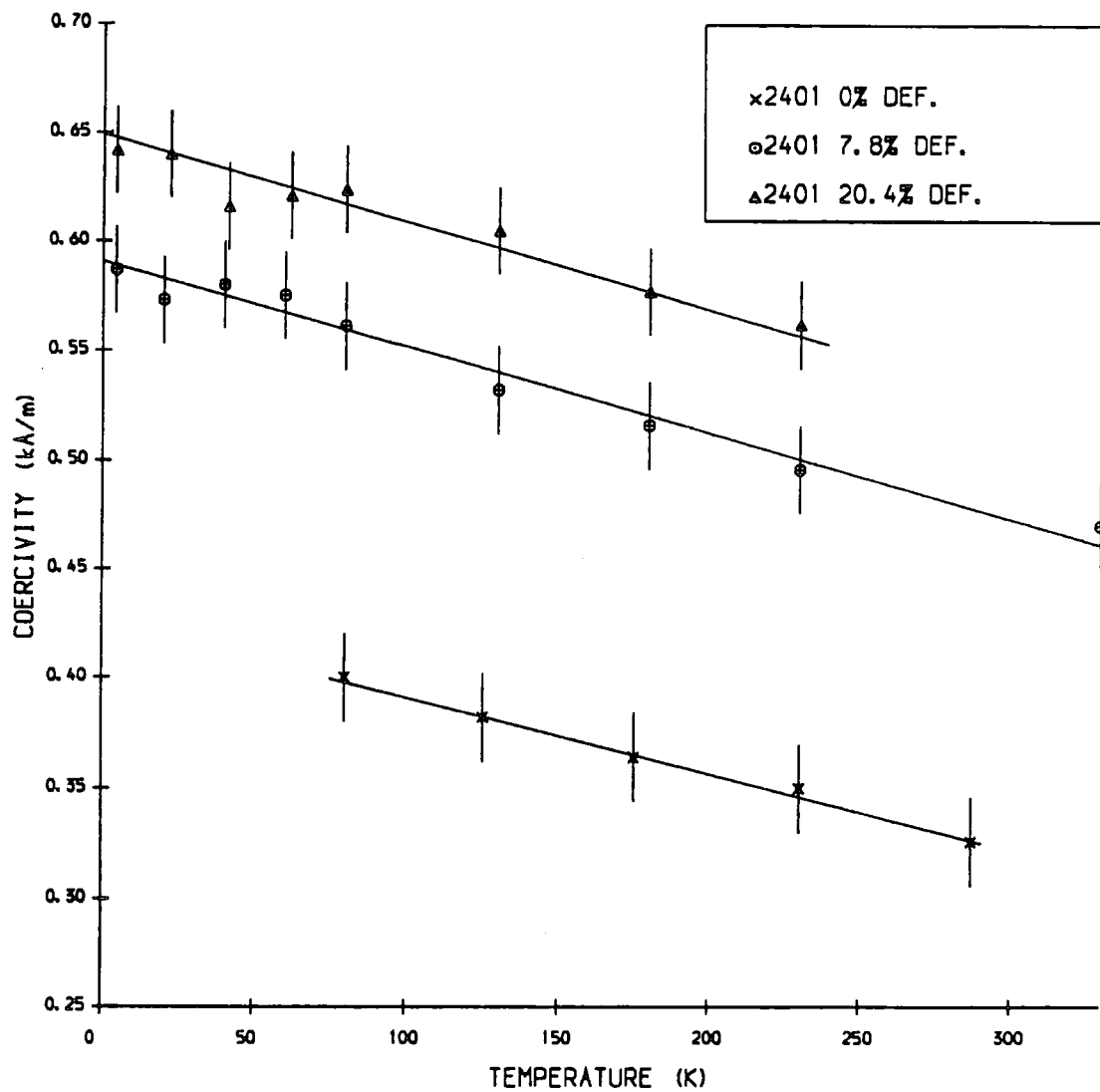
Figure 4.09 The Variation of Coercivity With Temperature for Three Values of Plastic Strain: 0%, 7.8% and 20%.
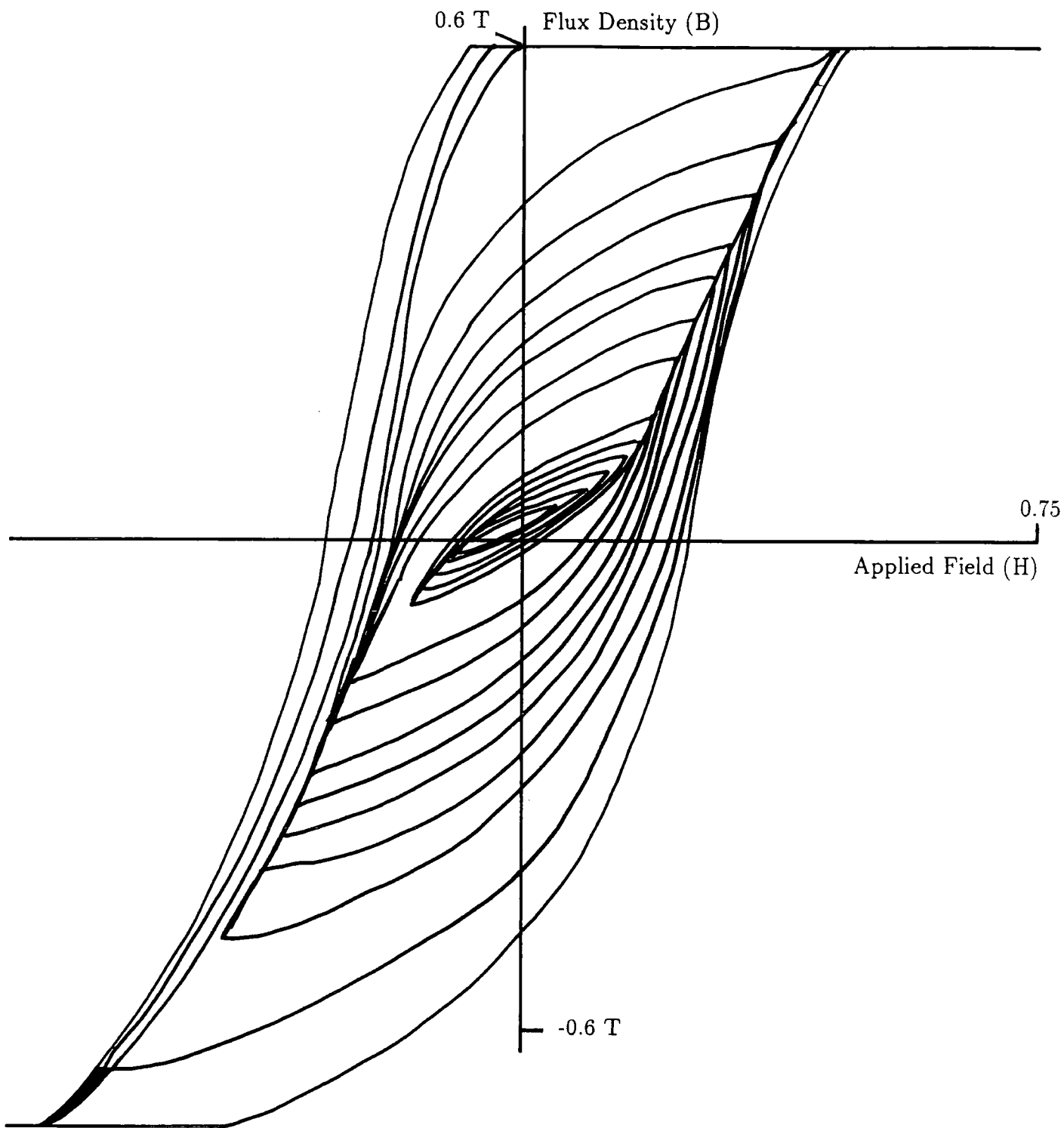
Figure 4.10a) Low Field Portion of Minor Loop Series for an Undeformed Sample.

87

Flux Density (B)

0.3 T

0.75

Applied Field (H)

-0.3 T
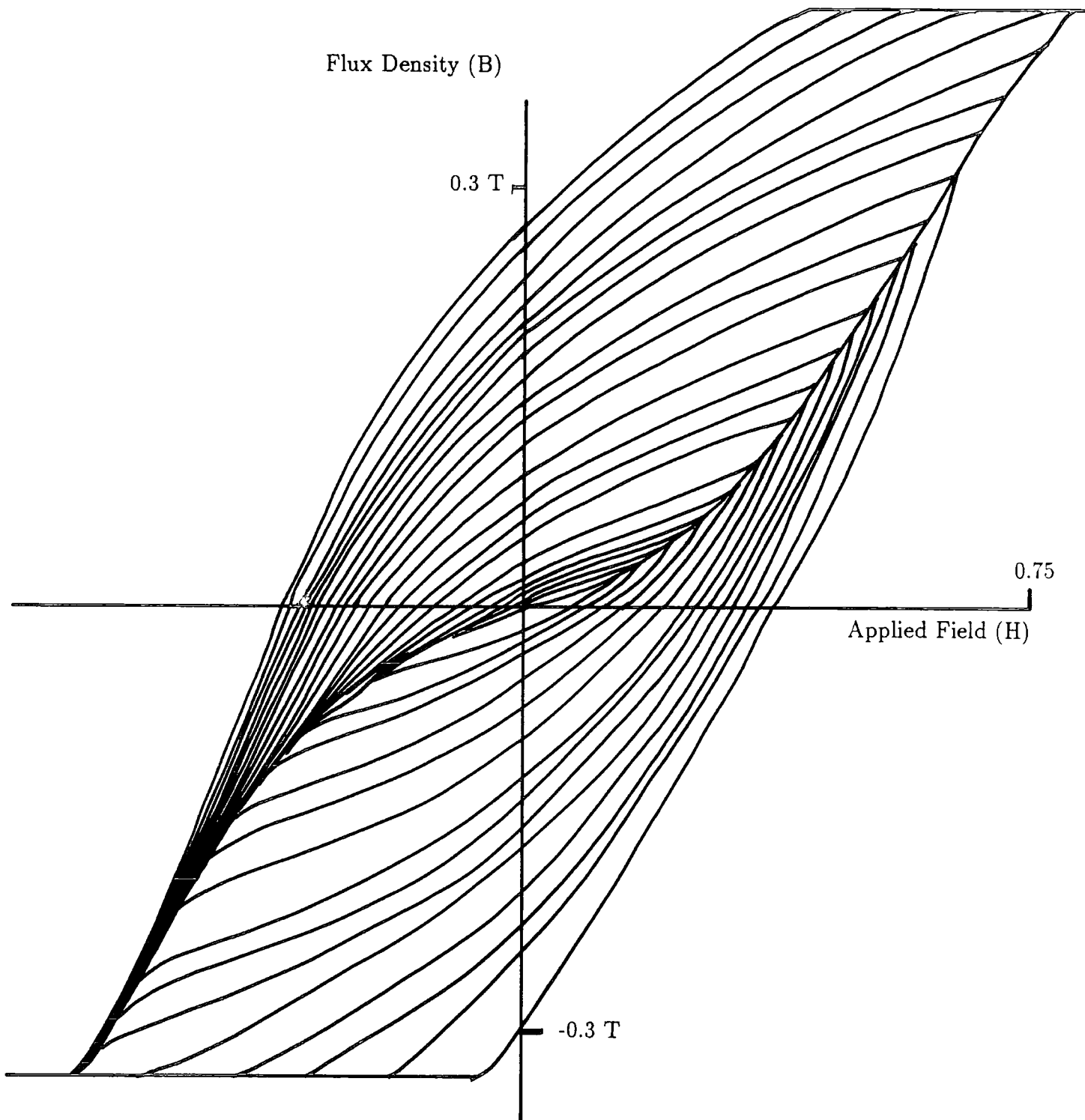
Figure 4.10b) Low Field Portion of Minor Loop Series for a 20% Deformed Sample.
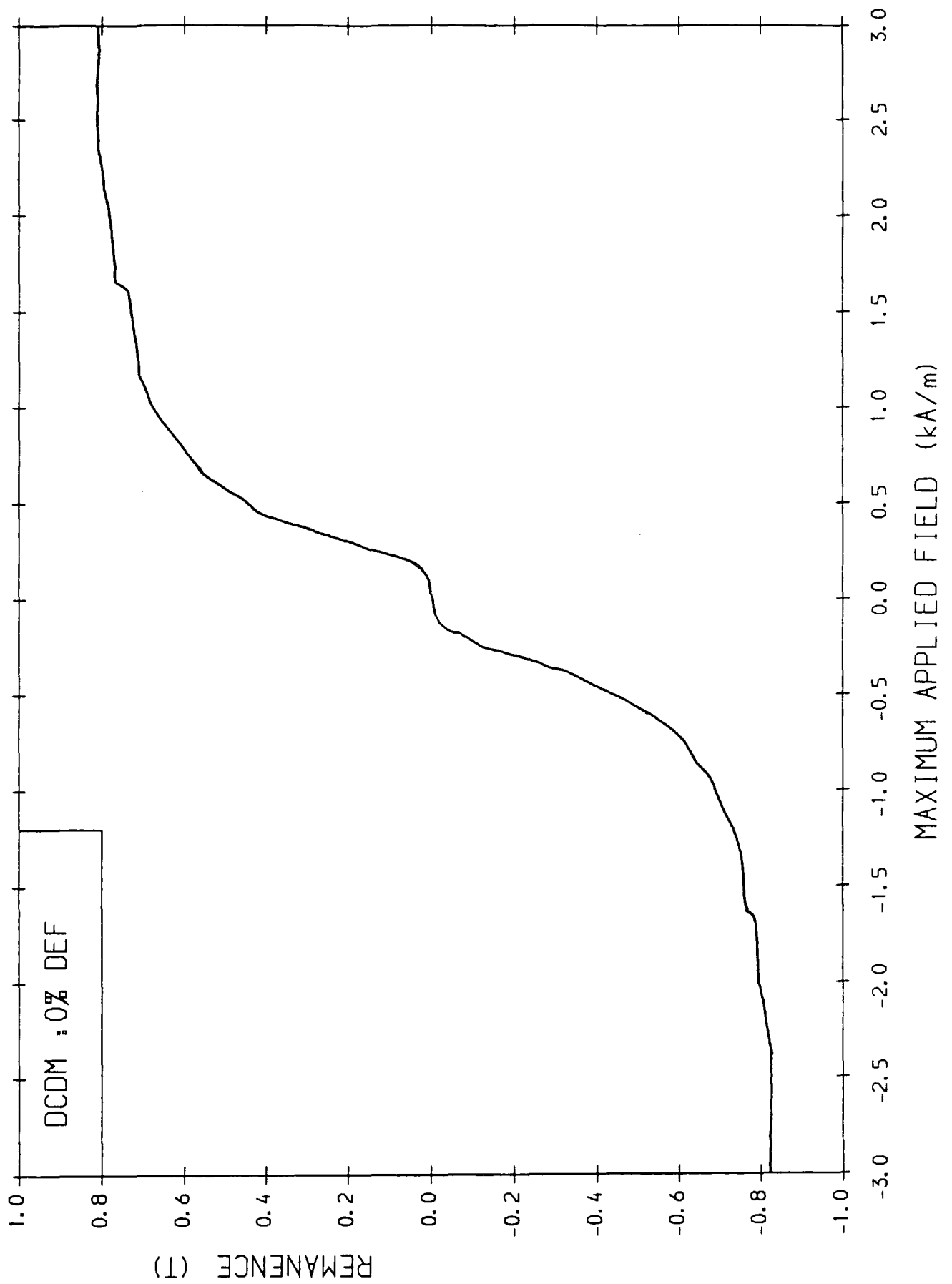
Figure 4.11 The Variation of Remanence With Maximum Applied Field (D.C.D.M.) For an Undeformed Sample.
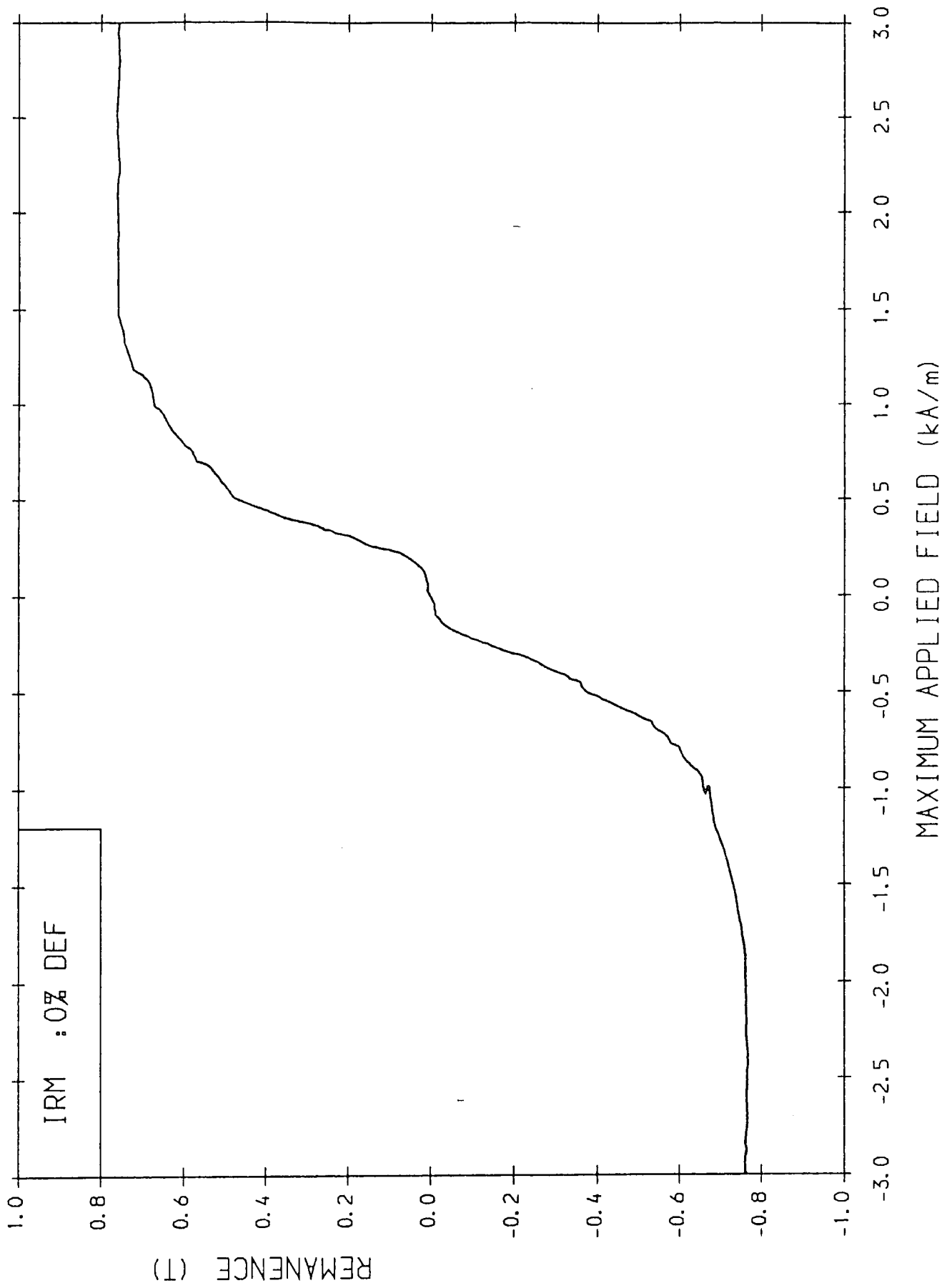
Figure 4.12 The Variation of Remanence With Maximum Applied Field (I.R.M.)
For an Undeformed Sample.
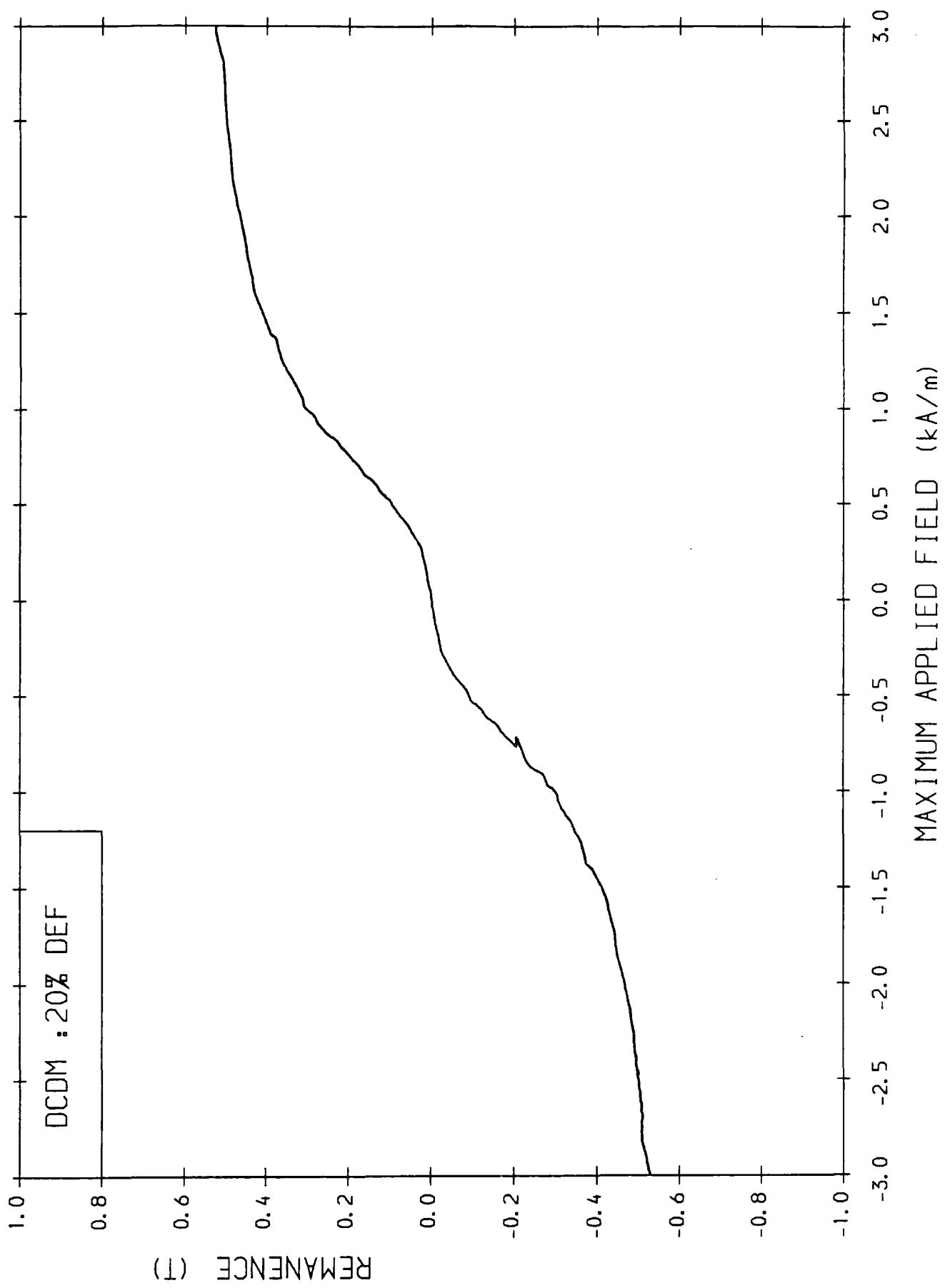
Figure 4.13 The Variation of Remanence With Maximum Applied Field (D.C.D.M.) For a 20% deformed Sample.

The plot is labeled DCDM :20% DEF. The x-axis is MAXIMUM APPLIED FIELD (kA/m) ranging from -3.0 to 3.0. The y-axis is REMANENCE (T) ranging from -1.0 to 1.0.
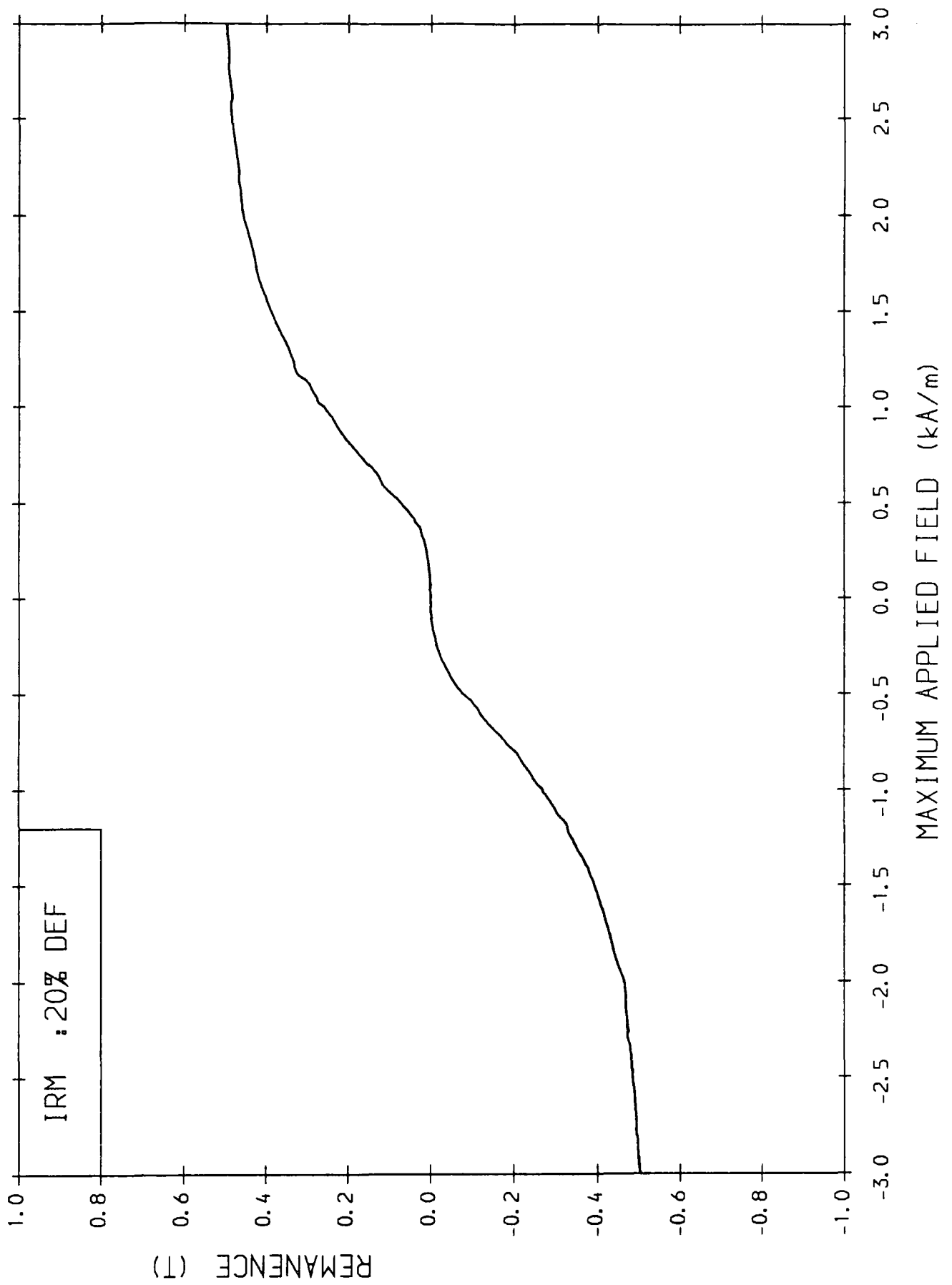
Figure 4.14 The Variation of Remanence With Maximum Applied Field (I.R.M.)
For a 20% deformed Sample.

92
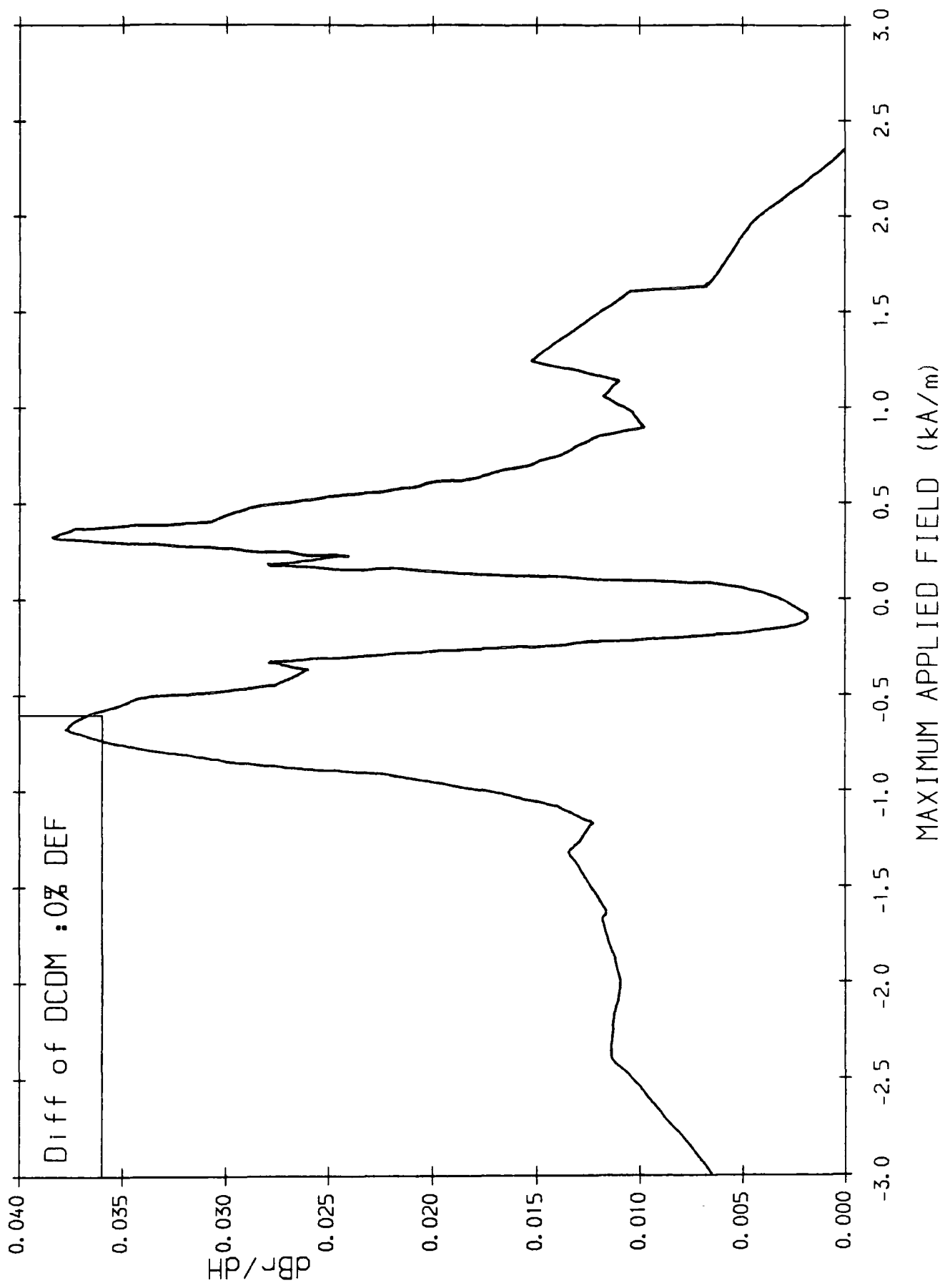
Figure 4.15 Differential of (D.C.D.M.) for Undeformed Sample.
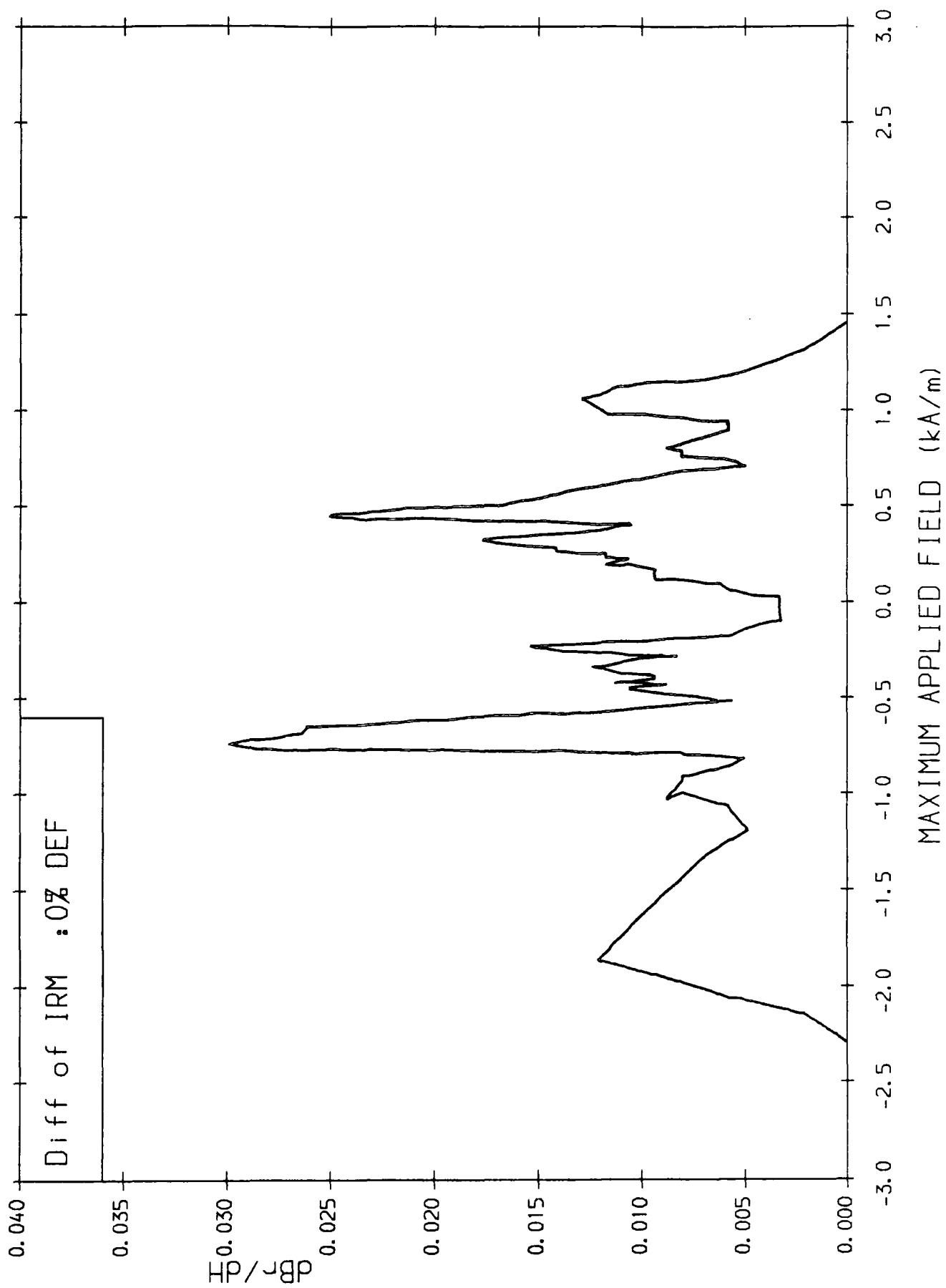
Figure 4.16 Differential of (I.R.M.) for Undeformed Sample.
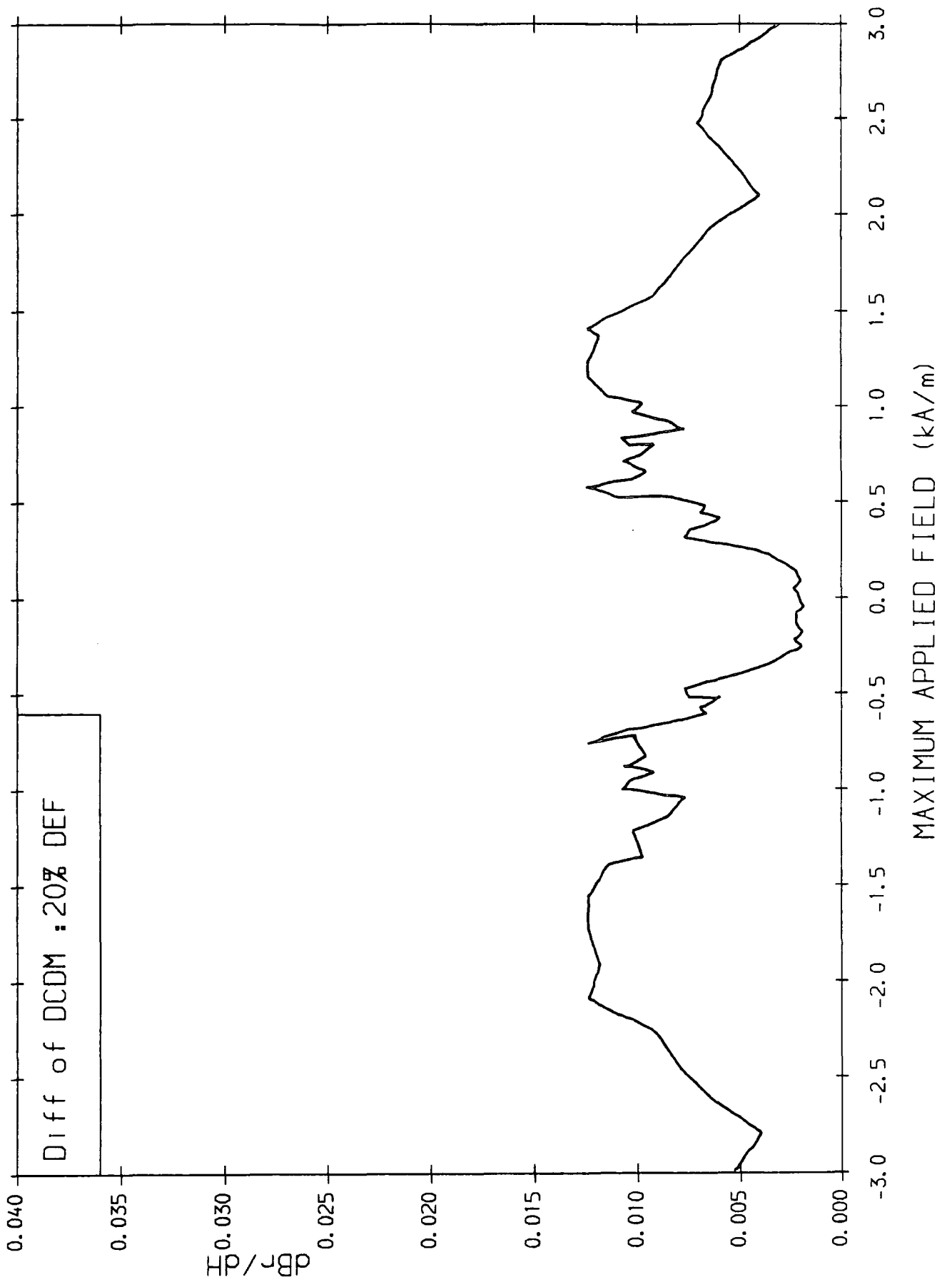
Figure 4.17 Differential of (D.C.D.M.) for 20% Deformed Sample.
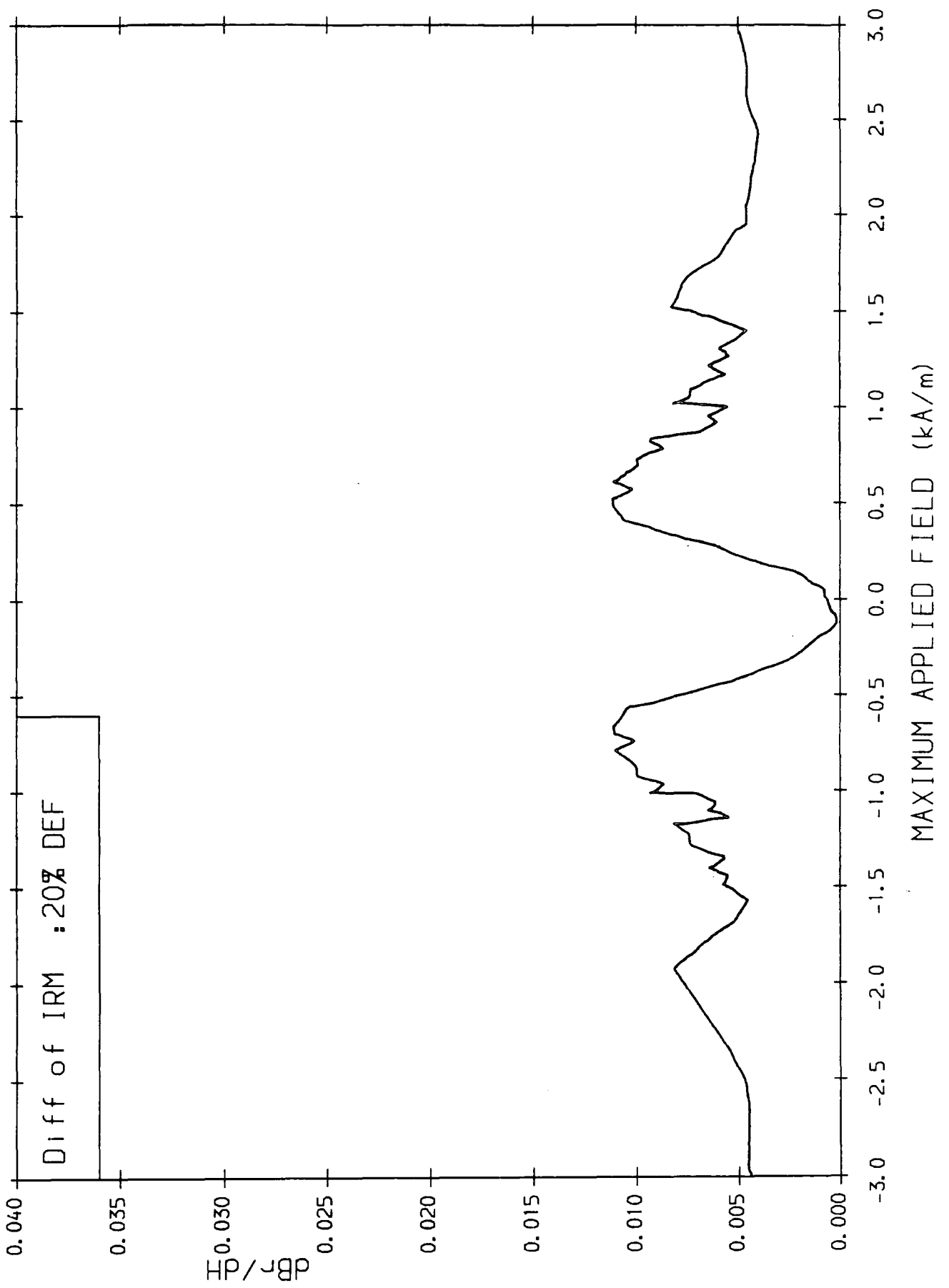
Figure 4.18 Differential of (I.R.M.) for 20% Deformed Sample.

96

4.5 Barkhausen Noise.

The Barkhausen noise of all the samples was recorded to further the investigations of A.J. Birkett (1985) into using the power spectra of the Barkhausen noise to characterise the magnetic properties of steel samples to include the effects of plastic deformation. The existing PET controlled Barkhausen noise detection system was used, dividing the 5 second half-loop into four sections and sampling at $31\mu s$ intervals. The calculation of the power spectra was carried out by Dr. Birkett after the data had been transferred to the NUMAC mainframe computer. The zero frequency intercept of the power spectrum decreased with plastic deformation as shown in figure 4.19.

4.6 Electron Microscopy.

A range of samples were studied using High Voltage Lorentz Electron Microscopy to observe the way in which the plastic deformation directly affects the domain configuration and subsequent domain wall movement under an applied field. The studies were undertaken using the EM7 High Voltage Electron Microscope at Oxford University using the Lorentz stage and for half the time with the magnetising coils in situ. Both the Fresnel and Foucault methods of domain wall imaging were used when no field was applied, but the delicate adjustment of the objective aperture necessary for Foucault imaging was found to be impractical when simultaneously applying a field as this in turn moves the image relative to the aperture. With no applied magnetic field the domain configuration was studied in all the samples in both ferrite and pearlite grains. With the magnetising coils in situ a magnetic field could be applied in a specific direction so as to encourage a particular domain in view to grow or contract and hence observe the change in domain configuration and movement of the domain wall through a minor hysteresis loop.

Domain configurations in the ferrite grains of the undeformed samples were usually uncomplicated and where a complex domain pattern was observed it often disappeared on the application of such low fields as $0.2kAm^{-1}$. Where the grains were relatively dislocation free the domain walls were straight but were influenced by the presence of ferrite-ferrite grain boundaries. Walls perpendicular to such

97
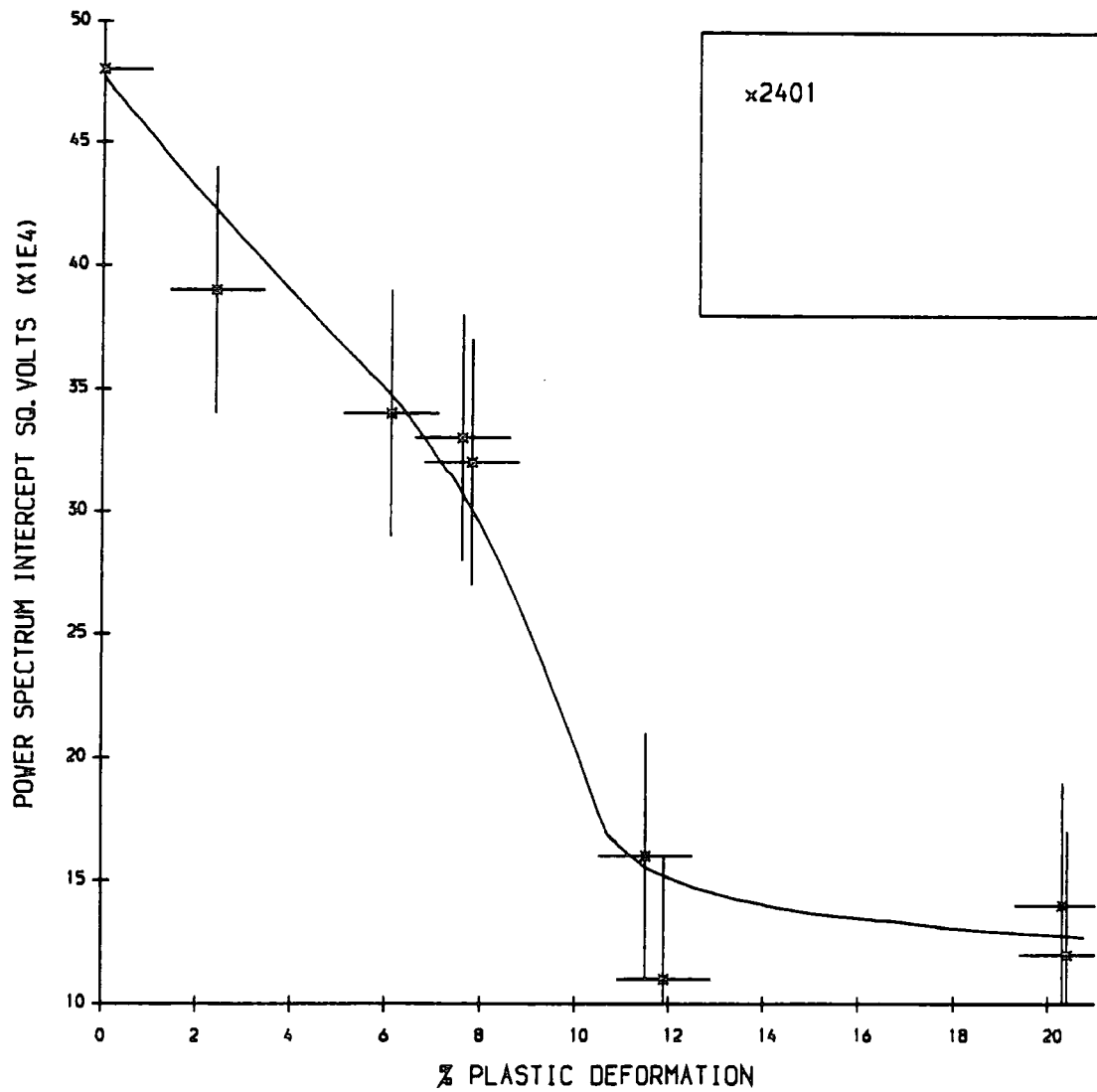
Figure 4.19 The Variation of the Zero Frequency Intercept of the Barkhausen Power Spectrum with Plastic Deformation.

98

boundaries were little affected, but when parallel were quite strongly pinned sometimes diverting a wall so that the nearest section could lie parallel to the boundary. The domain configuration and movement was dominated by the presence of the pearlite. The walls in the ferrite often formed closure domains onto large pearlite grains as shown in the Fresnel micrographs of figure 4.20 a) and b) and the walls themselves were often seen to splay at their actual point of contact with the grain. On the application of a field parallel to the main walls the configuration moved fairly easily along the grain. Domain walls were observed inside the pearlite grains running both parallel and perpendicular to the lamellae. Parallel walls can be seen in figure 4.20, such walls proved almost impossible to move with the maximum field available of $12kAm^{-1}$. Walls running perpendicular to the lamellae were both easier to see and to move under an applied field. The interior of a pearlite grain is shown in figure 4.21 where the individual cementite lamellae and dislocations in the ferrite are visible in the infocus micrograph . A number of perpendicular walls are visible in the accompanying fresnel pictures. The walls are affected by the presence of each lamellae giving it a disjointed undulating appearance and forming small closure domains onto some of the cementite lamellae as the wall is broken up along its length. Under an applied field some movement was observed with the wall retaining its overall orientation with the lamellae but not always remaining intact as the pinning effect varied across the grain. Small inclusions encountered in the direction of travel of a wall had a direct pinning affect restricting further movement until sufficient field was applied to overcome the pinning site.

Large areas of dense dislocation tangles were observed in all the deformed material. Walls running through these areas were no longer straight, but even with no applied field were curved or distorted. The sequences in figures 4.22 and 4.23 show regions of dislocated ferrite also including a ferrite-ferrite grain boundary. In both examples the affect of the overall configuration due to the grain boundary is evident by the closure domains that have formed and the bending of a wall so that it runs alongside the boundary. On a smaller scale the walls are affected by the presence of the dislocation tangles, some splaying is clearly visible in figure 4.22b) in the white wall pinned to the boundary, and none of the walls are straight along their length. A field was applied to the region illustrated in figure 4.22 before the photographs were taken in which the wall pinned to the boundary was initially

parallel to it before jumping across where it remained pinned for the rest of the magnetising sequence.

The way in which the domain walls moved was strongly affected by the presence of the dislocations. Smooth movement was no longer observed and was replaced by a series of domain wall bowing followed by release from the pinning sites. This situation is demonstrated in figure 4.24. The infocus micrograph shows the dislocation tangles and the ferrite grain boundary. In this case the walls are not affected by the boundary but are severely restricted by the high density of dislocation tangles. Figure 4.24b) is a fresnel micrograph taken in an applied field of $8.3kAm^{-1}$ in which strong bowing of the domain wall between pinning sites is observed before their release. This sequence has also been recorded on video.

It was rare to observe any domain movement at all at low fields in contrast to the undeformed sample where rapid domain rearrangement was often observed in this low field region. Less domain wall movement was observed within the pearlite grains than in the undeformed samples, and that that was appeared even more disjointed and difficult.

It was not possible to obtain good diffraction patterns in the limited microscope time available, but where movement in the region of a ferrite-ferrite grain boundary was being observed the diffraction pattern on either side of the boundary was observed to confirm that they were two distinct grains with different orientations.
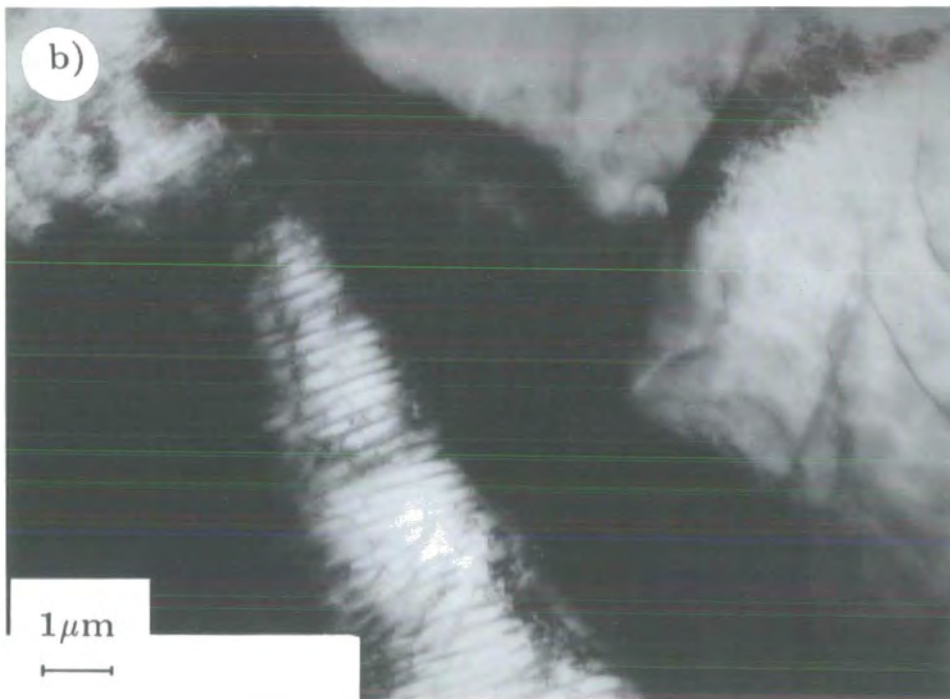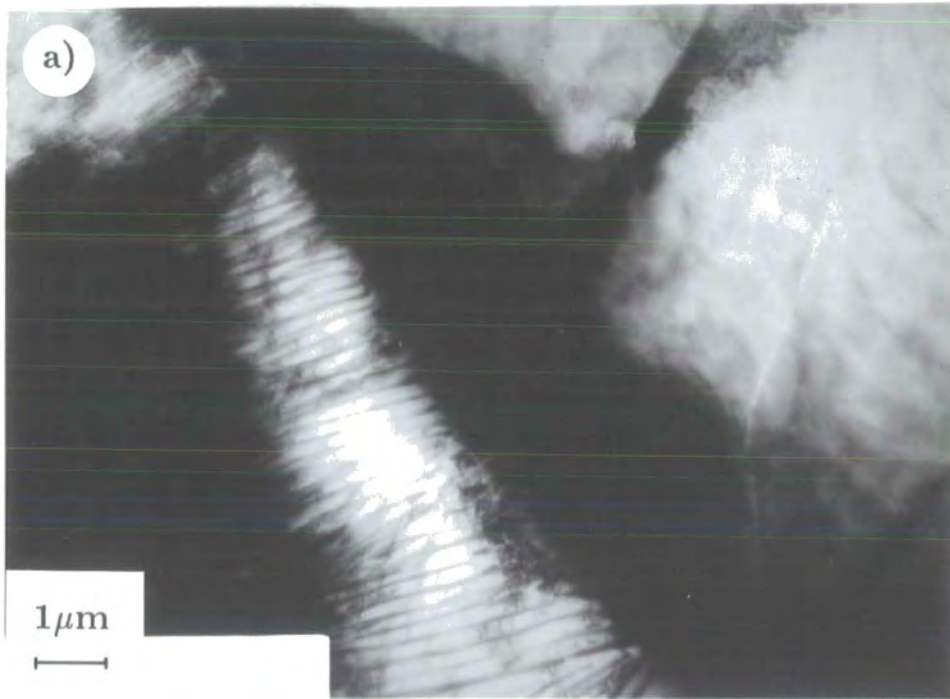
Figure 4.20 Fresnel electron micrographs of undeformed 2401 pipe steel : a) overfocus, b) underfocus.
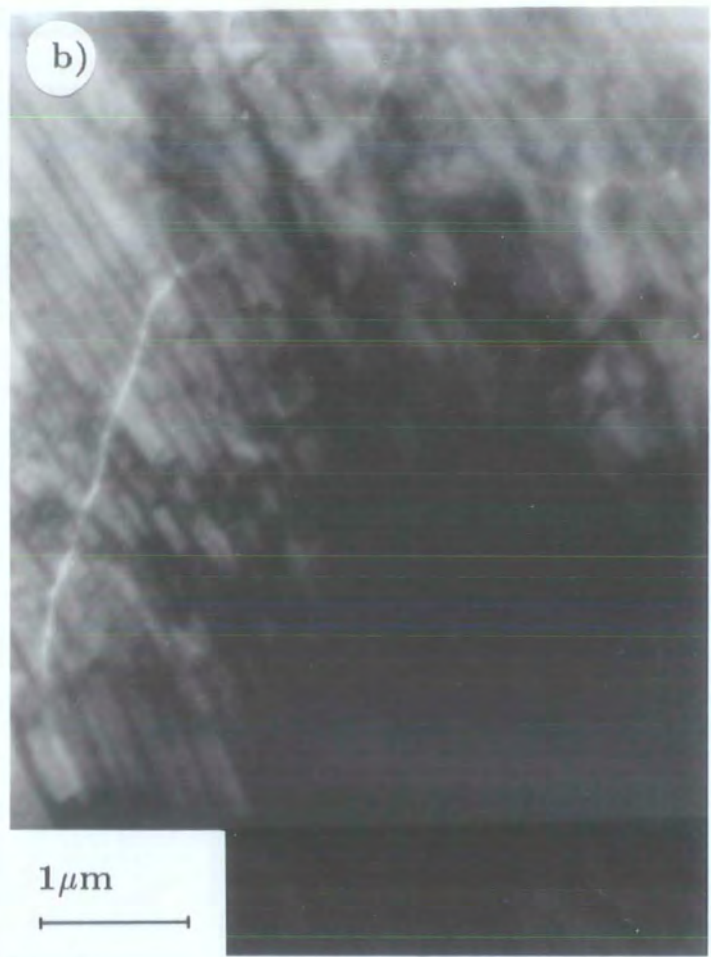
Figure 4.21 Fresnel electron micrographs of undeformed 2401 pipe steel : a) infocus, b) underfocus, c) overfocus.
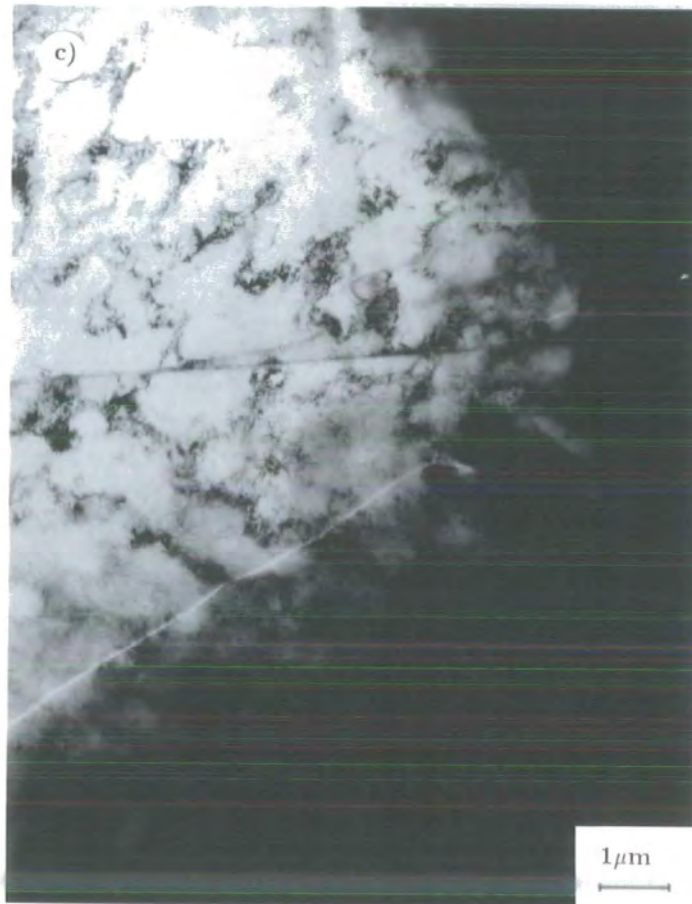
Figure 4.22 Fresnel electron micrographs of 20% deformed 2401 pipe steel : a) infocus b) underfocus, c) overfocus.
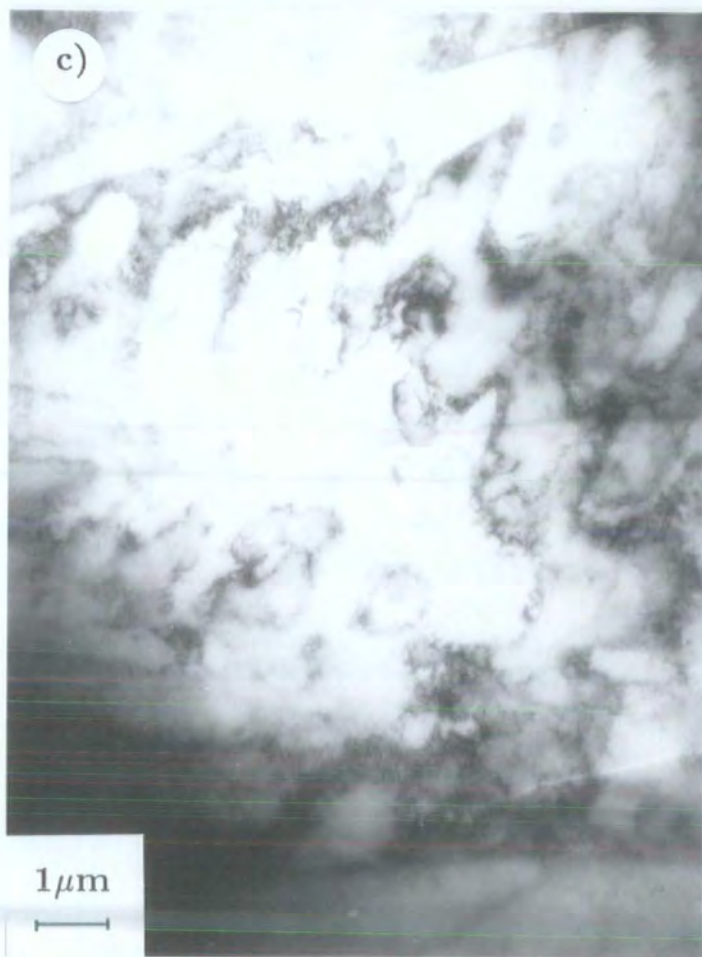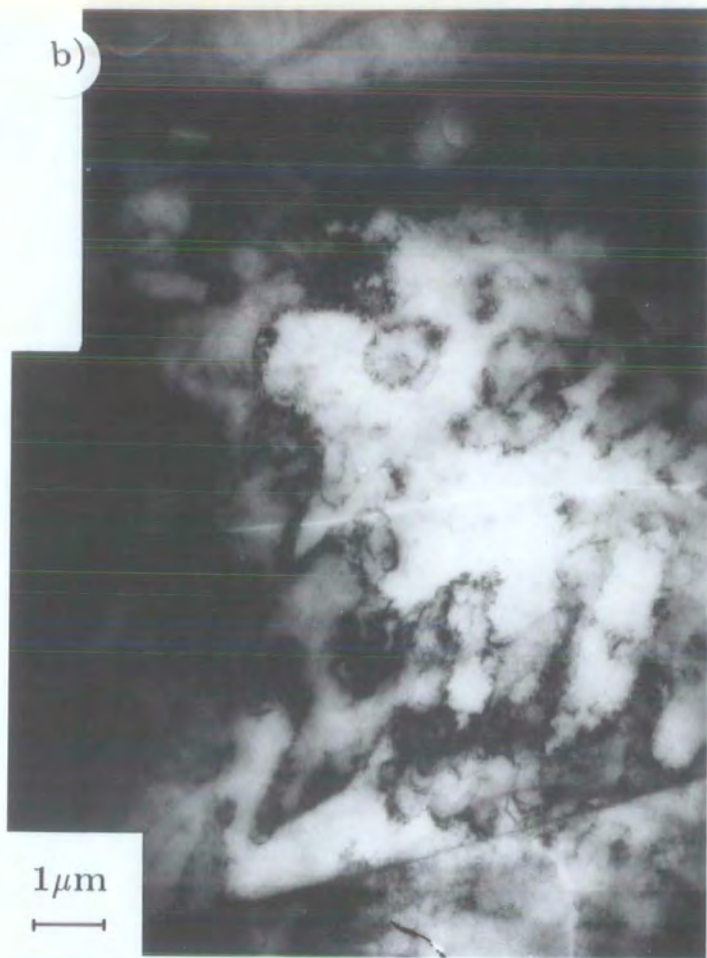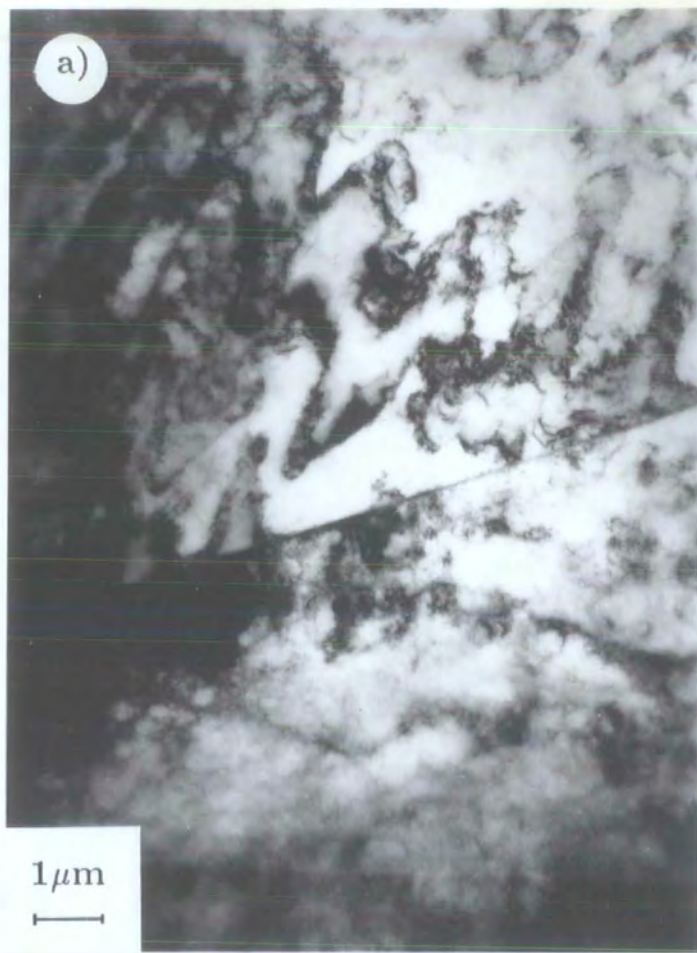
Figure 4.23 Fresnel electron micrographs of 20% deformed 2401 pipe steel : a) infocus b) underfocus, c) overfocus.
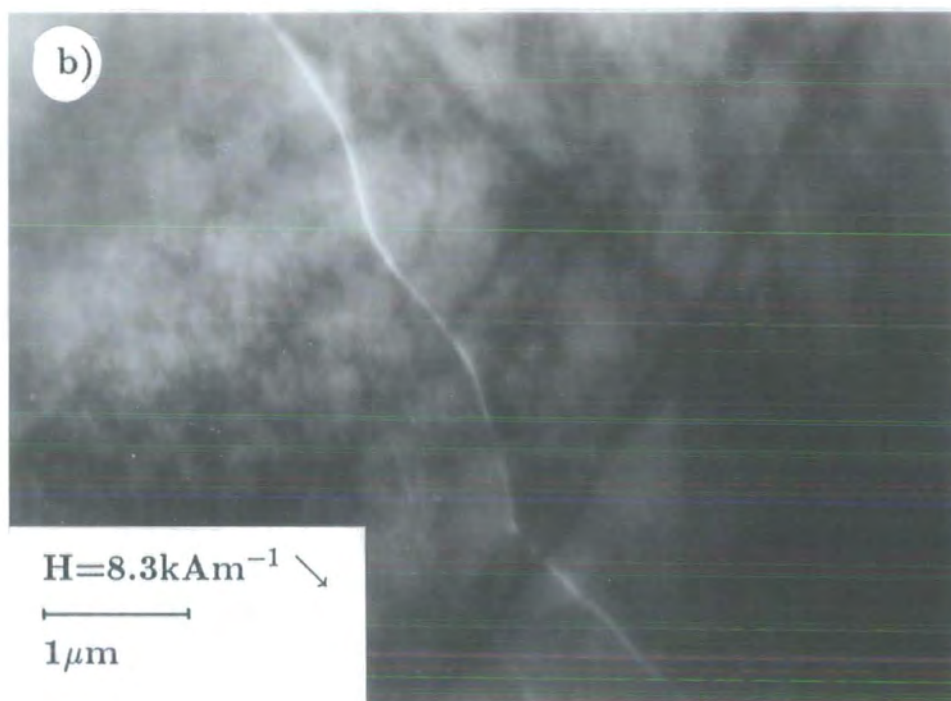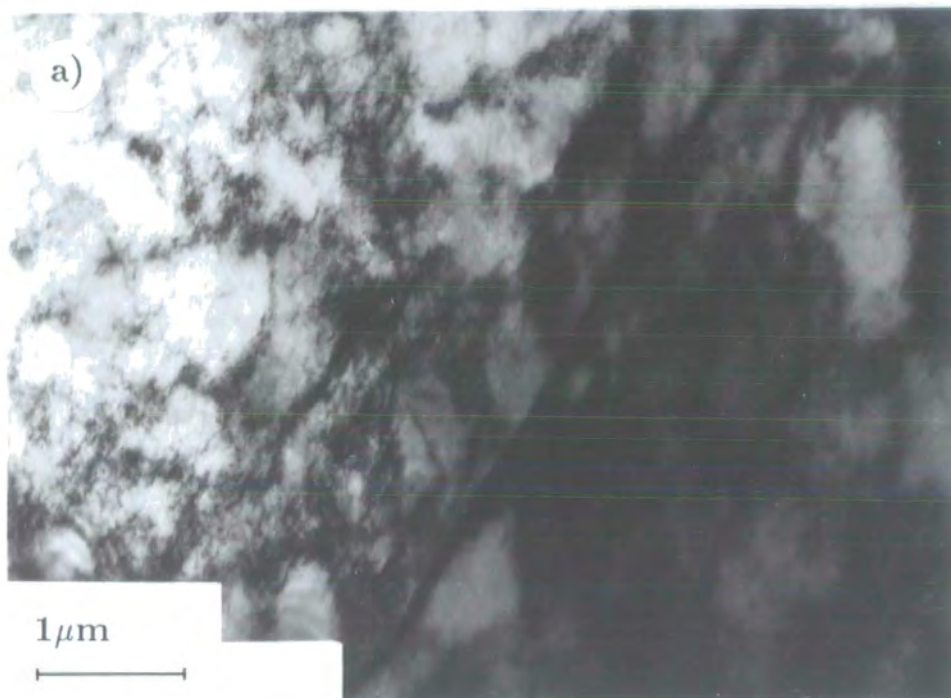
Figure 4.24 Fresnel electron micrographs of 7.8% deformed 2401 pipe steel : a) infocus, b) underfocus.

Chapter V

Experiments on Specially Prepared Steel.

5.1 Introduction.

As the iron-carbon system is very sensitive to added impurities, heat treatments and strain, it is difficult to separate these effects in the pipe-steel from the additional plastic strain subsequently induced. In order to investigate the independent effects of carbon content and heat treatment and their different responses to additional plastic deformation four batches of steel with nominal pearlite contents: 20%, 50%, 70%, 100% were obtained with additional heat treatment applied to some of the 20% pearlite bars. A similar series of experiments to those conducted on the pipe steel were carried out and the results of these experiments are recorded in this chapter.

5.2 Sample Details.

The four 10kg batches were manufactured at the Sheffield Metals Advisory Centre, under the supervision of Mr. A. Harvey, by the following process. The iron and excess carbon were heated under vacuum in an induction furnace with a small amount of argon added to reduce spitting; the excess carbon was then boiled off and the crucible left to cool in an argon atmosphere. Before any further treatment one gramme of the material was drilled from the billets and chemically analysed in a LECO Analyser in which the sample is heated in an induction furnace and the CO_2 and SO_2 emitted collected. The billet was then machined to a more uniform cylinder 730mm (2 7/8 inches) diameter 111mm (4 3/8 inches) long before extrusion at a temperature of 1175^oC to a bar approximately 3.35m long with a cross-section of 20mm x 10mm and air cooled. Seven or eight bars of length 440mm were then machined from the extruded metal to produce the bar samples as detailed in figure and table 5.1. The surface of the samples was prepared on a surface grinder operating at low speeds and making very shallow cuts in the presence of copious amounts of coolant.

106
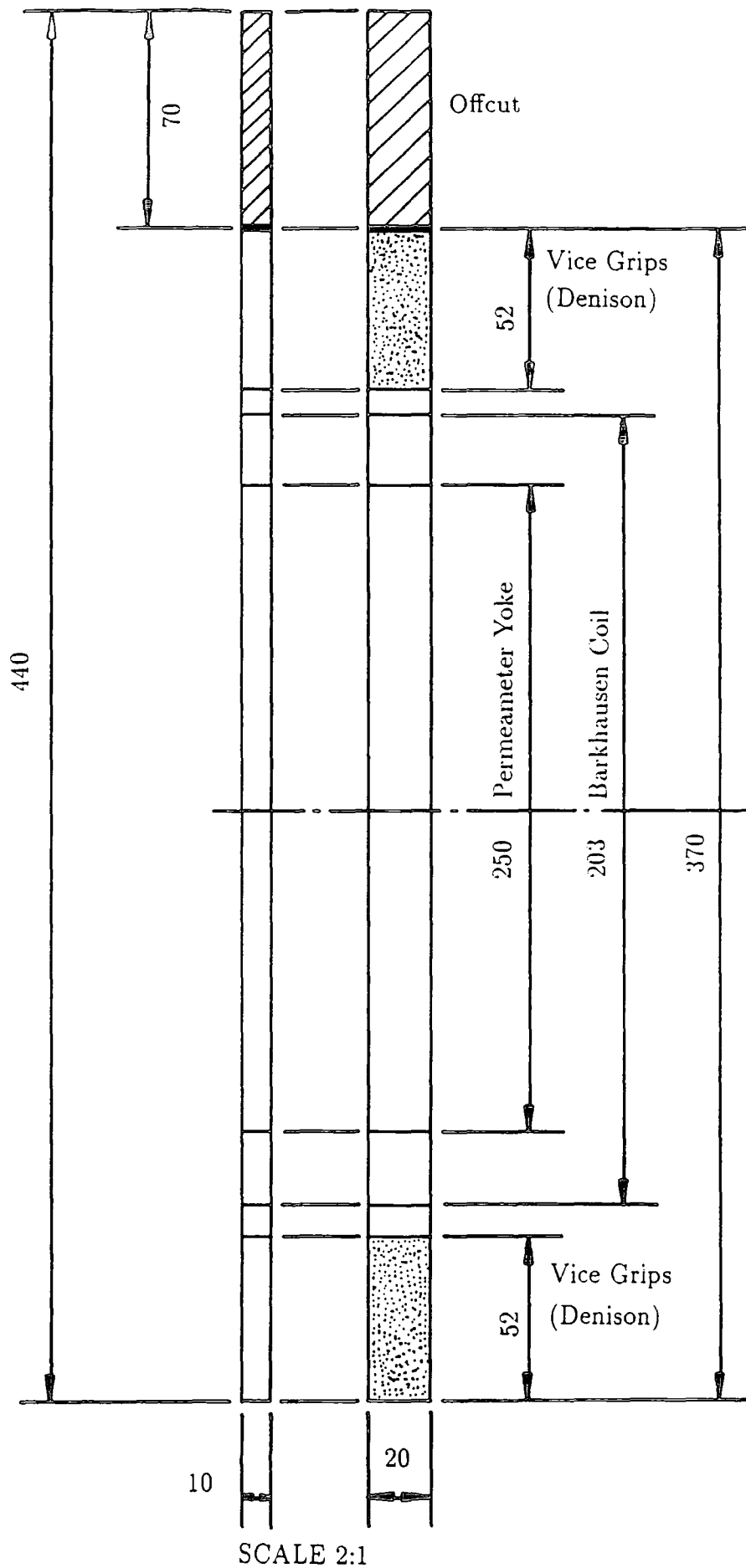
Figure 5.01 Details of the Bar Samples Showing Their Dimensions in Relation to the Various Types of Measuring Apparatus.

107

Steel batch	% Carbon	% Pearlite	% Sulphur
7091	0.17	19.5	0.003
7092	0.44	50.6	0.003
7093	0.67	77.0	0.003
7094	0.87	100	0.003

Table 5.01 Chemical Compositions of the Specially Prepared Samples.

5.3 Steel Properties prior to heat treatment.

The microstructure of each batch of steel was studied under an optical microscope at magnifications of ×100 and ×1000 and the micrographs are displayed in figures 5.02 and 5.03. At these magnifications non of the microstructures were affected by the subsequent plastic deformation. The relatively slow air cooling experienced by all the samples has resulted in quite a high transformation temperature and hence the pearlite is well dispersed and some coherent interfaces have formed.

In the 7091 ×100 micrograph the outline of the previous austenite grains is clearly visible due to the lath-like growth of both the ferrite and pearlite inwards from the grain boundaries. This structure is similar to that found in the heat-affected zone of welded samples which also experiences slow cooling. At the higher magnification the dark regions are confirmed to be lamellar pearlite accompanied by some smaller pearlite grains. Although it is not practical to define a grain size for such a microstructure the domain walls will be affected by the pearlite-ferrite boundaries and the size of these "grains" rather than the larger scale austenite boundaries.

The 7092 micrographs show a similar microstructure to 7091 with the outline of the austenite grains still visible. The microstructure is cellular with the proeutectoid ferrite enclosing the pearlite colonies. The pearlite within the colonies is denser than in 7091 and little of the interior structure can can be determined until the higher magnification picture is studied. There is quite a wide variation of lamellae spacing and orientation within the nodules and some of the cementite
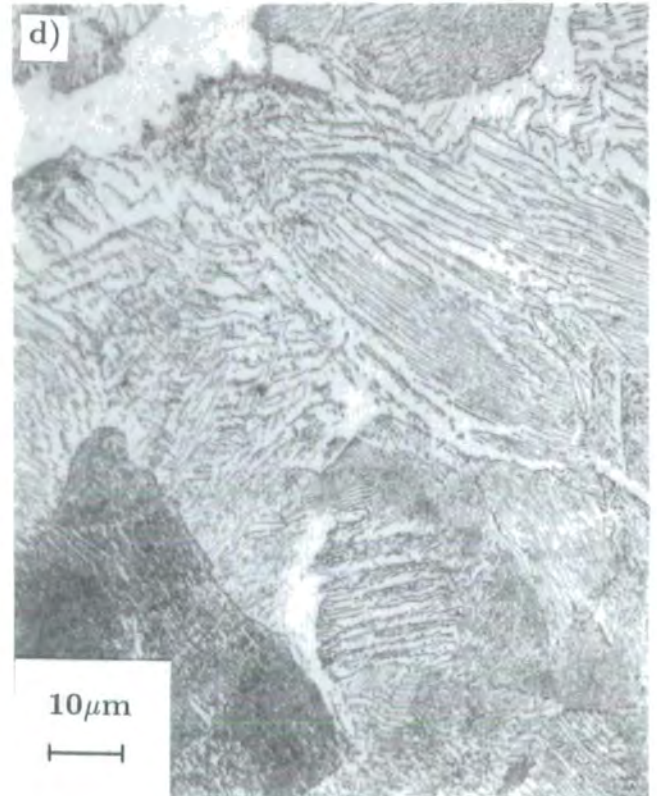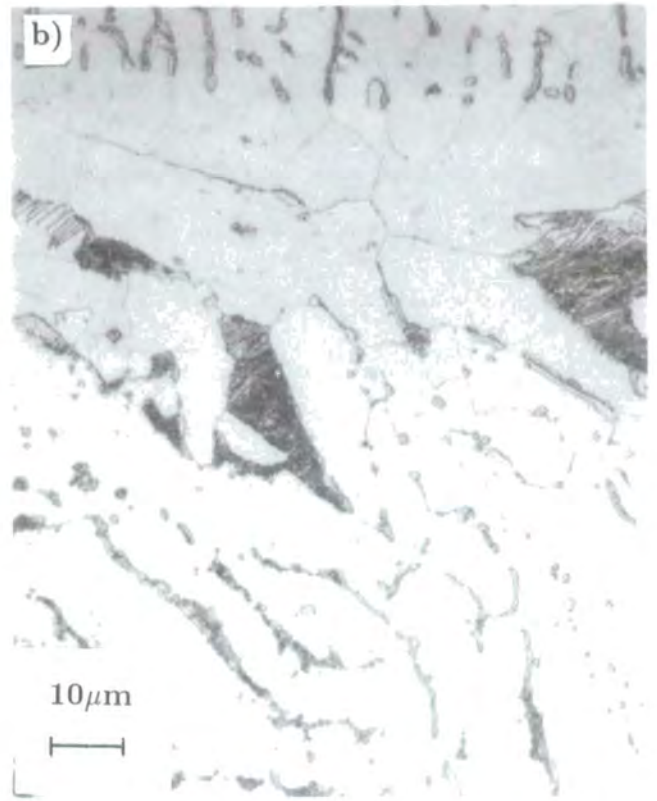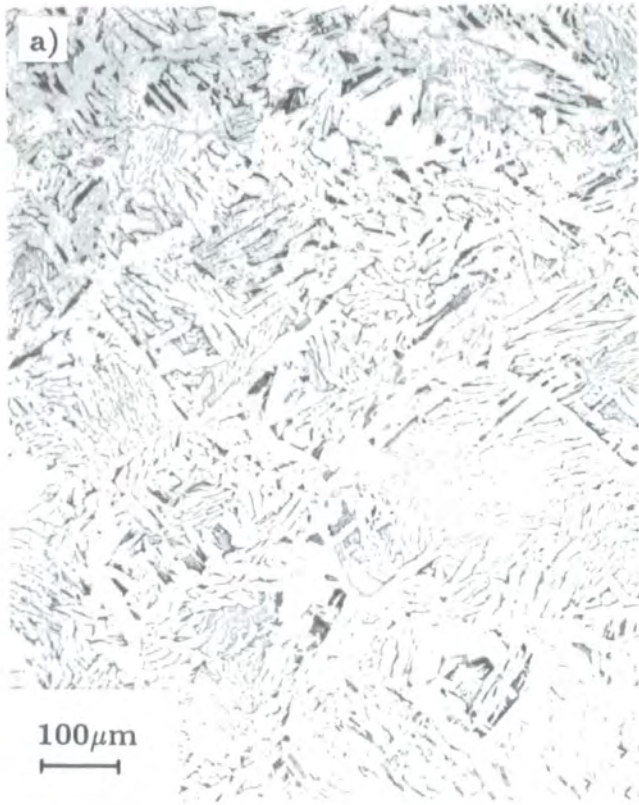
Figure 5.02 Optical micrographs of undeformed steel : a) 7091 ×100, b) 7091 ×1000, c) 7092 ×100, d) 7092 ×1000.
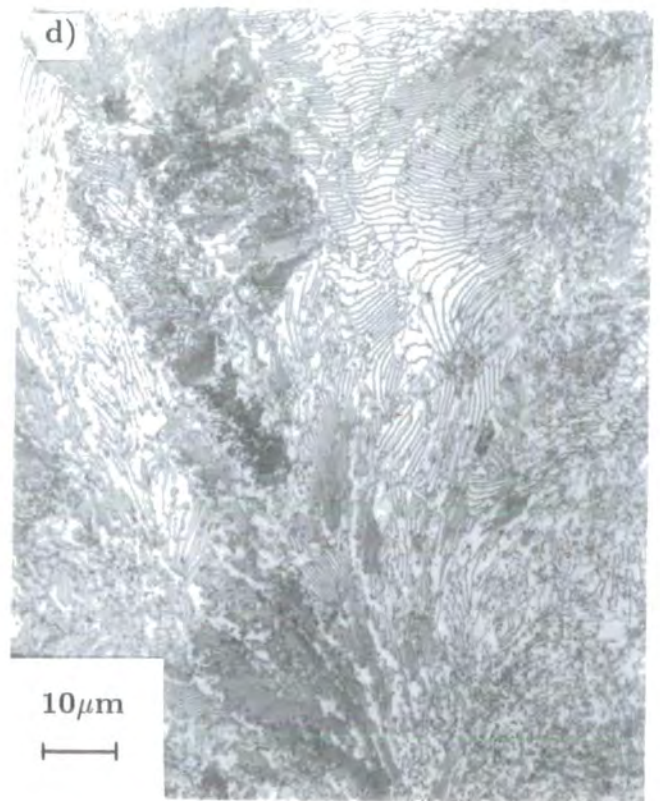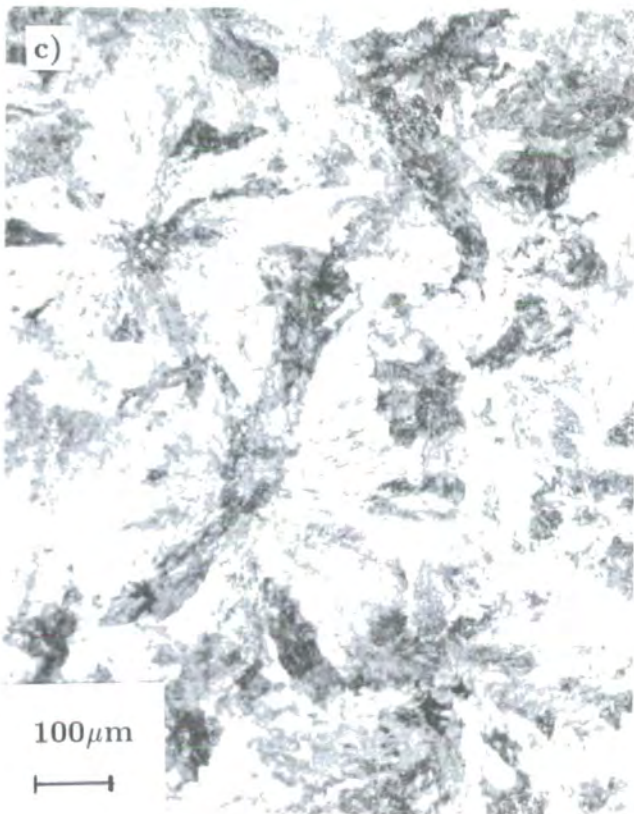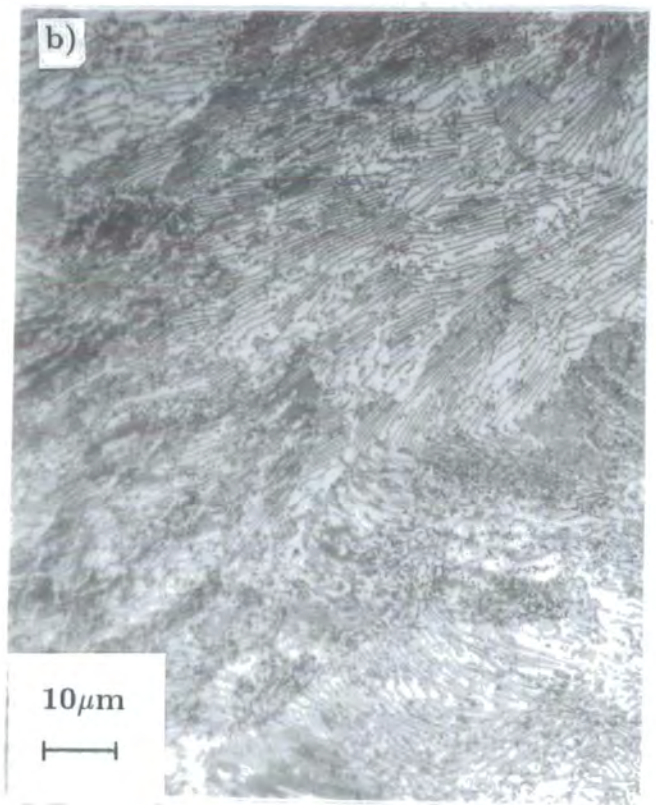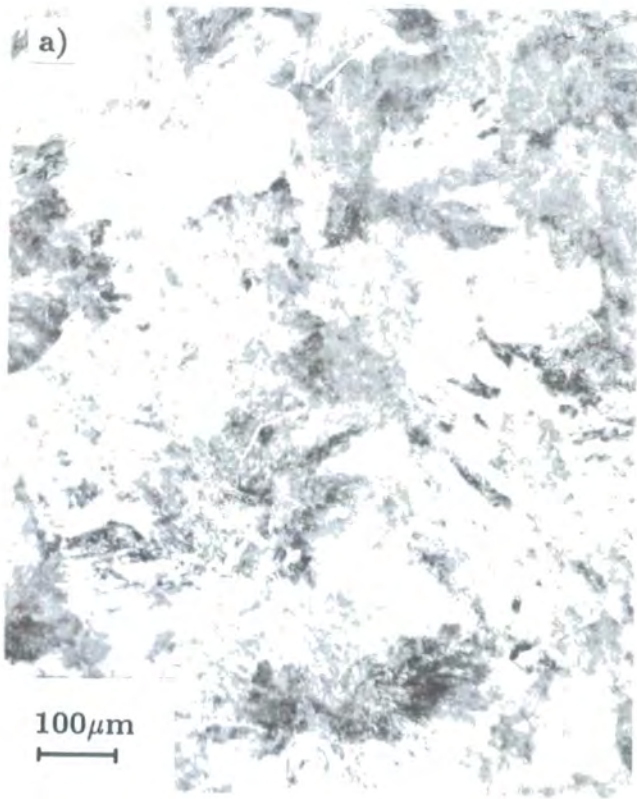
Figure 5.03 Optical micrographs of undeformed steel : a) 7093 ×100, b) 7093 ×1000, c) 7094 ×100, d) 7094 ×1000.

appears to be divorced.

The microstructures of 7093 and 7094 in figure 5.03 are very similar the only difference being the higher carbon content in the latter. Both samples appear to be almost entirely pearlite although some free ferrite is visible in both materials. The growth of the pearlite inwards from the austenite grain boundaries results in the "star-like" appearance of the microstructure on the ×100 scale. The ×1000 micrographs reveal the lamellar nature of the pearlite within which there is again a wide variation of lamellar spacing, colony size and divorced pearlite.

From each 440mm bar a 70mm section was initially removed so that a toroid and some 2.3mm discs could be extracted for further analysis of the undeformed properties. The 500kN Denison tensile testing machine in the School of Engineering and Applied Science at Durham University was used to plastically deform the samples up to plastic strains of 11%, example stress–strain curves are presented in figure 5.04. After deformation the Barkhausen noise from the samples was recorded, their Vickers Hardness (HV10) measured and their magnetic properties determined using the British Gas permeameter. If subsequent deformation was not required then a toroid and discs were extracted from the bar for further analysis and where applicable thinning in preparation for Lorentz Electron Microscopy. The restriction of the number of low carbon steel samples available necessitated redeforming the 7091 samples after each stage.

5.3.1 Bulk Magnetic Properties.

The yoke permeameter at British Gas was used to measure both the initial magnetisation and hysteresis curves of all the samples and hence determine the affect on the magnetic properties of the steel with increasing residual strain. A summary of these results follows in table 5.2 with the full details in Appendix B.

The bars were first measured in their initial, undeformed state from which the variation of the properties with carbon content could be studied. The expected increase in hardness is plotted in figure 5.05. The initial magnetisation curves for each of the four batches are plotted together in figure 5.06 illustrating the increasing magnetic "hardness" as the carbon content is increased. This trend is revealed by the decrease in maximum relative permeability μ_{max} and increase in the field
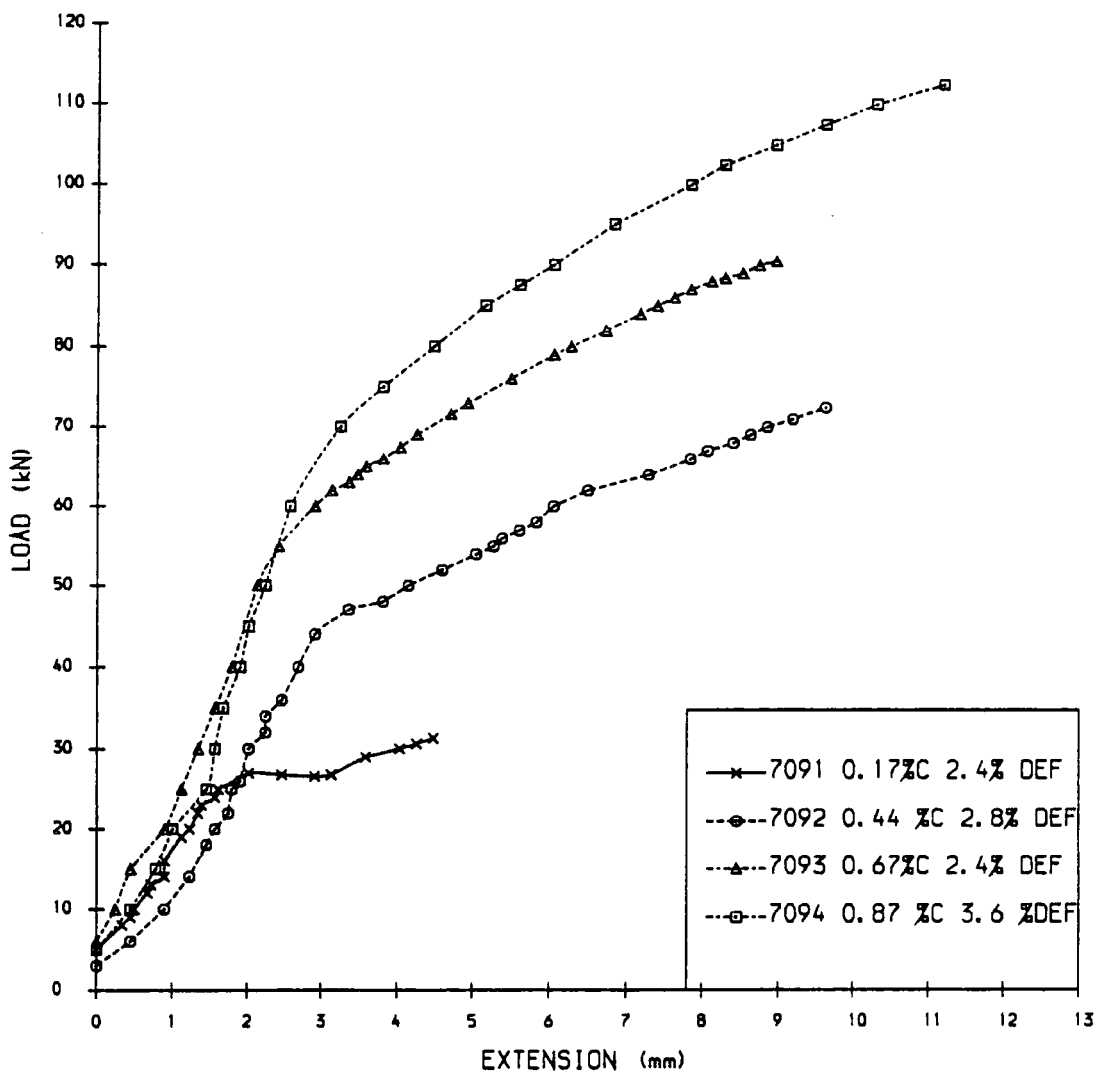
Figure 5.04 Load vs. Extension Curves for a Sample of Each Carbon Content
Deformed to a Nominal 3% Plastic Strain.

112
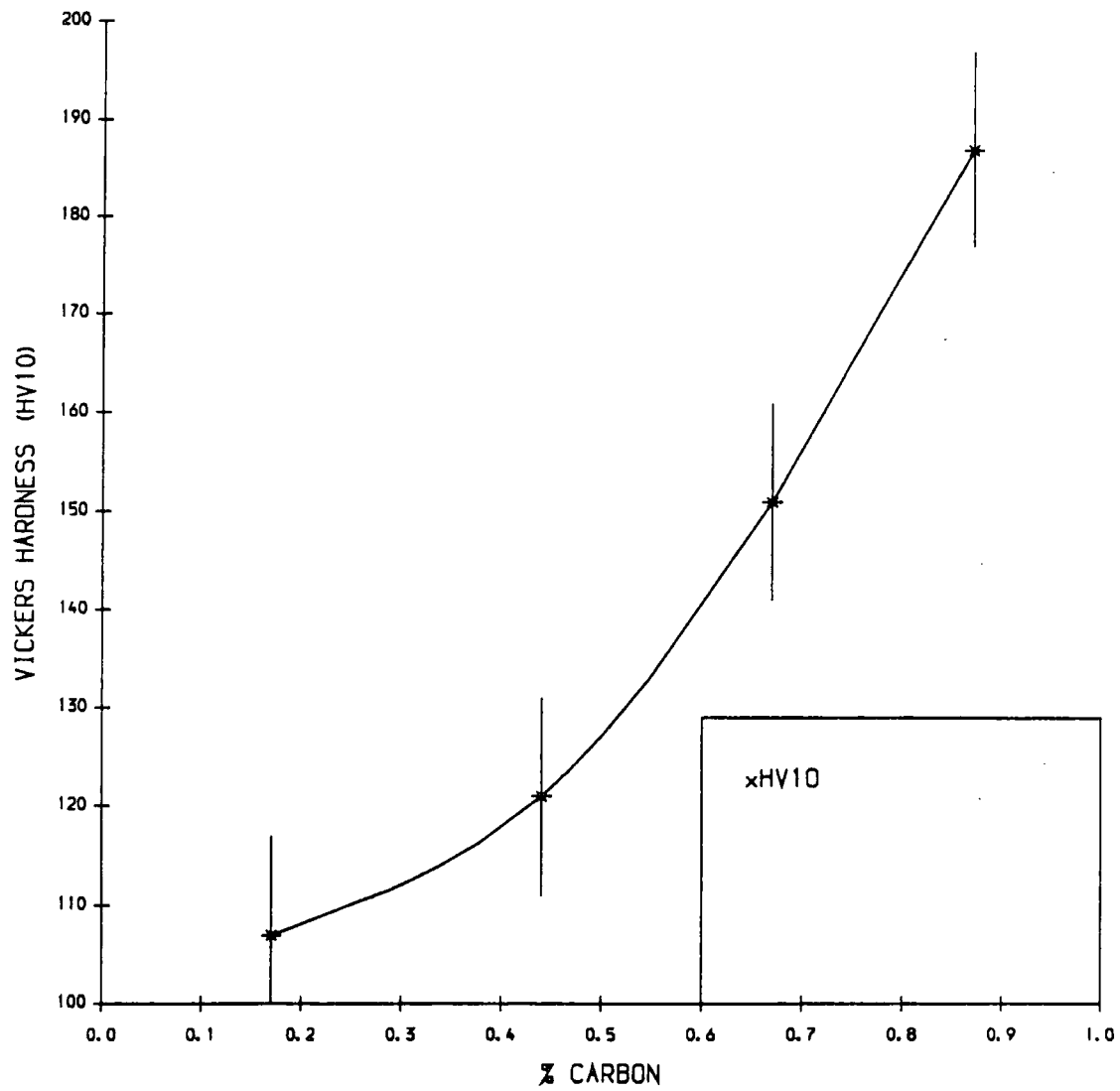
Figure 5.05 The Variation of Vickers Hardness With Carbon Content.

113
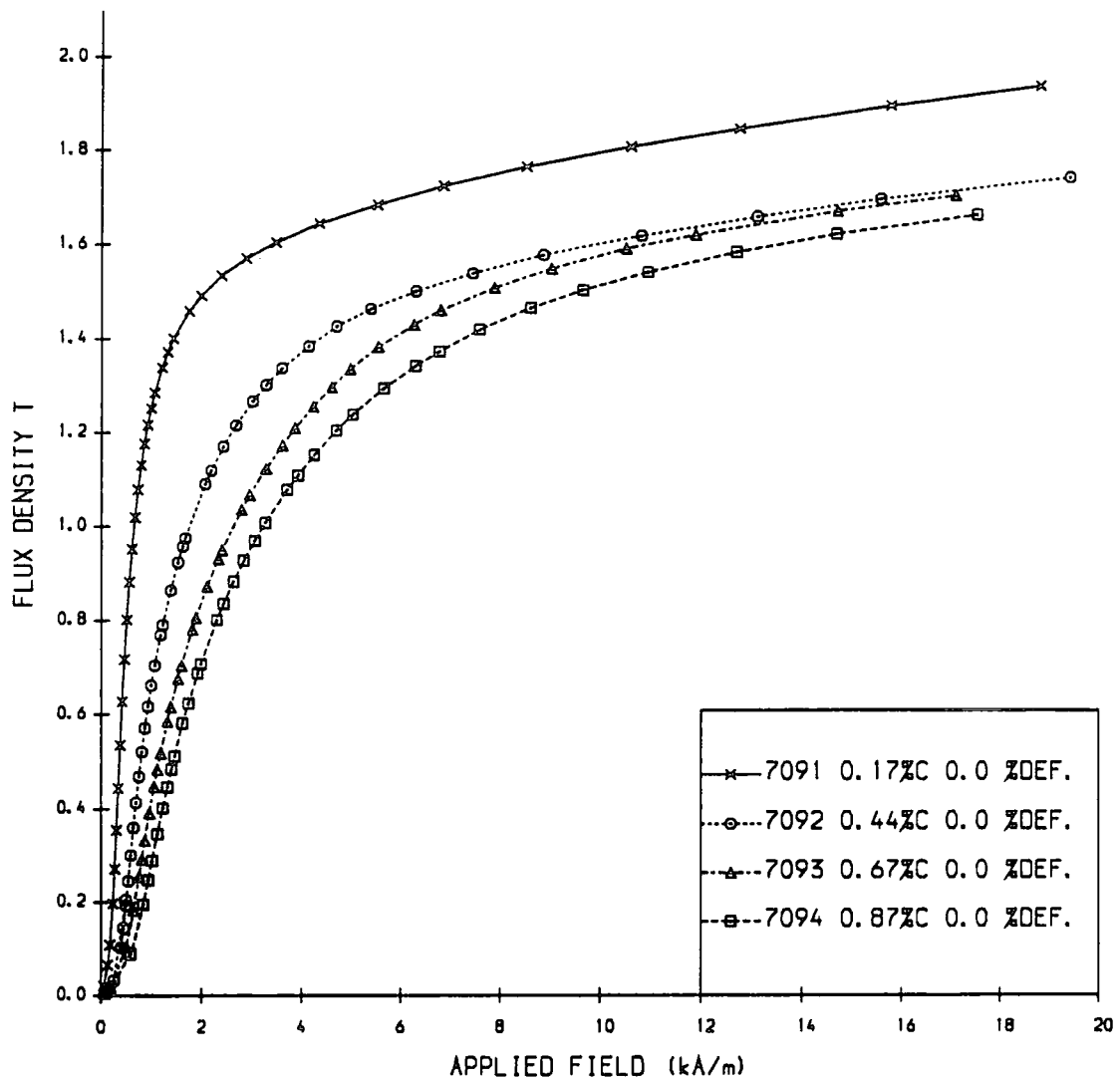
Figure 5.06 Initial Magnetisation Curves For an Undeformed Sample of Each Carbon Content.

114
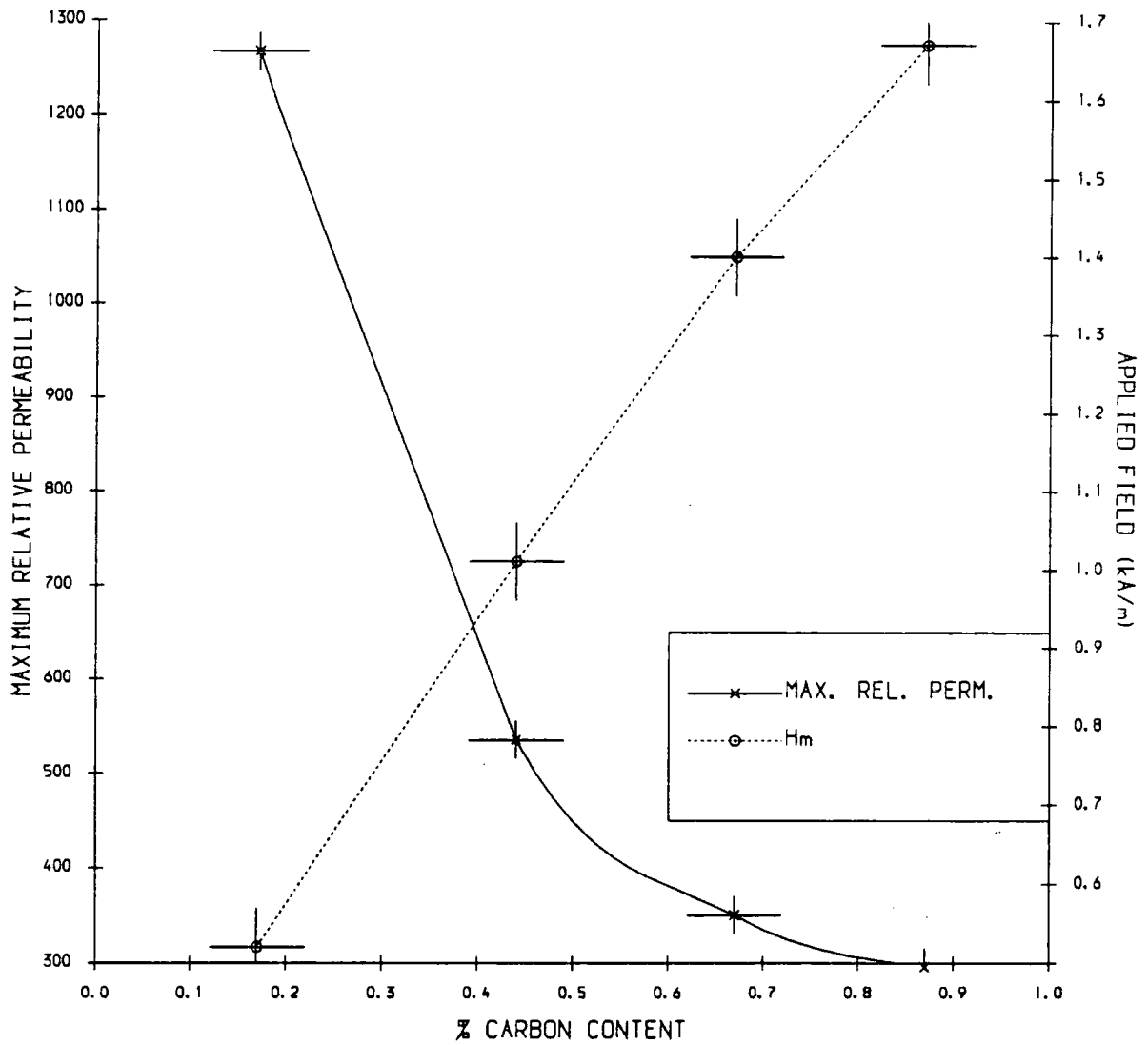
Figure 5.07 The Variation of Maximum Relative Permeability and the Field Hm
at Which This Occurrs With Carbon Content.

115
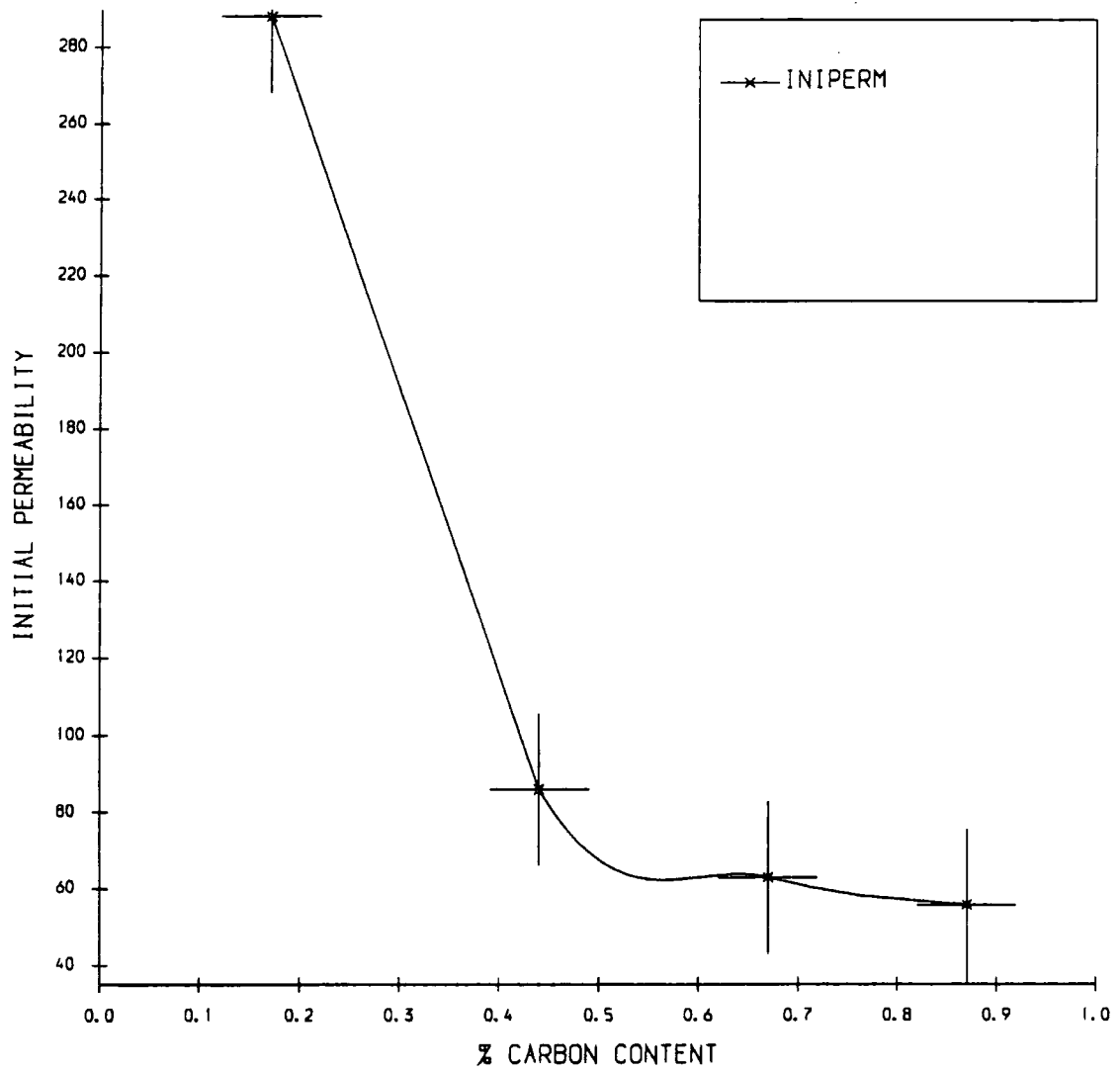
Figure 5.08 The Variation of Initial Permeability With Carbon Content.

116
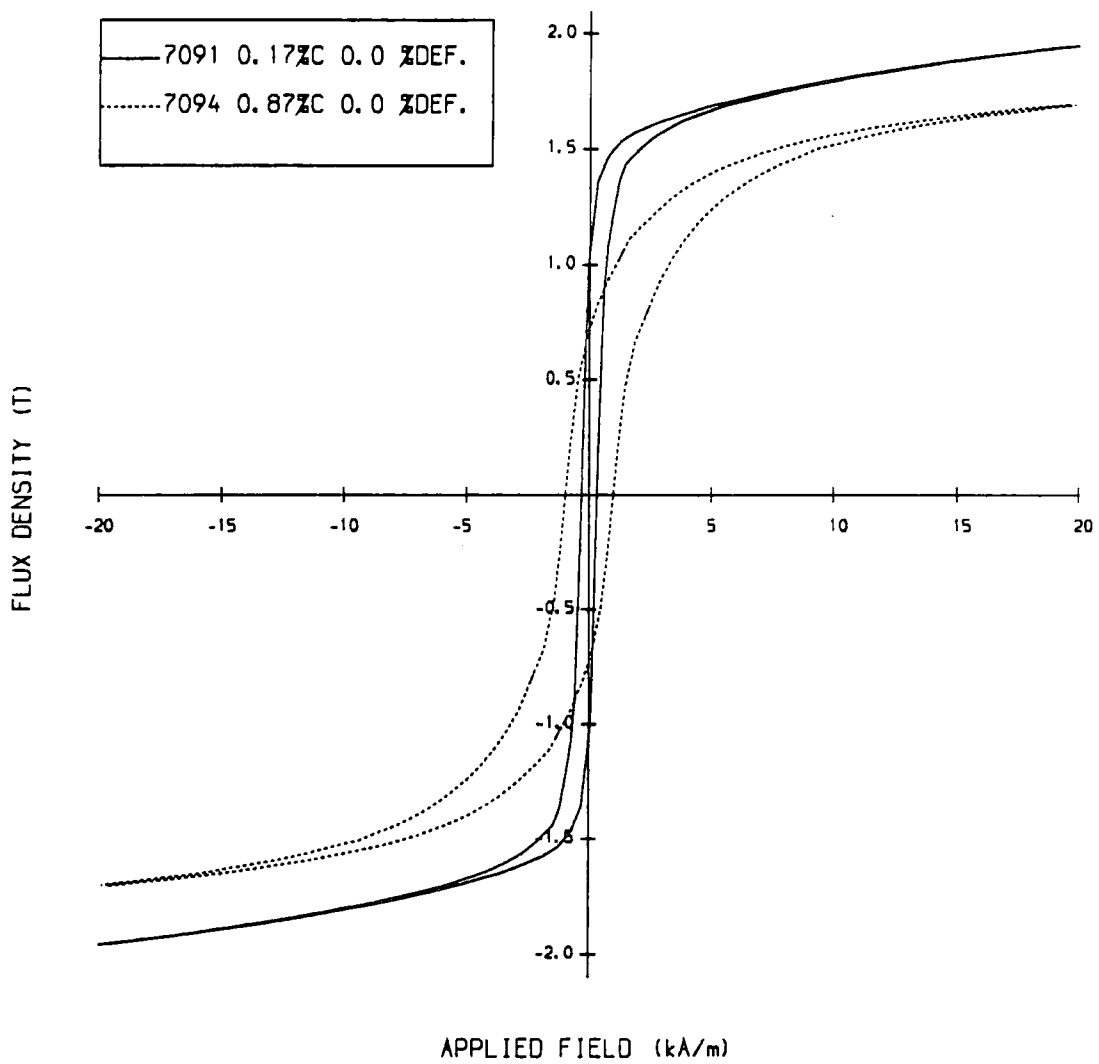
Figure 5.09 Example Hysteresis Curve For an Undeformed Sample with 0.17% and 0.87% Carbon Content.

117
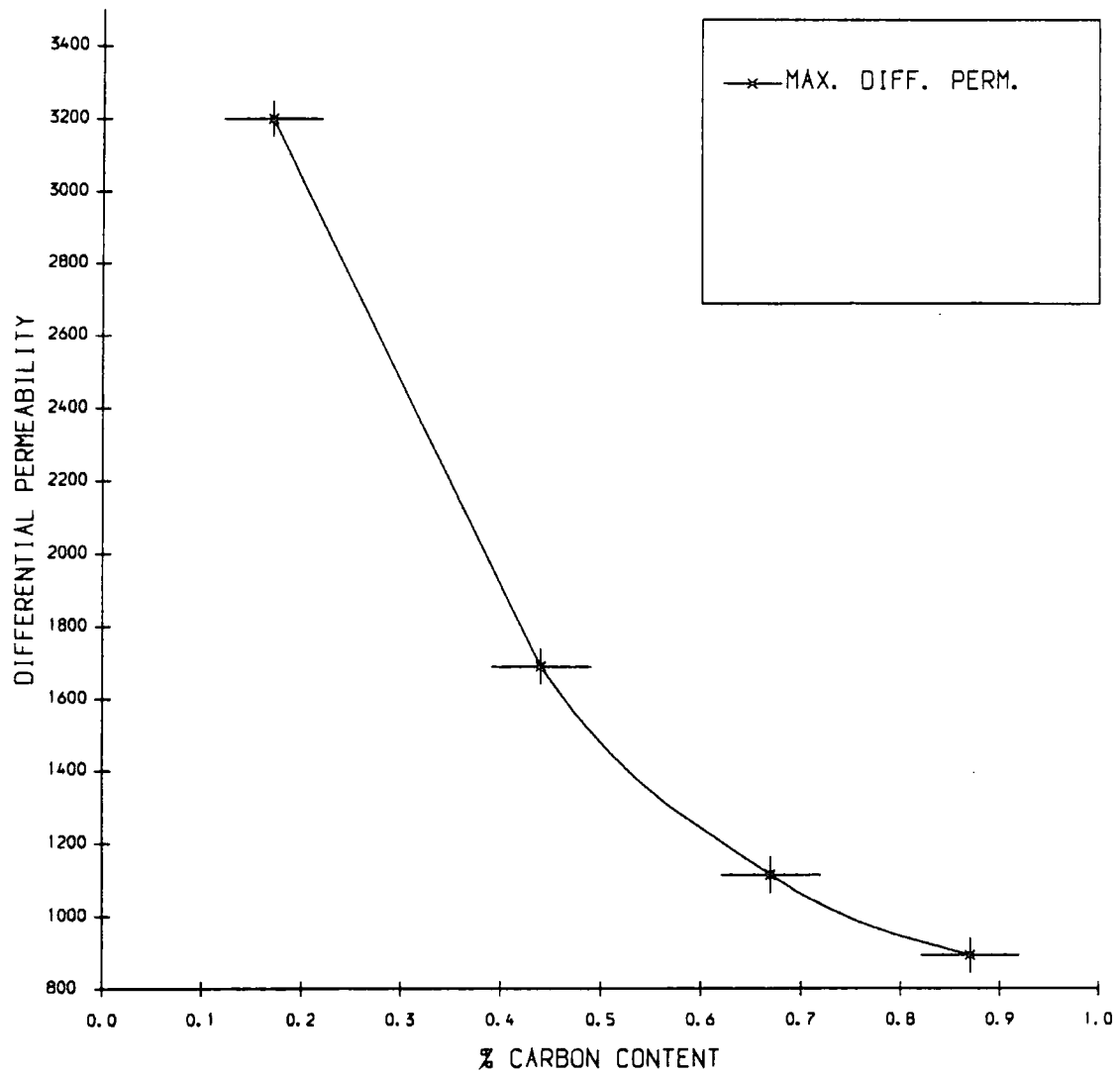
Figure 5.10 The Variation of Maximum Differential Permeability With Carbon Content.
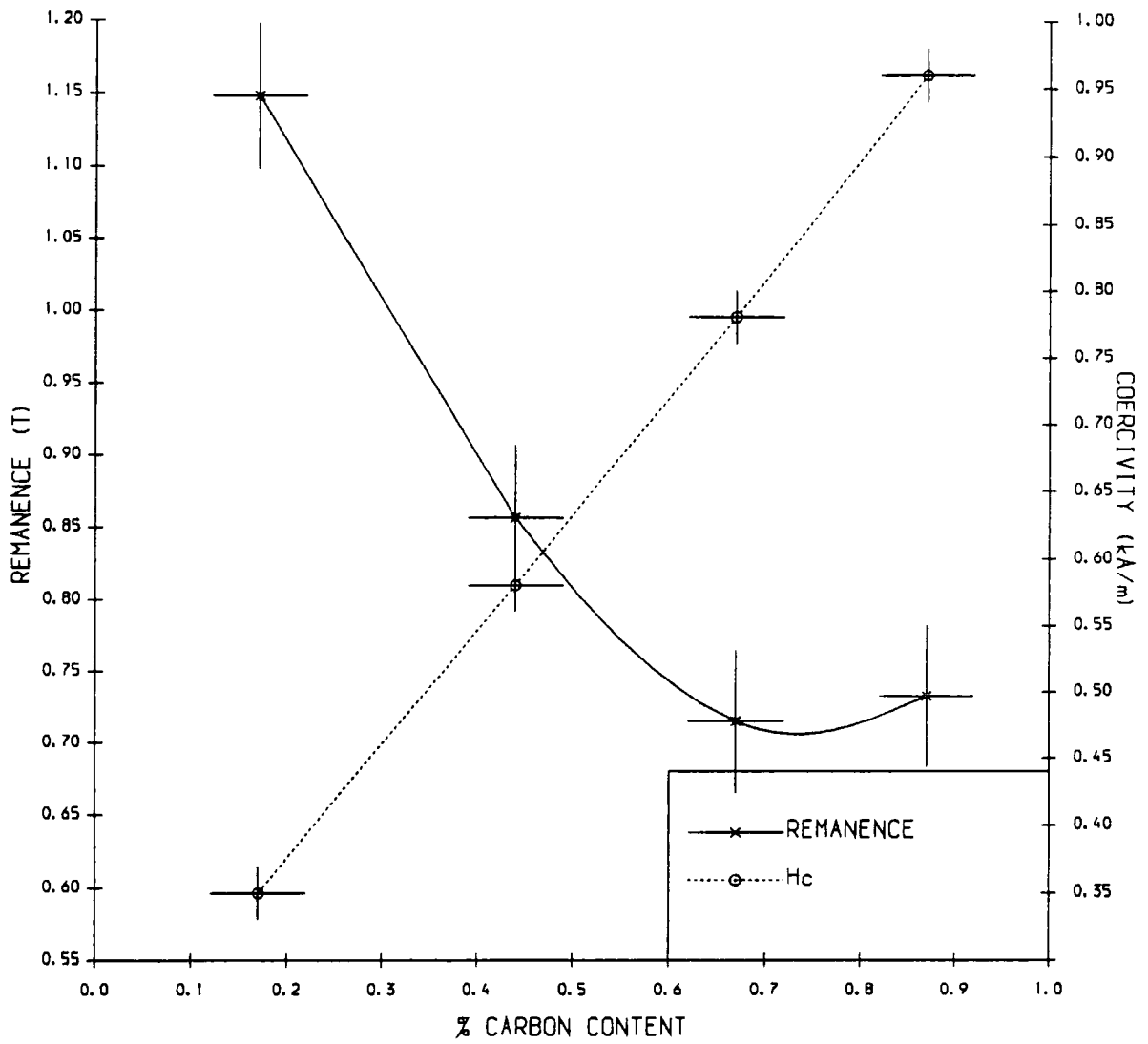
Figure 5.11 The Variation of Coercivity and Remanence With Carbon Content.

119

at which this maximum value occurs Hm both plotted in figure 5.07. The initial permeability μ_i also decreases (figure 5.08). Hysteresis curves determined for 7091 and 7094 are reproduced in figures 5.09 to illustrate the change in loop shape between minimum and maximum carbon concentration. From the hysteresis loops the decrease of maximum differential permeability μ'_{max} (figure 5.10), decrease of remanence and linear increase of coercivity (both figure 5.11) were measured. The toroids were wound and measured as for the pipe-steel as part of a third year undergraduate project by F.Coultard and G.Watson. These results, although suffering from larger errors, correlated with the permeameter measurements especially in the linear increase in coercivity with carbon content.

Batch	%Carbon	Max %Strain	μ_i	μ_{max}	Hm	Hc	Br	μ'_{max}
7091⟹	7094	0	⇓5.2	⇓4.3	⇑3.2	⇑2.7	⇓1.6	⇓3.6
7091	0.17	9.8	⇓4.1	⇓3.2	⇑4.2	⇑1.9	⇓3.3	⇓4.0
7092	0.44	6.0	⇓1.7	⇓2.2	⇑2.6	⇑1.7	⇓1.8	⇓2.7
7093	0.67	7.1	⇓4.6	⇓1.6	⇑1.8	⇑1.5	⇓1.3	⇓1.8
7094	0.87	10.2	⇓1.4	⇓1.7	⇑1.8	⇑1.5	⇓1.3	⇓1.6

Table 5.02 FACTORS by Which the Magnetic Properties of the Various Carbon Content Steels Changed Over the Maximum Range of Plastic Deformation.

The hardness of each batch of steel also increased during the initial stages of deformation and is shown in figure 5.12. The initial magnetisation curves for the series of plastic deformations for a low and high carbon content sample are plotted in graphs 5.13 and 5.14 and indicate the increased resistance to magnetisation as the degree of residual strain is increased. Decreases in μ_{max} for each batch, increases in Hm and the decrease of μ_i with plastic deformation are plotted in figures 5.15 to 5.17. Example hysteresis loops for the maximum deformation attained for each carbon content are displayed in figures 5.18 a) to d) to illustrate the alteration in the loop shape. This distortion is more pronounced in the lower carbon content steels. The increase in Hc and decrease in μ'_{max} and Br for each carbon content with increasing plastic strain are plotted in figures 5.19 to 5.21.
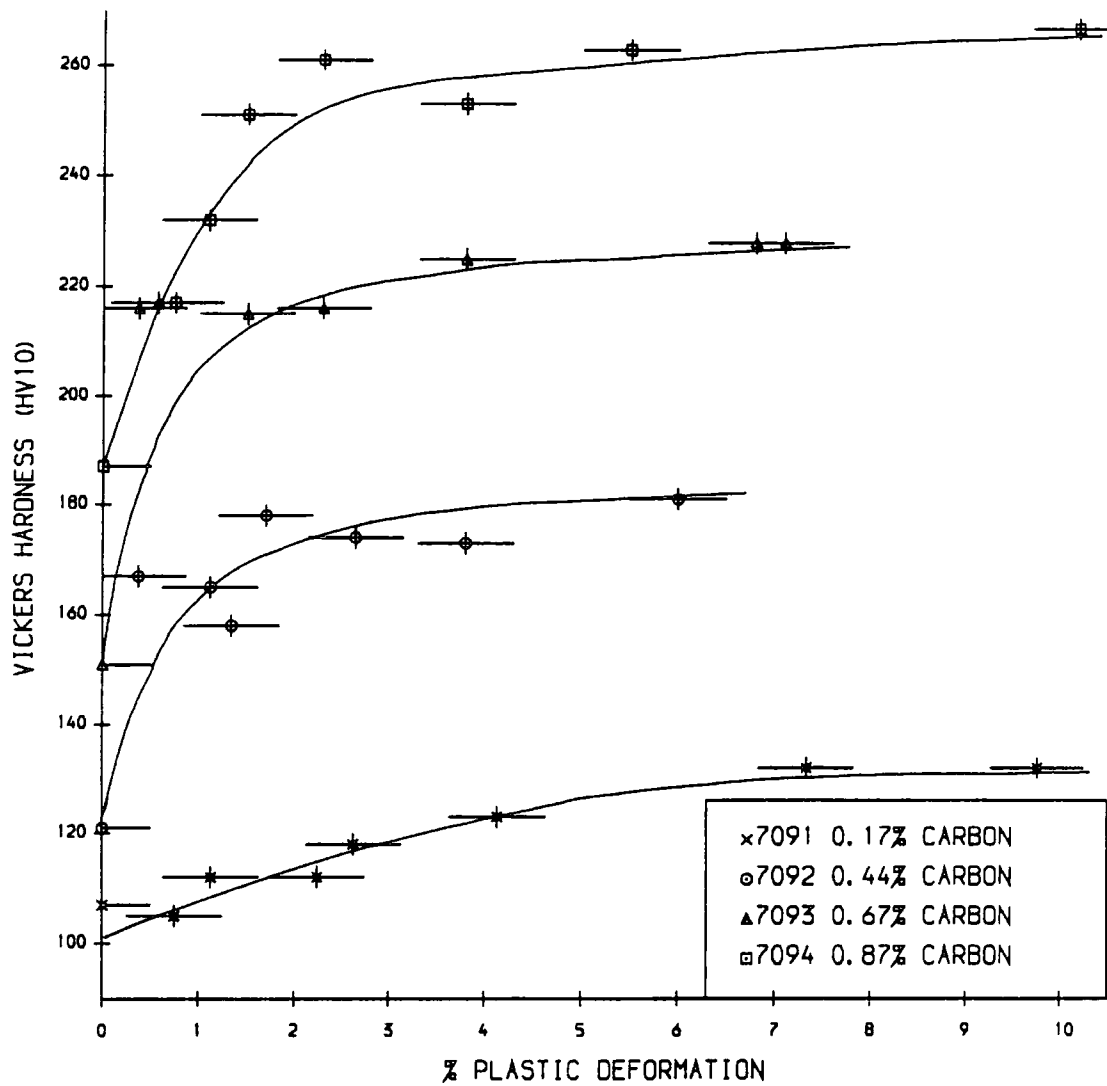
Figure 5.12 The Variation of Vickers Hardness With Plastic Deformation for a Range of Carbon Contents.

121
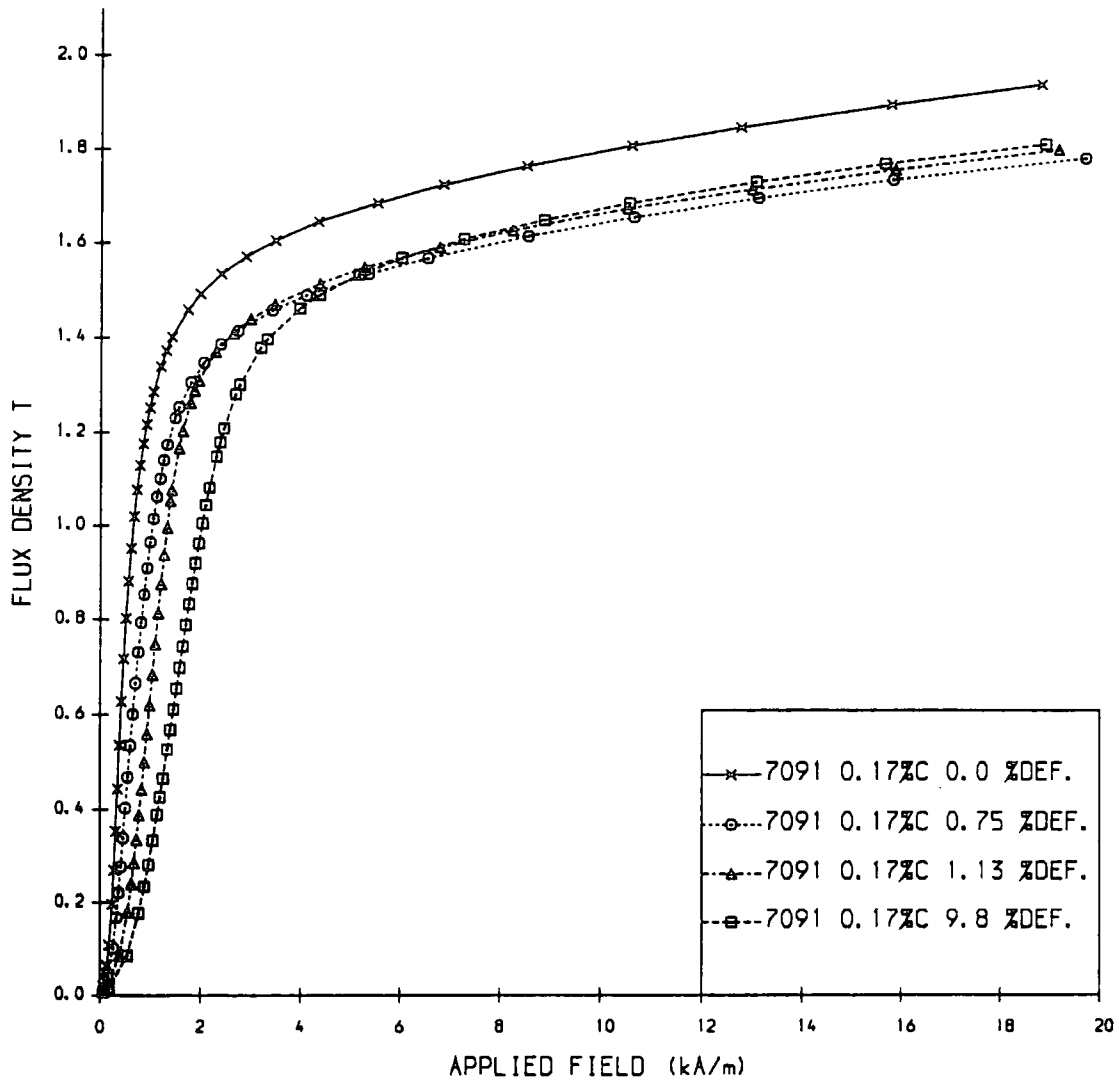
Figure 5.13 Set of Initial Magnetisation Curves for a Range of Plastic Deformations for Sample 7091: 0.17% Carbon Content.

122
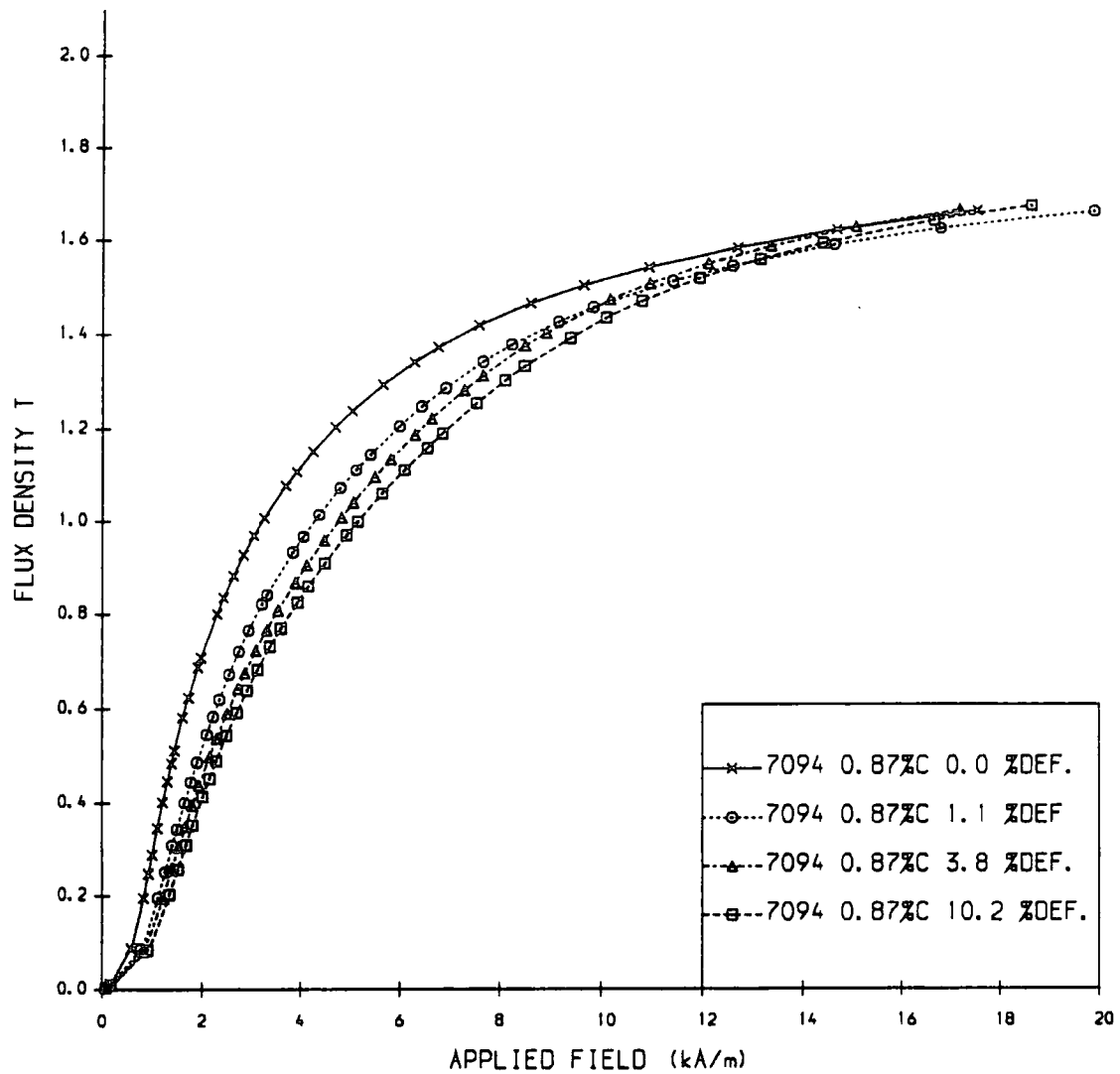
Figure 5.14 Set of Initial Magnetisation Curves for a Range of Plastic Deformations for Sample 7094: 0.87% Carbon Content.
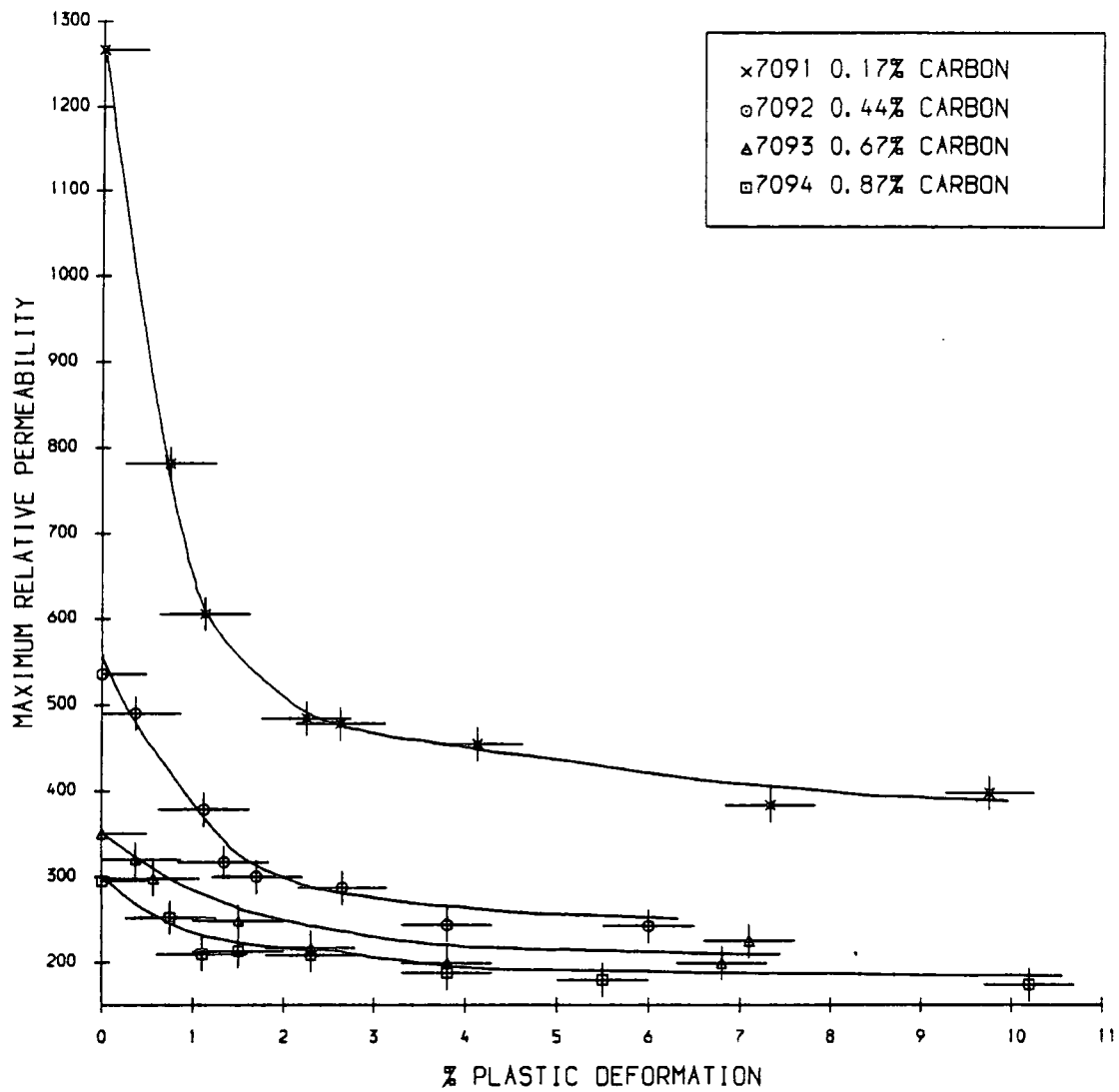
Figure 5.15 The Variation of Maximum Relative Permeability with Plastic Deformation for a Range of Carbon Contents.

124
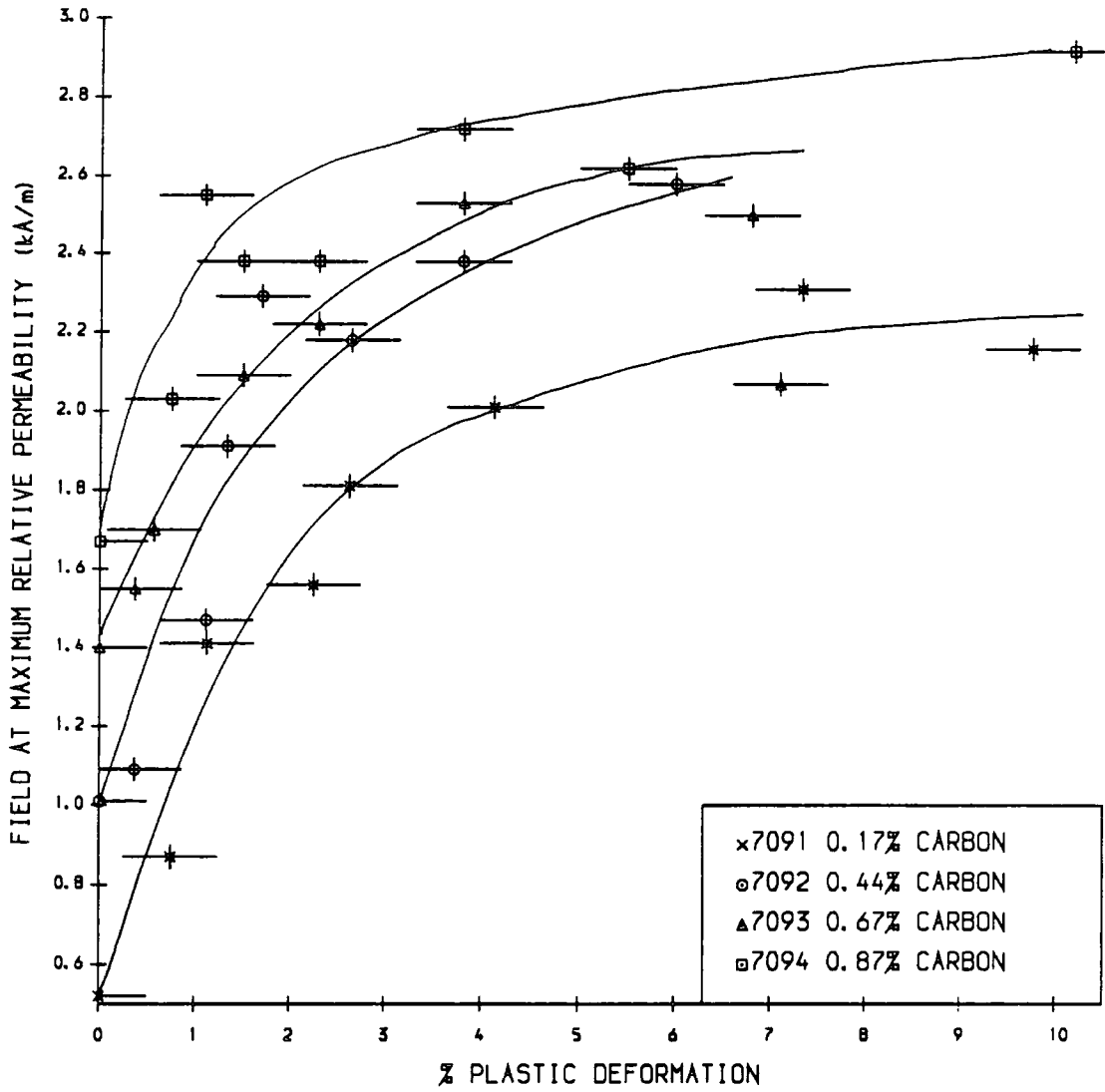
Figure 5.16 The Variation of Hm with Plastic Deformation for a Range of Carbon Contents.

125
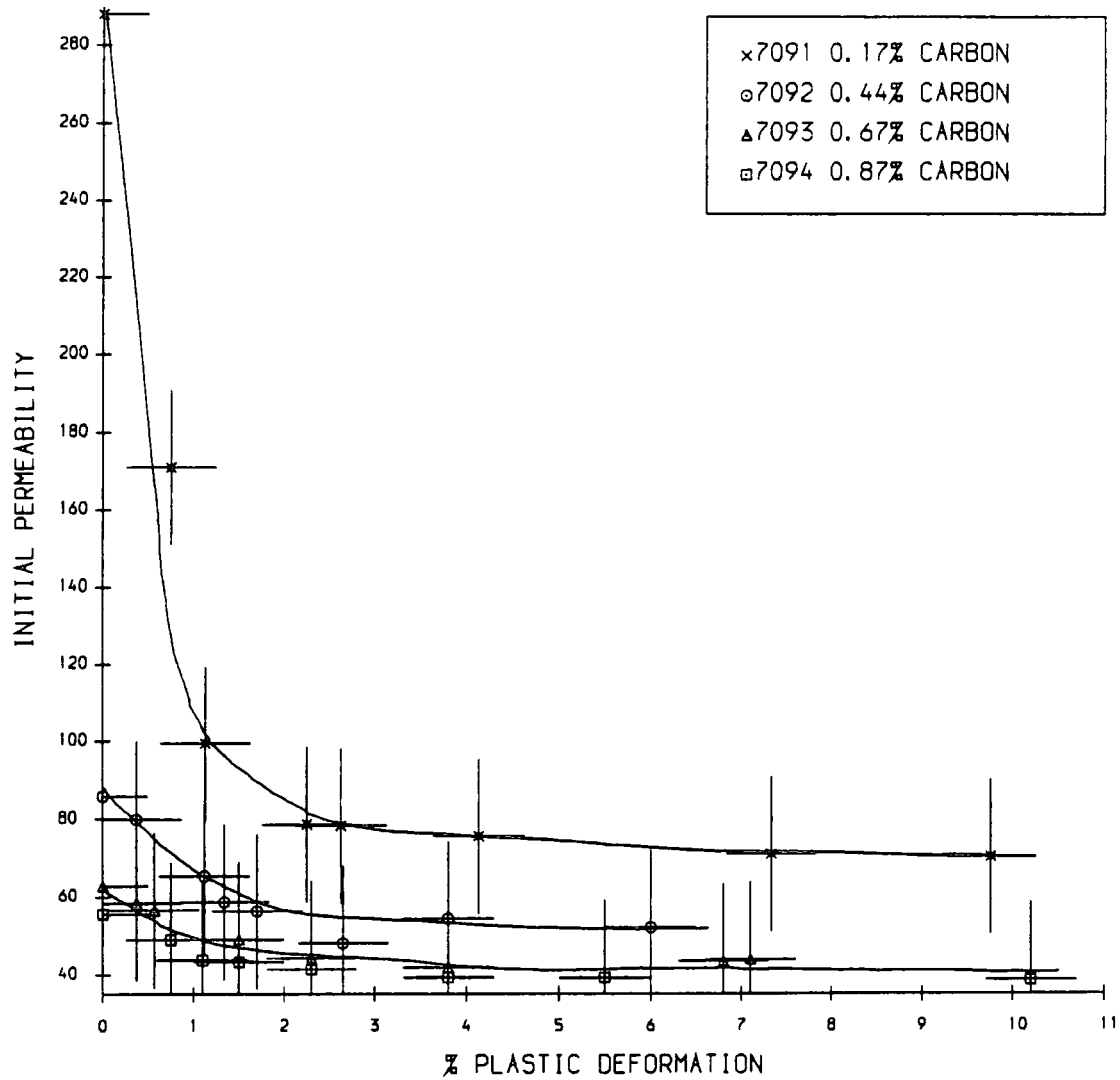
Figure 5.17 The Variation of Initial Permeability With Plastic Deformation for a Range of Carbon Contents.

126
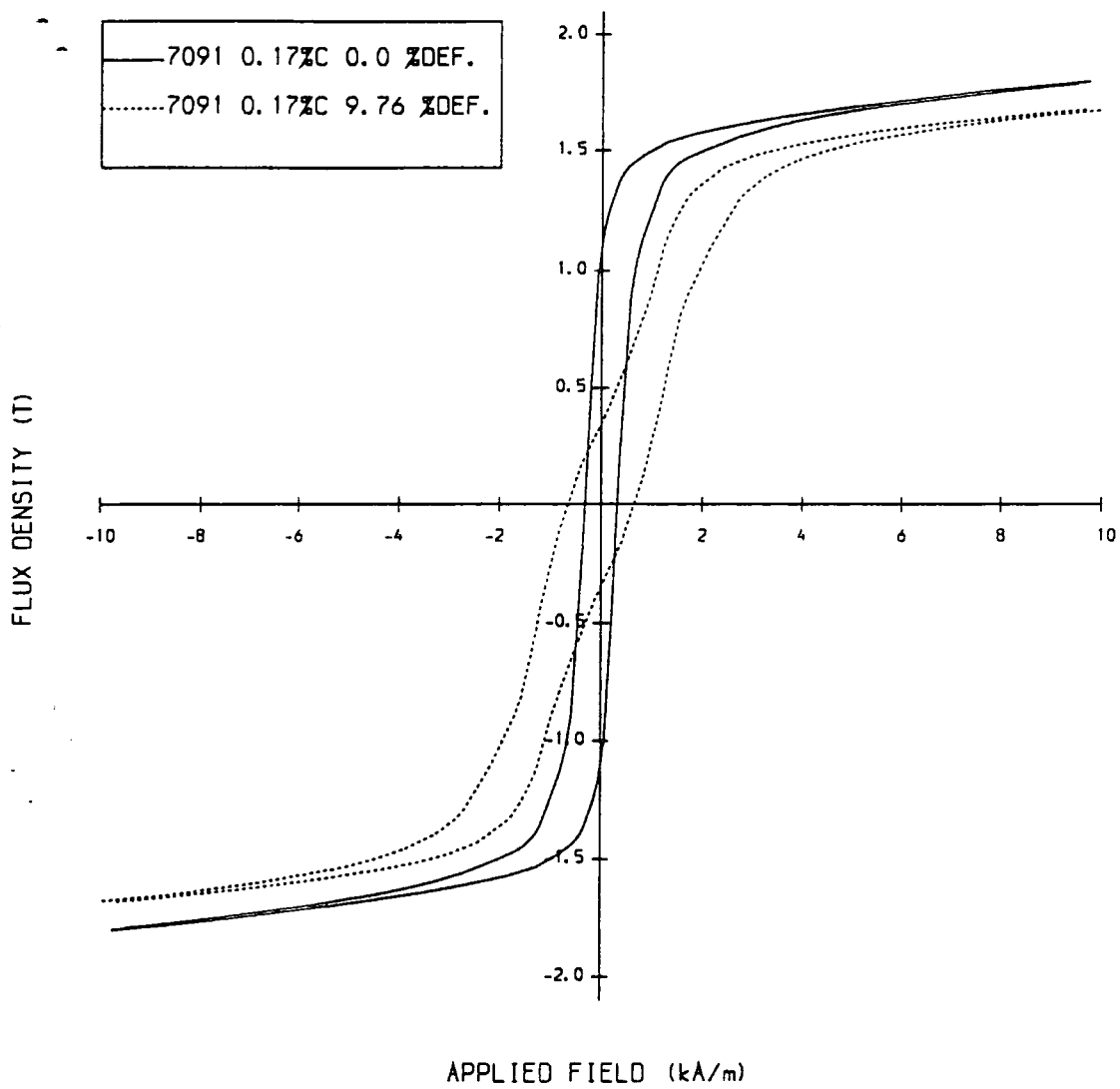
Figure 5.18a Hysteresis Curve for an Undeformed and Deformed Sample of 7091: 0.17% Carbon Content.

127
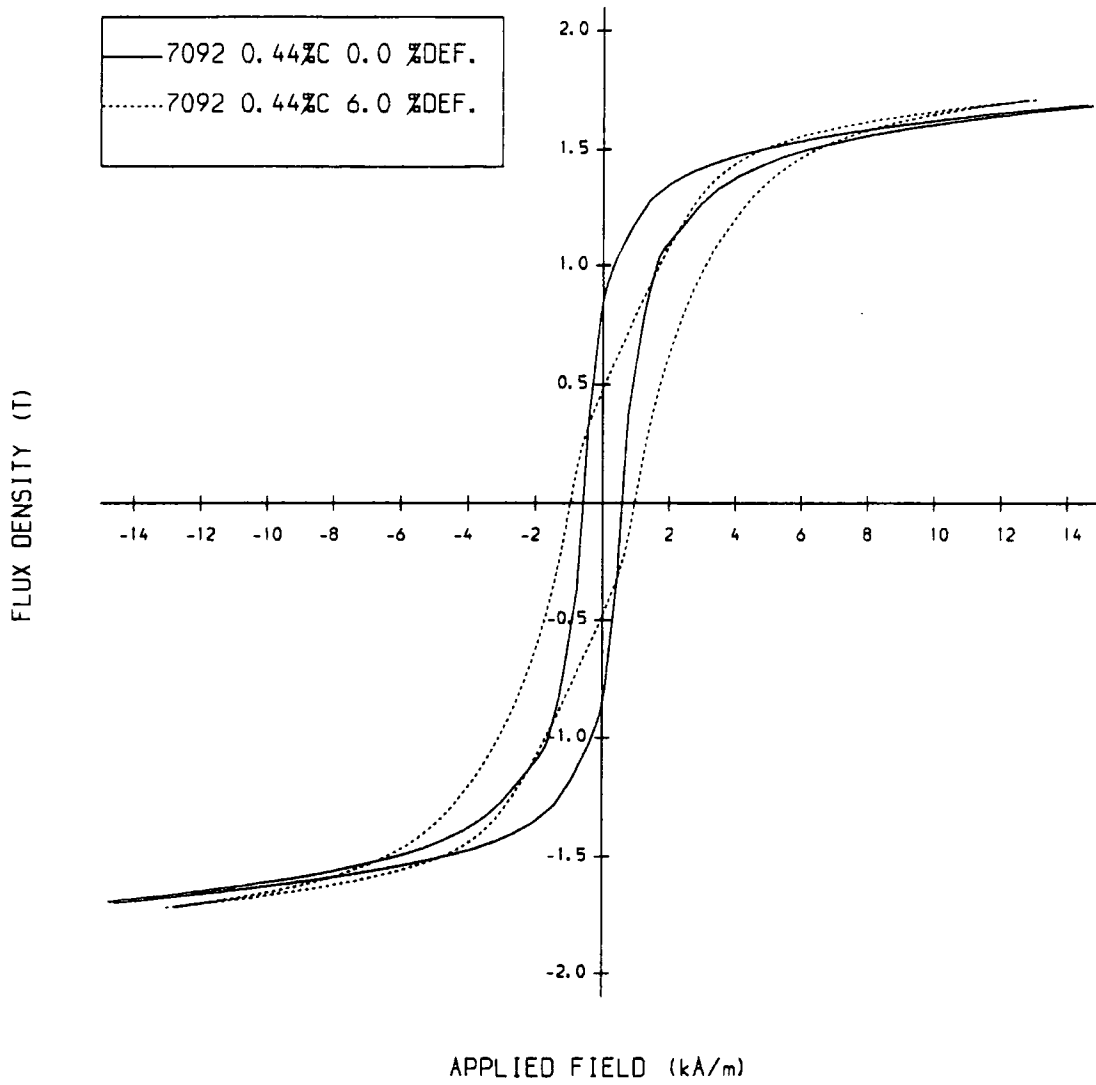
Figure 5.18b Hysteresis Curve for an Undeformed and Deformed Sample of 7092: 0.44% Carbon Content.

128
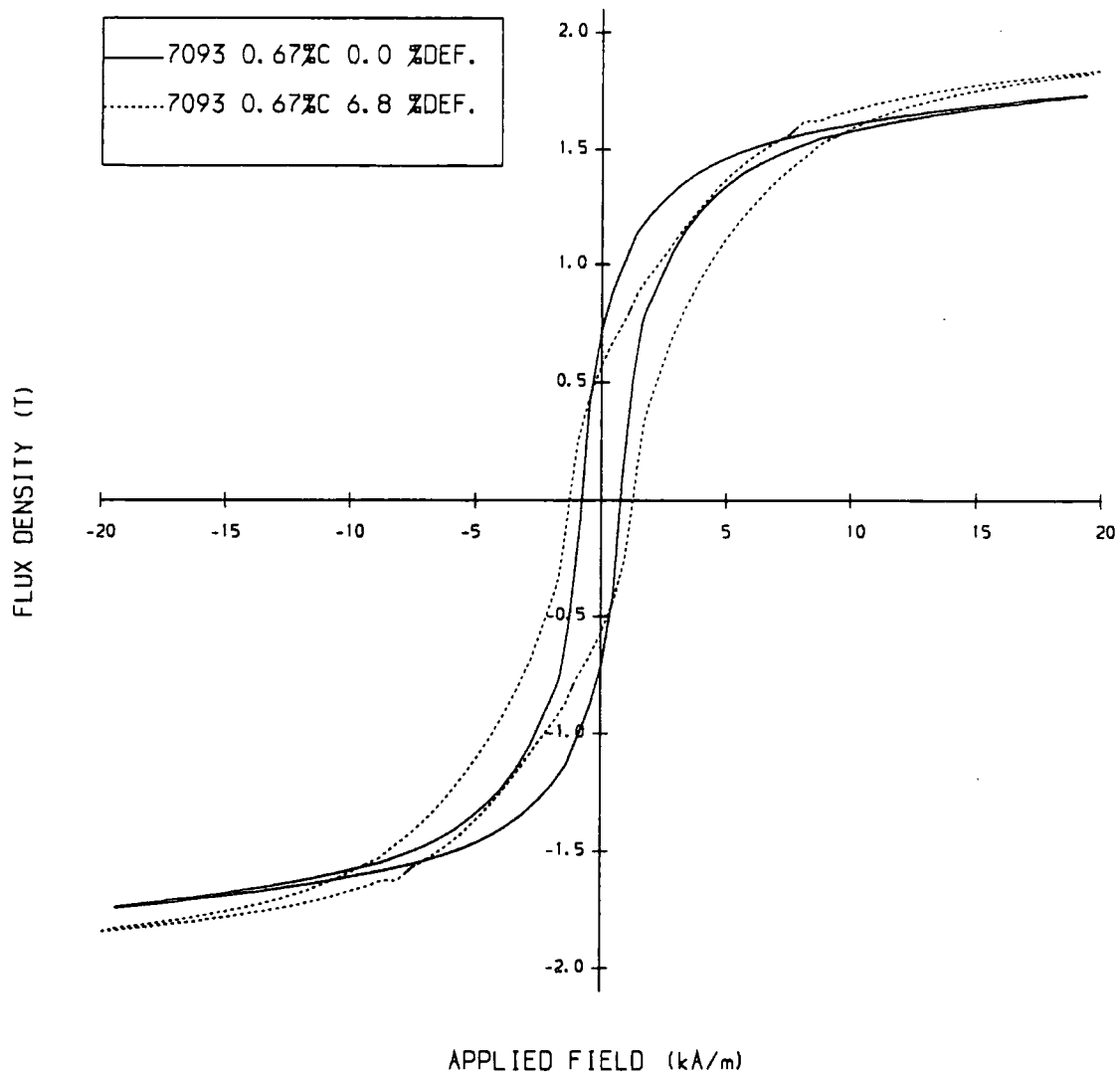
Figure 5.18c Hysteresis Curve for an Undeformed and Deformed Sample of 7093: 0.67% Carbon Content.
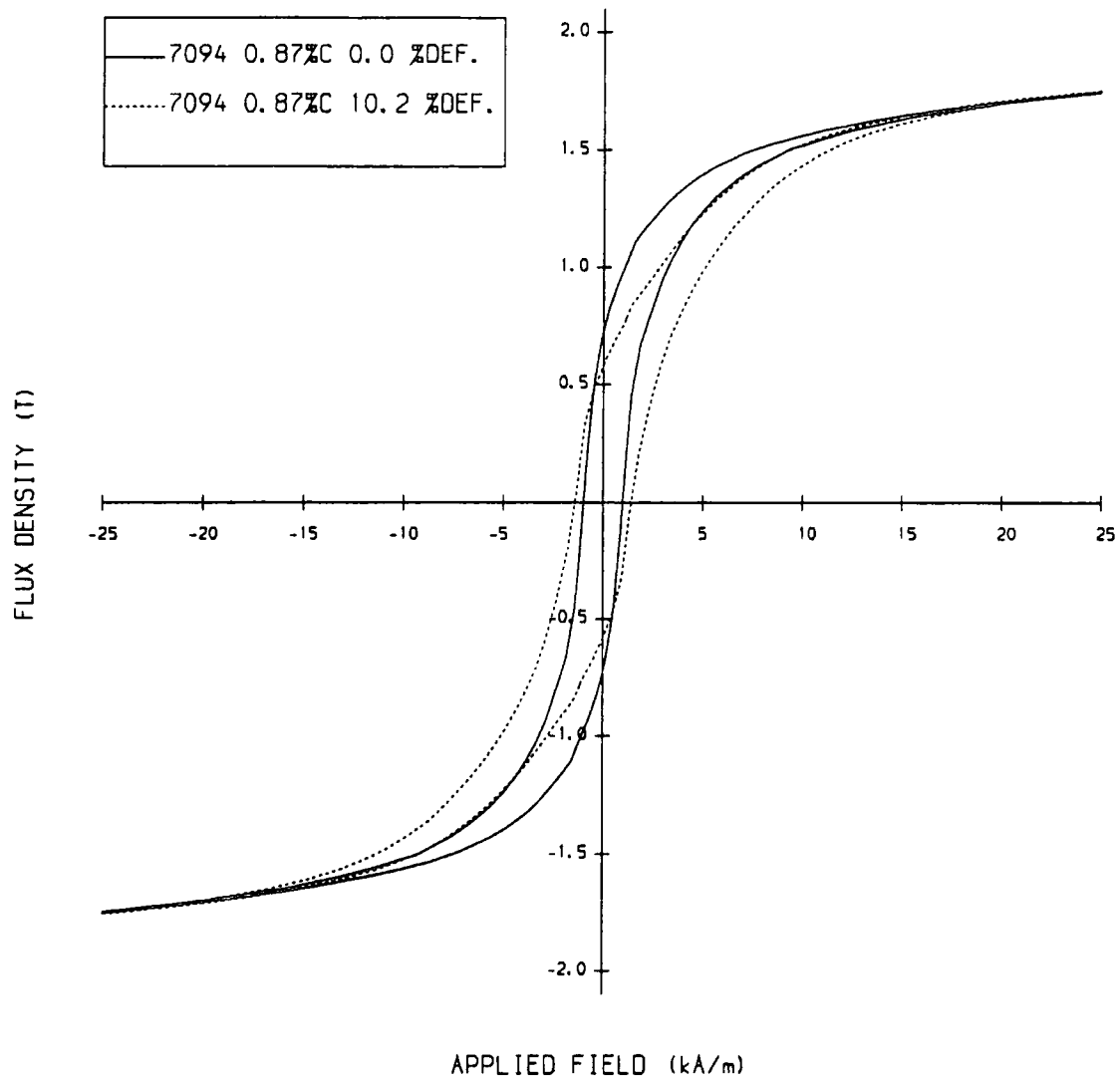
Figure 5.18d Hysteresis Curve for an Undeformed and Deformed Sample of 7094: 0.87% Carbon Content.

130
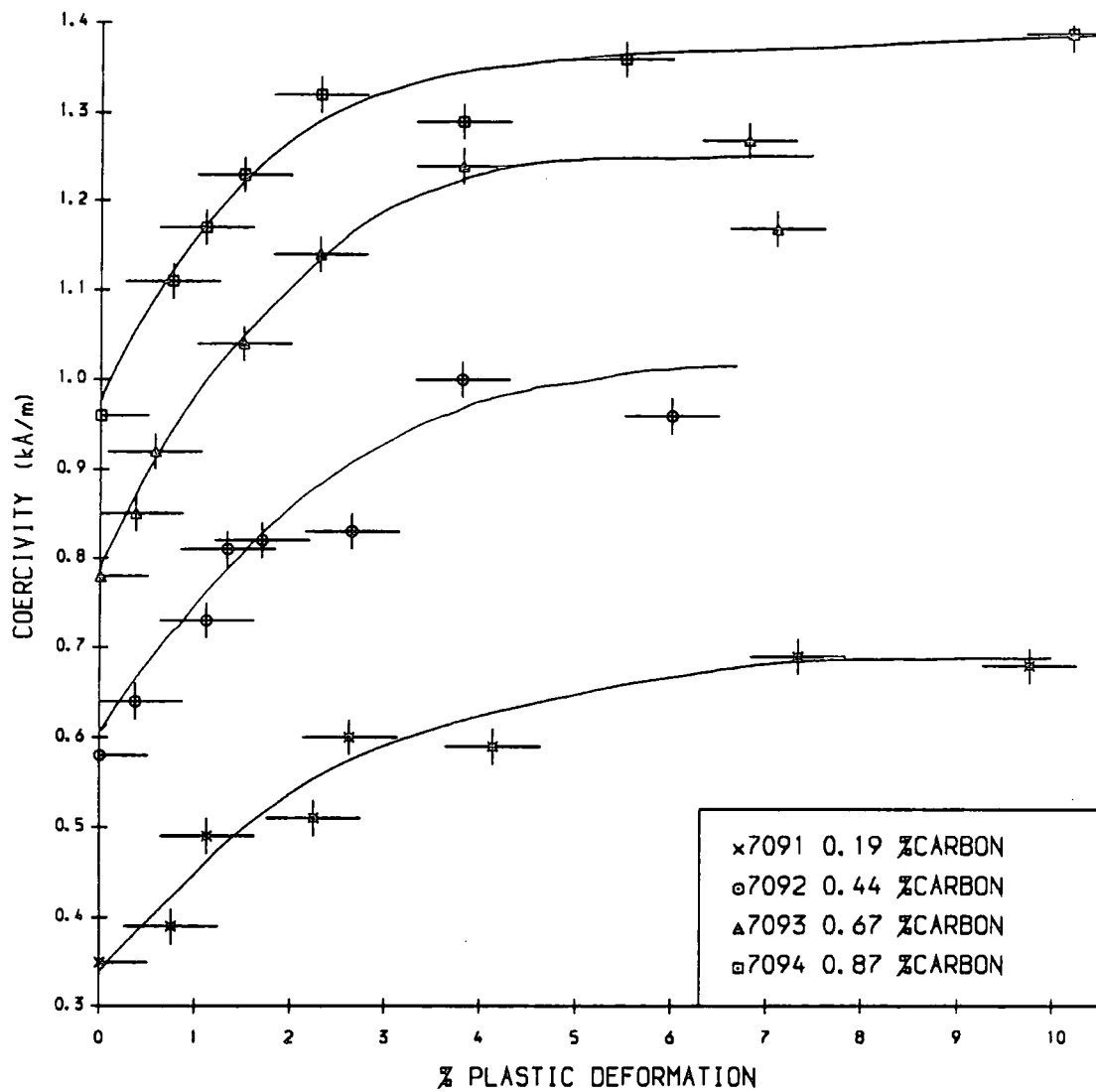
Figure 5.19 The Variation of Coercivity With Plastic Deformation for a Range of Carbon Contents.

131
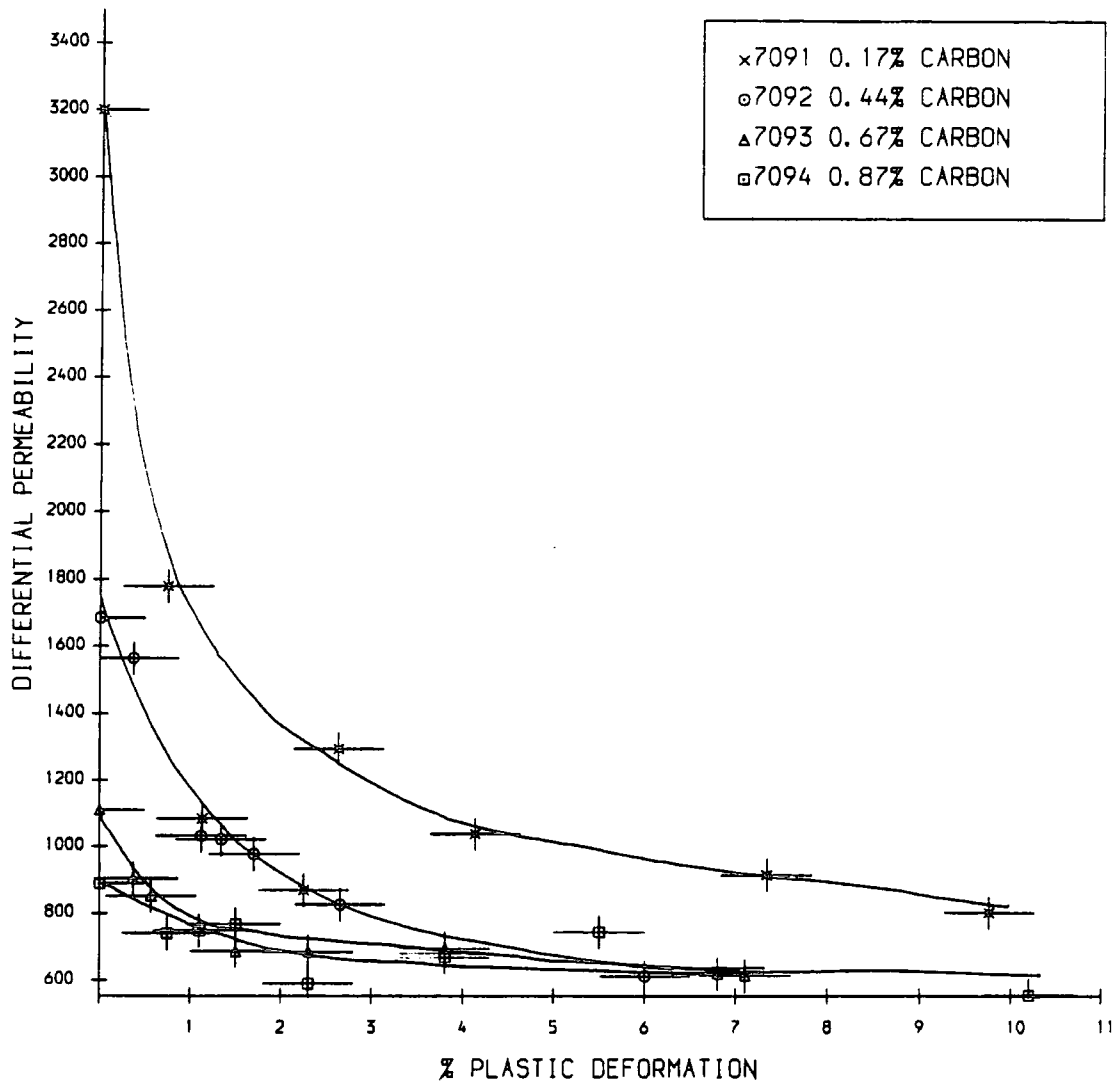
Figure 5.20 The Variation of Maximum Differential Permeability With Plastic Deformation for a Range of Carbon Contents.

132
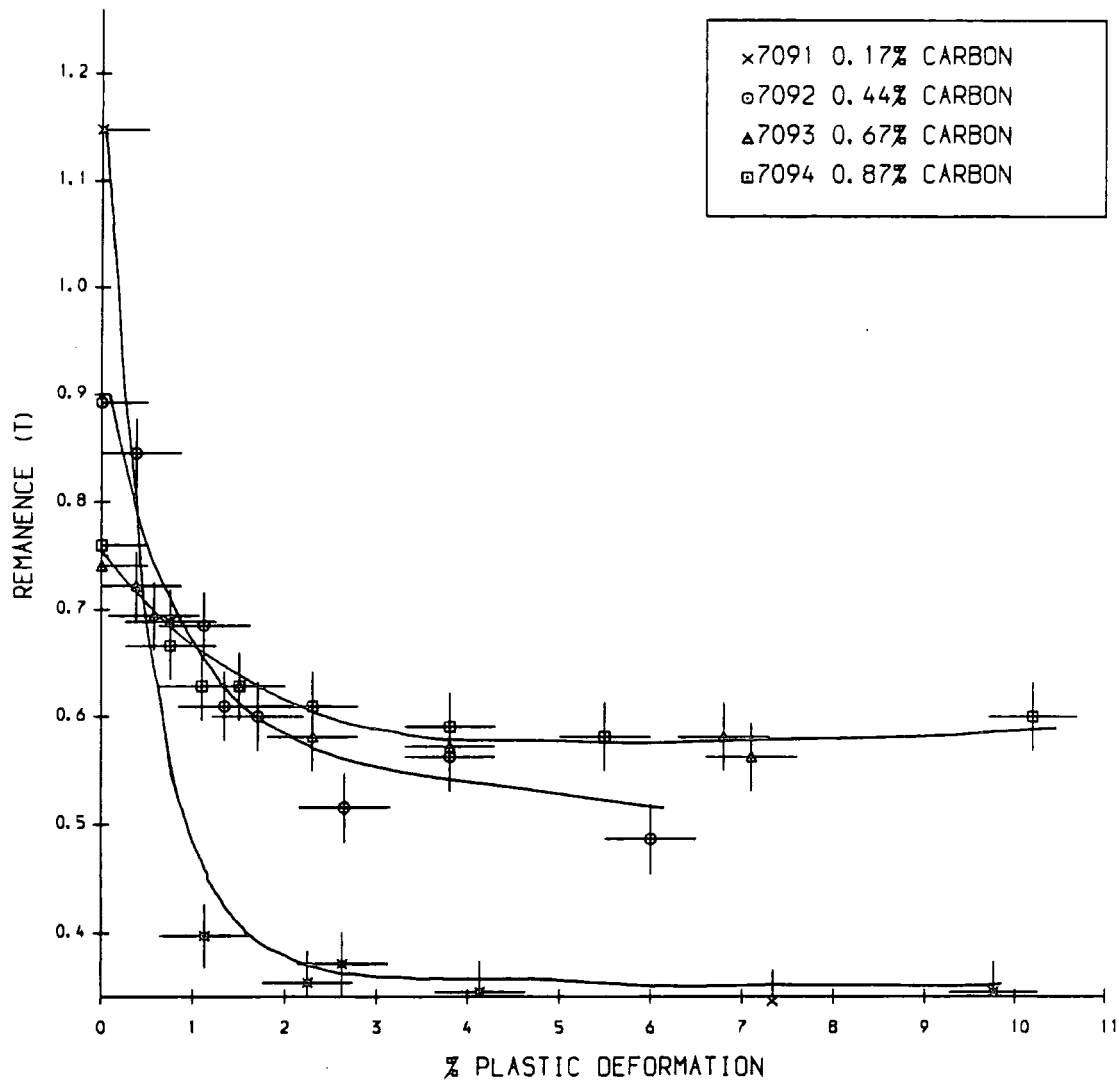
Figure 5.21 The Variation of Remanence With Plastic Deformation for a Range of Carbon Contents.

133

5.3.2 Barkhausen Noise

Studies of the nature of the Barkhausen noise of a steel can give an indication of the type of processes occurring as the sample is magnetised. To obtain this additional information the Barkhausen noise for samples of each carbon content was recorded before and after plastic deformation. The automated Barkhausen apparatus was used for these studies with three recordings made on each sample at magnetising currents of 1.0A, 2.5A and 3.5A corresponding to applied fields of 4.7kAm^{-1}, 11.75kAm^{-1} and 16.45kAm^{-1} respectively at a frequency of 0.1Hz. The full half cycle was recorded in each case and sampled at intervals of 152μs. Once transferred over to the mainframe computer at N.U.M.A.C. the data was averaged over 50 samples and plotted. The results obtained with a maximum field of 11.75 kAm^{-1} were found to be the most useful and the traces for the undeformed steel and one example of a recording from a deformed sample are presented in figures 5.22 to 5.29.

5.3.3 Electron Microscopy.

In order to determine the mechanisms by which the pearlite content of the steel affects its domain configuration and domain wall movement and how this is altered by plastic deformation; an undeformed and deformed sample of each carbon content were studied using High Voltage Lorentz Electron Microscopy. The A.E.I. EM7 microscope at Oxford University was used in both fresnel and foucault modes with the magnetising coils insitu, enabling observation of the domain wall movement under an applied field and the recording of magnetising sequences on video.

In the low carbon 7091 samples large ferrite grains were visible broken up by well defined pearlite nodules and ferrite-ferrite grain boundaries. A typical example of the uncomplicated domain structure observed in the undeformed material is shown in fresnel and foucault images in figures 5.30 a) and b). The dominant feature here is clearly the pearlite grain onto which the closure domains are forming. The walls however are not entirely straight, but affected by the dislocations present in the ferrite grain and the low angle grain boundary. The walls most distorted are the 90° walls forming the closure part of the domains. Once inside the pearlite grain it is difficult to see the domain walls, but a wall can be seen pinned between the two cementite inclusions attached to the bottom of the grain.
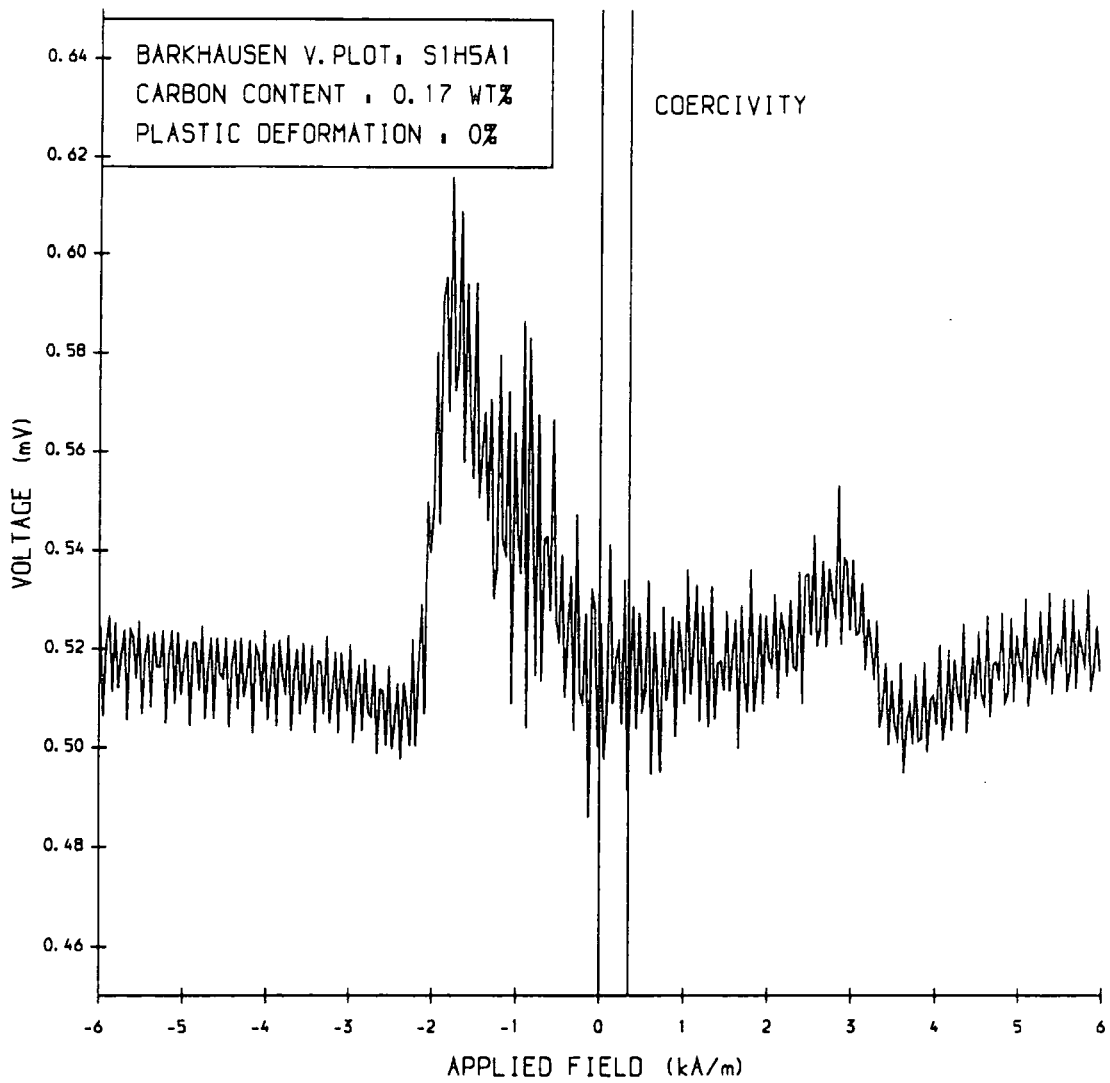
Figure 5.22 Barkhausen Noise for an Undeformed Sample of 7091: 0.17% Carbon Content. Magnetising Frequency 0.1Hz, Maximum Applied Field: 11kAm⁻¹.

135
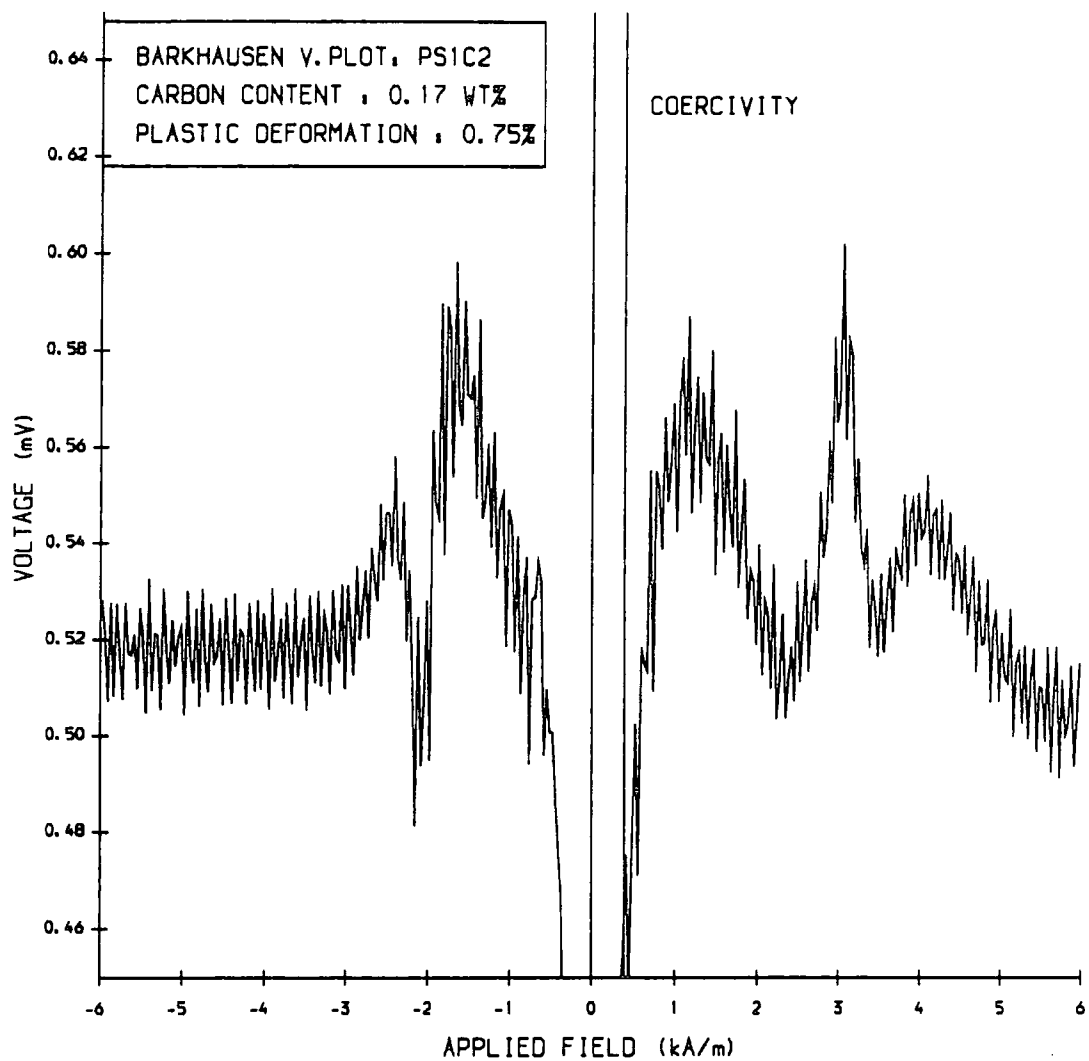
Figure 5.23 Barkhausen Noise for a 0.75% Deformed Sample of 7091: 0.17% Carbon Content. Magnetising Frequency 0.1Hz, Maximum Applied Field: 11kAm⁻¹.
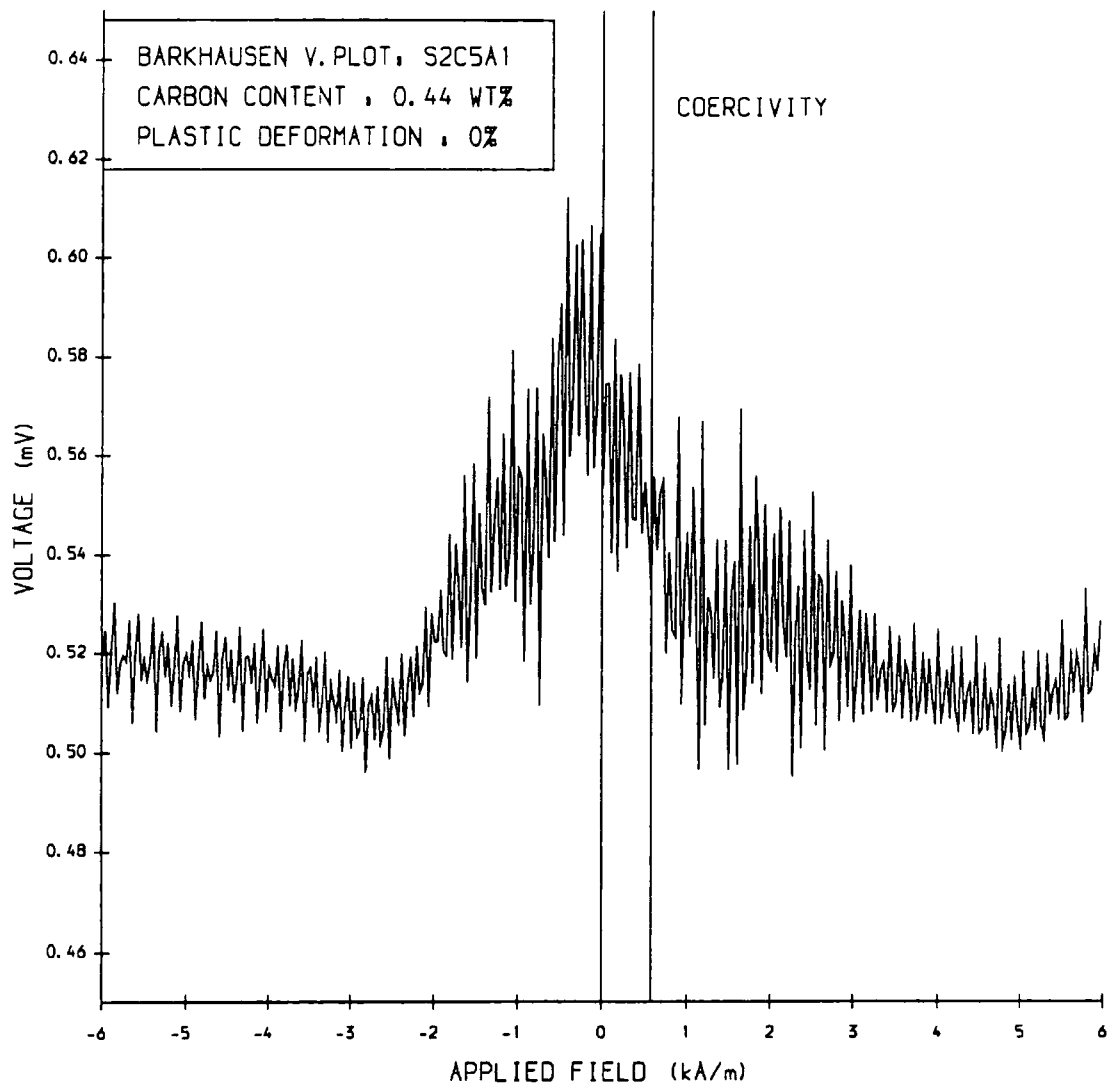
Figure 5.24 Barkhausen Noise for an Undeformed Sample of 7092: 0.44% Carbon Content. Magnetising Frequency 0.1Hz, Maximum Applied Field: 11kAm^{-1}.
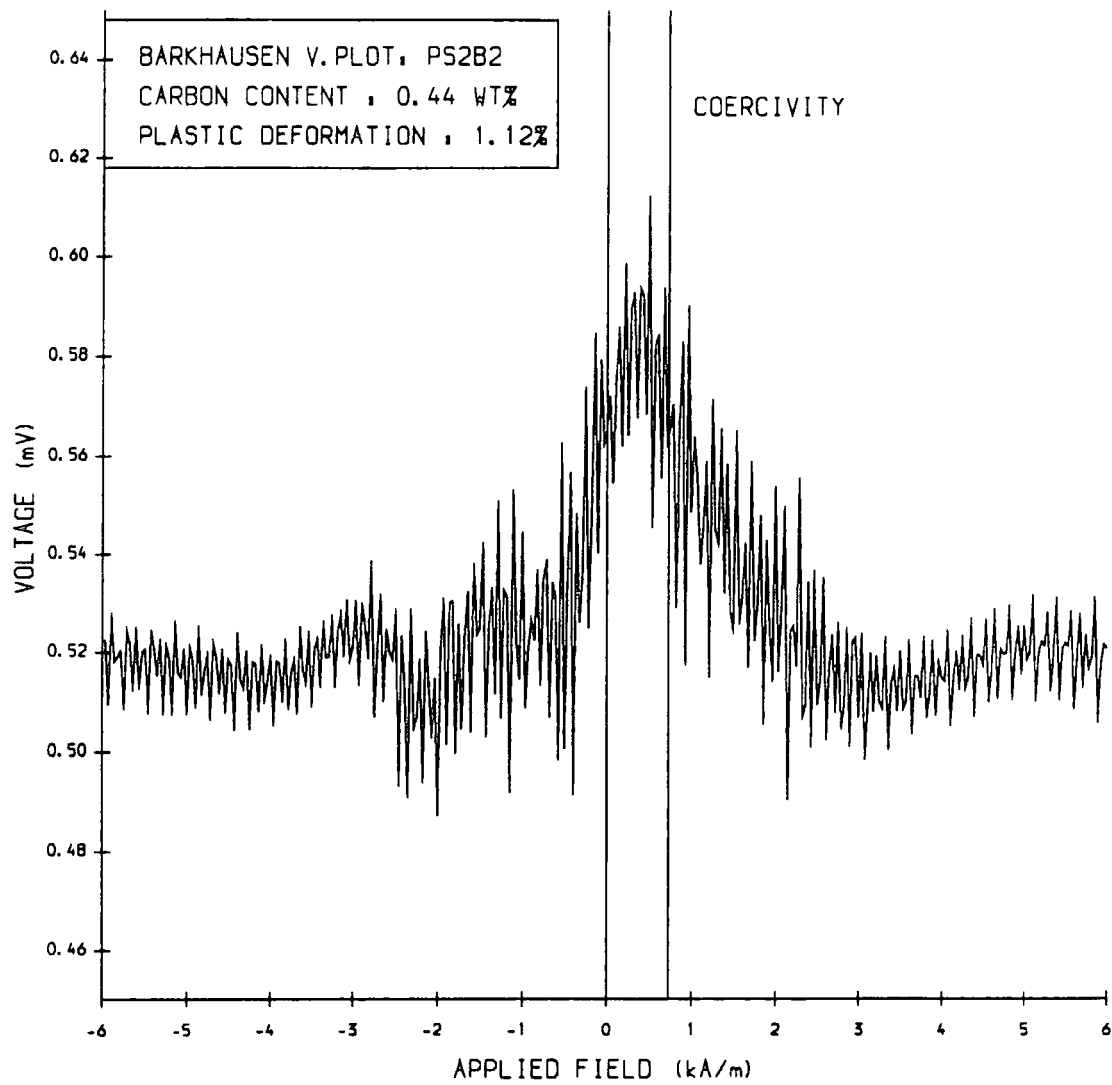
Figure 5.25 Barkhausen Noise for a 1.12% Deformed Sample of 7092: 0.44% Carbon Content. Magnetising Frequency 0.1Hz, Maximum Applied Field: 11kAm^{-1}.

138
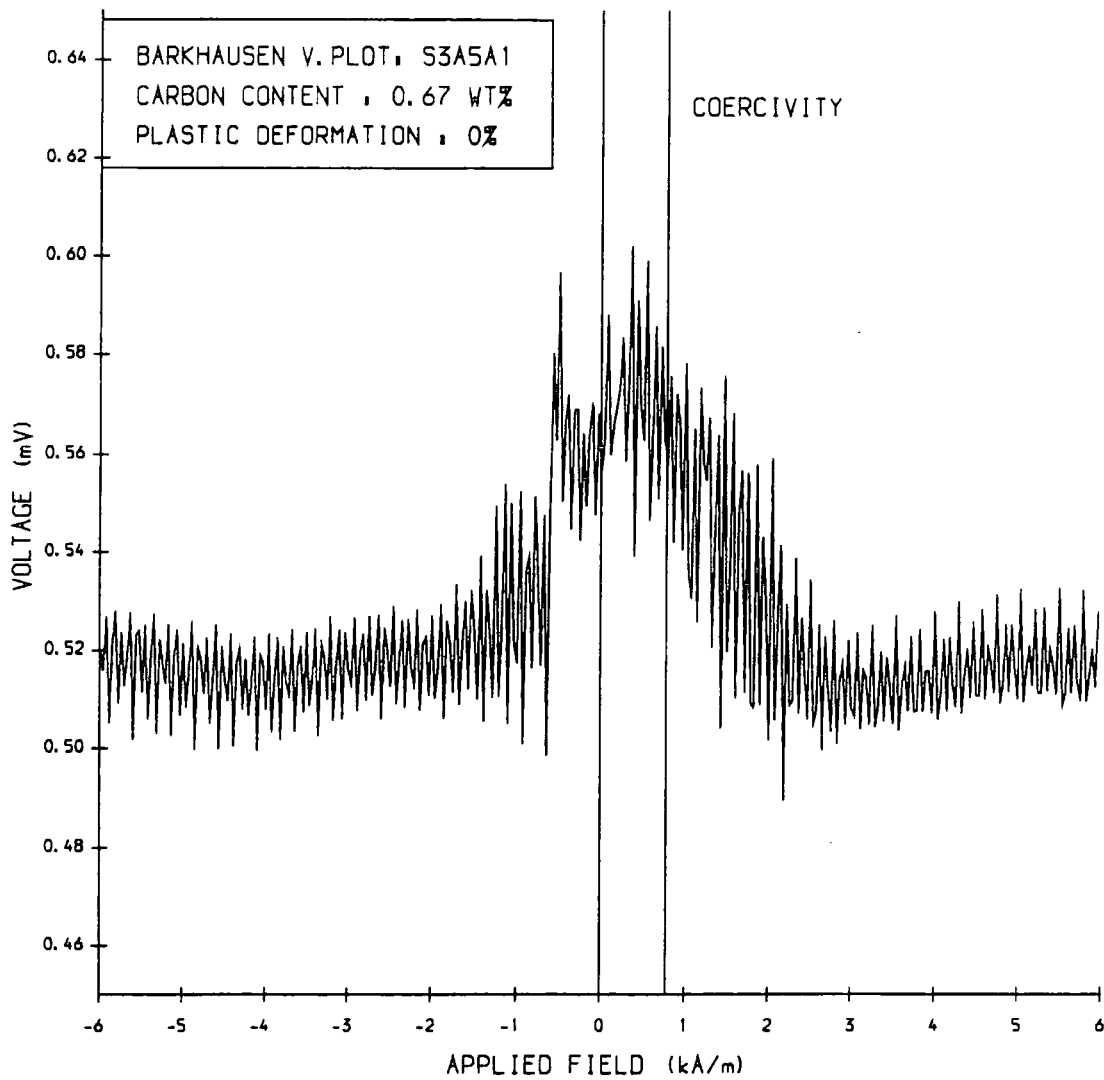
Figure 5.26 Barkhausen Noise for an Undeformed Sample of 7093: 0.67% Carbon Content. Magnetising Frequency 0.1Hz, Maximum Applied Field: 11kAm^{-1}.
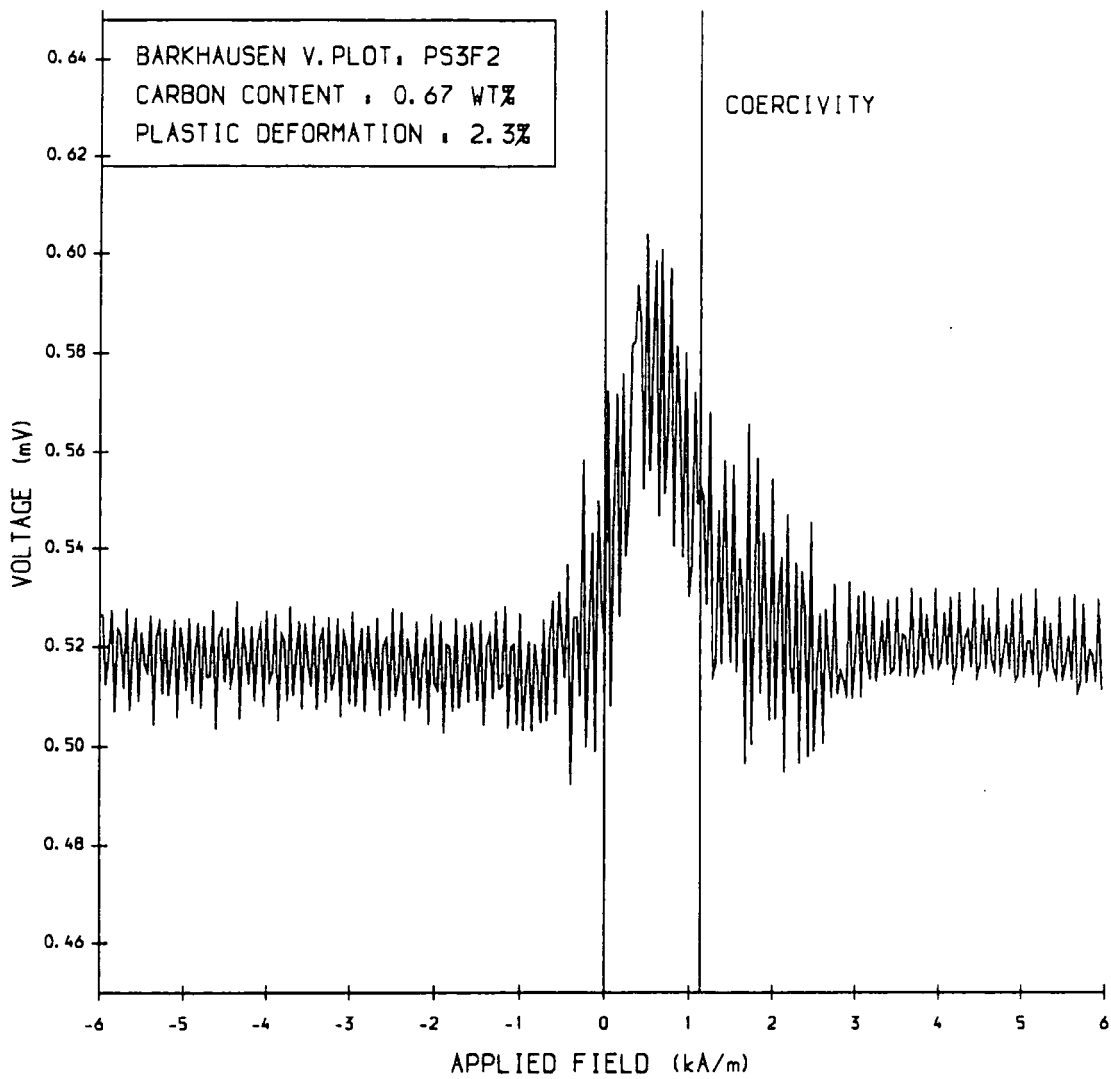
Figure 5.27 Barkhausen Noise for a 2.3% Deformed Sample of 7093: 0.67% Carbon Content. Magnetising Frequency 0.1Hz, Maximum Applied Field: 11kAm^{-1}.

BARKHAUSEN V. PLOT: S4A5A1
CARBON CONTENT : 0. 87 WT%
PLASTIC DEFORMATION : 0%

COERCIVITY

0. 64
0. 62
0. 60
0. 58
0. 56
0. 54
0. 52
0. 50
0. 48
0. 46

VOLTAGE (mV)

-6 -5 -4 -3 -2 -1 0 1 2 3 4 5 6
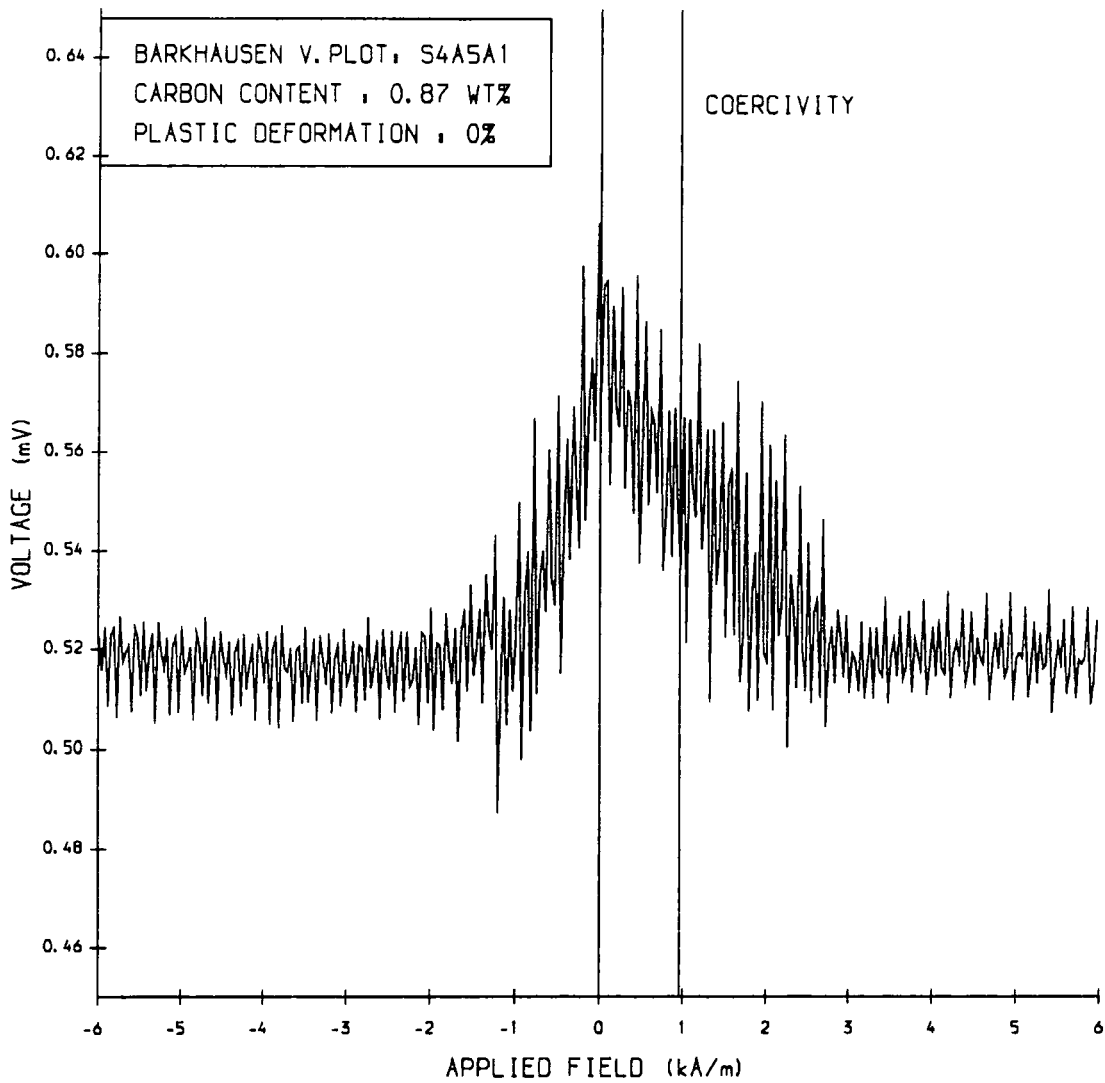
APPLIED FIELD (kA/m)

Figure 5.28 Barkhausen Noise for an Undeformed Sample of 7094: 0.87% Carbon Content. Magnetising Frequency 0.1Hz, Maximum Applied Field: $11kAm^{-1}$.
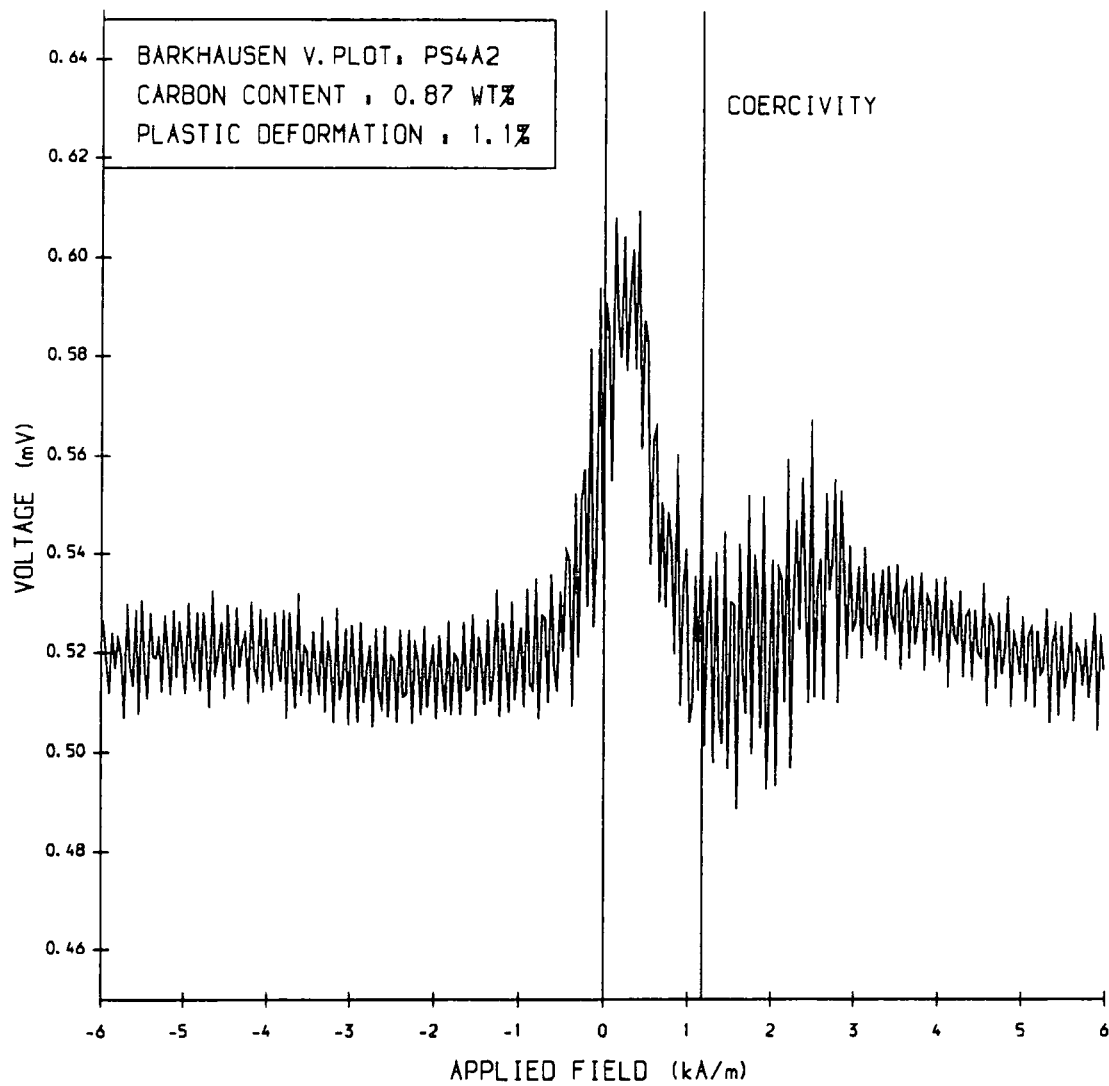
Figure 5.29 Barkhausen Noise for a 1.1% Deformed Sample of 7094: 0.87% Carbon Content. Magnetising Frequency 0.1Hz, Maximum Applied Field: 11kAm^{-1}.

142
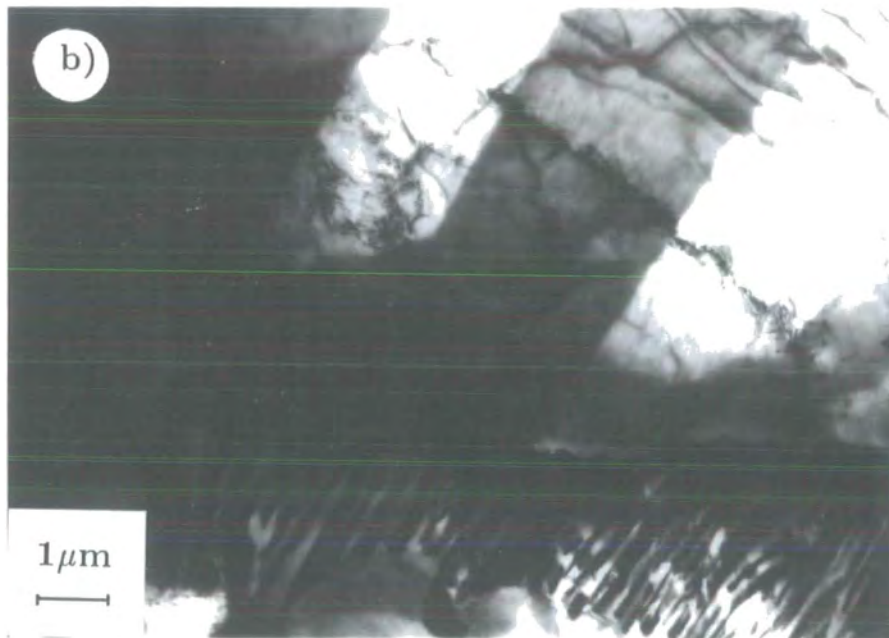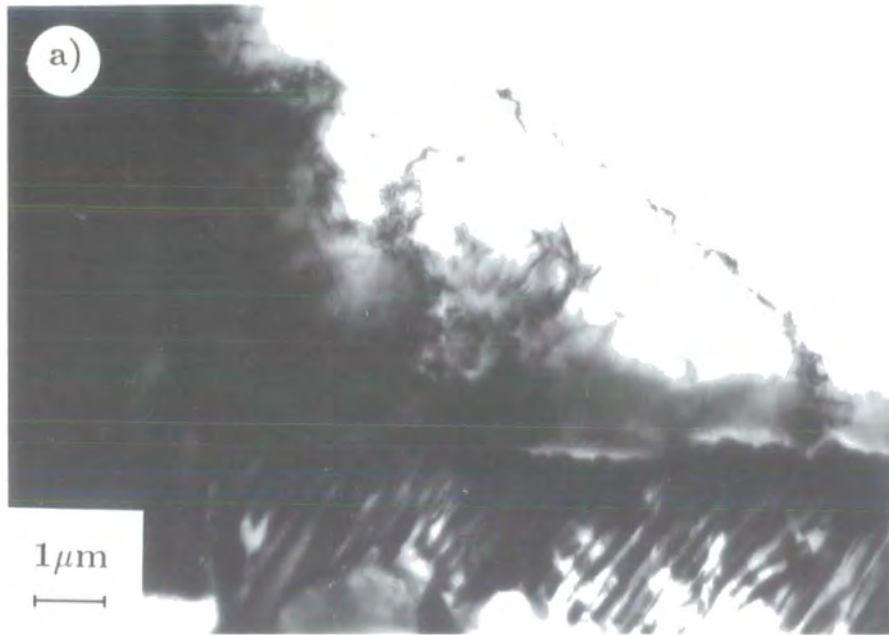
Figure 5.30 Electron micrographs of undeformed 7091 : a) infocus, b) foucault contrast.

A dislocated ferrite grain in a 10% deformed sample is shown in figure 5.31; across the grain is a low-angle grain boundary and the surrounding ferrite grain is relatively dislocation free. A pair of domain walls run along the grain parallel to the grain boundary. Movement was observed at low applied fields of $2kAm^{-1}$ parallel to the grain boundary, but due to preferential wall movement occurring in the relatively undeformed ferrite outside the grain the two walls inside the grain sometimes moved in the same direction. The grain boundary is the dominant feature in this case with the walls eventually becoming pinned to it. The wall movement, although sudden and not steady, is not strongly affected along its length by the dislocations and is only slightly disturbed by the low angle boundary running across the grain.

The series of micrographs in figure 5.32 of a deformed sample illustrates the large variation in dislocation density within the samples. The first fresnel micrograph is at the maximum applied field of $15kAm^{-1}$ and shows the domain walls strongly pinned to the carbide particle to the left of the picture. It is also pinned by the dislocations between it and the ferrite grain boundary to the bottom as the domain between the two walls tries to contract. As the field is reduced the wall is eventually released at $9.4kAm^{-1}$ and rests pinned to the heavily dislocated ferrite particle at the right of photographs 5.32 c) and d) which show different areas at the remanent point. The white wall on the right has also been bent around to the left reducing the angle between it and the grain boundary running across the picture. The walls are not straight in this region but vary along their length as they encounter the different pinning sites in the shape of dislocation tangles and grain boundaries.

As was expected the 7092 samples contained significantly more pearlite, but the microstructure was similar to the 7091 samples in that the pearlite grains were well defined. This is illustrated in the sequence of an undeformed sample recorded in figures 5.33 a) to d); the region appears similar to figure 5.30 of a 7091 sample in which a ferrite region is bounded at the top and bottom by pearlite grains. In the over- and under-focus micrographs with no applied field the straight domain walls running across the grain form closure domains onto the pearlite and to the small cementite inclusions in the lower half of the picture. The photographs are taken at low magnification so these domains are relatively large. When a field was applied

144
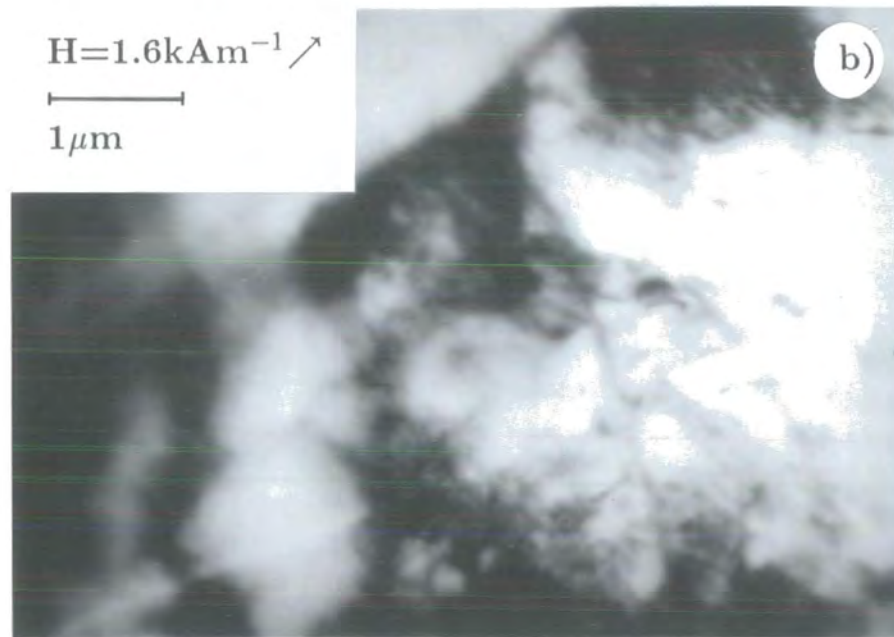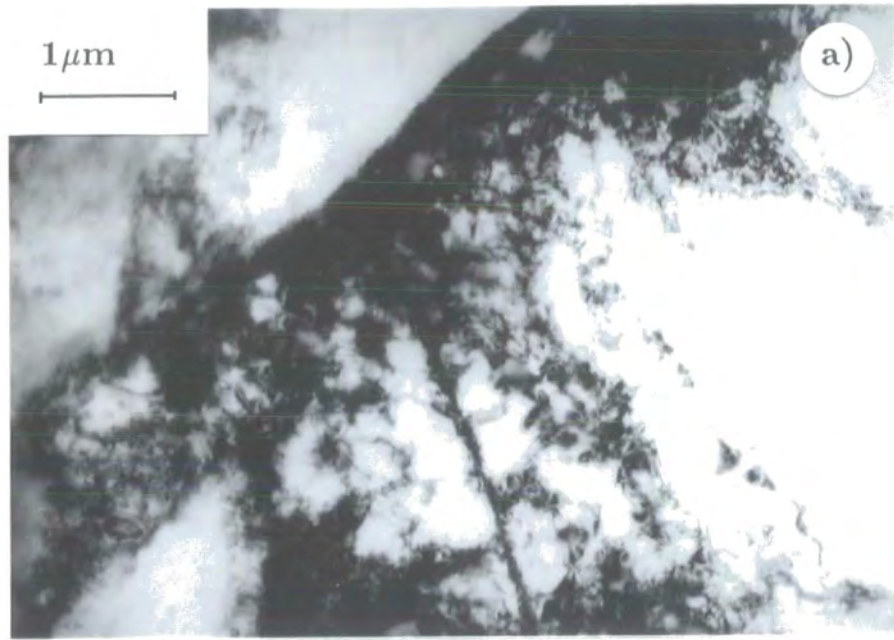
Figure 5.31 Fresnel electron micrographs of 10% deformed 7091 : a) infocus, b) underfocus at 1.6kAm⁻¹.
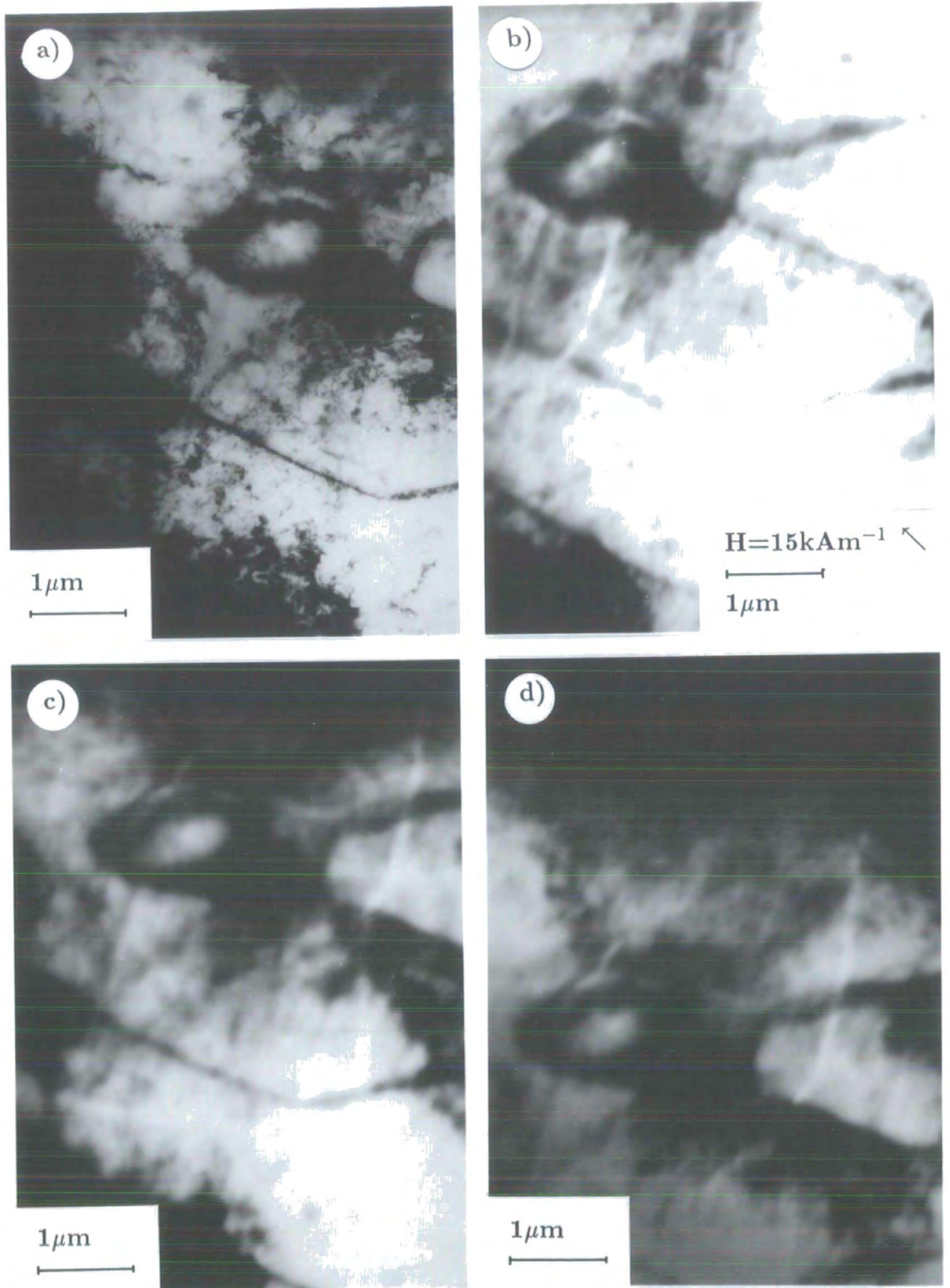
Figure 5.32 Fresnel electron micrographs of 10% deformed 7091 : a) infocus,
b) underfocus at maximum applied field of 15kAm^{-1}, c) and d)
underfocus at end of magnetising sequence.

Figure 5.33 Fresnel electron micrographs of undeformed 7092 : a) infocus, b) underfocus, c) underfocus, at 7.2kAm^{-1} and d) underfocus after reducing to -14.1kAm^{-1}.

parallel to these domain walls most of the steady movement along the pearlite boundary occurred at low fields with no movement at all above $10kAm^{-1}$. Figure 5.33 c) shows the situation at an increasing field of $7kAm^{-1}$ in which a white wall can be seen coming into the picture from the left slightly pinned by the small inclusions and dislocation tangles encountered along its length. The situation in the maximum negative applied field is shown in d) where the bottom part of the black wall has moved to the left to become pinned to the inclusion there.

Figure 5.34 is an infocus foucault micrograph inside a rather irregular undeformed pearlite nodule which illustrates how complex the domain configuration can be in such an area. On application of an applied field slow restricted domain wall movement was observed in this region.

A largely pearlitic area is shown at low magnification in figure 5.35a) where a complex array of domain walls can be seen running both across and along the lamellae. The more irregular the pearlite, the more irregular the domain pattern. The following five micrographs are taken at higher magnification of the relatively regular area to the right of the picture which is shown in focus in figure 5.35b). This clearly shows the cementite lamellae and the dislocations present in the ferrite. The magnetising sequence is taken in the overfocus position and records the domain wall movement up to a maximum applied field of $16kAm^{-1}$ and then finally after removing the applied field. The walls running across the colony are invariably affected by the presence of each cementite lamella, the wall's direction bending towards the lamella as it passes through each one. Some of the walls stop abruptly with closure domains onto a lamella or a heavily dislocated region. The actual wall movement, mainly across the lamellae and parallel to the applied field, although disjointed as the walls changed shape, was relatively steady and started at low fields.

A dislocated ferrite region in a 4% strained sample is shown at high magnification in figures 5.36a) and b). The overfocus micrograph shows a white domain wall attached to the dense dislocations to the right by a closure domain. To the left the wall splits again as it reaches another dislocated area. On the application of an applied field the wall bowed along its length before moving irreversibly. The photograph in 5.36 b) was taken after the field had been removed, but some

148

Figure 5.34 Foucault electron micrograph of undeformed 7092.
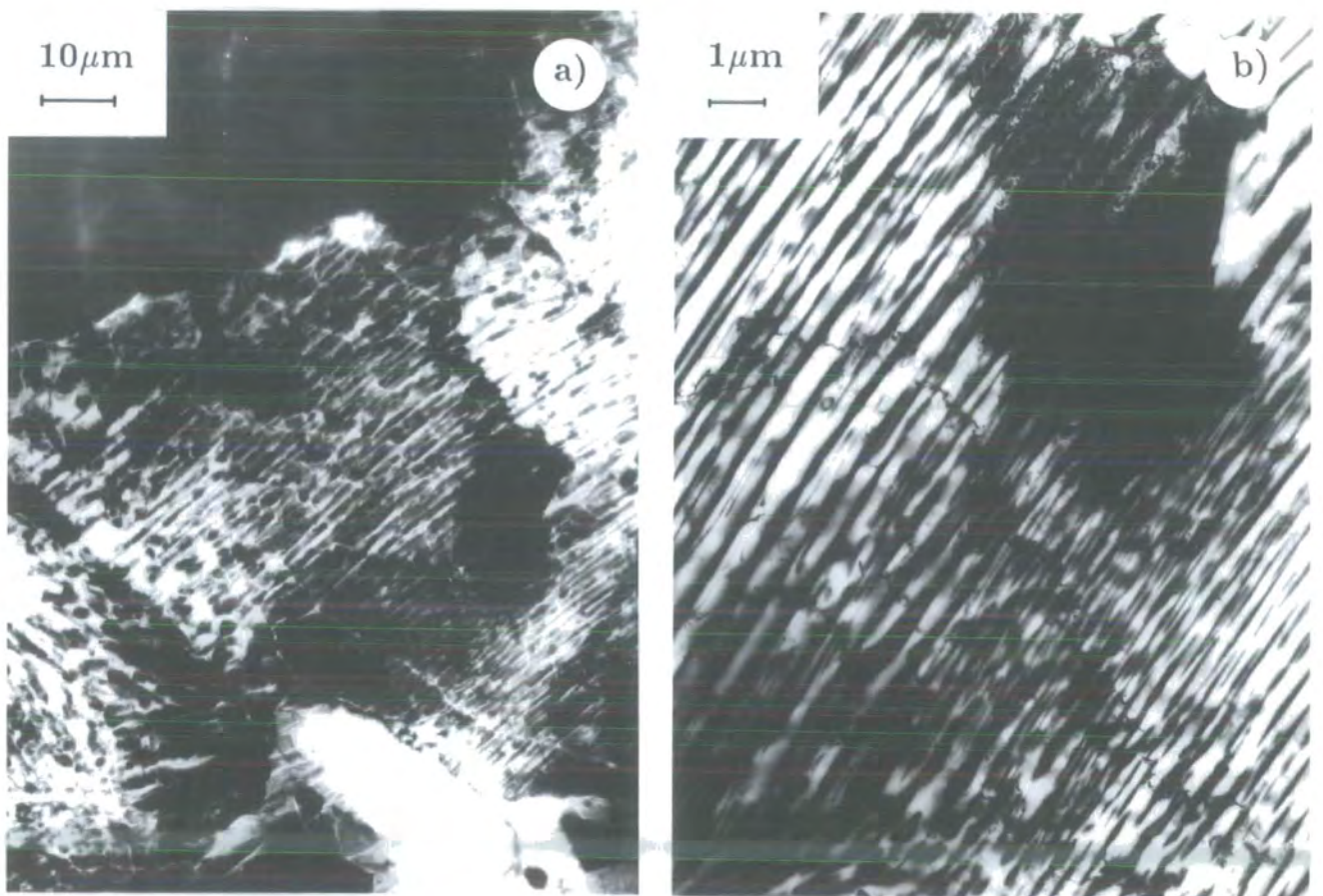
Figure 5.35 Fresnel electron micrographs of undeformed 7092 : a) and b) infocus.
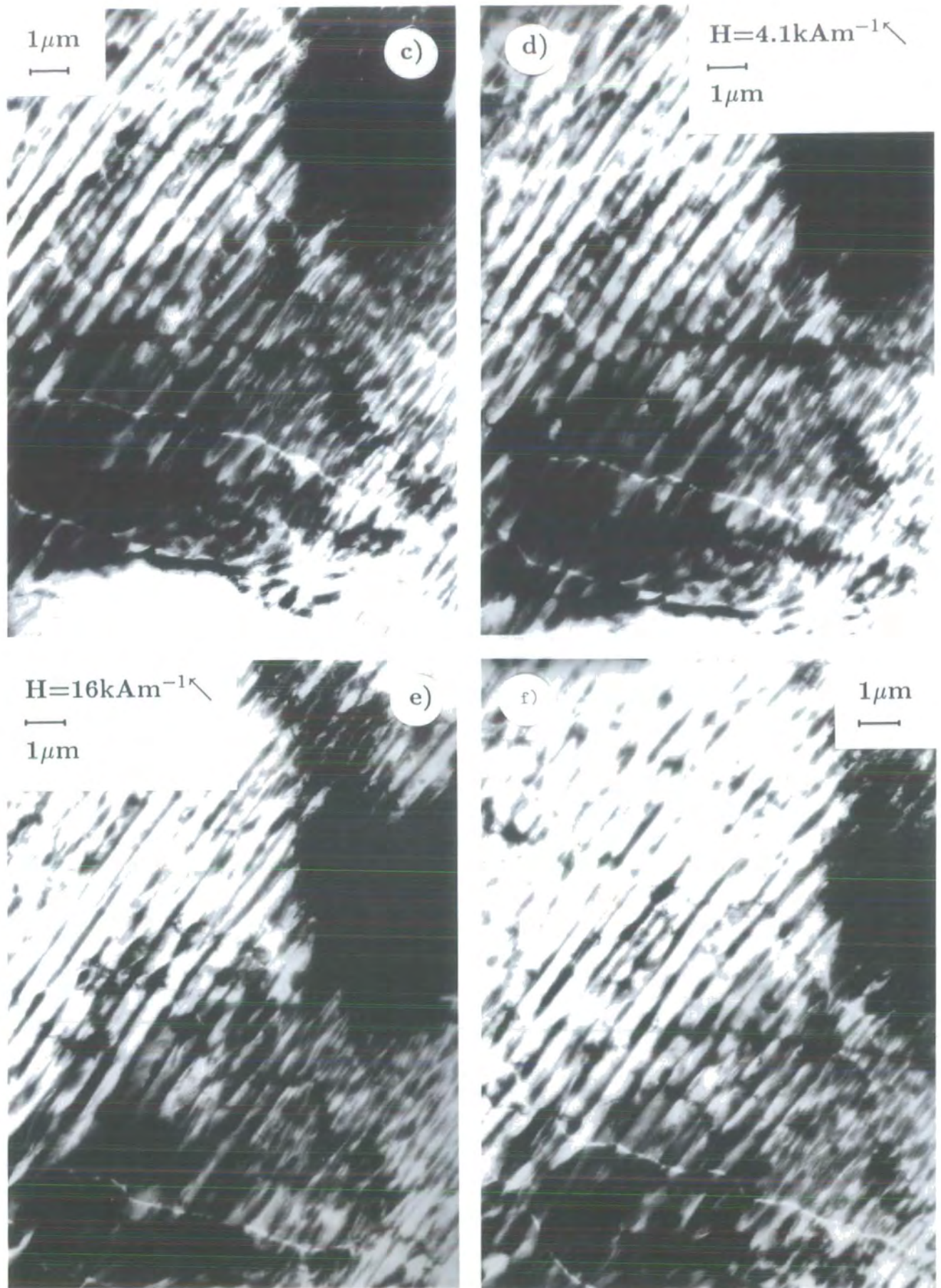
Figure 5.35 contd. c) overfocus, d) underfocus at 4.1kAm^{-1}, e) underfocus at 16kAm^{-1}and f) after removing the applied field.
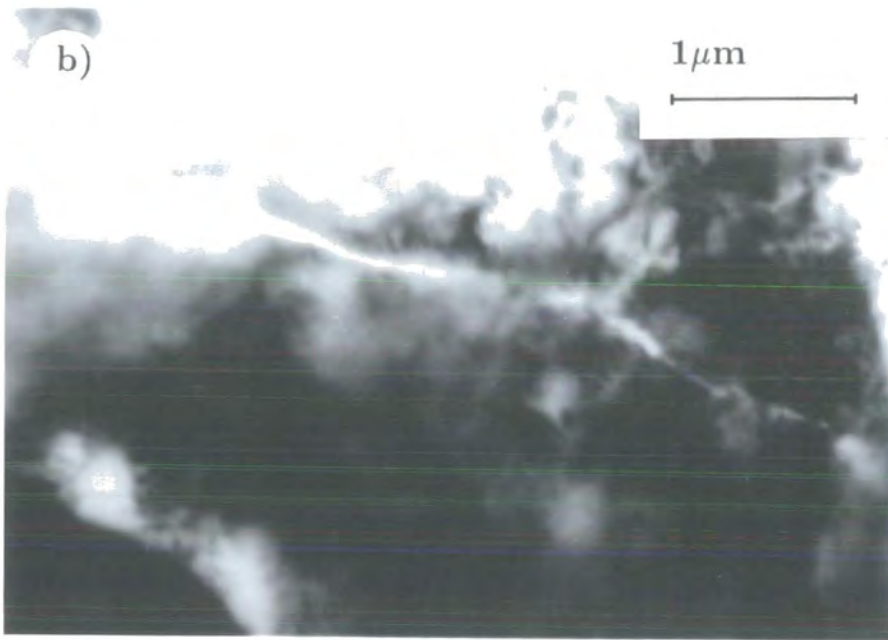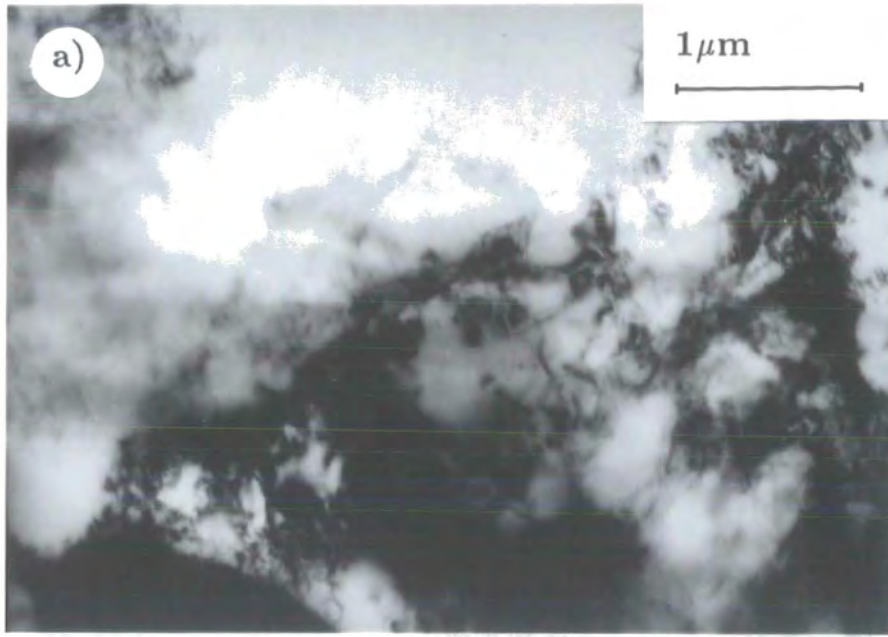
Figure 5.36 Fresnel electron micrographs of 4% deformed 7092 : a) infocus and b) overfocus.

of the bowing still remains and the wall also suffers further distortion where the dislocations are densest.

The four infocus micrographs in figure 5.37 illustrate the variety of pearlite structures to be found within one sample. These particular pictures were taken of a strained sample but similar microstructures were also observed in the undeformed material although the dislocation density is higher here. Figure 5.37a) is taken at a lower magnification to demonstrate how the pearlite microstructure can change from a fine divorced state such as that at the top left to a widely spaced lamella structure in the bottom right. The other three micrographs are taken at higher magnification to observe the pearlite on a scale that the domain walls encounter it. Broken up pearlite of this type was frequently observed in the 7092 and 7093 samples; it is not thought that the apparent shearing effect is due to the plastic strain, but that it is due to the low transformation temperature allowing nucleation within the grains as well as at the boundaries. A video sequence was taken in a similar pearlitic region where the domain wall movement was most disturbed in the irregular areas forming closure domains onto the disjointed lamellae and bowing in-between inclusions.

Samples 7093 and 7094 appeared to be almost 100% pearlite although even in the 7094 samples the occasional clear area of ferrite was present. As the ferrite etches preferentially to the pearlite these samples were more consistently electro-polished. The first sequence of micrographs displayed of the 7093 samples in figure 5.38 is of an undeformed pearlitic region at the junction of two pearlite colonies. At the higher magnifications the regular, although broken up, nature of the lamellae becomes clearer. In the fresnel micrograph a white domain wall runs down the picture diagonally across the lamellae. The wall is quite straight and moves relatively steadily towards the colony boundary, distorting a little as it crosses the lamellae, where it becomes pinned.

Figure 5.39 shows three further examples of different pearlite lamellae at high magnifications. At a lower magnification figure 5.40 shows a disjointed pearlite region both in and out of focus. The domain configuration is very complex with short distorted domain walls which rearranged rapidly on the application of an applied field making it difficult to follow a magnetising sequence.
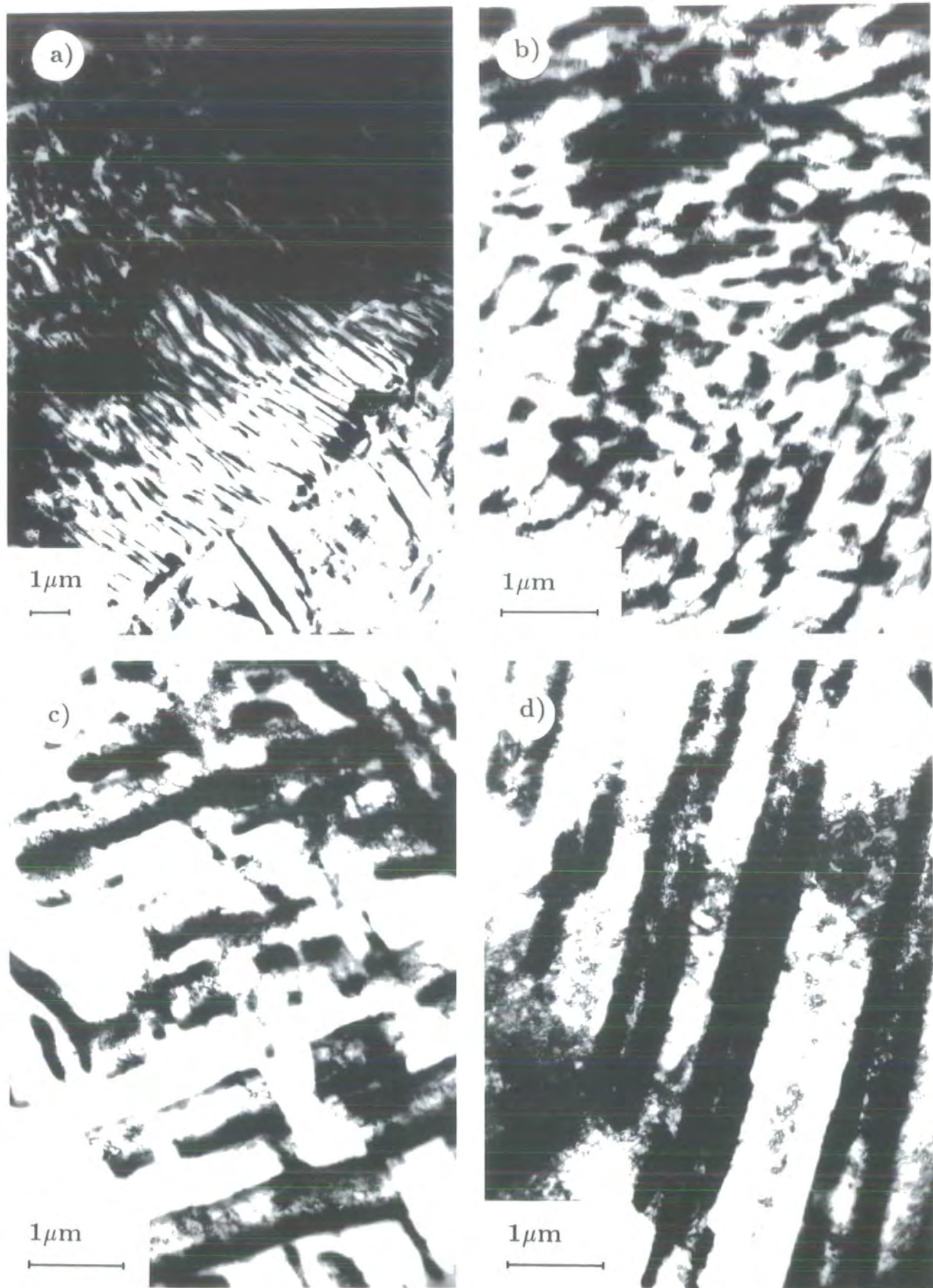
Figure 5.37 Infocus electron micrographs of 4% deformed 7092.
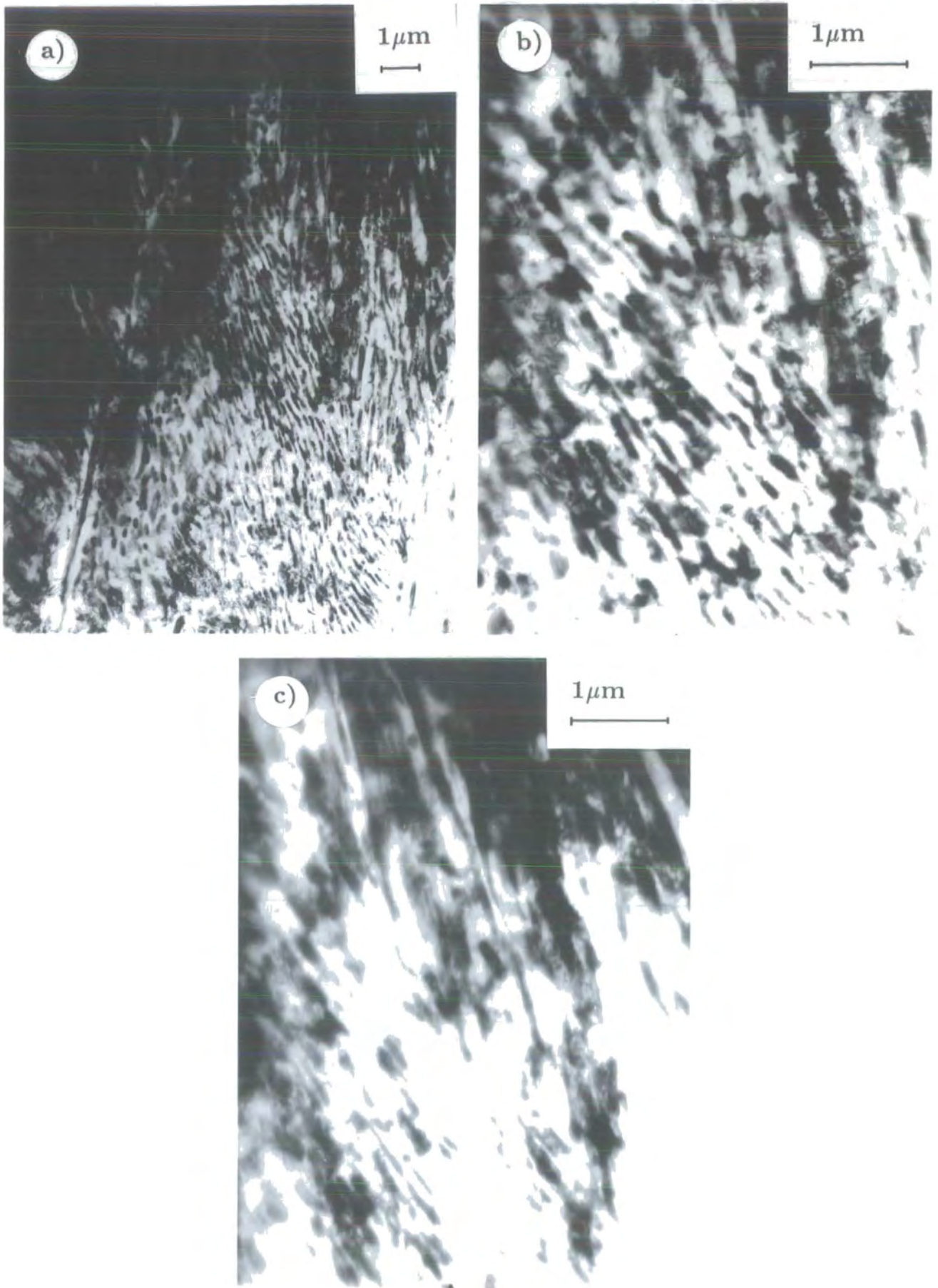
Figure 5.38 Fresnel electron micrographs of undeformed 7093 : a) and b) infocus and c) underfocus.
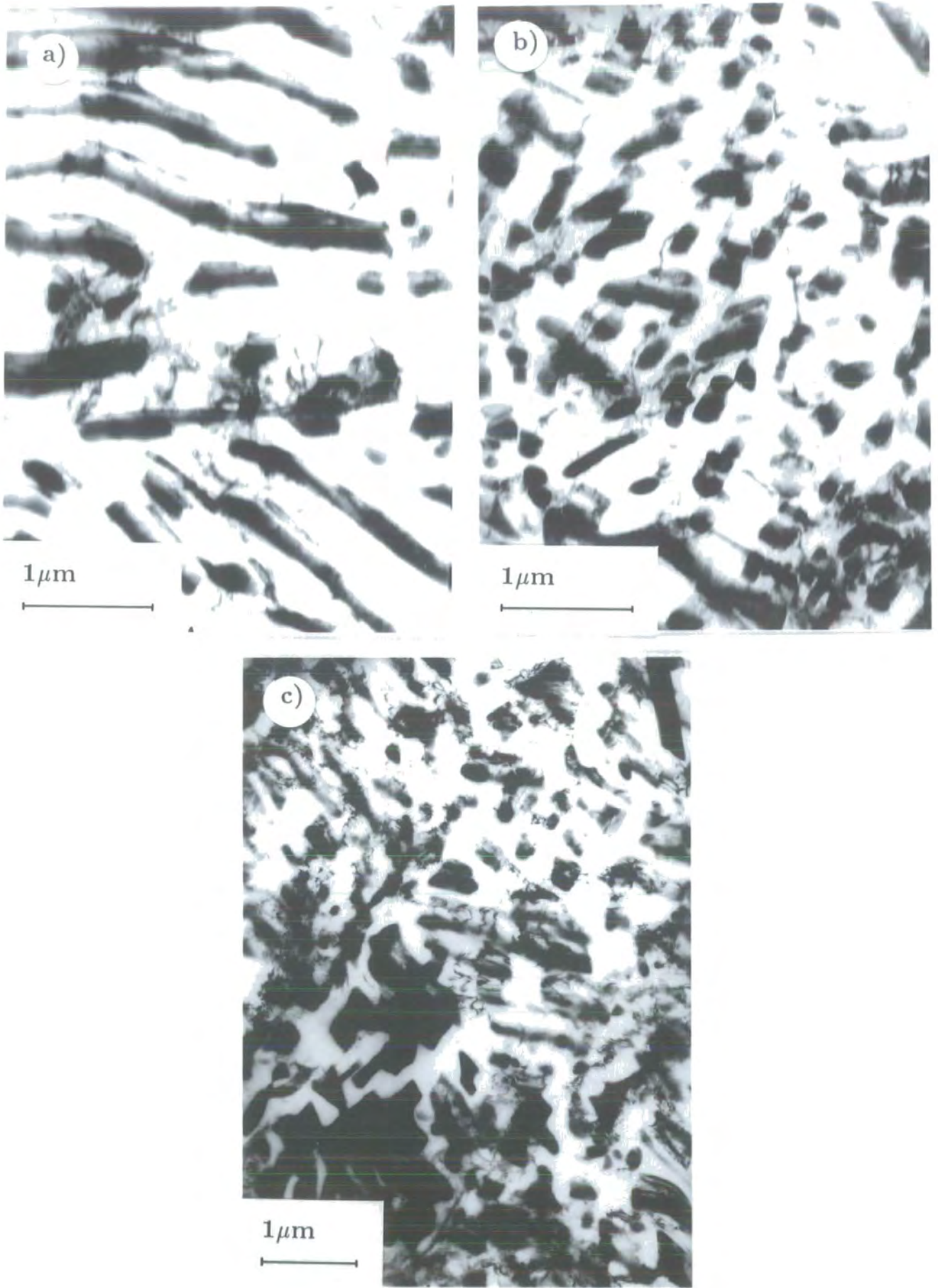
Figure 5.39 Infocus electron micrographs of undeformed 7093.
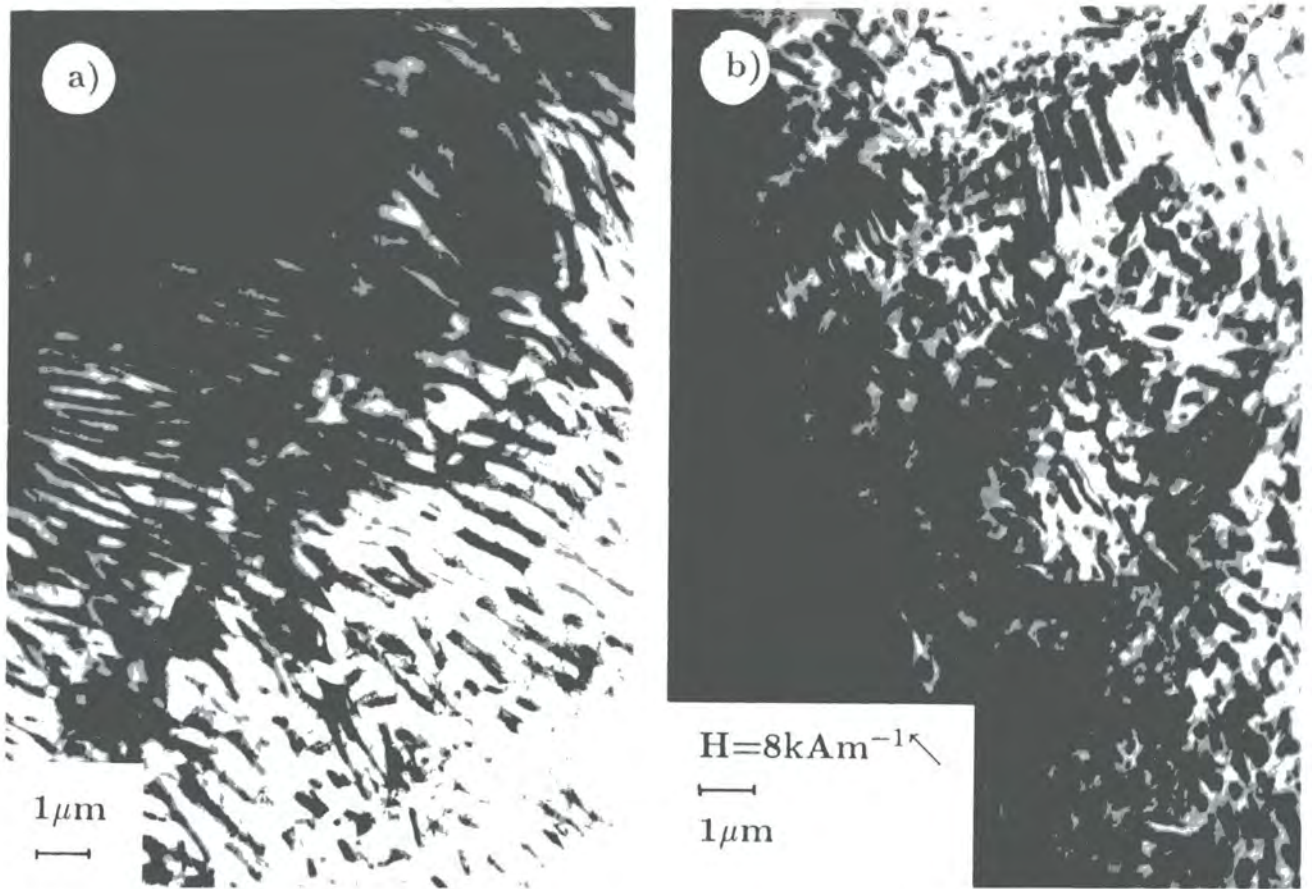
Figure 5.40 Fresnel electron micrographs of undeformed 7093 : a) infocus and b) underfocus at 8kAm^{-1}.
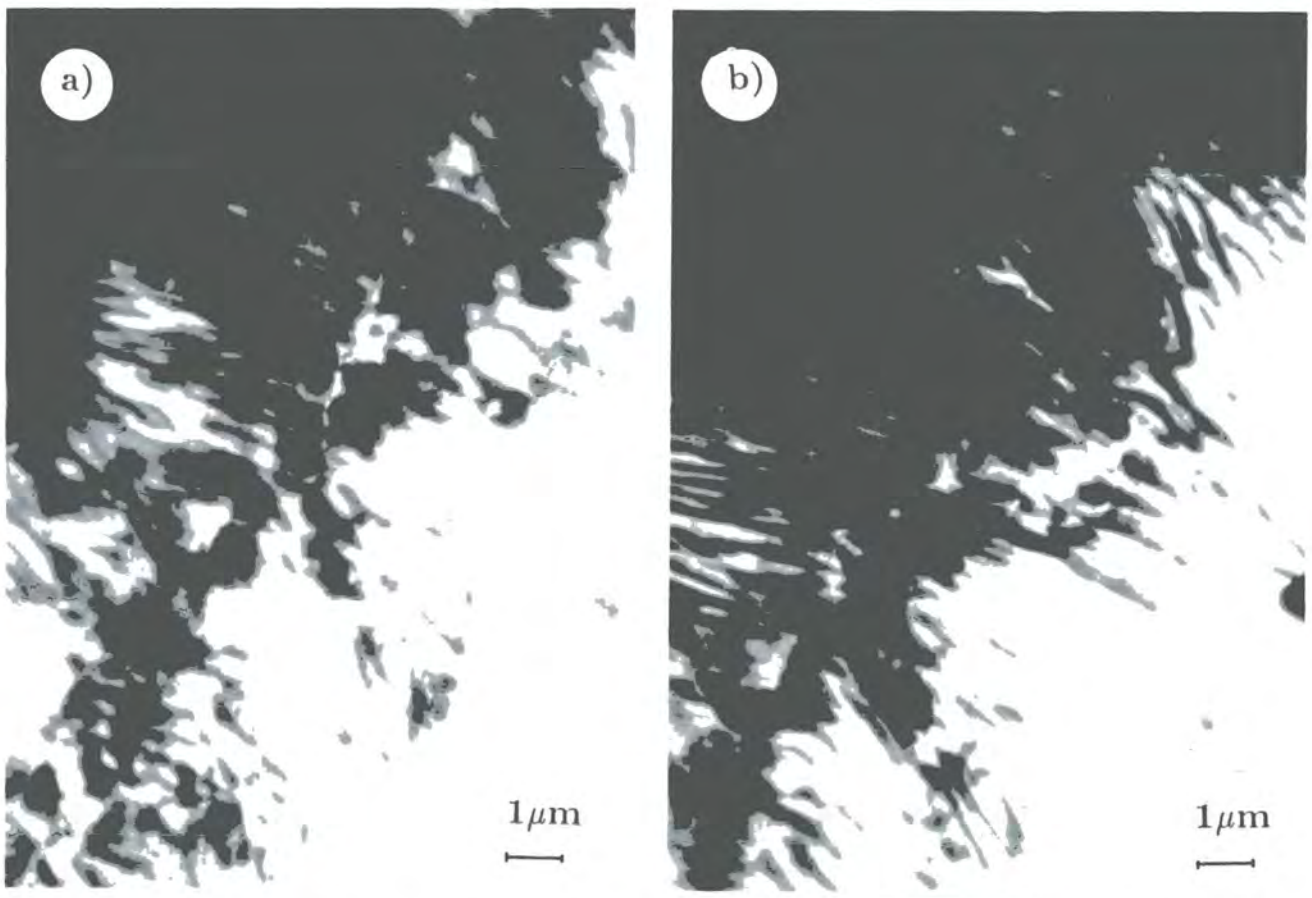
Figure 5.41 Fresnel electron micrographs of undeformed 7093 : a) overfocus. b) underfocus.

A more ordered undeformed pearlitic region is presented in figure 5.41 with a long domain wall running across the lamellae. Although the wall is strongly affected by the cementite forming closure domains and splitting in places along its length, when a field was applied it was able to remain largely intact as it moved across the lamellae.

Two infocus examples of the microstructure in a strained 7093 sample are presented in figure 5.42.; a) is a dislocated ferrite region and b) a pearlitic region where the dislocations are visible in the ferrite.

The improved electropolishing of the 7094 100% pearlite resulted in better contrast and hence it was possible to successfully photograph some full magnetising sequences. The first (figures 5.43 a) to h)) is taken in a regular pearlitic region of an undeformed sample with the major walls running across the lamellae. As usual the walls are distorted along their length by the occasional closure domain and split wall. As a positive field is applied the main white wall in the overfocus fresnel micrographs moves upwards towards the pearlite boundary, but becoming strongly pinned by the dark tangled region within the grain, bowing substantially before being released and attaching itself to the boundary at maximum applied field (5.43 e)). On removing the field the wall is released from the boundary and has reached the tangled area again by the remanent point. Subsequently applying a reverse magnetic field the wall becomes pinned again and eventually breaks up as it tries to pass the pinning area.

The second sequence in figures 5.44a) to h) is also in an unstrained sample and illustrates a small ferrite grain sandwiched between two pearlite grains with their lamellae parallel to the ferrite-pearlite grain boundaries. Domain walls can be seen in the ferrite running between these two pearlite grains and walls in the pearlite in the same direction across the lamellae. A wall is also visible running diagonally between the two pearlite grains . As the field is increased in a direction perpendicular to the lamellae this diagonal wall jumps to become parallel to the pearlite grain boundary where it becomes pinned and at the same time another, similar wall at the same orientation detaches itself from the opposite side of the pearlite grain moving in the same direction. The two walls in the ferrite running directly between the two grains quickly disappear, while the walls in the pearlite
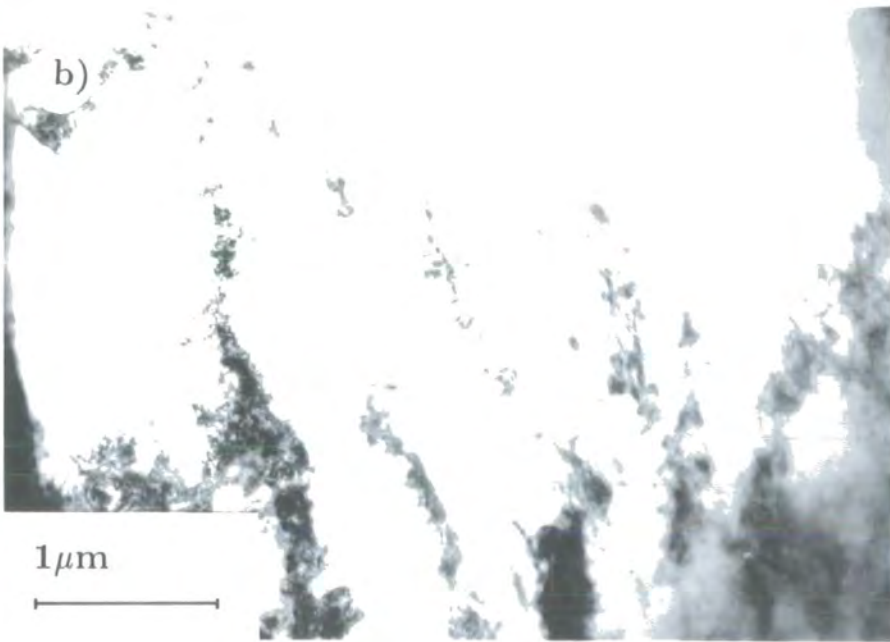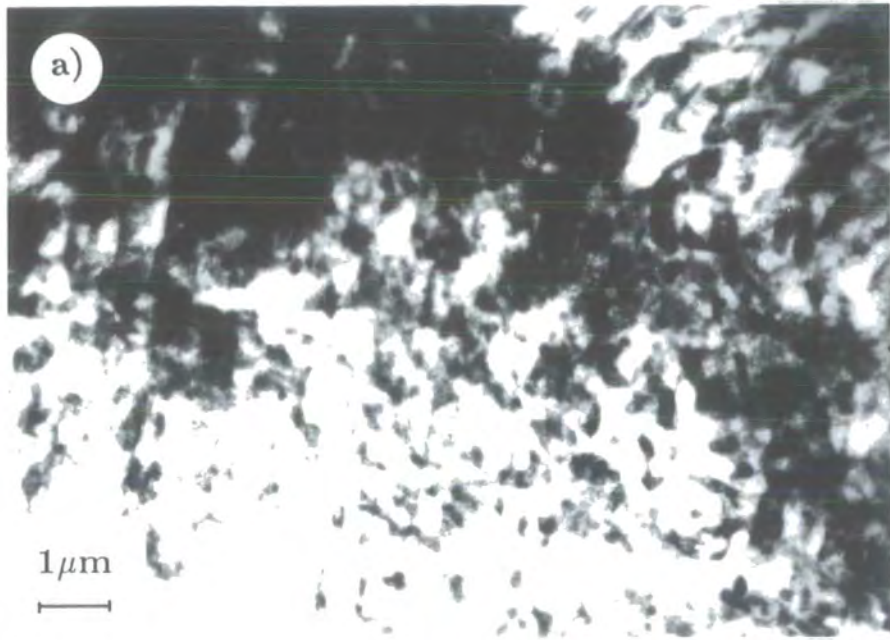
Figure 5.42 Infocus electron micrographs of 7% deformed 7093.
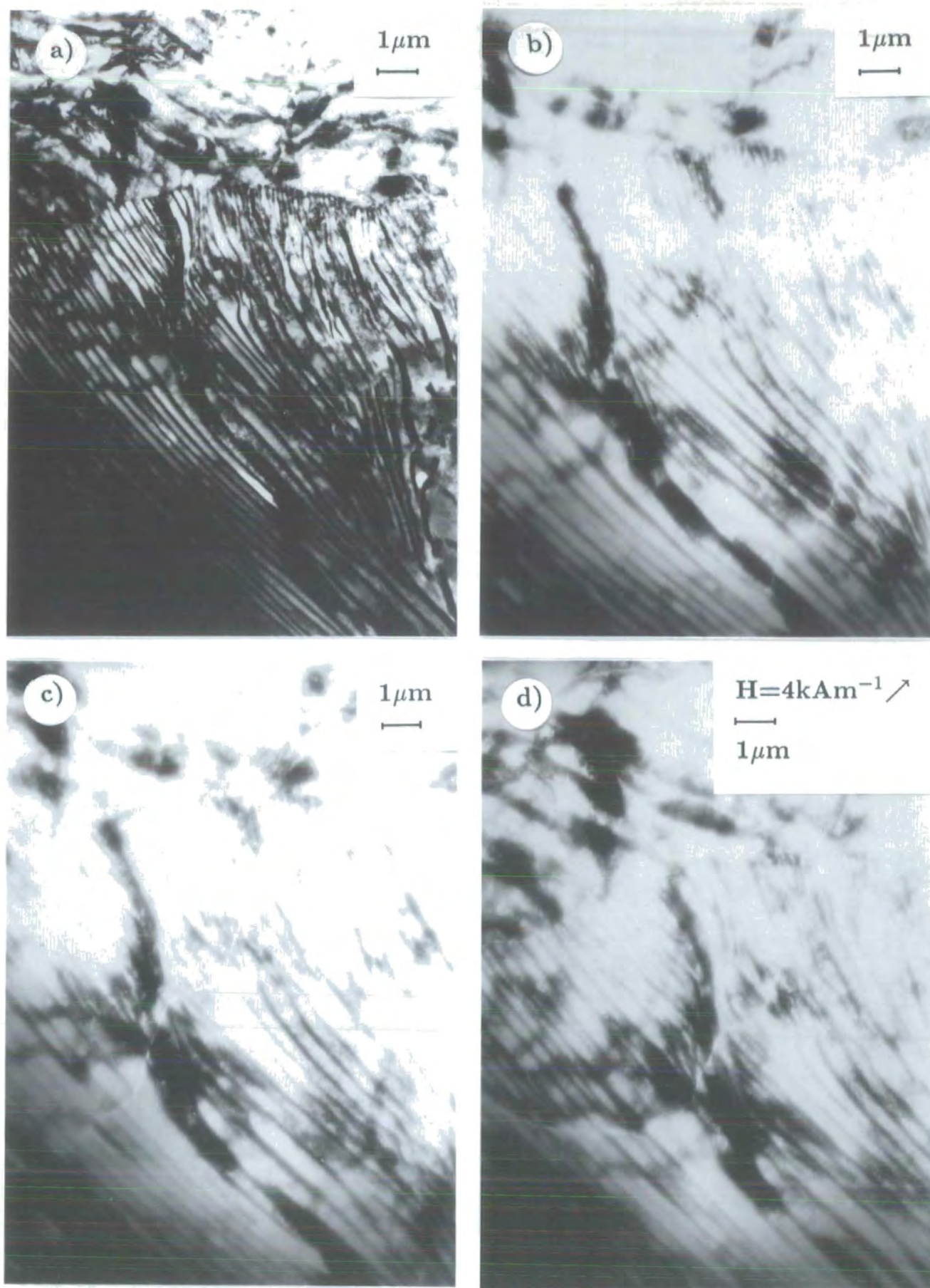
Figure 5.43 Fresnel electron micrographs of undeformed 7094 : a) infocus, b) underfocus, c) overfocus and d) at 4kAm^{-1}.
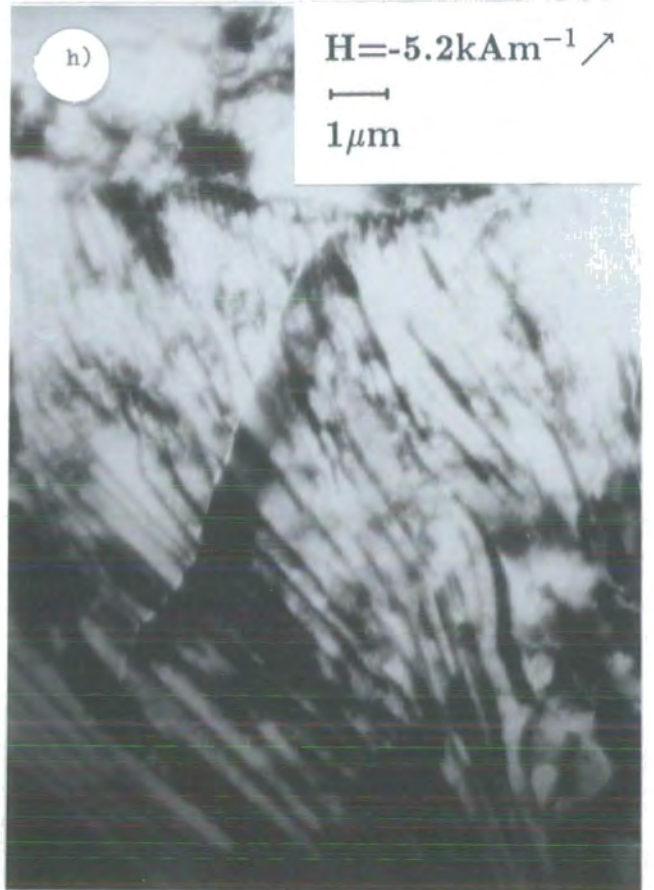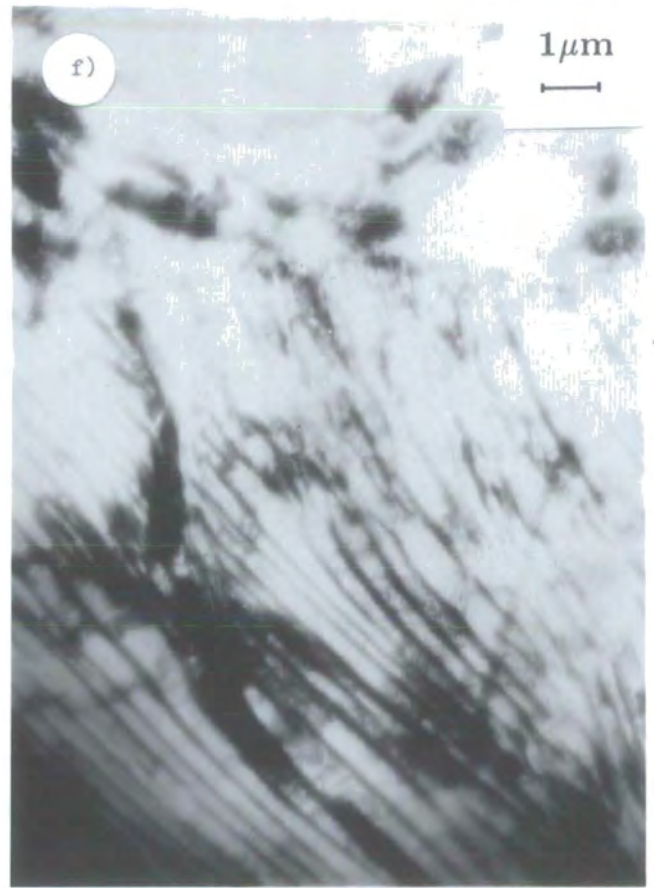
Figure 5.43 contd. e) overfocus at 8.3kAm^{-1}, f) overfocus after removing the field, g) overfocus at -8.3kAm^{-1} and h) after reducing the field to -5.2kAm^{-1}.
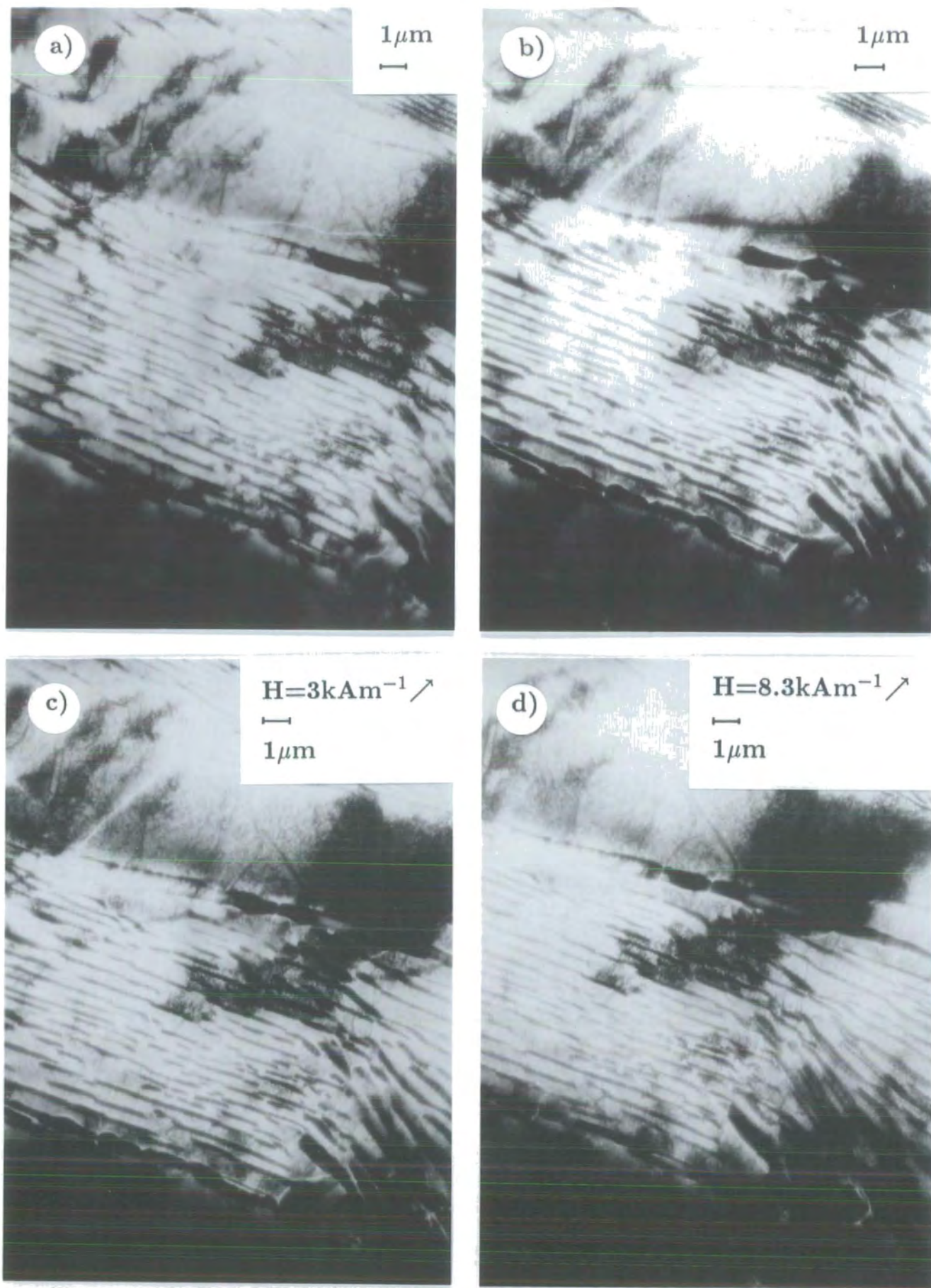
Figure 5.44 Fresnel electron micrographs of undeformed 7094 : a) overfocus, b) underfocus, c) underfocus at $3kAm^{-1}$ and d) underfocus after increasing the field to $8.3kAm^{-1}$.
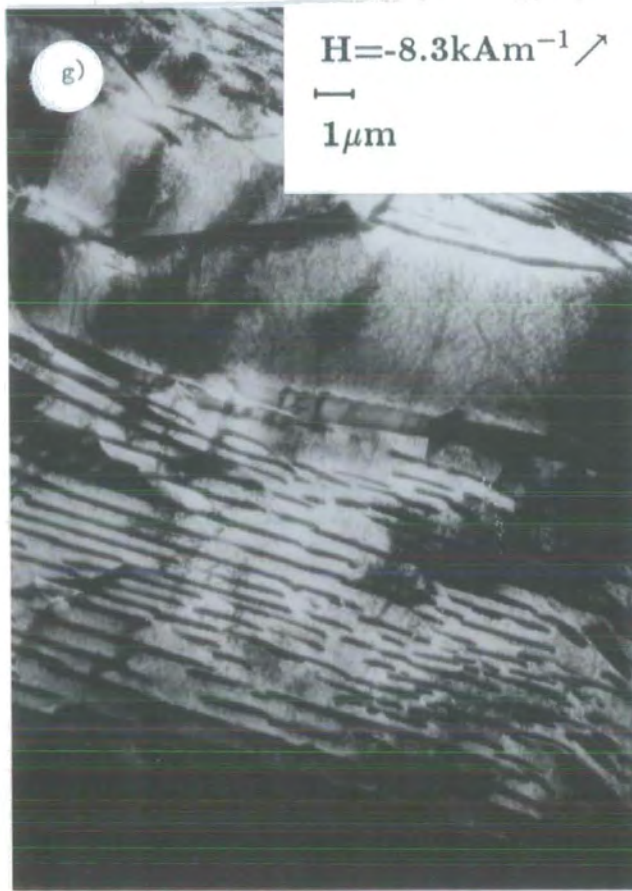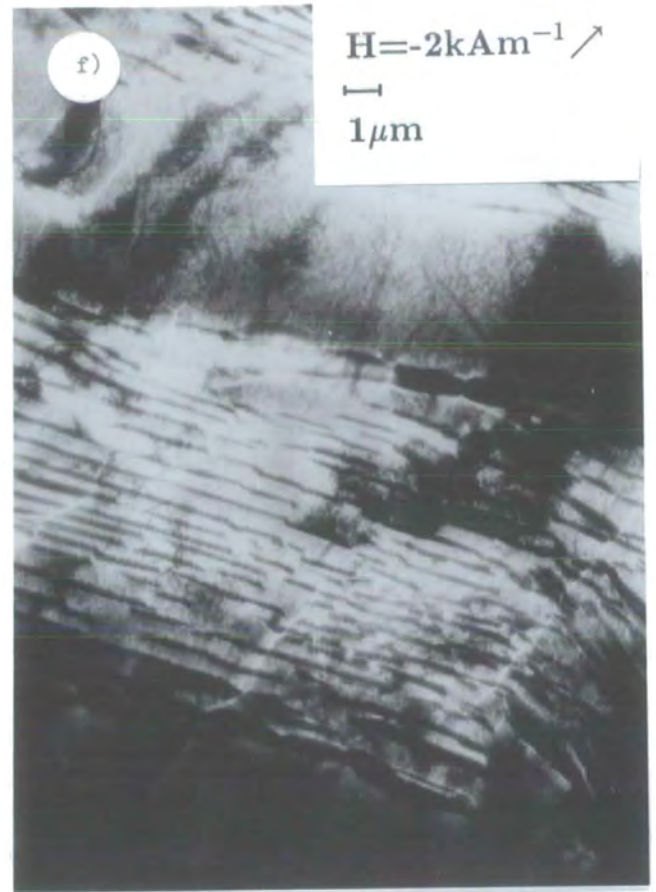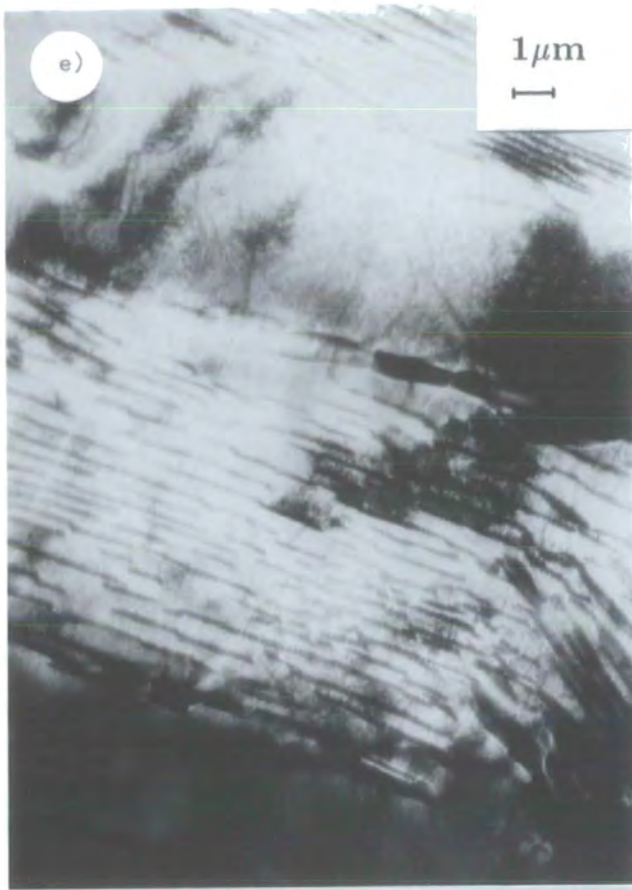
Figure 5.44 contd. e) underfocus after removing the field, f) underfocus at -2kAm^{-1}, g) underfocus at -8.3kAm^{-1} and h) after removing the negative field.

slowly make their way across the lamellae. This is the only movement still visible above $4kAm^{-1}$. As the field is removed and a negative field applied the diagonal wall returns again to the top ferrite grain.

The final magnetising sequence (figures 5.45 a) to g)) is taken in a pearlitic region within a 10% deformed sample. The area, which is a junction of three pearlite colonies, is shown infocus first at different magnifications to illustrate the heavily dislocated ferrite. The domain walls run mainly across the lamellae and move intact as the field is applied. In addition to the usual distortions the wall experiences whilst in pearlite it also bows over quite a large scale as it moves across the grain. When the field is reduced to zero the wall splits around a particularly tangled region as it tries to move to the left and is finally released from this pinning site when a negative field is subsequently applied.

5.4 Heat Treated Samples.

For steels with pearlite contents greater than 20% the changes in microstructure induced by different heat treatments are largely dominated by the effect of the presence of the carbon itself. However for lower carbon content material the changes in carbon morphology and in grain size can have a significant effect on the properties of the steel. To investigate how the response of these materials to plastic deformation is affected by its microstructure four of the 20% pearlite bars were subjected to different heat treatments.

5.4.1 Sample Details.

Initially the heat treatments were tested on the 70mm offcuts from the bars by F.Coultard and G.Watson as part of their final year project. Toroids were cut from these bars to measure their bulk magnetic properties and samples examined under the optical microscope.

Four of the 370mm bars were then subjected to the same heat treatments, samples cut from them examined under the optical microscope and their magnetic properties measured using the permeameter and compared to those determined prior to heat treatment. The samples were then progressively deformed in four

163
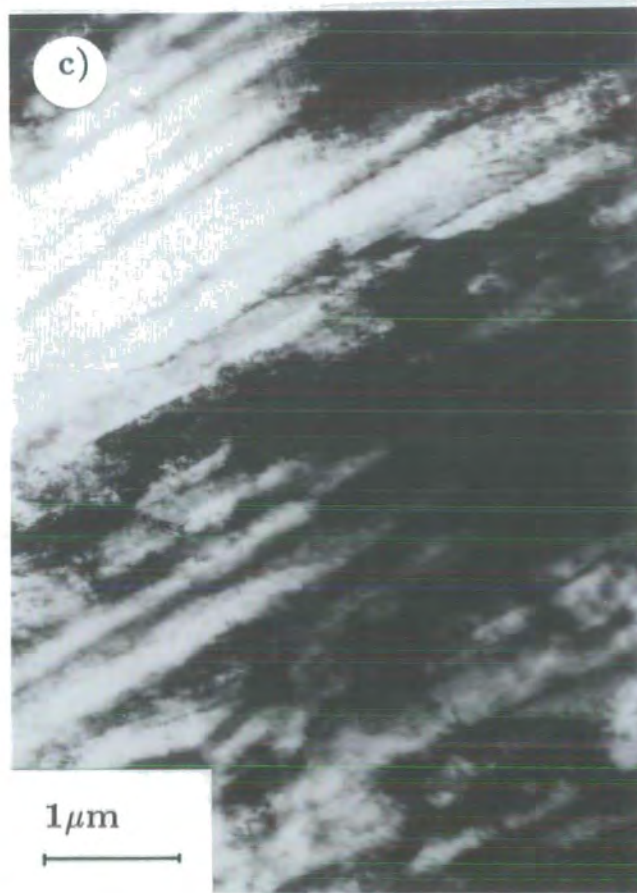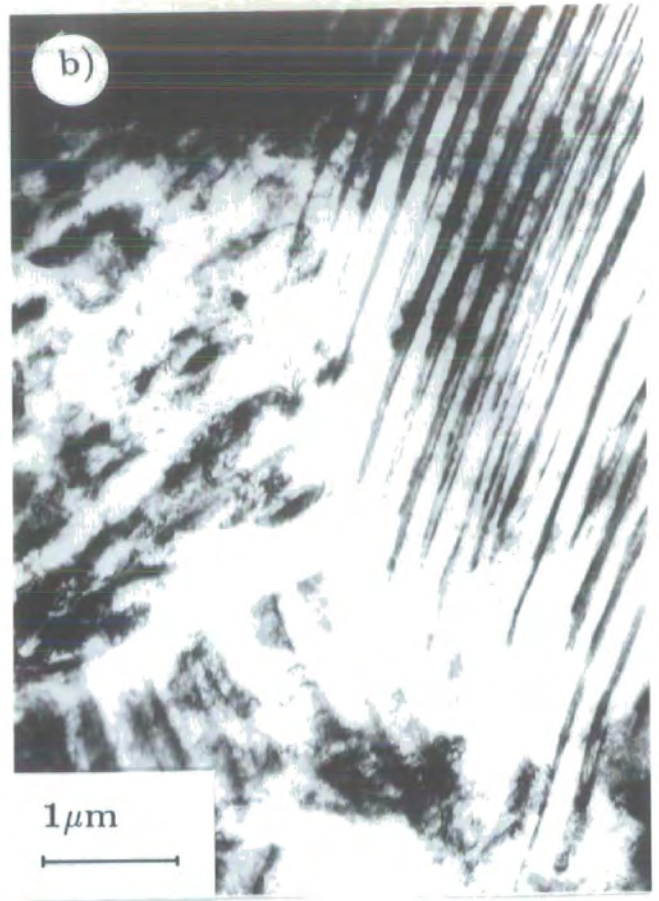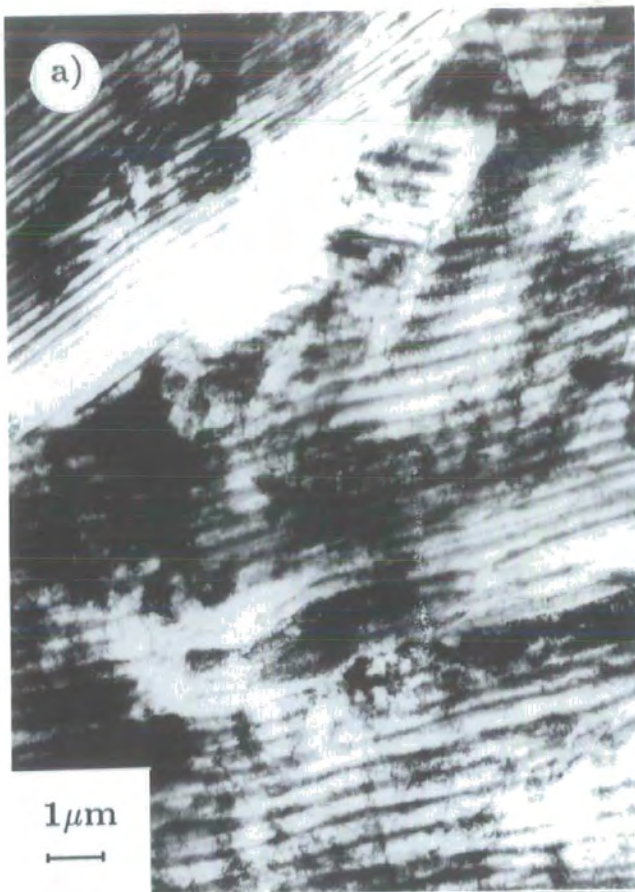
Figure 5.45 Fresnel electron micrographs of 10% deformed 7094 : a), b) and c) infocus.
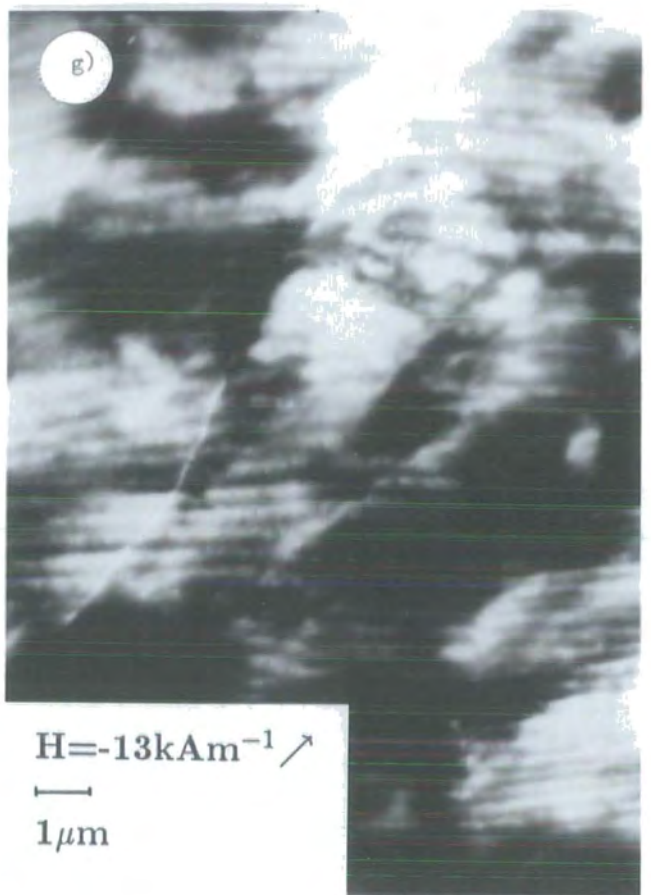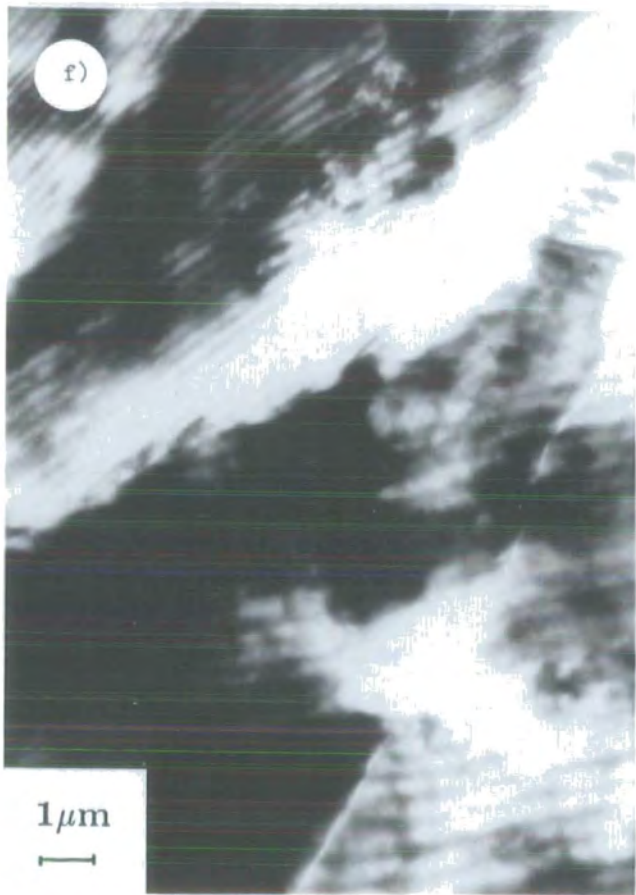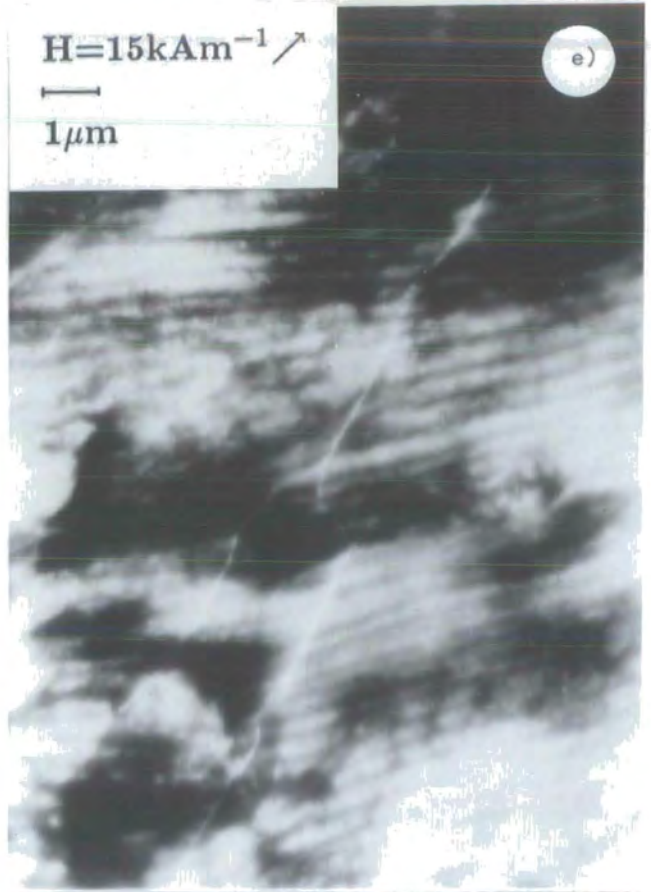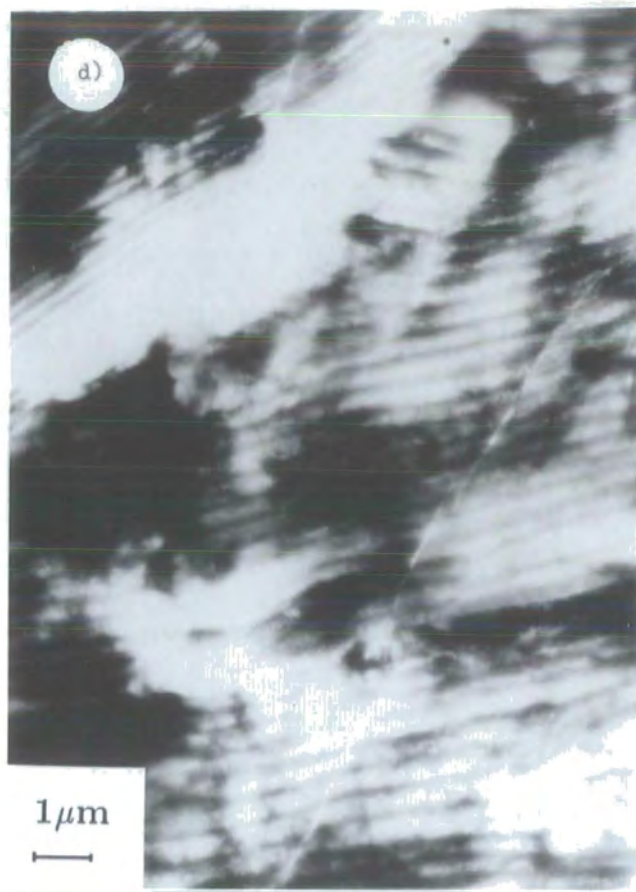
Figure 5.45 contd. d) overfocus, e) overfocus at $15kAm^{-1}$, f) overfocus after removing the field and g) overfocus at $-13kAm^{-1}$.

stages on the 500kN Denison tensile testing machine, measuring the Vickers Hardness, Barkhausen noise and magnetic properties on the permeameter between each stage.

All the heat treatments involved renormalisation at 860°C for 90 minutes followed by four different cooling rates to encourage varying grain size and degrees of spheroidisation between the samples. The process of normalising alone will relieve some of the stresses induced during the extrusion process. While the samples were in the furnace they were kept enclosed in a silica tube in an argon atmosphere throughout. Details of the four treatments used are given in table 5.03.

Type	Sample	Heat Treatment
A	7091E	1.5 hours at 860°C, air cooled
D	7091A	1.5 hours at 860°C, furnace cooled
B	7091G	1.5 hours at 860°C, 1 hour at 600°C
C	7091B	1.5 hours at 860°C, 2 hours at 600°C

Table 5.03 Heat Treatments for the Low Carbon Content Steel.

The optical micrographs taken for both the bars and offcuts are presented in figures 5.46 to 5.49. All the microstructures showed an irregular grain size indicative of incomplete austenisation. As only those grains that have transformed are able to then nucleate the growth of ferrite and pearlite on retransformation some of the ferrite grains will remain in their initial state. Where samples were air-cooled the increased cooling rate of the smaller 70mm offcut samples has resulted in different microstructure from the full 370mm bars.

The air-cooled sample of heat treatment "A" has cooled quite rapidly resulting in a low transformation temperature enabling nodular pearlite growth by nucleation similar to that in the pipe-steel. The higher magnification micrograph shows the lamellar pearlite structure within the pearlite nodules along with some free carbides in the ferrite grains. The more rapid cooling of the offcut has resulted in a smaller and more regular grain size. The fast cooling has also caused some

166
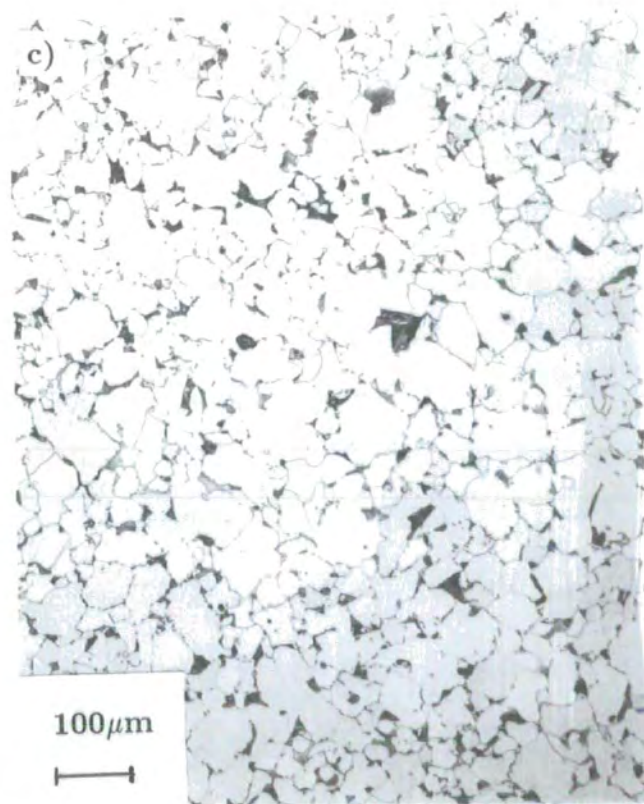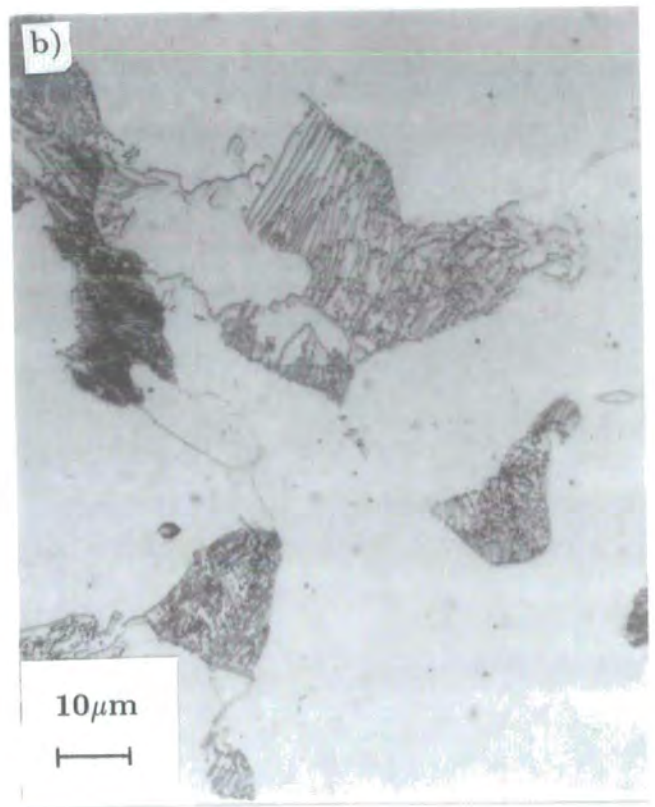
Figure 5.46 Optical micrographs of undeformed 7091 Heat treatment "A" : a) ×100, b) ×1000, c) offcut ×100.
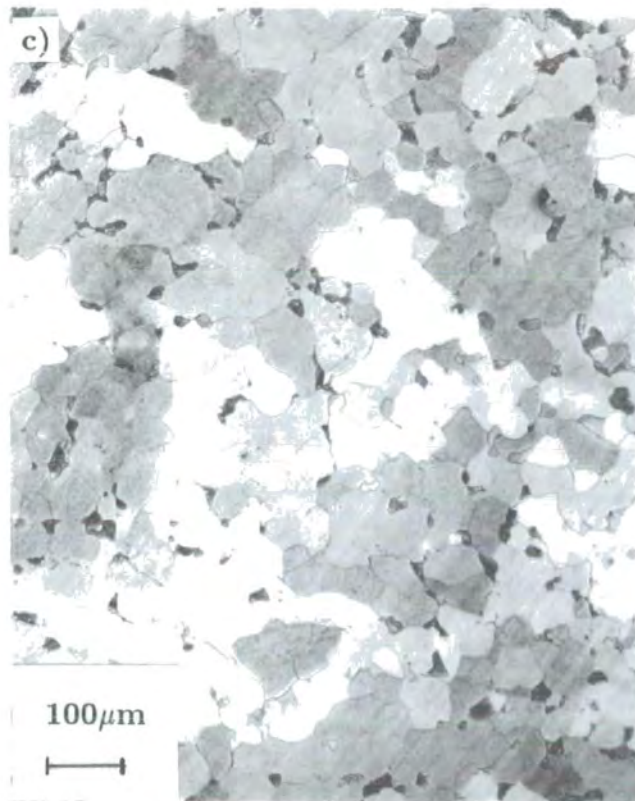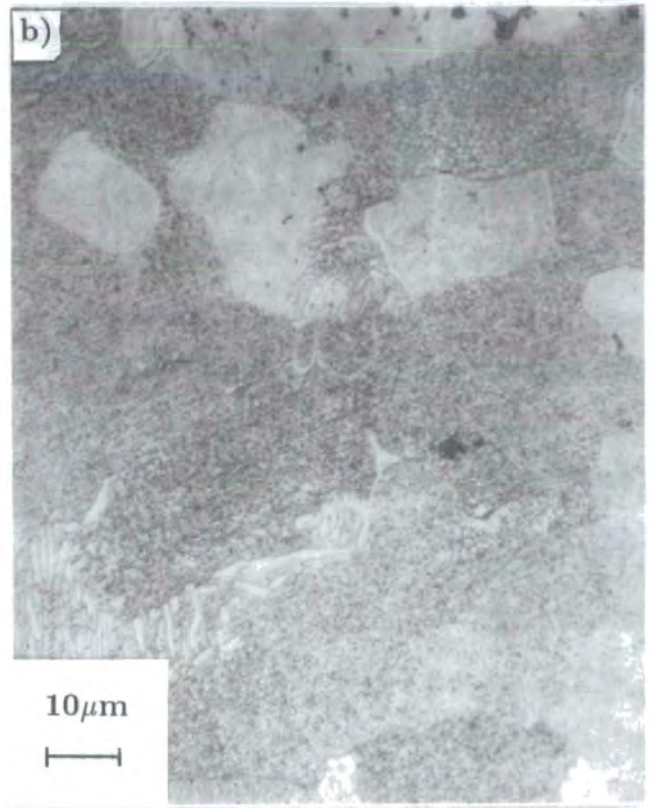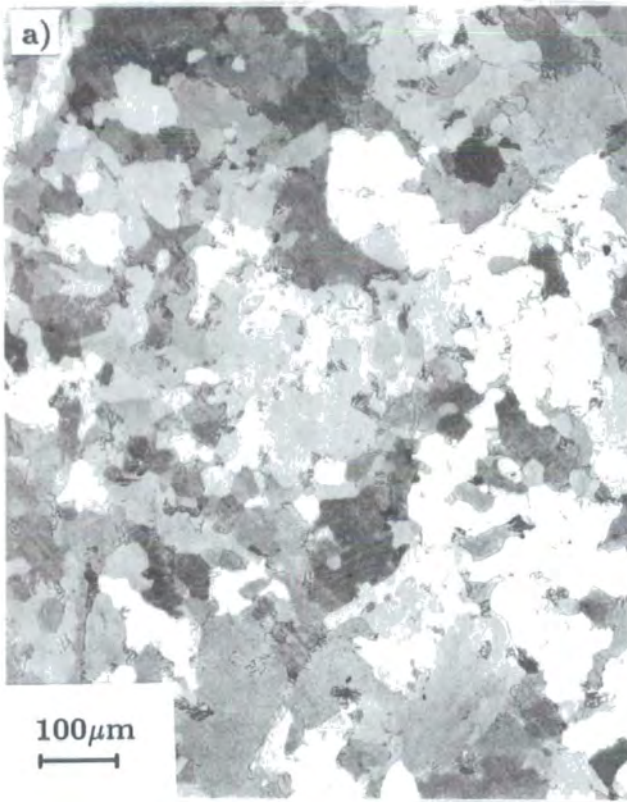
Figure 5.47 Optical micrographs of undeformed 7091 Heat treatment "D" : a) ×100, b) ×1000, c) offcut ×100.
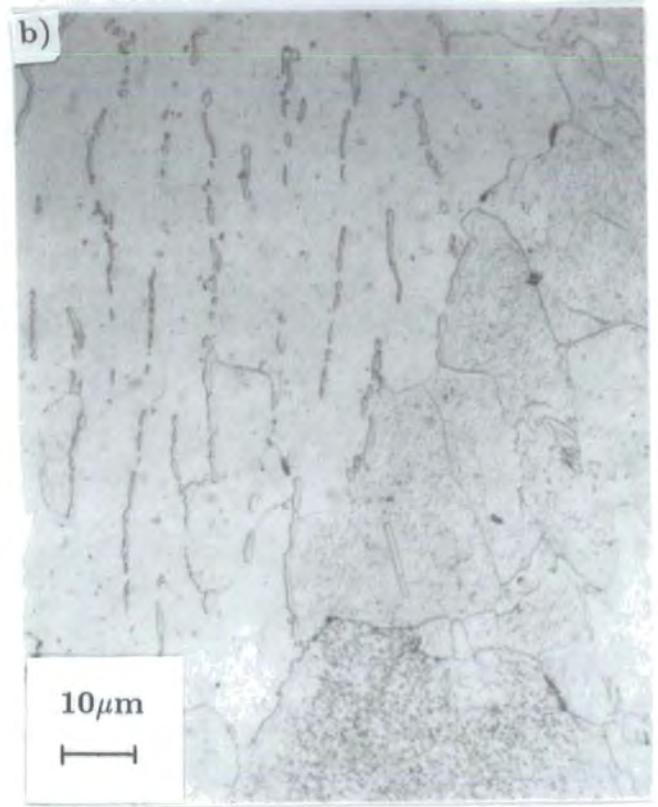
Figure 5.48 Optical micrographs of undeformed 7091 Heat treatment "B" : a)
×100, b) ×1000, c) offcut ×100.
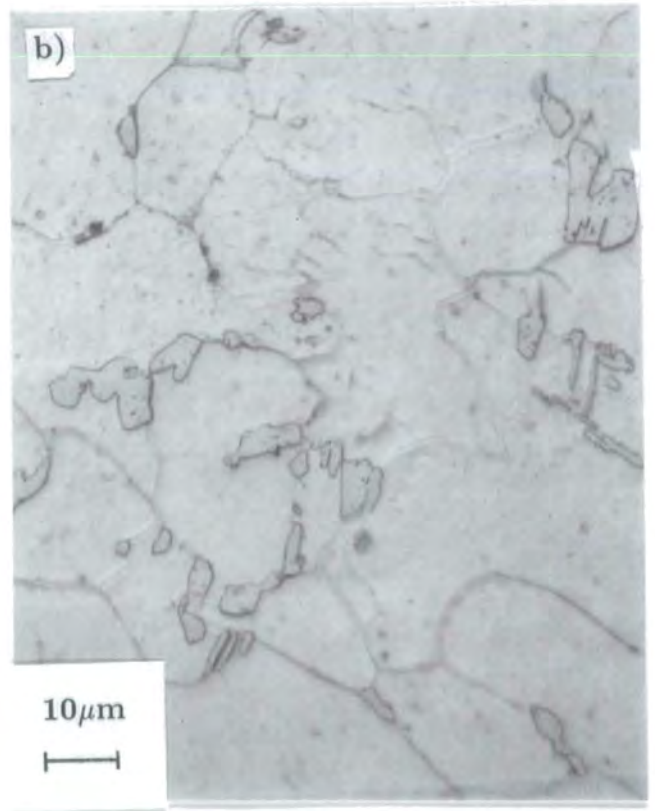
Figure 5.49 Optical micrographs of undeformed 7091 Heat treatment "C" : a) ×100, b) ×1000, c) offcut ×100.

carbides to be deposited around the ferrite grains, this can have a drastic effect on the toughness of the material. Some free carbides are also visible.

The slower cooling rate during the furnace cooling of heat treatment "D" has enabled more complete nulcleation growth with larger ferrite grain sizes and pearlite more dispersed through the sample. As the sample was furnace cooled the offcut shows a very similar microstructure.

Heat treatments "B" and "C" which involved holding the sample subcritical for one and two hours respectively after normalisation show the effects of carbide growth over this period. The microstructure is similar to that prior to heat treatment in that due to the slow cooling the pearlite growth is very dispersed with fewer nodules and some lath-type growth. Very little of the pearlite now shows a lamellar structure and some of the free carbides especially in "C" are exceptionally large. The offcuts were cooled more rapidly to 600°C by removing them from the furnace briefly and hence the lower transformation temperature has resulted in a microstructure similar to that of the air-cooled offcuts of heat treatment "A", but without the free carbides deposited on the grain boundaries and with larger ferrite grains.

Further observations under the optical microscope showed that in some cases there had been a loss of carbon at the surface and in all the samples the microstructure at the surface was not representative of the bulk. Due to the small surface penetration of Barkhausen noise it was decided that any such recordings of the heat treated samples could not be relied upon to give a true indication of the magnetisation processes within the sample.

The variation of Vickers Hardness with plastic Deformation for the various heat treatments are displayed in figure 5.50.
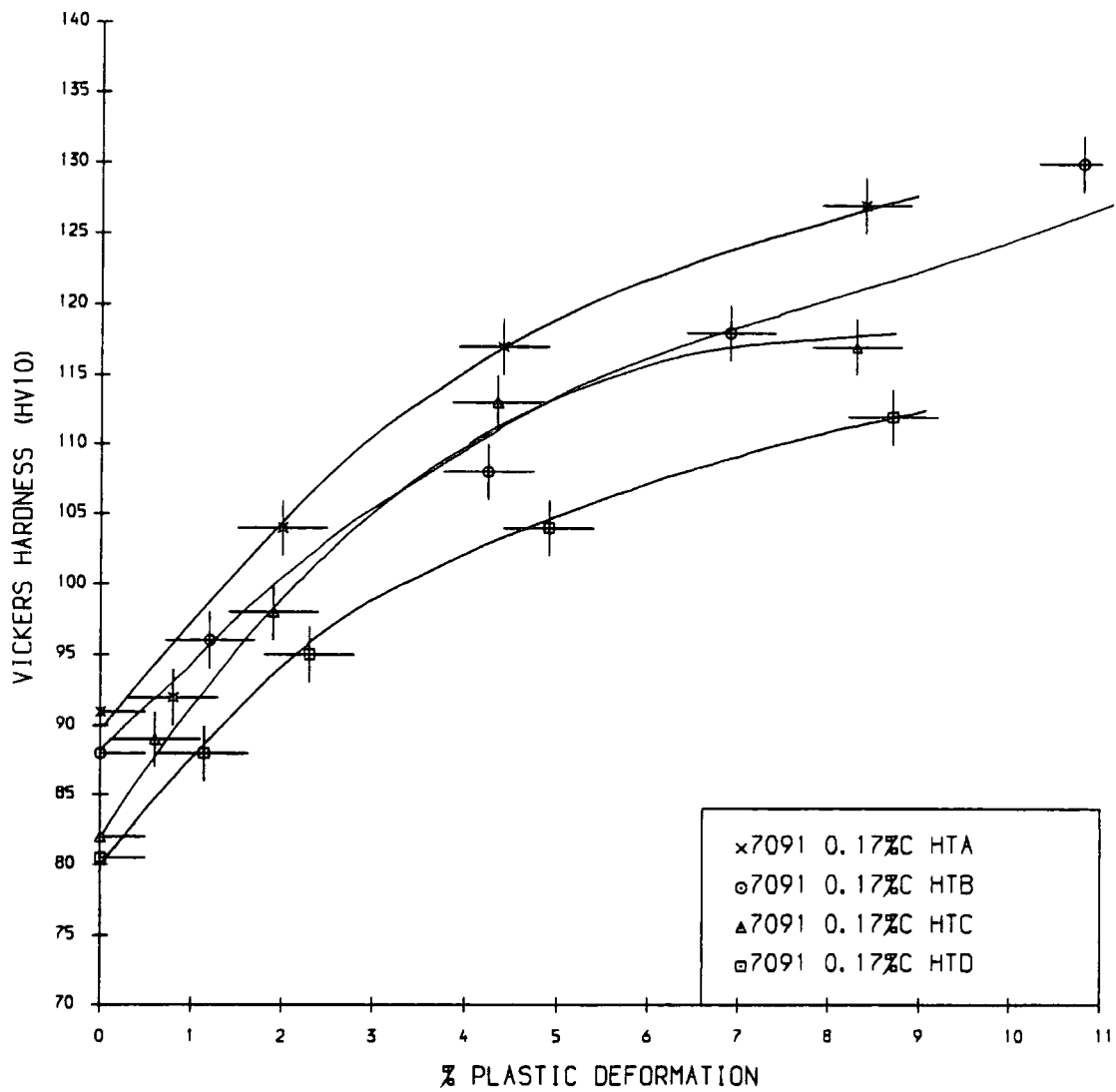
Figure 5.50 The Variation of Vickers Hardness With Plastic Deformation for the Heat Treated Samples of 7091: 0.17% Carbon Content.

172

5.4.2 Bulk Magnetic Properties.

The initial magnetisation curves for each of the undeformed heat treated samples are displayed in figure 5.51 to illustrate the differences between them; and for the various stages of plastic deformation for heat treatment "A" in figure 5.52. For each heat treatment the variation of magnetic properties with plastic deformation followed the same trends as they did prior to heat treatment although the factors by which the properties changed were greater. A summary of these results is presented in table 5.04 with a detailed table in Appendix A. Graphs showing the variation of μ_{max}, Hm and μ_i with plastic deformation are plotted in figures 5.53 to 5.55 followed by a typical example of a B-H loop for a highly strained sample demonstrating the marked distortion in the central region in figure 5.56. Figures 5.57 to 5.59 plot the increasing coercivity, μ'_{max} and decreasing Br with plastic deformation respectively.

Heat Treatment	Maximum %Deformation	μ_i	μ_{max}	Hm	Hc	Br	μ'_{max}
A	8.4	⇓8.0	⇓4.3	⇑6.9	⇑3.2	⇓3.2	⇓4.7
D	8.7	⇓8.6	⇓5.0	⇑8.5	⇑3.4	⇓3.2	⇓6.9
B	8.3	⇓8.8	⇓4.8	⇑8.4	⇑3.4	⇓2.6	⇓6.9
C	10.8	⇓8.6	⇓5.1	⇑8.0	⇑3.4	⇓3.5	-

Table 5.04 FACTORS by Which the Magnetic Properties of the Heat Treated Steels Changed Over the Maximum Range of Plastic Deformation.

The measurements on the toroids were only made on the undeformed material. They all demonstrated that the heat treated material was magnetically "softer" and also showed an inverse dependence of coercivity and hysteresis loss and a linear increase of maximum susceptibility with estimated grain size.
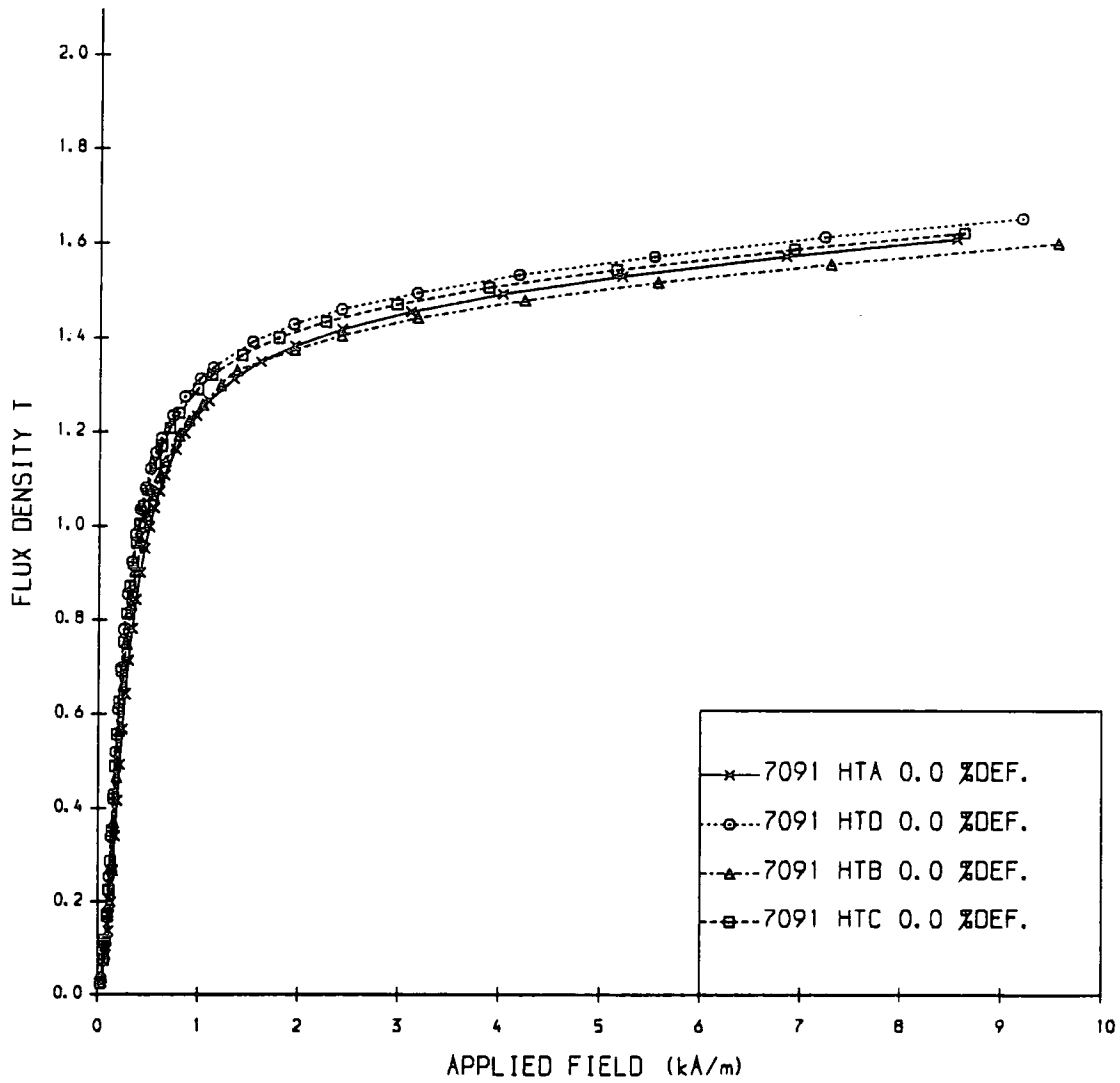
Figure 5.51 Initial Magnetisation Curves for the Range of Heat Treated Samples of 7091: 0.17% Carbon Content.
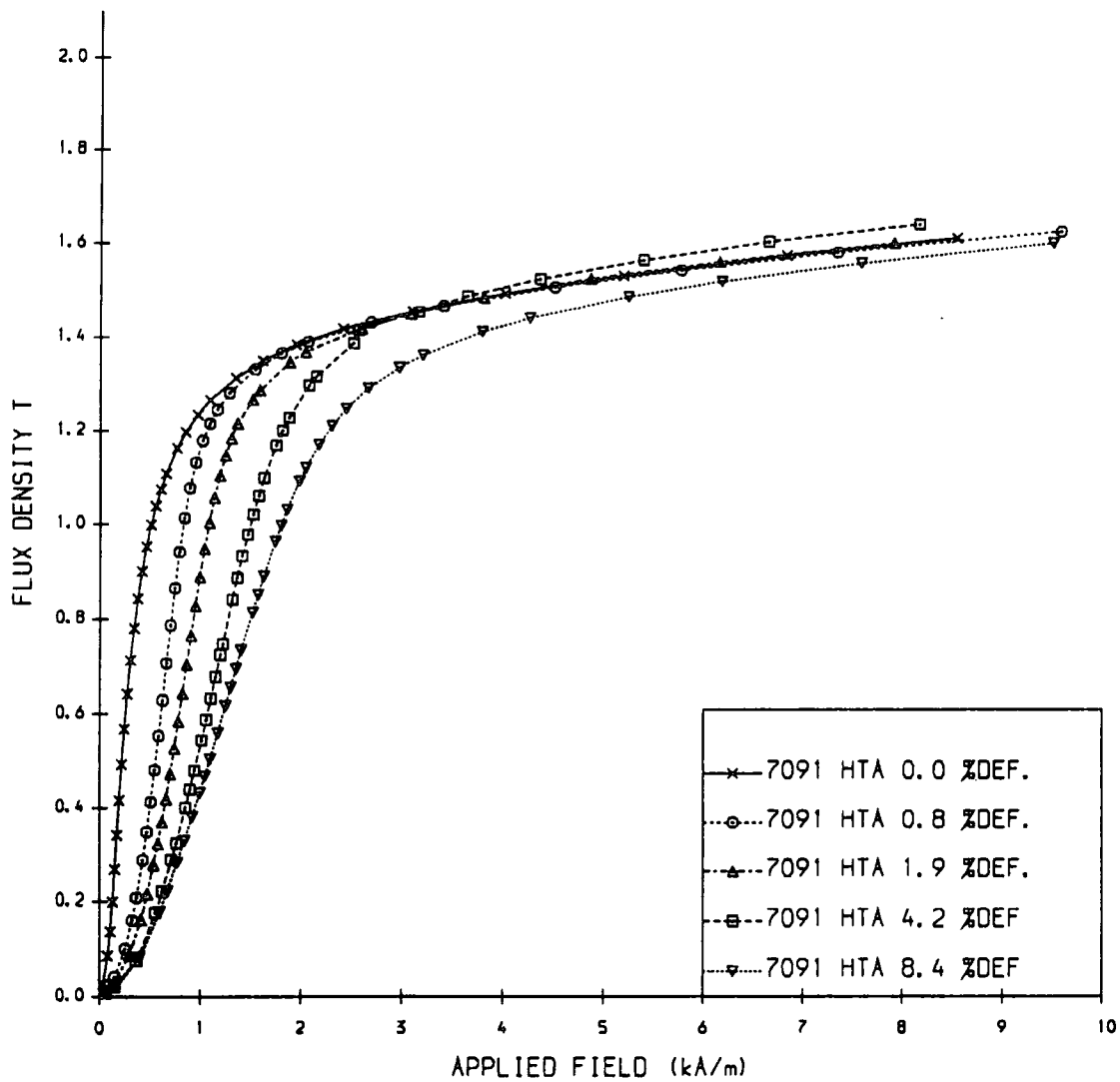
Figure 5.52 Initial Magnetisation Curves for the Range of Plastic Deformations applied to the 7091: 0.17% Carbon Content Heat Treated "A" Sample.

175
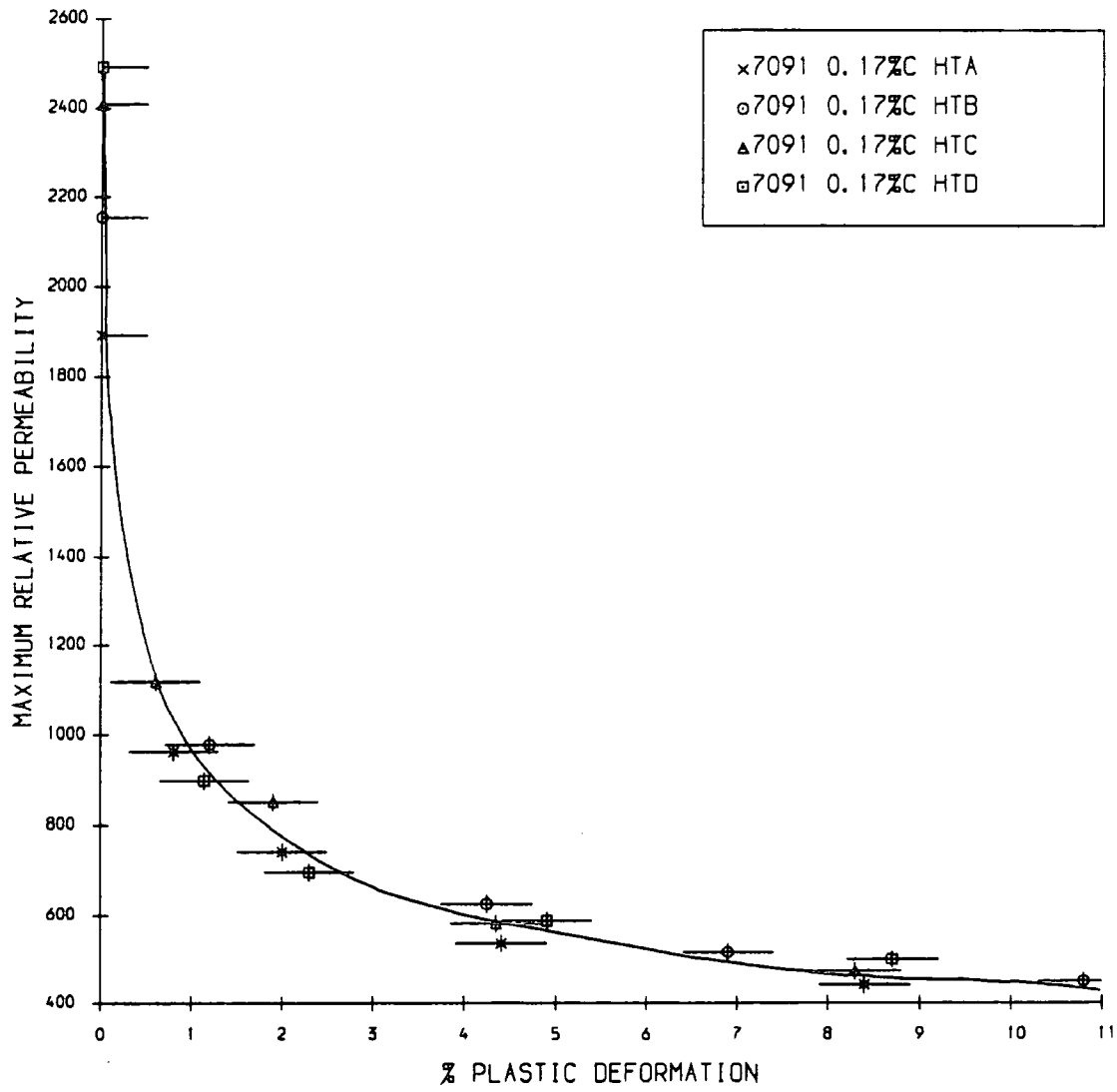
Figure 5.53 The Variation of Maximum Relative Permeability With Plastic Deformation for the Heat Treated Samples of 7091. 0.17% Carbon Content.
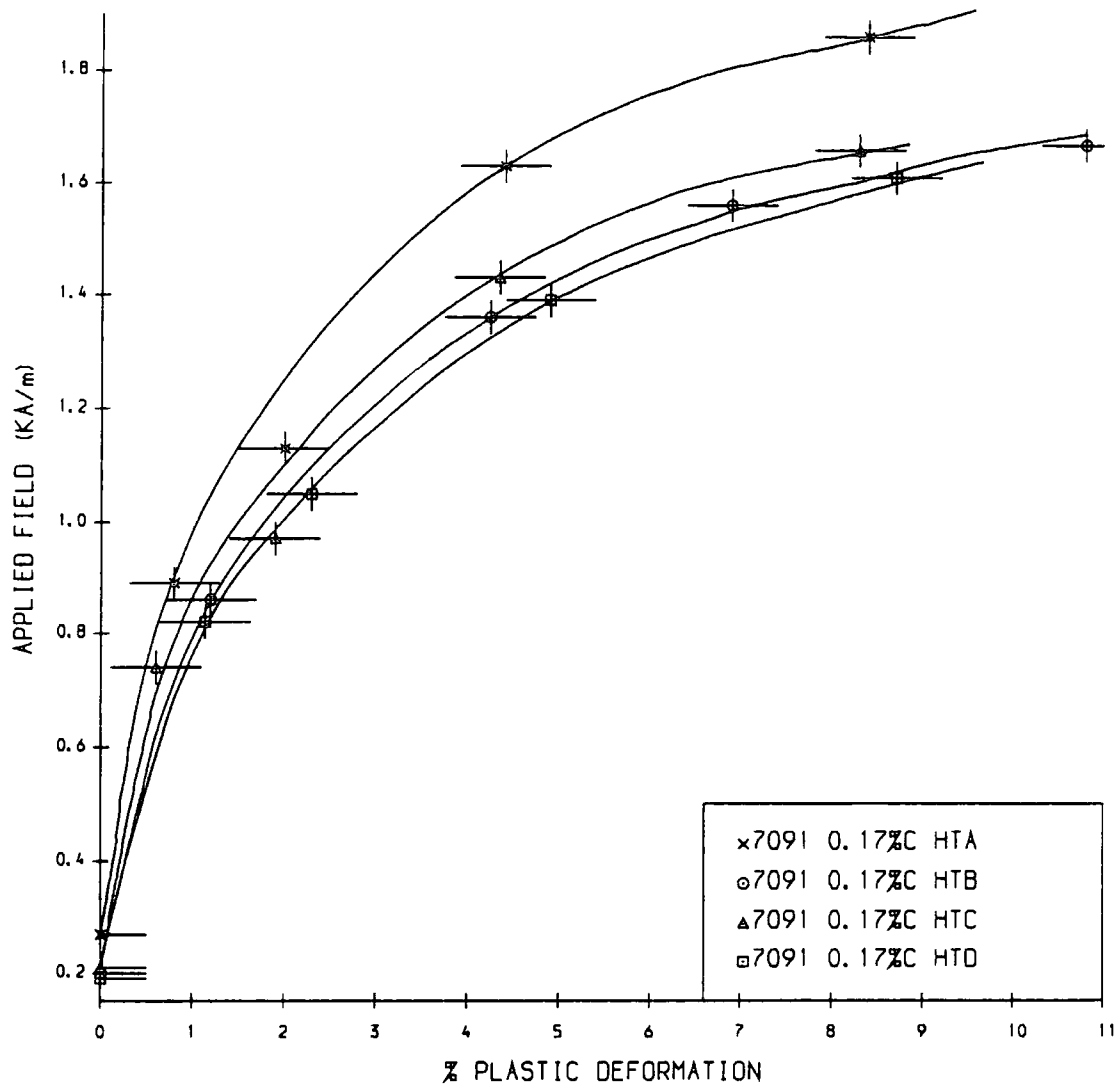
Figure 5.54 The Variation of Hm With Plastic Deformation for the Heat Treated Samples of 7091: 0.17% Carbon Content.
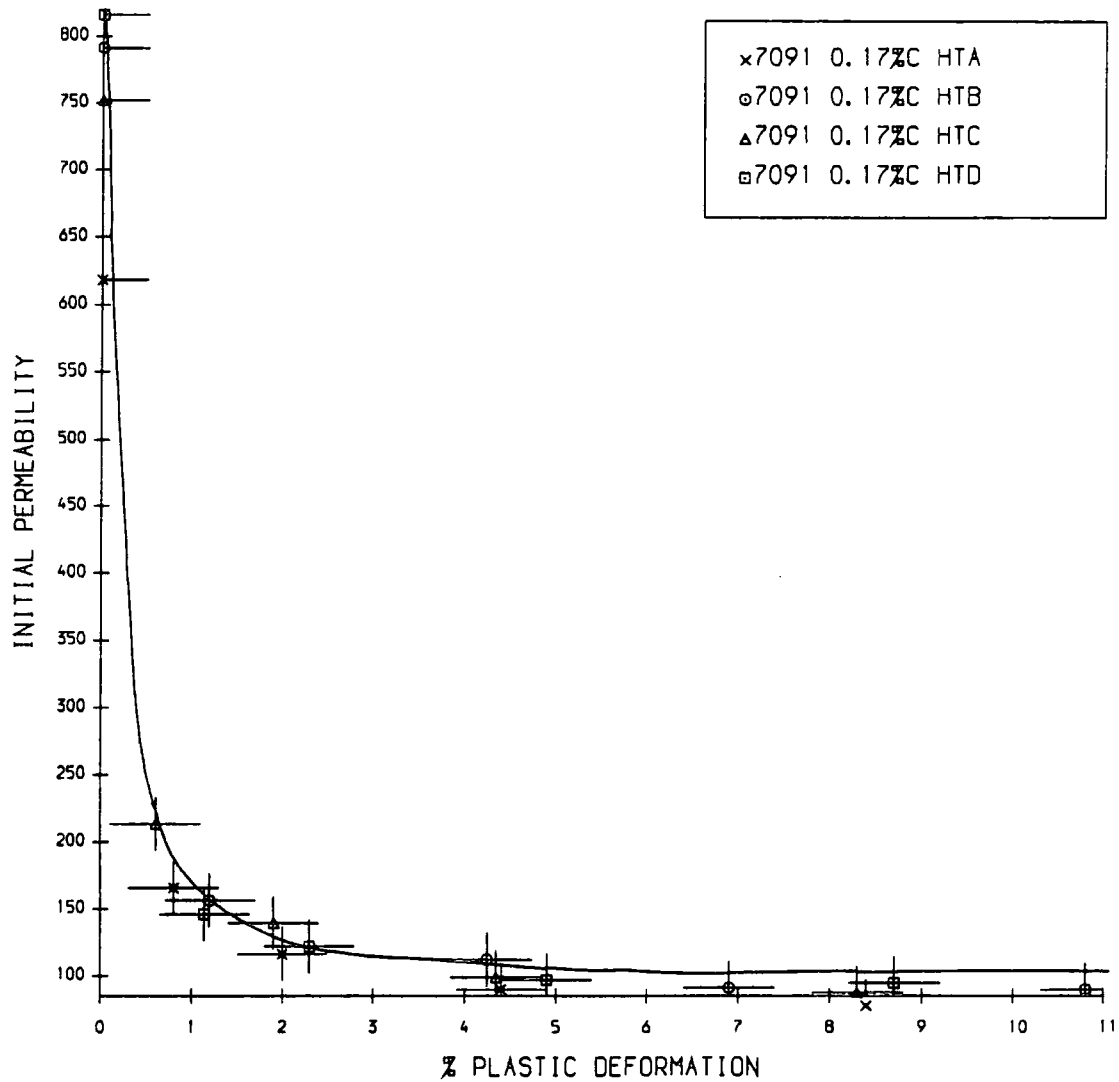
Figure 5.55 The Variation of Initial Permeability With Plastic Deformation for the Heat Treated Samples of 7091: 0.17% Carbon Content.

178
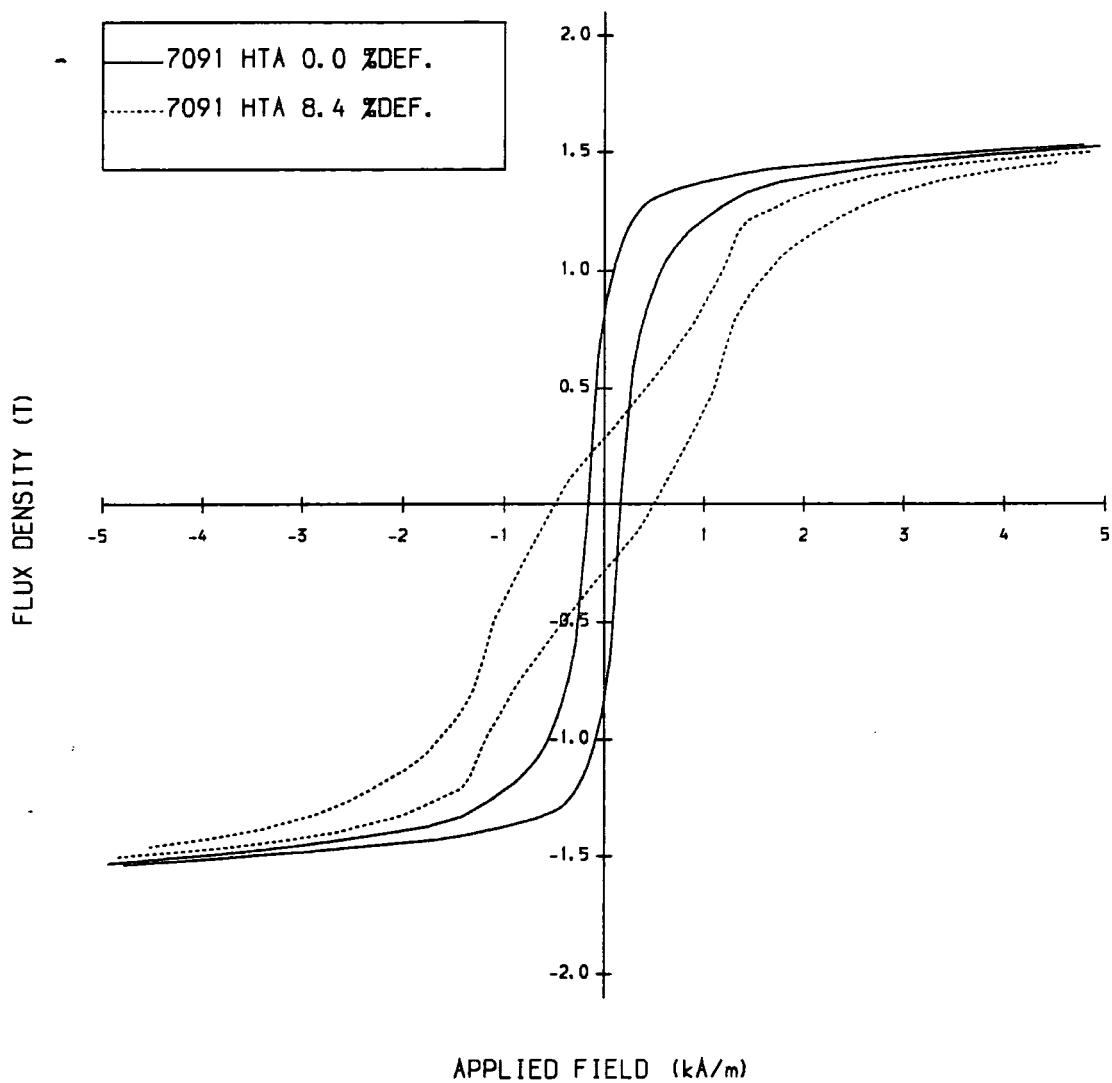
Figure 5.56 Hysteresis curve of the undeformed and 8.4% Deformed Heat Treated "A" Sample of 7091: 0.17% Carbon Content.

179
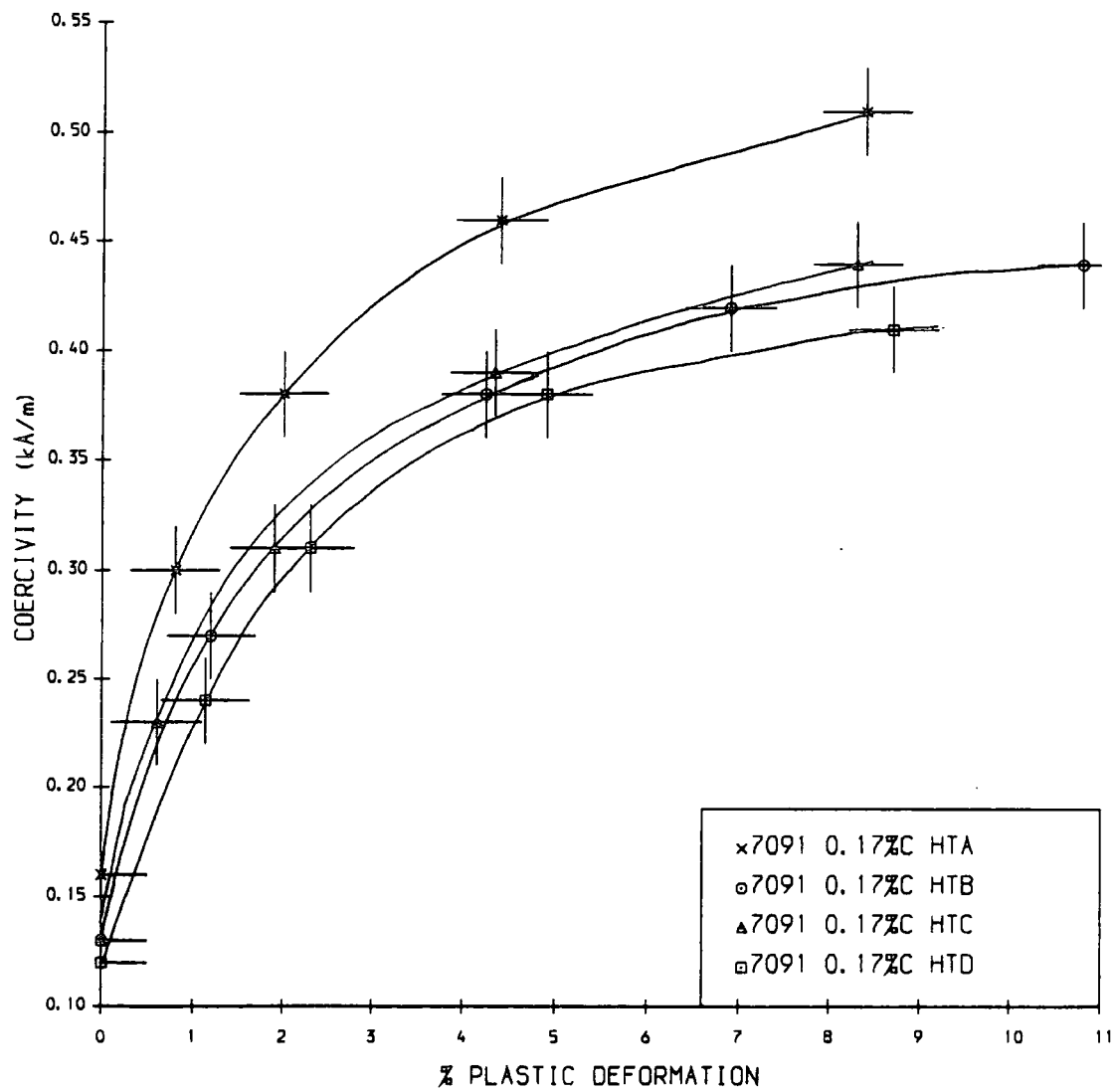
Figure 5.57 The Variation of Coercivity With Plastic Deformation for the Heat Treated Samples of 7091: 0.17% Carbon Content.

180
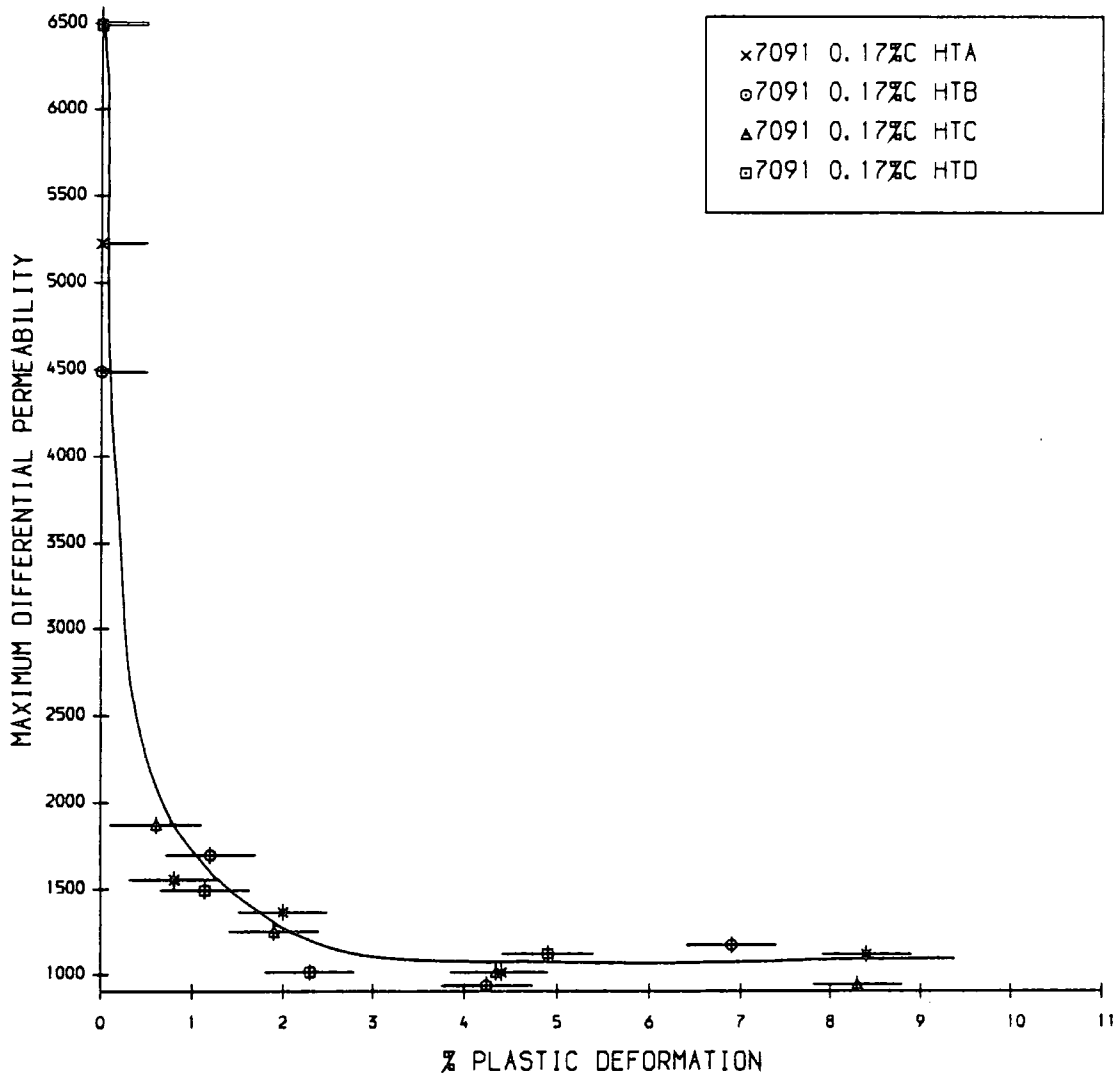
Figure 5.58 The Variation of Maximum Differential Permeability With Plastic Deformation for the Heat Treated Samples of 7091 0.17% Carbon Content.

181
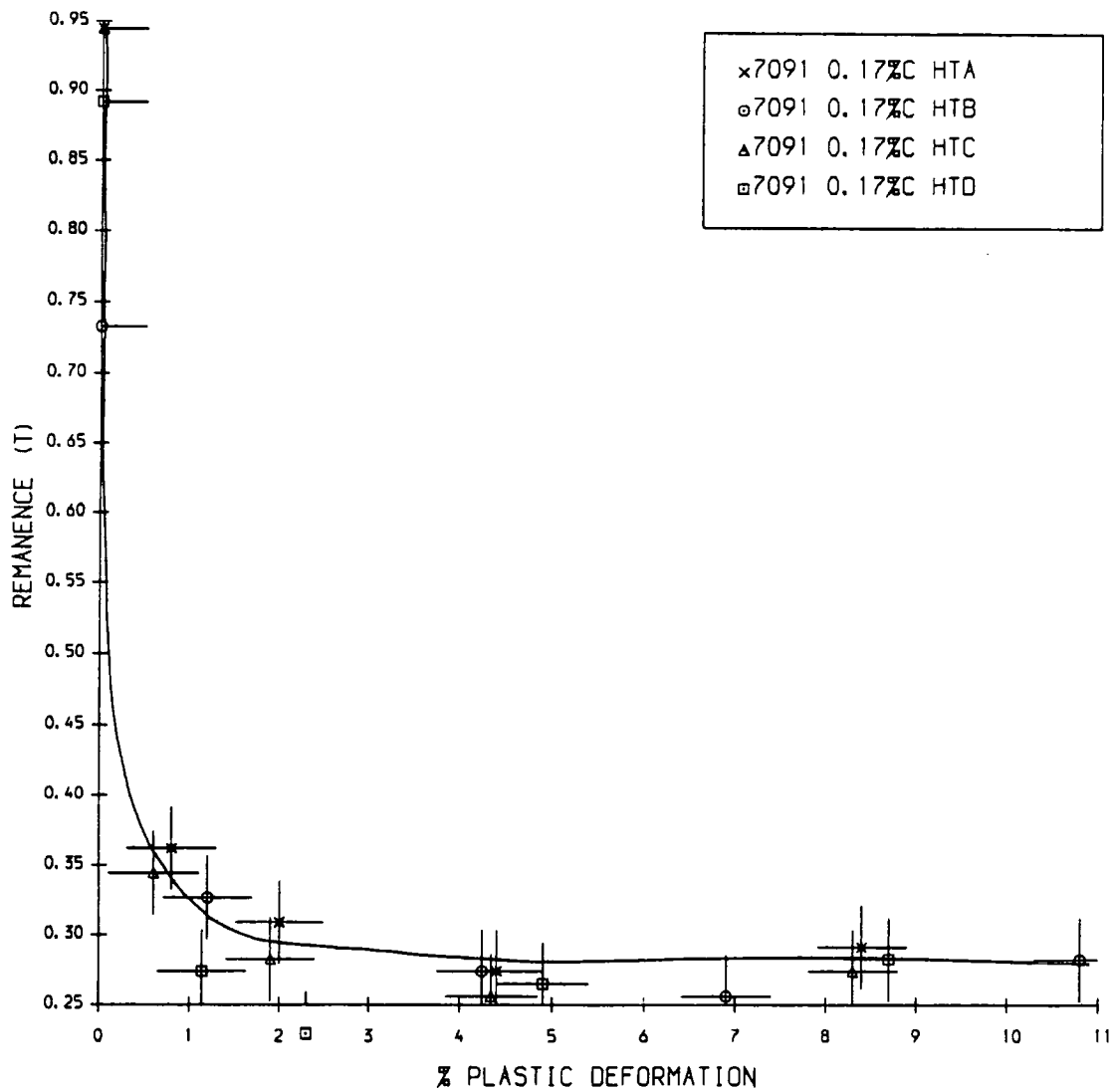
Figure 5.59 The Variation of Remanence With Plastic Deformation for the Heat
Treated Samples of 7091: 0.17% Carbon Content.

182

Chapter VI

Analysis.

In this chapter the electron microscope observations are correlated with the bulk magnetic measurements and used to explain the effects of carbon content, heat treatment and in particular plastic deformation on the magnetic properties of pearlitic steel.

6.1 Undeformed Steel.

The shearing of the hysteresis loop as the pearlite content is increased and the ensuing degradation in magnetic properties demonstrate the increasing magnetic hardness of the steel.

The results of Schwerer et al (1978) and English (1967) indicated that pearlite could not be considered to be a non-magnetic inclusion below its Curie temperature of 483K. They found a maximum in the coercivity at this point, which became more pronounced as the carbon content was increased illustrating its increased importance in the magnetising process. Spherodised pearlite did not exhibit a peak which is supported by the measurements of Jiles (1988a and b) on steels subjected to different heat treatments in which he found spherodised pearlite did not reduce the coercivity of the steel as much as lamella pearlite. Orthorhombic Cementite has a very high anisotropy energy and both the Pitsch-Petch and Bagaryatskii crystallographic relations show that its easy ⟨001⟩ direction does not coincide with that of the interspersed ferrite. Schwerer et al derived a limited model for the magnetic coercivity of pearlite based on minimising this anisotropy energy and the magnetostatic energy due to the plate form of the layers. They commented that in a real situation the loss of regularity in the lamellae would probably have a significant affect; this was found to be the case in this study

A general theory of the coercive force for materials in which the magnetising process is dominated by domain wall movement has been developed by Freidburg and Paul (1975) and Paul (1976, 1982a and b). This takes into account the wave

nature of the domain wall and considers it to behave as a pulse travelling through the material. Defects are considered where it is assumed that the curvature of the defect is less than that of the wall so that it can be treated as planar. Where the wall thickness is small compared to the defect width some dispersion will occur in the wall as it passes through it. A set of non-linear differential equations are formulated taking into account the different magnetisations and anisotropies in the defect region (although the easy direction is assumed to be the same). The equations are then solved and a set of solutions obtained for the given boundary conditions. The local coercive force is determined to be the largest stable solution. From this modelling some general conclusions were made, the most general of which stated that in such a material the coercive force is linked to the difference in magnetic parameters between the defect material and the host. The equations also predicted an increase in local coercive force with defect width, but also that this increase would eventually saturate. For a wide enough defect the far side of the defect will be invisible to the domain wall and the problem reduced to one of a single boundary. The effect of different easy directions of magnetisation was later considered for a permanent magnet material (Paul 1980) and found to increase the effect of the defect and hence the coercivity.

In the context of Paul's theory the cementite lamellae within a pearlite grain can be considered to be planar defects and a complete pearlite grain a single boundary situation across which the domain structure will not be continuous. If the case of regular pearlite is considered first, a domain wall energy vs. position graph can be sketched for the situations where the wall is lying along and across the lamellae (figure 6.01). By considering only the decreased wall energy in the pearlite a wall running along the lamellae will be very strongly pinned as in Paul's theory and domain wall movement across the lamellae will be relatively easy. The more irregular the pearlite microstructure, the greater the variation of wall energy will be along the wall's path and hence the more difficult the movement. In samples where a relatively regular pearlite structure exists extra pinning will result from the branching out of the lamellae at the junction of two pearlite colonies. Cementite lamellae become more effective at pinning domain walls as their thickness increases and spacing decreases. The probability of closure domains forming at cementite-ferrite interfaces within the pearlite increases with the width of the cementite lamellae.

184
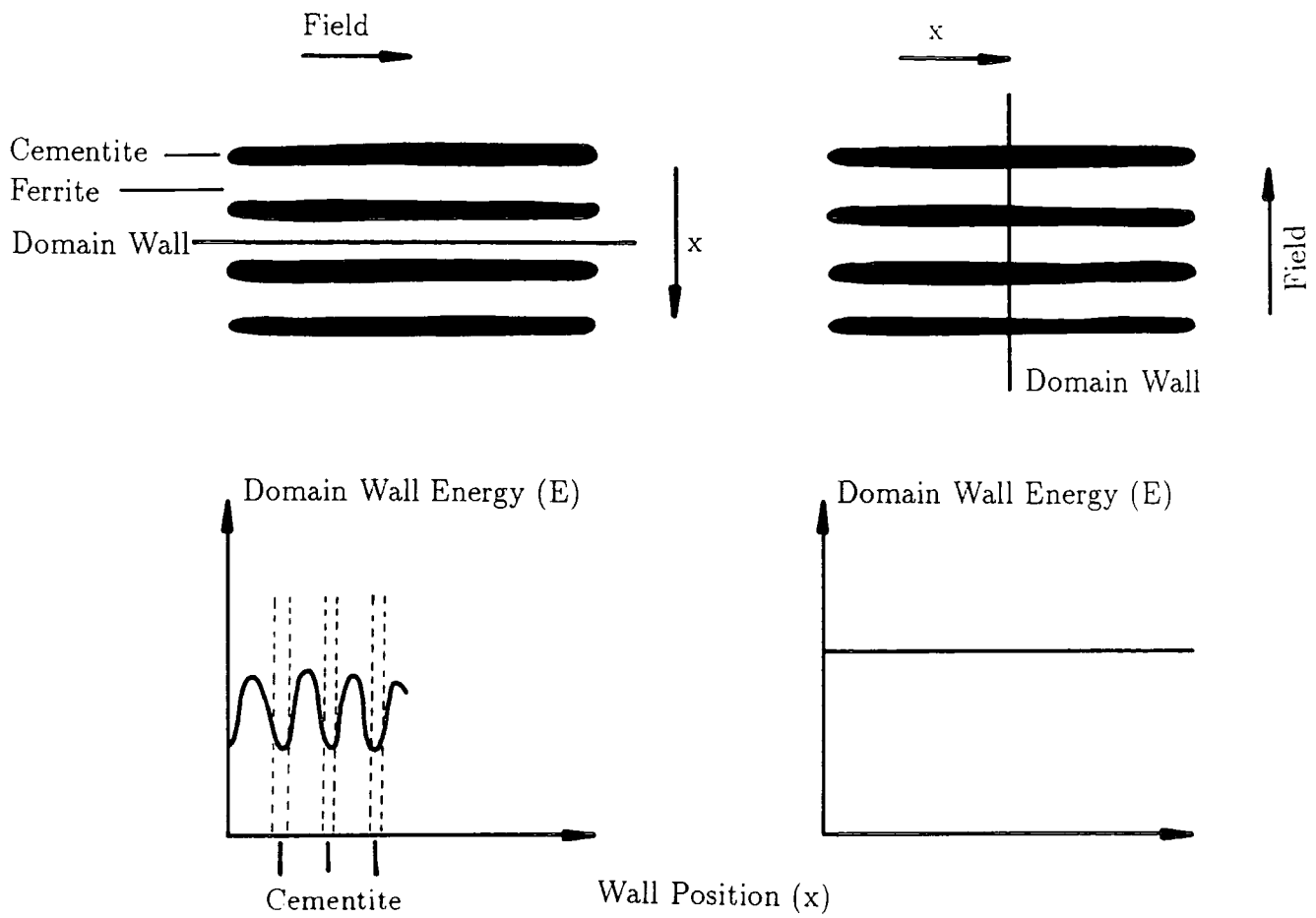
Figure 6.01 Schematic Domain Wall Energy vs. Position Graphs for a Wall Running a) Along, and b) Across the Cementite Lamellae in a Pearlite Grain.

185

6.1.1 Electron Microscopy Observations.

All these effects of the microstructure on the domain wall motion were observed by electron microscopy as described in chapters four and five. Walls running across pearlite grains seemed to alter their orientation as they crossed each cementite lamella, due to the strong anisotropy energy of the cementite. The small inclusions of cementite particles provide extra isolated pinning sites within the material. Some of the very irregular pearlite structures contained extremely complex domain configurations. The domain observations made under the microscope were similar to those made by Hetherington (1985) on a variety of constructional steels and Alcock (1988) on a fully-killed steel. Taylor (1983) also observed the interaction of domain walls with non-magnetic precipitates in some ferromagnetic materials.

When the lamella pearlite content is close to 100% almost all the domain wall motion in the material has to occur within the pearlite nodules. However at lower carbon contents the effect of both ferrite-ferrite and ferrite-pearlite grain boundaries and hence grain size must be considered. In the case of ferrite-ferrite grain boundaries the change of easy direction of magnetisation between the two grains is an important factor in determining the change in wall energy as the boundary is crossed. In general the domain walls were less affected by ferrite-ferrite boundaries to which they were perpendicular than by boundaries parallel to the walls which provide very strong pinning sites along the wall length. Low angle boundaries only affected the walls at the point of intersection by interaction with the line of dislocations. Pearlite grain boundaries were always found to have a significant affect on the domain configuration with closure domains often forming onto the boundary regardless of the orientation between the domain walls and the lamellae inside the grain. Walls running parallel to a pearlite boundary subsequently became strongly pinned to it during a magnetising sequence. An inverse relationship has previously been found (Hetherington et al 1987) between coercivity and grain size in low carbon steels. The median value of the Barkhausen noise also increases with grain size (Tittio 1977 and 1978, Bertotti et al 1989). This relationship was observed in the heat treated offcuts of 7091. Domain configurations were significantly simpler and wall movement easier within the ferrite grains.

6.1.2 Barkhausen Noise.

A study of the Barkhausen noise traces obtained for samples of each carbon content (figures 5.22, 5.24, 5.26 and 5.28) gives an insight into the differences in the magnetisation processes between them. In the trace for the low carbon 7091 sample there is a high initial and final peak either side of the zero field region. This has been attributed by Buttle (1986 and 1987) to the presence of ferrite, he found the size of this peak to increase with annealing times and hence ferrite grain size. As the field is reduced from saturation there is a lot of easy irreversible domain wall movement in the ferrite resulting in the high initial peak; as the remanent point is reached the magnetic force is sufficient to cause discontinuous domain wall movement within the pearlite. In this sample there is little pearlite and so the central peak is very low. In magneto-acoustic measurements made by Buttle (1987) he was able to identify the central peak to be mainly due to 180° wall movement and the initial and final peaks to both 90° and 180° movement. As the pearlite content is increased to 50% in the 7092 sample the initial peak is lowered due to the reduced amount of clear ferrite in which easy domain wall motion can occur. The noise in the central portion increases indicating that a greater amount of irreversible motion now occurs in the harder pearlite with its inherent complex domain configurations. The traces for the higher pearlite content samples of 7093 and 7094 are almost identical, the microstructures for both these samples appeared under the microscope to be almost entirely pearlite. There is now no initial peak and the central peak is very much higher as almost all the domain wall movement is now within pearlite.

6.1.3 Variation of the Magnetic Properties with Carbon Content.

The increased number of pinning sites provided by the pearlite can be directly related to the linear increase in coercivity with carbon content. Tanner et al (1988) found a direct relationship between coercivity and percentage carbon and manganese content for pipe-steels of which the 2401 steel used here was one. This relationship:

$$Hc = 1.186\%C + 0.237\%Mn \dots (6.01)$$

compares with the one found from figure 5.11:

$$Hc = 0.87\%C + 0.2 \ldots (6.02)$$

Using Willcock's formula to predict the coercivities of these samples and plotting these against those found experimentally (figure 6.02) show quite a good correlation with a gradient of: 1.09+/-0.2. The gradients for the two sets of steels are very similar but the values for the pipe steels are displaced due to additional impurities and microstructural factors which increase the coercivity in the commercial material. When the 7091 samples were heat treated their coercivity was reduced by half; the variation between the microstructures of the different heat treatments was much smaller indicating that the main reason for this reduction was the release of internal strains during the normalising process. These few examples alone indicate how sensitive the magnetic properties of the iron-carbon system are to changes in carbon content, residual strain and microstructure.

The mechanical properties of the steel are also directly affected by the increase in carbon content with both the yield strength and Vickers Hardness increasing. Both these mechanical properties can be directly related to the coercivity, the linear relation for yield strength is plotted in figure 6.03: $Y.S. = 305Hc + 52$. The yield strength of the pipesteel was found to be significantly higher ($409MNm^{-2}$ for 2401 compared to $135MNm^{-2}$ for 7091). The Vickers Hardness values for all the steels including the plastically deformed ones are plotted against coercivity in figure 6.04 to show the generality of this relation. Experiments carried out on undeformed pipe steels by S.N.M.Willcock (Tanner et al 1988) found the relation for Vickers Hardness to be: $VH = 166Hc + 93$ compared to: $VH = 129Hc + 73$ for this study. Indicating again the greater hardness of the pipe steel.

In addition to the increased pinning which results in the increased coercivity and decreased initial permeability the addition of the pearlite also restricts the proportion of ferrite that can be magnetised in the easy direction and so the hysteresis loop shears over, and decreases in remanence and differential permeability μ'_{max} result. The smooth shape of the loop however remains intact and plots of differential permeability against applied field (6.05) show a smooth curve with a peak near the increasing coercive force. The lowering of the peak and the broadening
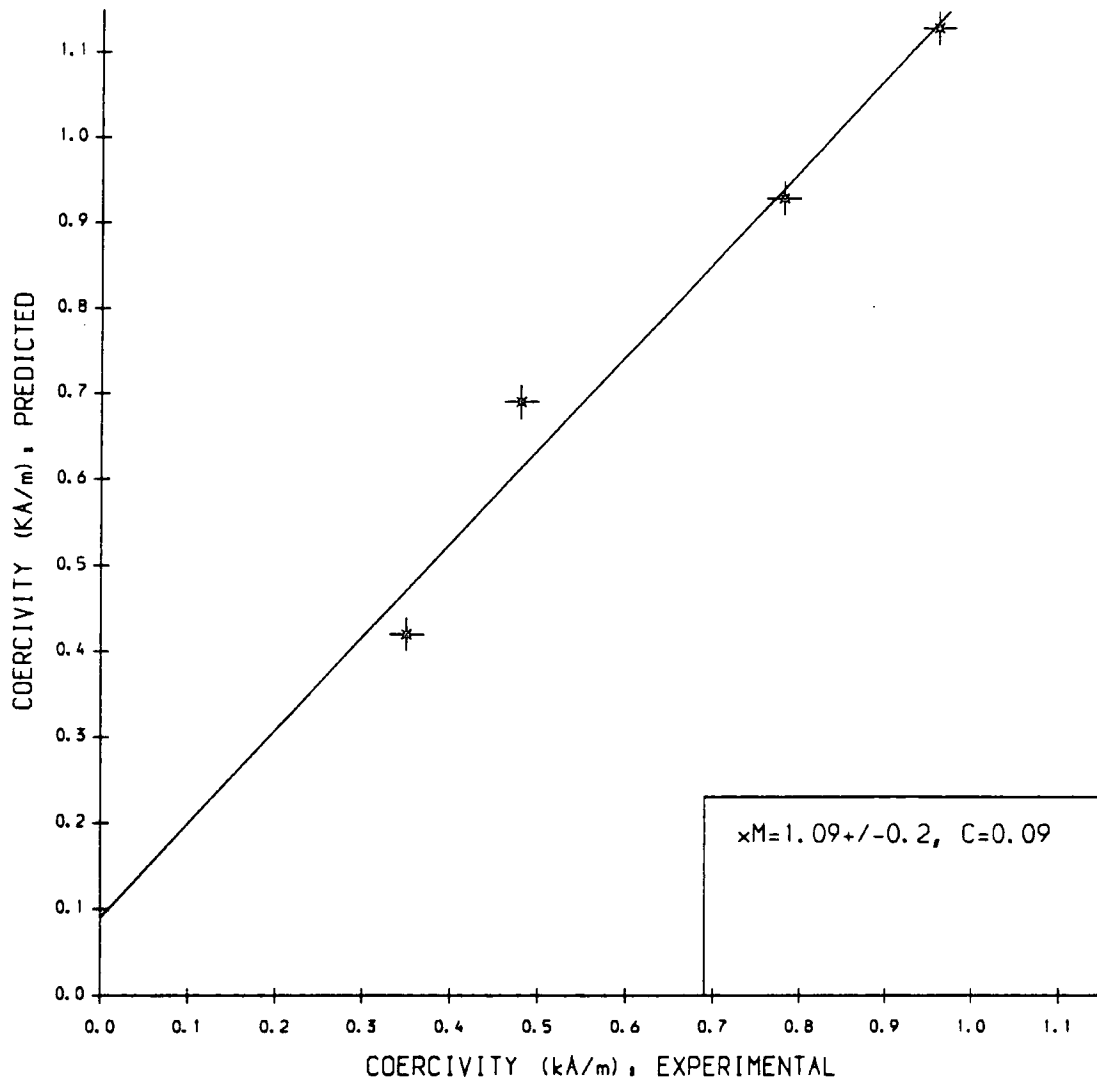
Figure 6.02 Predicted Values of Coercivity from Willcock's Formula against the Experimental Values.

189
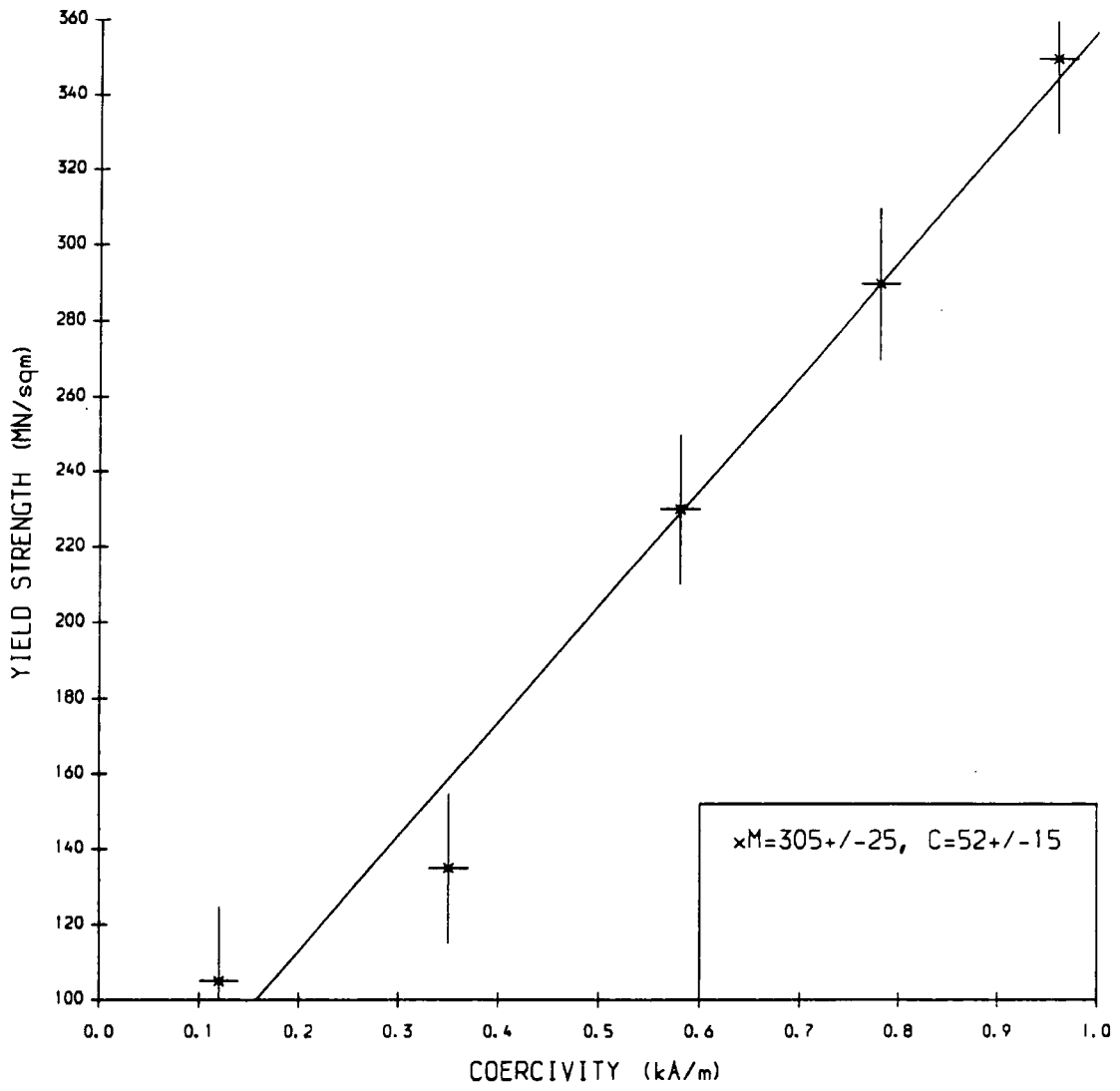
Figure 6.03 Variation of Yield Strength with Coercivity.

190
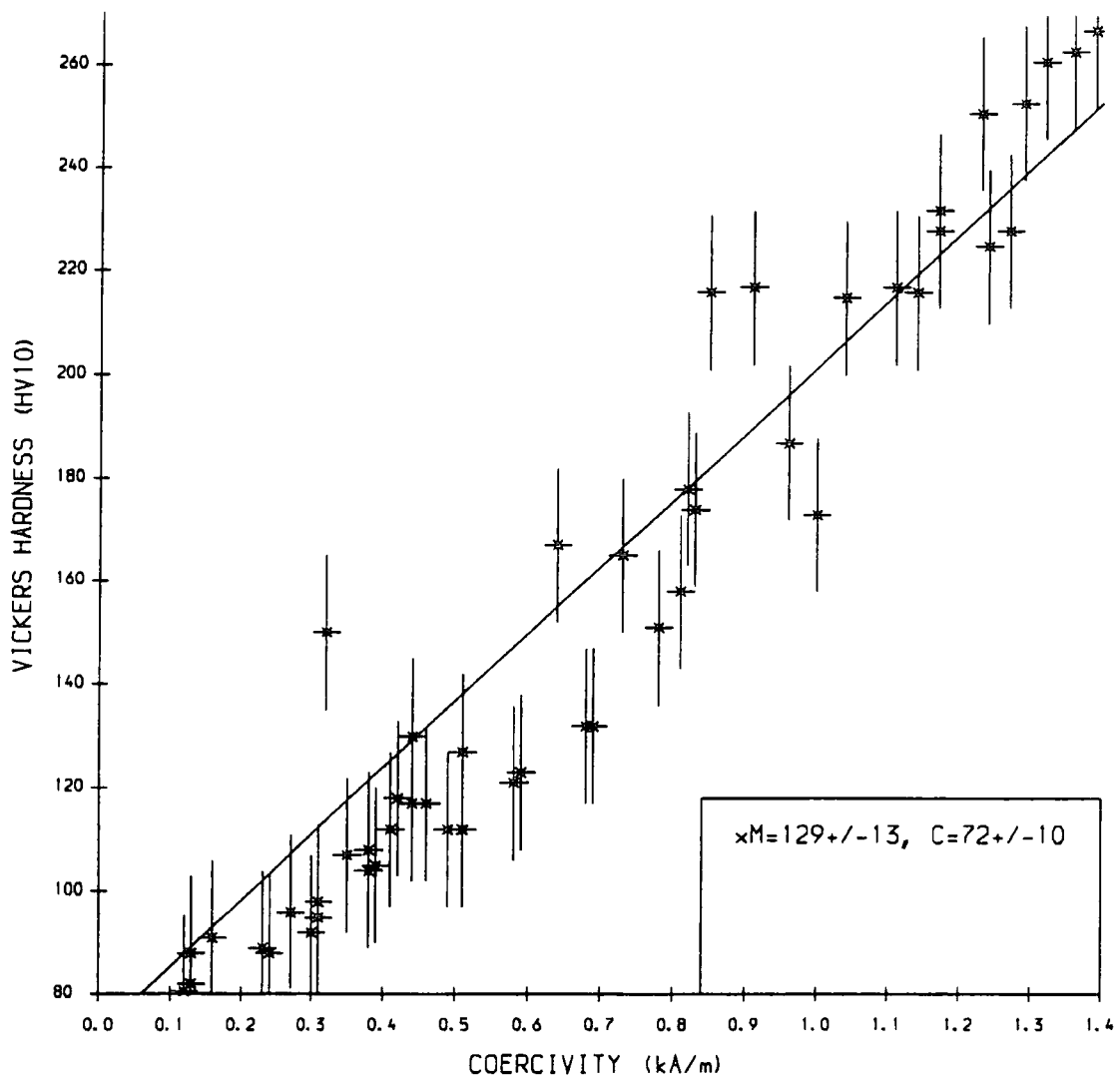
Figure 6.04 Variation of Vickers Hardness with Coercivity for Both Deformed and Undeformed Steel.

191
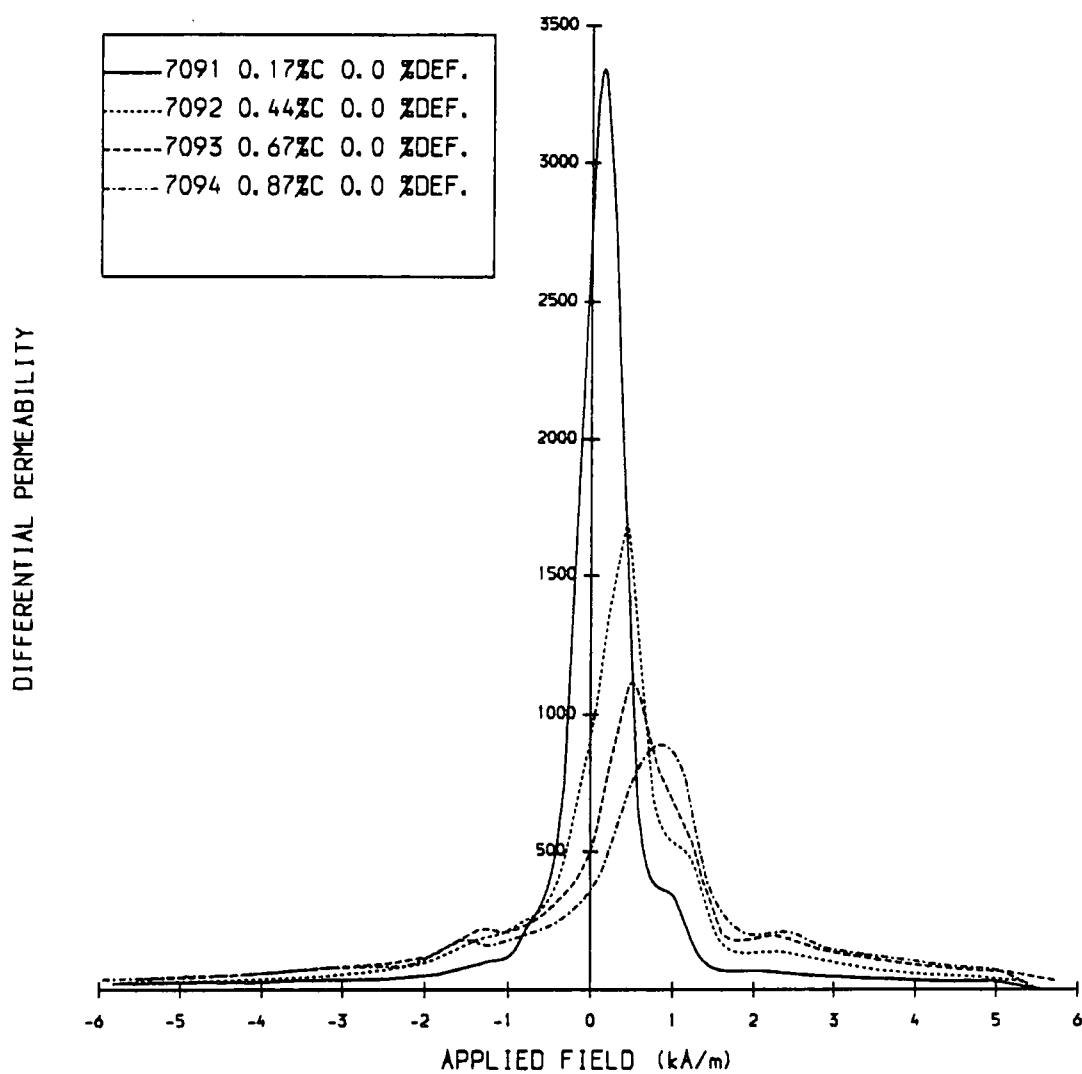
Figure 6.05 Differential Permeability as a Function of Applied Field for an Undeformed Sample of Each Carbon Content.

192
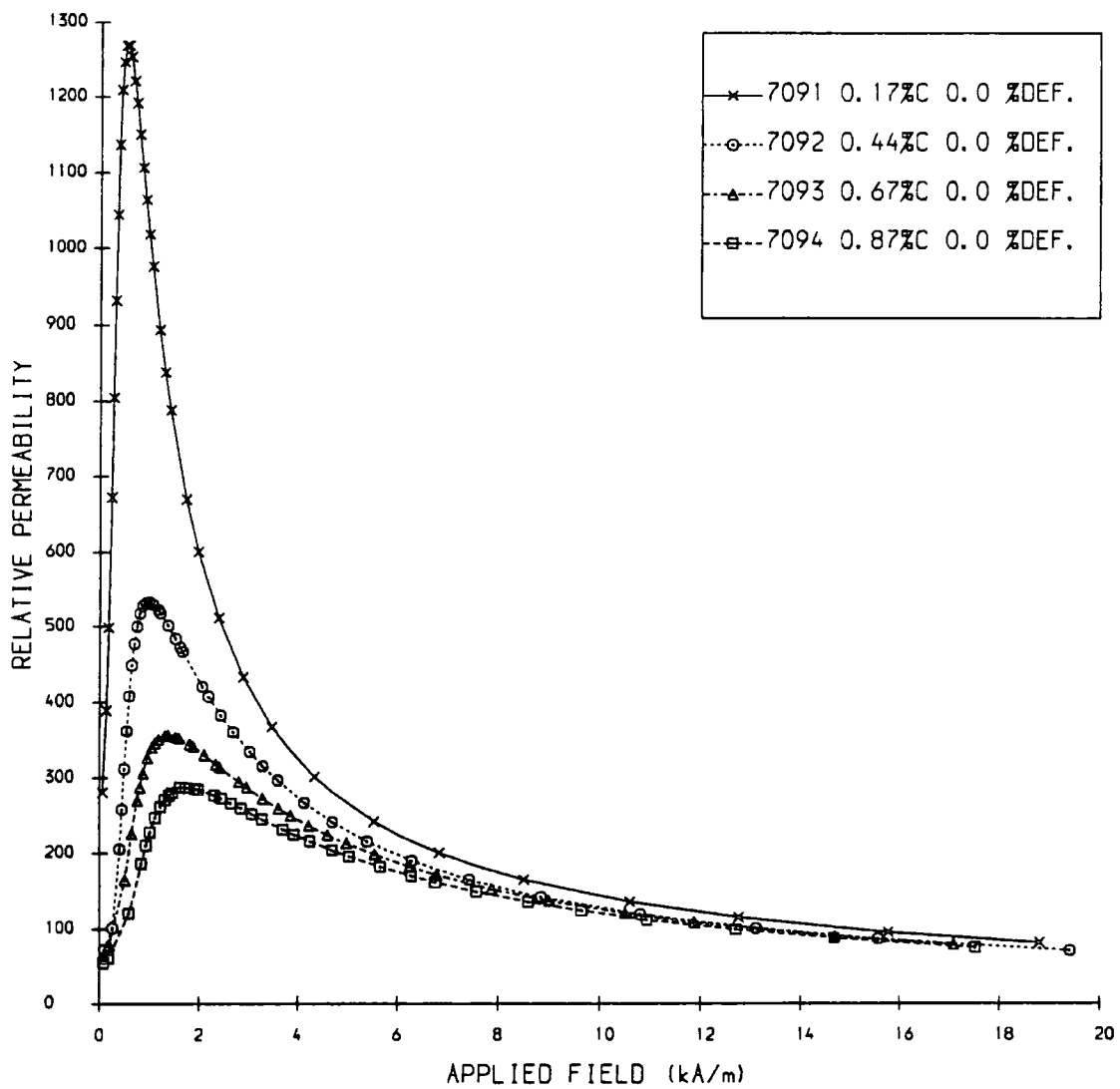
Figure 6.06 Relative Permeability as a Function of Applied Field for an Undeformed Sample of Each Carbon Content.

193

of the curve can be attributed to the slower approach to saturation. The reduced gradients of the initial magnetisation curves are well described by the variation in relative permeability with applied field (6.06) illustrating the slower approach to saturation by the lower and broader curve with the peak occurring at a higher field Hm.

6.1.4 Heat Treated Samples.

The most significant affect of the heat treatments was the normalisation and subsequent strain relief resulting in a much softer steel mechanically and magnetically. This is reflected in the low coercivity, hardness and yield stress values which have been included in figures 6.03 and 6.04 relating the coercive force to these mechanical parameters.

Heat treated samples "A" and "D", air and furnace cooled respectively, will be considered together followed by "B" and "C", held subcritical for one and two hours respectively. Plots of relative permeability against applied field for each of the samples are plotted in figure 6.07.

The finer grain size of the air cooled sample "A" resulted in harder mechanical and magnetic properties compared to "D". Vickers Hardness, coercivity and the field at maximum permeability were all higher for "A" whereas the maximum differential permeability, initial and maximum permeabilities were all lower. The remanence was also a little higher; as little change is expected in the residual strain or the available easy directions in the ferrite this can be explained by an increase of the irreversible nature of the magnetising process as the grain size is reduced.

The properties of "B" and "C" were very similar although the increased annealing time of "C" caused it to exhibit slightly softer characteristics. The values were usually intermediate between "A" and "D" with a coercivity nearer that of the furnace cooled "D". A much longer time at 600°C would be necessary to determine the effects of the carbide growth which has only just begun in parts of the samples at this stage.

194
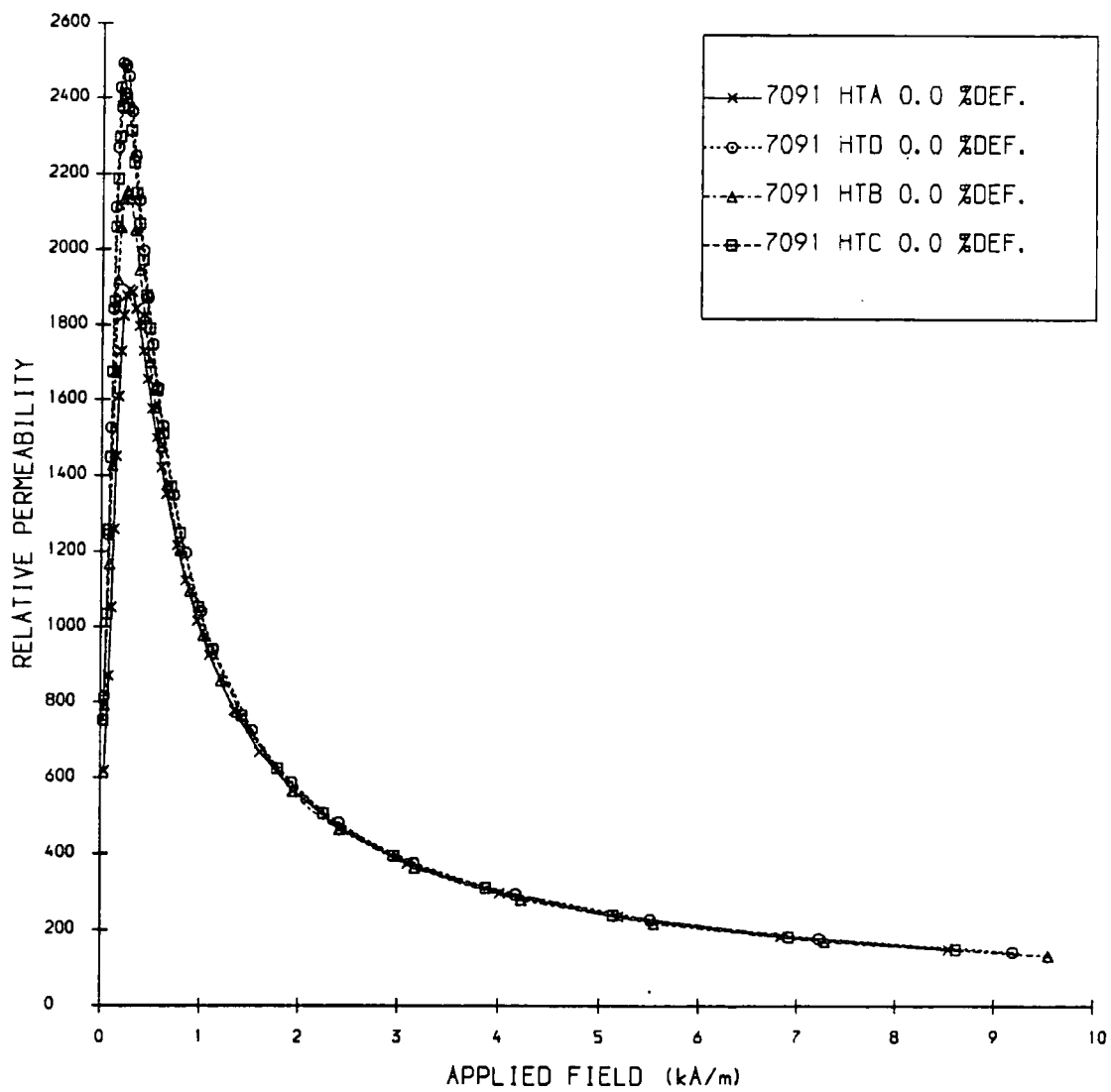
Figure 6.07 Relative Permeability as a Function of Applied Field for an Undeformed Sample Subjected to Different Heat Treatments.

195

6.2 Elastic Deformation.

During elastic deformation the crystal lattice is distorted and magnetostrictive effects occur. For a material with positive magnetostriction such as iron, tensile stress enhances the magnetisation parallel to the applied stress and compressive stress hinders it. This effect has been the subject of many research programmes and recently that of Atherton and Jiles (1983) and Kwun et al (1987). They have recorded the shearing of the loop under compressive stress and the resulting decreases in saturation, remanence, relative and differential permeability and the lack of any change in coercivity. The opposite affects of tensile stress were not as large for the same amount of applied compressive stress. As the steel is compressed the lattice distortion causes the magnetisation vectors to rotate away from their axes reducing the overall magnetisation. This slows the approach to saturation decreasing both the relative and differential permeability, shears the hysteresis loop, reduces the saturation induction and increases the rate of demagnetisation reducing the remanence. The effect has been exploited independently by Abuku (1977) and Langman (1981a and b, 1982, 1983 and 1985) who have used the anisotropy of the permeability and the rotation of the easy direction of magnetisation respectively to develop a magnetic probe to detect stress in a steel. The number of pinning sites is not much affected and hence there is little change in the coercivity; however some interaction can be expected between the pinning sites and the change in internal stress fields hence a change in coercivity is sometimes detected. In their consideration of elastic stress Jiles and Atherton (1984) postulated that this interaction would release some walls from their pinning sites so that the magnetisation curve will always move towards the anhysteretic on the application of stress. For compressive stress this can result in a small increase in coercivity parallel to the direction of stress and a smaller decrease perpendicular to it. For tensile stress the reduction parallel to the stress direction will be greater than the increase perpendicular. As this effect depends on the nature of the pinning sites different microstructures will be affected differently.

The effect on Barkhausen noise of elastic stress has been studied by various authors, using a variety of techniques. They have all found that the Barkhausen noise increases with tensile stress and decreases with compressive stress. This effect is explained by the preferred arrangement of the domains parallel to tensile stress

and perpendicular to compressive stress. Altpeter et al (1990) identified the outer peaks, containing most of the 90°walls, to be most stress sensitive and Buttle et al (1986 and 1987) described the same effect using the reduction of their initial peak. Kwun (1985) measured the amplitude (B.N.A.) as a function of angle between the stress magnetisation directions. Jagadish et al (1990) found the rms voltage and the total number of pulses to decrease with compressive stress while the pulse size distribution shifted to lower amplitudes. Rautioaho et al (1986) measured an increase in the power spectra at all frequencies for tensile stress and noted that the effect reduced with increased tension which they attributed to the fact that most of the domain rearrangement occurs at low stress levels and Tittio (1977) has used the observed changes in noise level for the commercial development of a probe for detecting residual stresses in engineering components. This reduction in noise is explained by the magnetostrictive effect and the rearrangement of the domains to favour the direction perpendicular to the applied compressive stress.

Jiles and Atherton (1983 and 1986) have been responsible for developing a new model of hysteresis. This is based on an effective field model for the anhysteretic curve to which a pinning parameter "k" is added to generate the hysteresis. This expression is further modified to include the effect of reversible domain wall bowing by incorporating a parameter "c", the ratio of normal to anhysteretic susceptibilities. Sablik et al. (1987) extended the model to include the effects of elastic strain by adding an additional magnetostrictive term, H_σ, to the expression for the effective field, He:

$$He = H + \alpha M + H_\sigma(\sigma, M) \ldots (6.03)$$

where α is the effective field parameter. The stress term is modelled as:

$$H_\sigma(\sigma, M) = \frac{3}{2} \frac{\lambda}{\mu_o M_s} \frac{M}{M_s} \sigma \ldots (6.04)$$

The field and stress dependence of the magnetostriction were then studied and three different expressions tested by comparison with their experimentally determined variations of Ms and Br. They found the expression that best described the increased curvature of the compressive curve and the smaller effect for tensile stress was:

$$\lambda = \frac{3}{2} [\lambda_s(\sigma)] (\frac{M}{M_s})^2 \ldots (6.05)$$

197

where:

$$\lambda_s(\sigma) = \begin{cases} (\lambda_{s_o} - \lambda_{s_t})[1 - (\frac{\sigma}{\sigma_t})^{\frac{1}{2}}] + \lambda_{s_t}, & \text{if } \sigma \geq 0; \\ (\lambda_{s_o} - \lambda_{s_c})[1 - (\frac{\sigma}{\sigma_c})^{\frac{1}{2}}] + \lambda_{s_c}, & \text{if } \sigma \geq 0. \end{cases} \quad \dots(6.06)$$

This theory was successfully applied to the stress dependent anhysteretic curves of AISI 4130 steels by Garikepati et al (1988) and Dobranski et al (1985). Sablik et al (1988) also used their theory to explain the effects of stress on the amplitudes of the 1st and 3rd harmonic amplitudes as determined by Willcock et al (1983) and Szpunar et al (1984) attempted to extend this theory to plastic strain by alteration of the damping parameter "k". Recent results of Pitman (1990) on elastically strained steel also support Jiles's analysis.

6.3 Plastic Deformation.

Measurements of residual stress using x-ray diffraction techniques indicate that tensile plastic deformation results in compressive residual stress (Rusnak et al 1969, Bagchi et al 1967 and Cullity 1964). Abuku (1973 and 1977) extended this work using the magnetic stress probe; its output was monitored as the steel sample was cycled through increasing stress cycles continuing past the yield point. When applying tensile stress the positive output of the probe increased until the yield point was reached when the output decreased, becoming negative as the tensile load was removed. On successive cycles the output never again reached the positive maximum at the "magnetic yield point". These results were explained by considering the different magnetostrictions and yield stresses of the $\langle 100 \rangle$, $\langle 110 \rangle$ and $\langle 111 \rangle$ grains. As the magnetostriction of ferrite is far stronger than that of cementite, this dominates the measurements of the probe. Abuku (1973) noted that the compressive residual stress found in plastically deformed steel increased significantly with increasing carbon content. As pearlite workhardens more readily than ferrite the larger tensile deformation there is balanced by the high compressive residual stress in the ferrite.

As tensile stress is applied to the steel sample and taken through the yield point, rapid dislocation multiplication occurs. The dislocations readily pile-up creating dense dislocation tangles with a high degree of tensile deformation leaving the bulk of the sample in residual compression. The increase in workhardening

198

and its sudden increase as fracture approaches is illustrated by a plot of the gradient of the stress-strain curve as the load is removed against final strain value as in figure 4.04. It is the combination of these two effects that causes the changes in the magnetic properties of the steel as it is plastically deformed. As in the steel that is subjected to compressive elastic stress, the residual compressive stress reduces both the relative and differential permeabilities and the remanence, shearing the hysteresis loop. The low field movement in the initial magnetisation curve is inhibited reducing the initial permeability. In addition, the dislocation tangles form very effective pinning sites increasing the coercivity and hence hysteresis loss. The increase in individual pinning energies also tends to reduce the remanence. These results (pipesteel: Thompson et al 1990a) are in complete agreement with those made on 50D steel by the late M.R. Anderson (1980). This analysis also explains the results of D.C.Jiles's experiments on the effects of compressive deformation on A.I.S.I. 4130 (1988c) and 4140 (1988d) steels. He found for his lamellar pearlite samples not only that coercivity increased and initial permeability decreased, but that maximum differential permeability and remanence also showed small increases. His results for remanence were particularly inconclusive which could be explained in the case of compressive deformation by the combination of the tensile residual stress tending to increase the remanence and the increasing dislocation density tending to decrease it. The changes due to the tensile residual stress were also smaller than those for compression as was predicted from the dependence of the magnetostriction on stress.

It is therefore suggested that not only can the increase in plastic deformation be detected from a measurement of coercivity, but that by measuring a parameter such as the maximum differential permeability at the coercive point, it should be possible to determine whether the deformation is tensile or compressive. In addition, for steels in which the coercivity is little affected by elastic stress, any confusion that may arise from isolated measurements made to detect elastic stress due to the onset of plastic deformation could be resolved by a single coercivity measurement parallel to the direction of strain.

6.3.1 Barkhausen Noise.

Fewer measurements have been made of the Barkhausen noise from plastically deformed steel and not all the authors are in agreement as to the effect of the deformation. In general the level of noise has been seen to decrease as the yield point is reached. This has been observed in both silicon-iron (Tittio 1976) and mild steel (Karjalainen et al 1979, 1980, Rautioaho et al 1986) although Buttle et al (1986) found all three peaks recorded for 4.9% cold-worked polycrystalline iron to decrease after annealing. Karjalainen et al (1979) also investigated the effects of repeated cycling of the material above and below the yieldpoint and were able to detect a change in the trend of the noise as fatigue was approached. The effect of plastic strain on the power spectra of the Barkhausen noise also seems to depend on the initial microstructure; Rautioaho et al (1986) found a decrease in the low frequency noise with increasing deformation for their mild steel samples as did Lieneweg (1976) with silicon-iron, however Hwang et al (1988) recorded a decrease in their low frequency noise as their mild steel was deformed.

The Barkhausen measurements on the 2401 pipe steel were a continuation of the work of A.J. Birkett (1988) on 12″ pipesteel in which the low frequency intercept of the power spectrum had been found to decrease with both plastic compression and tension. The power spectrum of the 2401 steel also decreased with increasing strain (Birkett et al 1989). In the theory for the clustering of individual pulses described in chapter one it was assumed that the number of elementary pulses per cluster is proportional to the time interval between the cluster and the previous discontinuity. At low frequencies it is possible to approximate the equation for the power spectrum (1.31) to:

$$\Phi(0) \simeq 2\varphi(0)\rho \ldots (6.07)$$

hence the low frequency intercept is determined solely by ρ the number of elementary pulses per cluster. The restriction of the domain wall movement due to the dislocation tangles has been observed under the electron microscope and would seem likely to reduce the probability of more than one jump occurring at the same time. This will reduce the number of pulses occurring in one cluster and hence the value of the low frequency intercept as observed experimentally.

The actual Barkhausen traces were studied for the second series of experiments on the pure steel, examples of the plots for the deformed steel are in figures 5.23, 5.25, 5.27, and 5.29. For all the samples the overall volume of noise decreased for the deformed samples. The initial peak of 50% pearlite sample 7092 reduced and then disappeared completely at the low deformations of 0.4% and 0.8% respectively as the 90°wall motion is completely suppressed by the residual compressive stress. What was then a single 180°wall peak for all the samples became sharper and narrower as the onset of wall motion became more abrupt and only larger jumps were feasible. The peak also shifted towards the right, occurring at a higher field, this shift can be correlated with the increase of coercivity.

6.3.2 Shape of the Hysteresis Curve.

It is remarkable in itself that plastic deformation of as little as 5% can cause a similar change in magnetic properties as an increase from 20% to 100% of pearlite content with its associated change in microstructure. Although for tensile deformation the changes in properties for the two situations are similar, the increase in carbon content does not distort the shape of the hysteresis loop as was observed for the plastically deformed samples (figure 5.18). A simple change in the ratio of Br/Hc is not sufficient to produce this distortion as this ratio decreases faster for the increase in carbon content than for the increase in plastic deformation. The observed bulge in the central portion of the loop is accentuated in the plots of differential permeability against applied field shown for 7091 in figure 6.08 and after heat treatment "A" in 6.09. As plastic deformation increases, and with it the density of the dislocation tangles, the pinning forces due to these tangles also increases and hence easy domain wall movement is greatly reduced. As the field is reduced from saturation very little irreversible domain wall movement is possible due to the very high pinning energies and magnetisation is forced to occur either by rotation or by reversible bowing between pinning sites. As zero field is reached there is sufficient magnetic force to overcome these strong pinning sites. However this movement is very difficult and the permeability drops dramatically when this point is reached. This is reflected in the dip in the differential permeability that develops around the remanent point as the degree of plastic deformation is increased. The dip in the curve also broadens as the deformation progresses and an increased proportion of the magnetisation reversal must take place in this way.

201
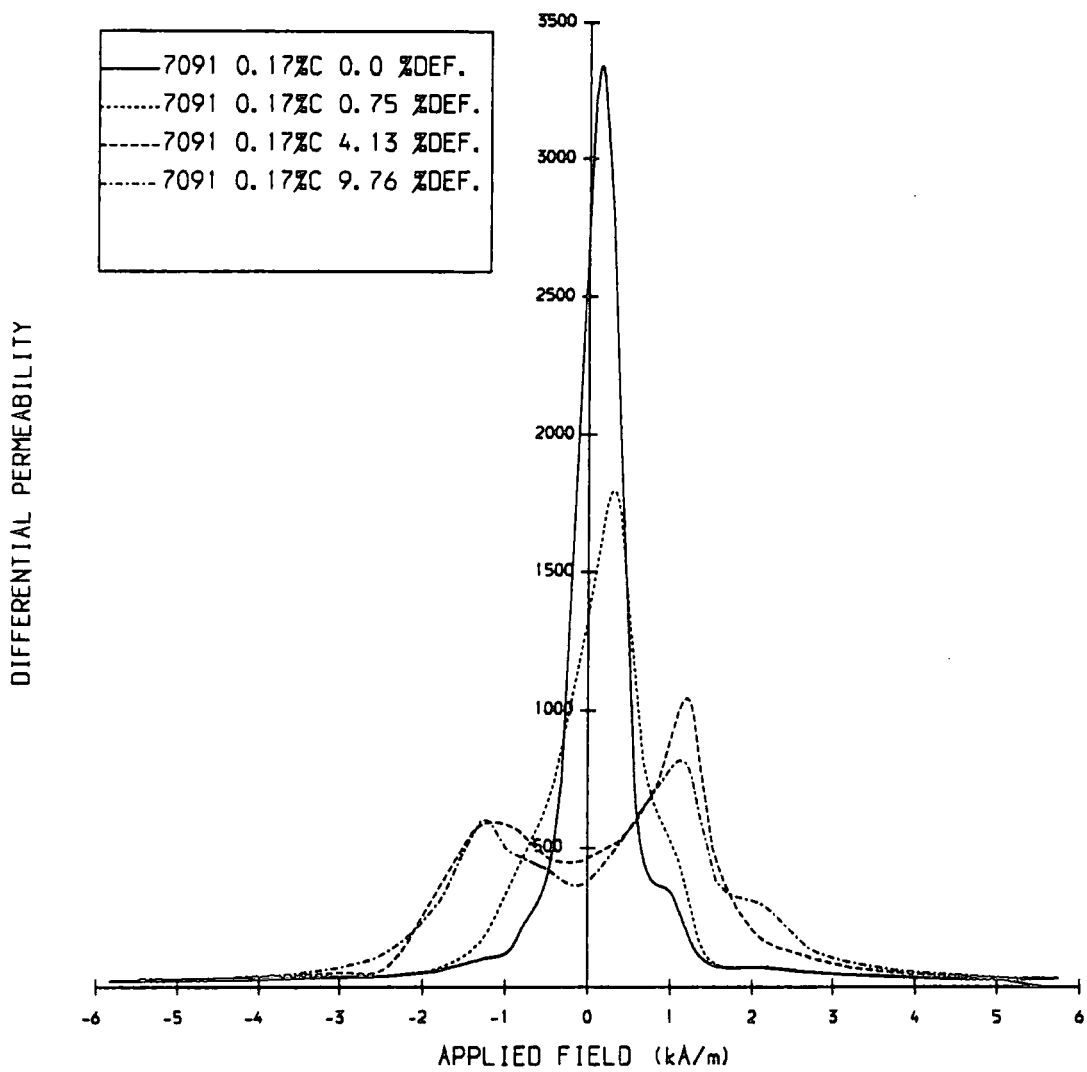
Figure 6.08 Differential Permeability as a Function of Applied Field for a Range
of Plastic Deformations of Sample 7091.

202
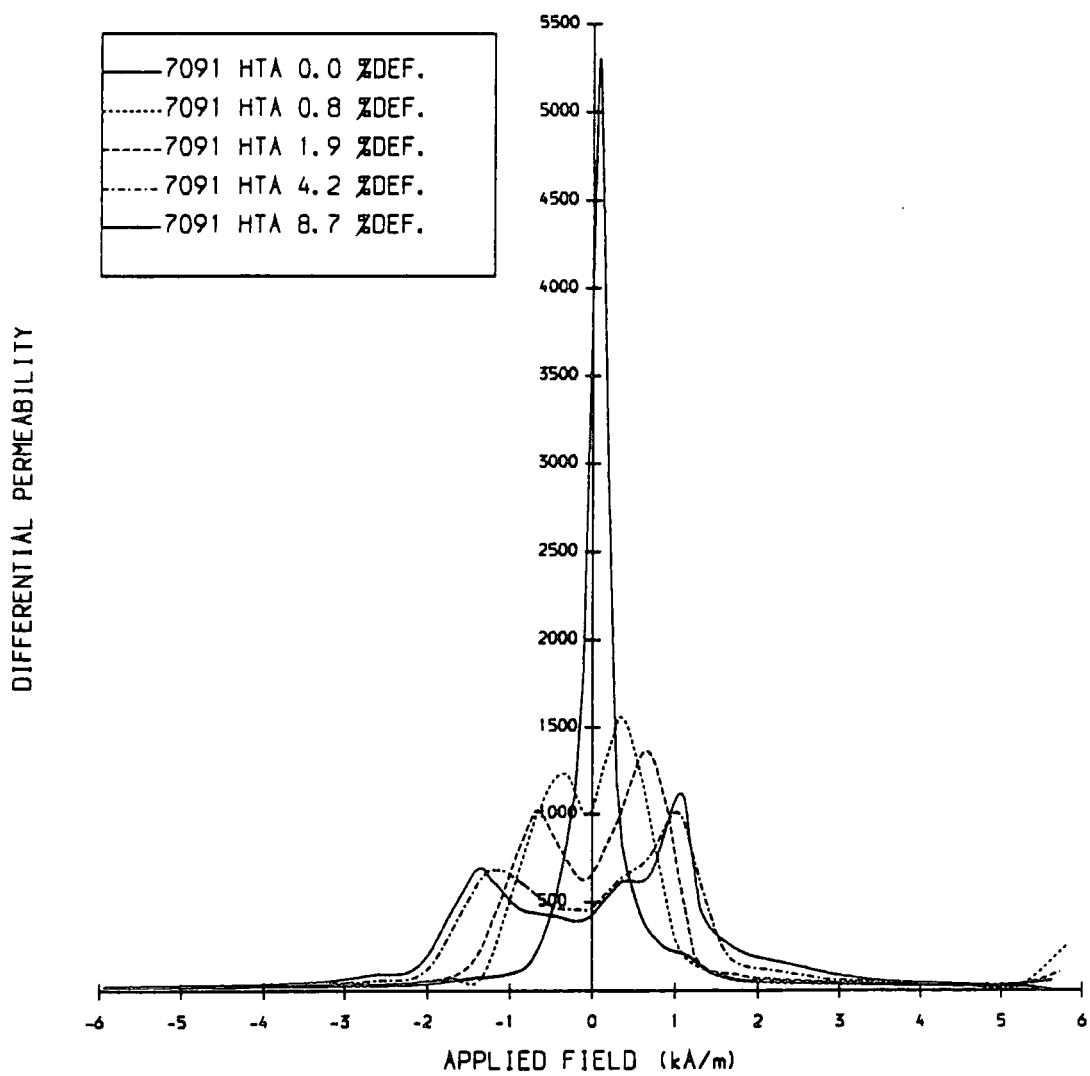
Figure 6.09 Differential Permeability as a Function of Applied Field for a Range of Plastic Deformations of a Heat Treated Sample of 7091 (HTA).

203

This marked decrease in the gradient of the hysteresis curve around remanence gives the distorted hysteresis loop its characteristic bulge. The interaction in some steels between internal stress and the pinning sites that results in an increase in coercivity even for elastic compressive stress, also has a bulging hysteresis curve.

This reduction in discontinuous low field movement is also demonstrated by the results of the minor loop data. At very low maximum fields, Hmax, values of coercivity and remanence are both extremely low as most of the magnetisation takes place by reversible low energy domain wall movement. As Hmax is increased enough energy is eventually supplied by the applied field to release some of the walls from their pinning sites, irreversible motion increases rapidly as do values of Br and Hc until high field reversible rotation begins to dominate. The low field region of reversible domain wall motion is represented by the flattening of the Br vs. Hmax curves (figures 4.12 to 4.15). This region was found to be wider for the deformed sample due to the higher field necessary to overcome the increased pinning energies. The energy distribution of these barriers can be represented by the differentials of these curves (figures 4.16 to 4.19). The higher the outer peaks of these curves the faster the increase of Br with Hmax i.e the easier it is to unpin the walls. The broader the peaks the greater the amount of high field motion and the wider the central dip the higher the field/energy required to overcome the smallest pinning sites. The curve for the deformed sample had lower, broader peaks and a wider central portion than the undeformed one. This broader central trough in the graph of dB/dHmax for a plastically deformed sample makes it especially important that a sample is saturated before either Br or Hc are determined.

6.3.3 Electron Microscopy Observations.

The observations made of domain wall movement under the electron microscope support this analysis and extended the previous observations of plastically deformed high purity polycrystalline iron made by Astie et al (1981), Degauque et al (1982) and R.A.Taylor (1983). Hetherington (1985) studied some undeformed constructional steels and commented that the dislocations present had little effect on the domain wall movement. This supports the statement that it is the dense tangles of dislocations that are effective as pinning sites.

204

Dislocated areas were present in both deformed and undeformed steel due to the inherent microstructure of the steel and the extrusion process, but far more dense dislocation tangles were observed in the deformed samples. Wherever domain walls encountered these regions their movement was affected. In some cases this resulted in noticeably more movement taking place in surrounding dislocation free areas, but in most cases the domain walls were locally affected weaving through the dislocated areas in which the stress fields will be very non-uniform to find the minimum wall energy. Where a domain wall was pinned by dislocations it would bow between the strongest pinning sites under an applied field until sufficient energy was acquired to release it; some bowing often remained after the applied field had been removed. These observations describe a more difficult magnetisation process with an increase in high field reversible motion in highly dislocated areas. It is possible to derive expressions for the interaction of domain walls with various dislocations (Cullity 1972); but such equations are specific for types of dislocation and orientation with the domain wall. It is difficult to generalise these expressions for such an inhomogenous material (Jiles et al 1983), but the prediction that the dislocations will have a greater effect on $90°$walls than on $180°$ones is supported by figure 5.30 in which the walls forming the closure domains are more distorted than the main $180°$walls. Seeger et al (1964) have discussed the effects of dislocations on domain walls in f.c.c. crystals.

6.3.4 Inter-relationship of Magnetic Properties.

Hc, Hm and μ_i are all affected by the reduction of easy domain wall movement due to the increased domain wall pinning and some covariance can be found between these parameters (Jiles 1988a, b c and d), and (Tanner et al 1988).

For the initial magnetisation curve, the increase in the proportion of domain wall movement that occurs at higher fields is demonstrated by the lowering and broadening of the plots of relative permeability against applied field shown for a range of deformations for 7091 and 7094 in figures 6.10 to 6.11 and for heat treatment "A" in figure 6.12. The field at which the maximum permeability occurs increases in line with the coercivity as this represents the point on the initial magnetisation curve where most of the pinning sites have been overcome and rotational processes start to dominate. Graphs showing Hm as a function of Hc are plotted
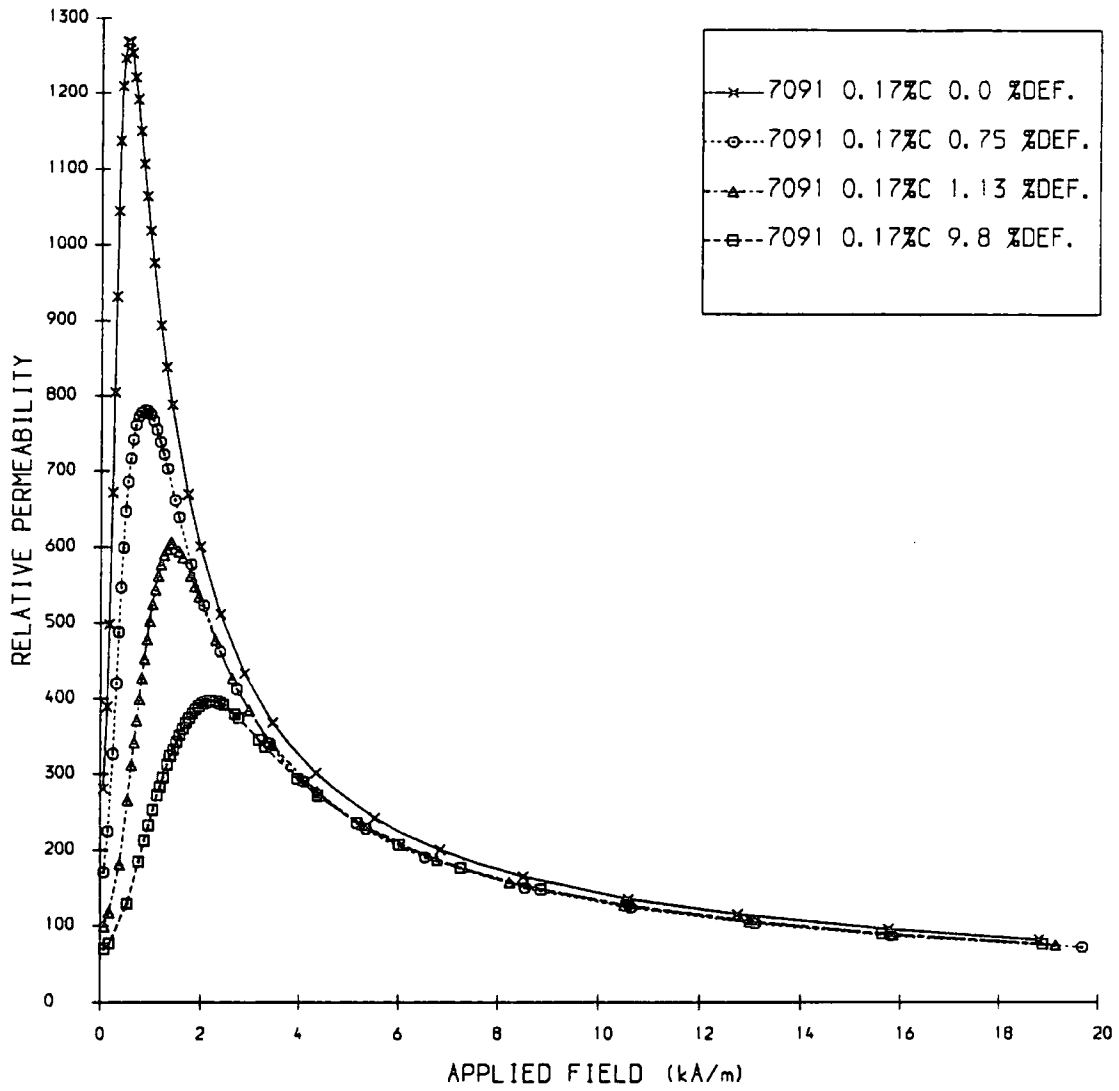
Figure 6.10 Relative Permeability as a Function of Applied Field for a Range of Plastic Deformations of Sample 7091.
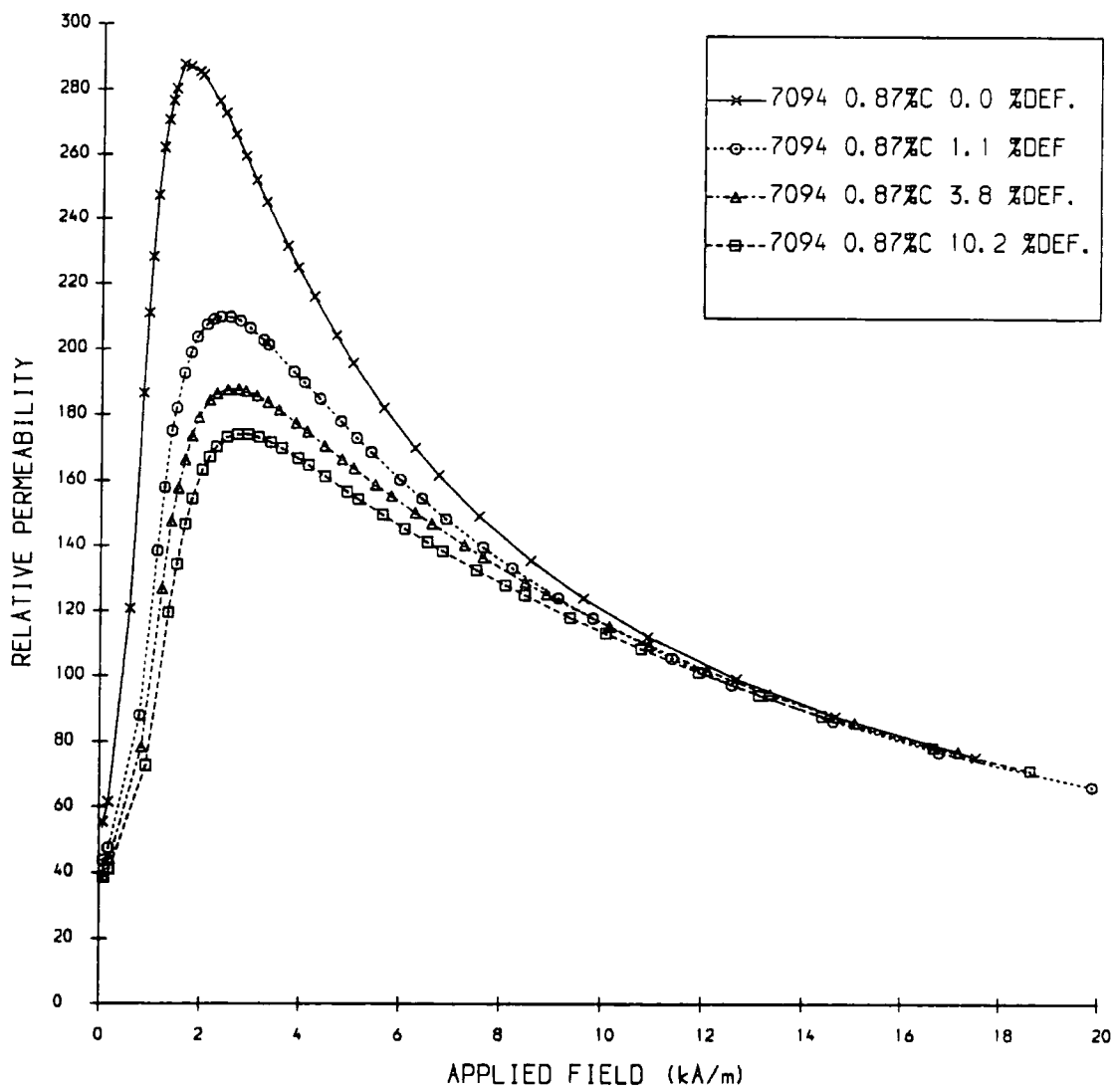
Figure 6.11 Relative Permeability as a Function of Applied Field for a Range of Plastic Deformations of Sample 7094.
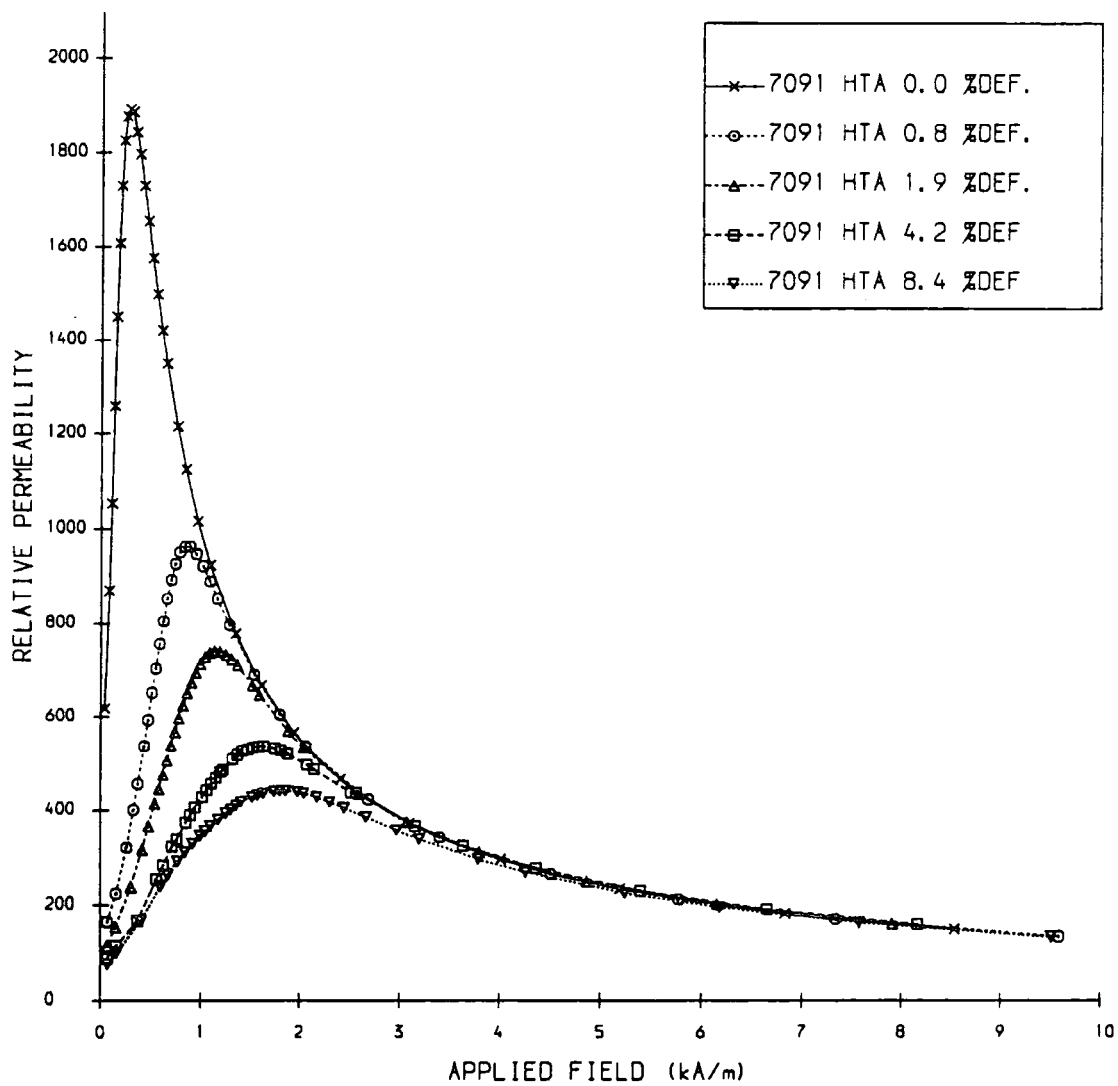
Figure 6.12 Relative Permeability as a Function of Applied Field for a Range of Plastic Deformations of a Heat Treated Sample of 7091 (HTA).

208
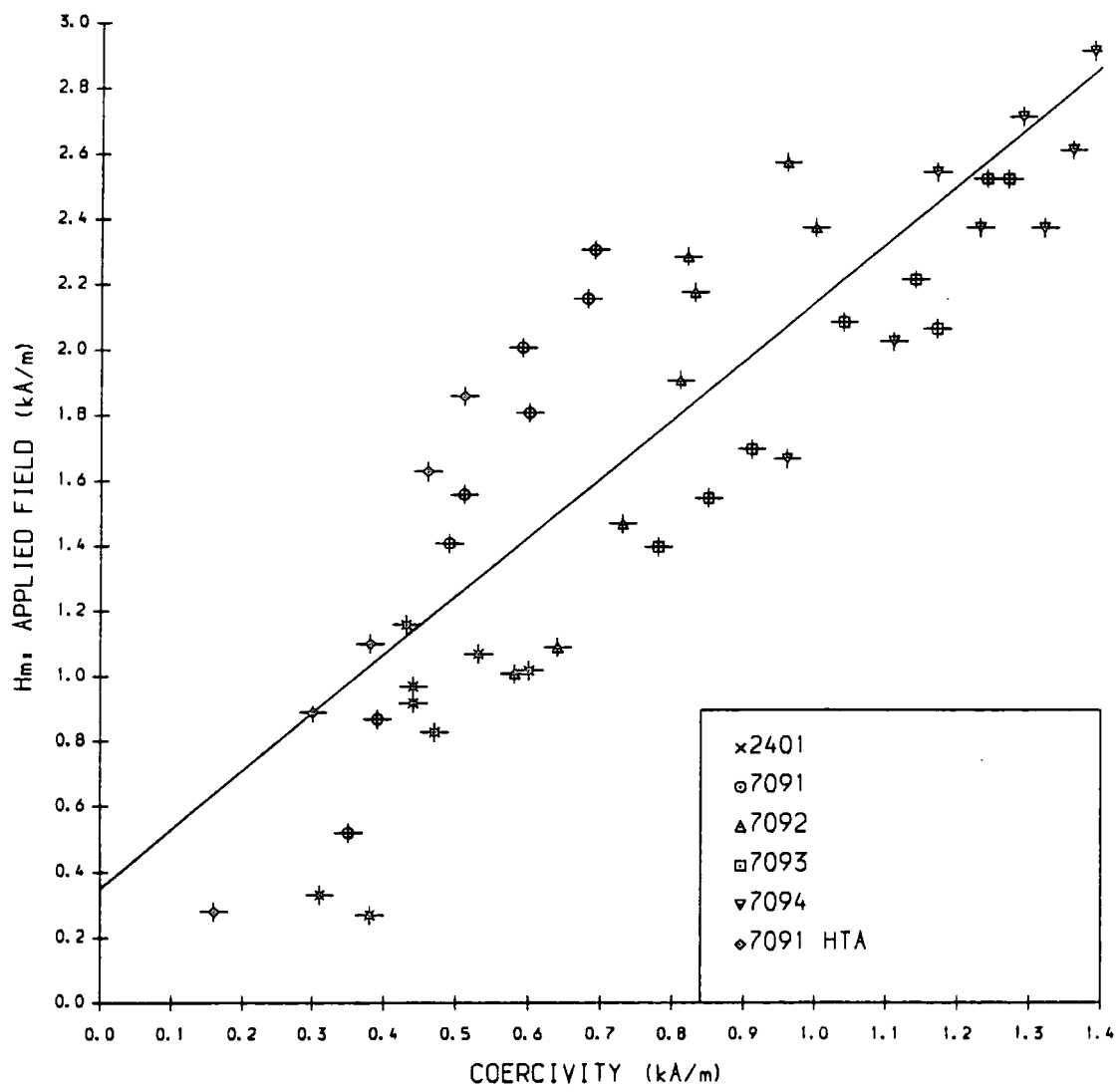
Figure 6.13 The Linear Relation of Hm With Coercivity for All the Steels Used in this Study.

209

for each carbon content and the pipe steel in figure 6.13. This linear dependence also holds for increasing carbon content although the gradient is significantly lower indicating the increased shearing of the loop for the plastically deformed steel.

The very rapid increase of dislocations in the early stages of deformation followed by the reduction in the flow stress increment as workhardening increases causes the initial rapid change in magnetic properties. As workhardening progresses the dislocation tangles become denser and the pinning forces stronger. As observed under the electron microscope the bowing of the domain walls between strong pinning sites becomes more noticeable and the ratio of reversible to irreversible processes that occur increases and hence the rate of increase in the coercivity decreases. The dislocation density of iron has been found to be proportional to the square root of the deformation for iron:

$$N = \text{const}\varepsilon^{\frac{1}{2}} \ldots (6.08)$$

Quereshi et al (1977) successfully tested predictions that the coercivity should be proportional to the square root of the dislocation density on SiFe. Combining this relation with equation 6.08 we have the relation between coercivity and deformation:

$$Hc = D\varepsilon^{\frac{1}{4}} \ldots (6.09)$$

where D is a constant. This equation has been tested by plotting Hc against $\varepsilon^{\frac{1}{4}}$ in figure 6.14. The fit is reasonably good for the low pearlite steels, but as the percentage of pearlite, which is more readily workhardened increases, the dislocation density in the ferrite will not increase as rapidly as $\varepsilon^{\frac{1}{2}}$ reducing the effect on Hc and causing the curve to flatten out at higher deformations. The actual change in coercivity as plastic deformation increases is independent of the carbon content and hence the initial value of coercivity. This is demonstrated in figure 6.15 in which $\Delta Hc = Hc(\varepsilon) - Hc(0)$ is plotted against $\varepsilon^{\frac{1}{4}}$ for all carbon contents, heat treated samples and 2401 pipe steel producing the general relation for all but the pipesteel:

$$\Delta Hc = 33.5\varepsilon^{\frac{1}{4}} - 15.5 \ldots 6.10$$

The pipesteel also increases linearly, but with a lower gradient: 16.6. Although the points are scattered most of the steels generally follow this relation, but as for the variation of Hc with $\varepsilon^{\frac{1}{4}}$ the curve for the 100% pearlite 7094 is convex.
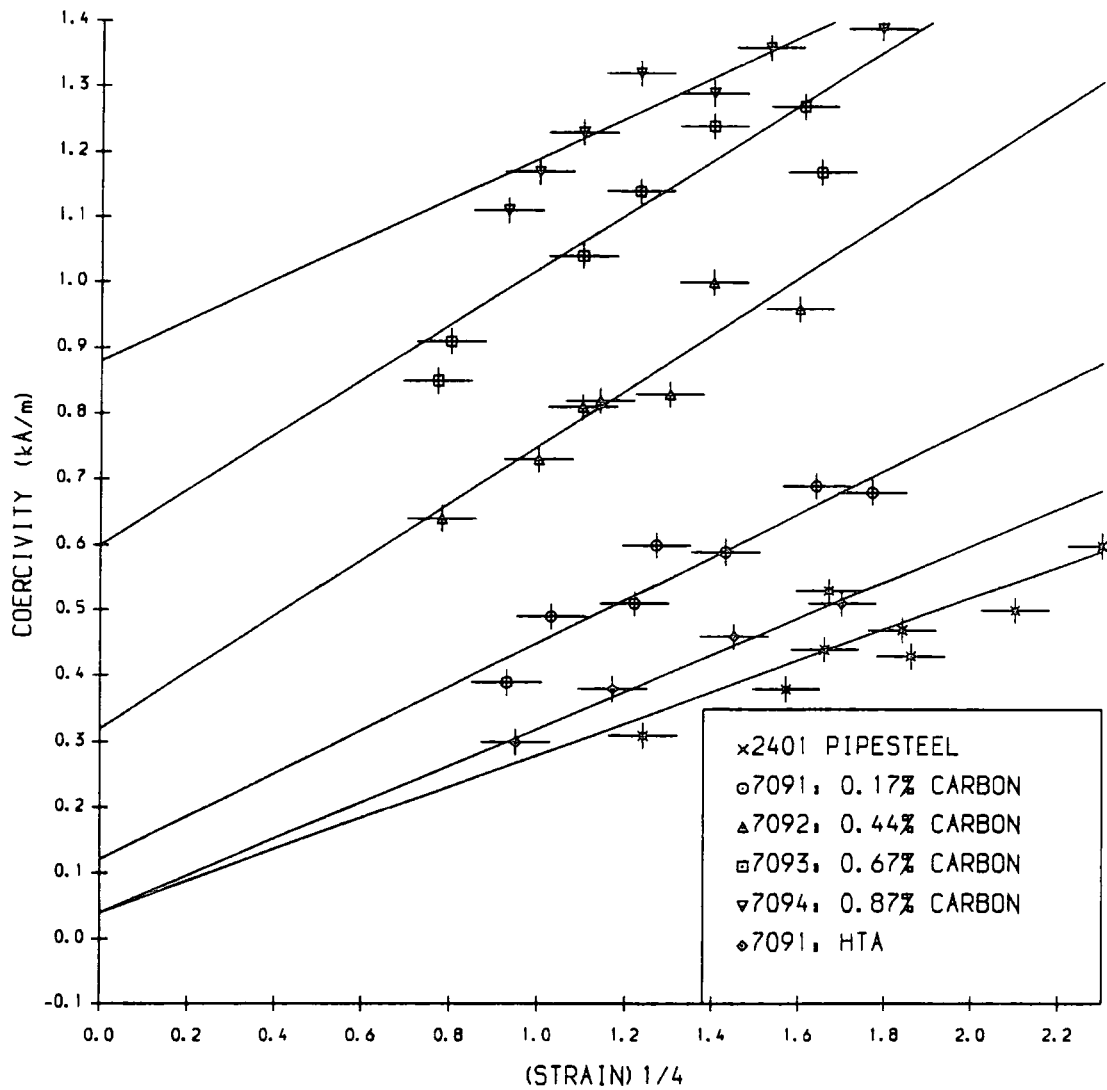
Figure 6.14 The Linear Relations of Coercivity With $\varepsilon^{\frac{1}{4}}$ for All the Steels Used in this Study.
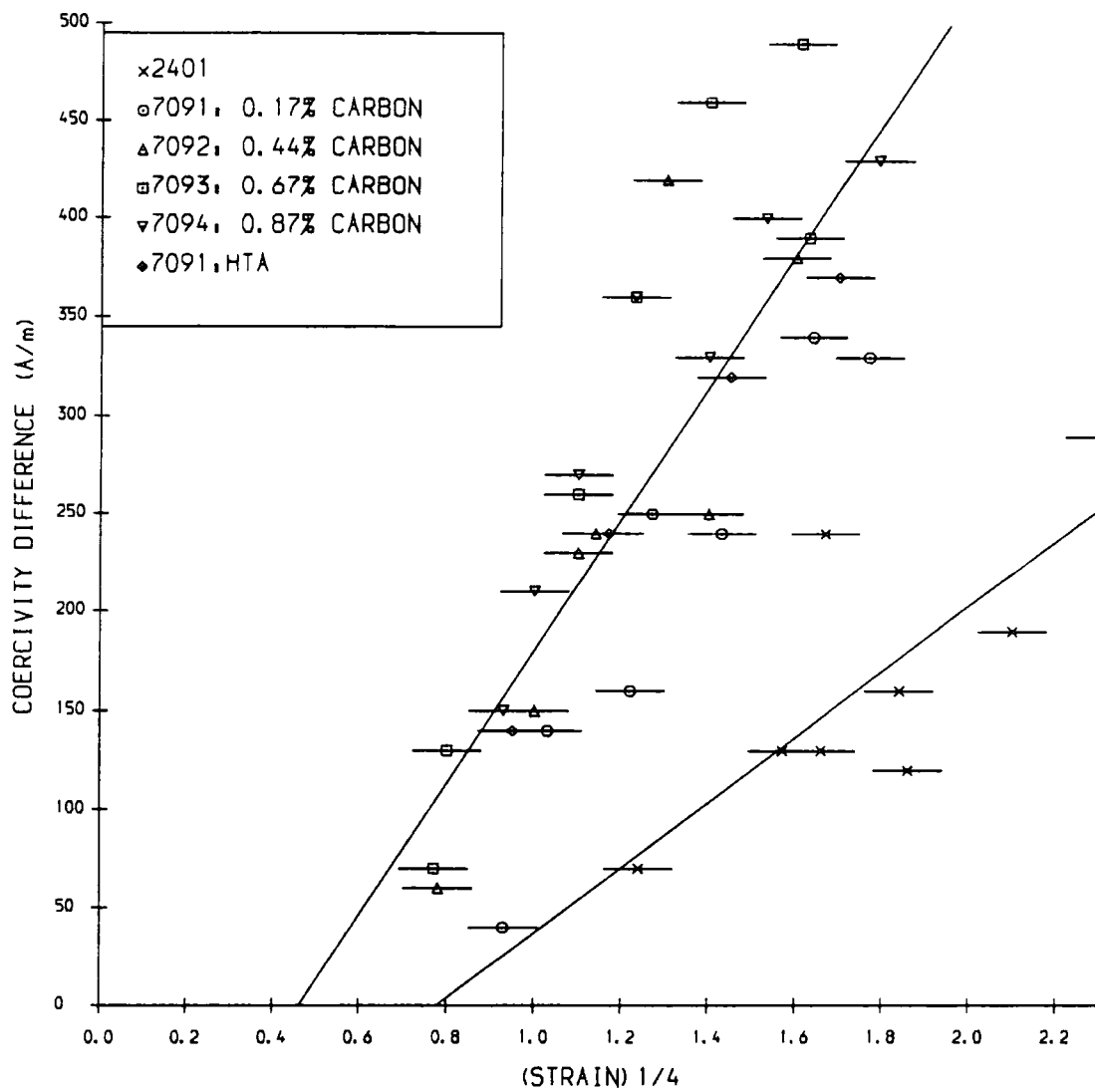
Figure 6.15 The Linear Relation of ΔHc With $\epsilon^{\frac{1}{4}}$ for All the Steels Used in this Study.

212
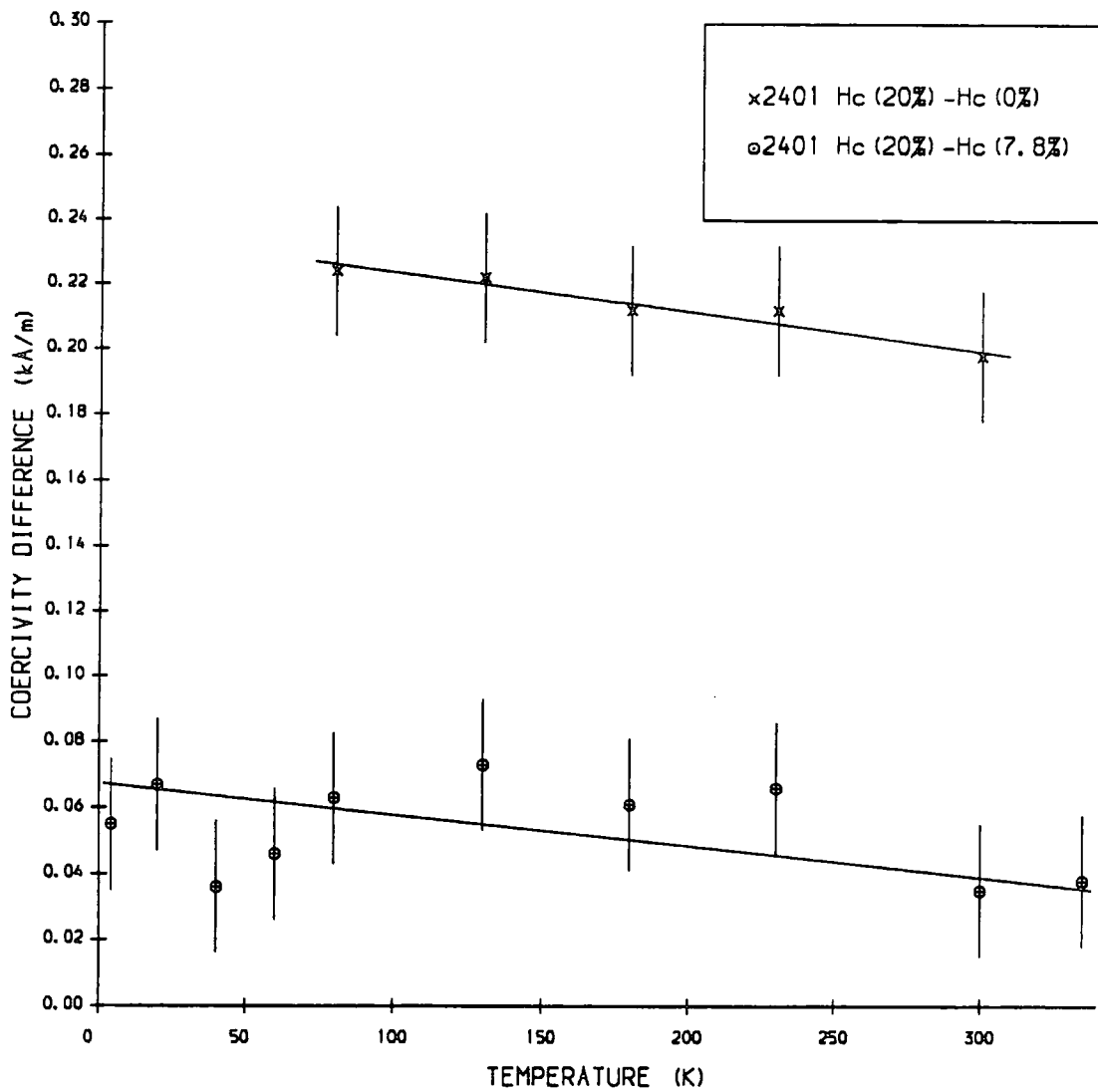
Figure 6.16 The Differences Between the Linear Relations of Coercivity With
Temperature for Different Plastic Deformations (Figure 4.09) With
Temperature.

213

As observed under the electron microscope it is in fact the dislocation **tangle** density that has the pinning effect on the domain walls and not simply the dislocation density. Hence the above equations should to be modified with a prediction as to how the tangle density increases with external strain. This is not a simple prediction to make as it will vary with the different microstructures, Fortunately dislocation density seems to provide a convenient approximation.

Measuring the reduction in coercivity with temperature (figure 4.09) showed that the contribution to the coercivity from the dislocations remained constant within the temperature range 4.2K to 300K. This is emphasised in figure 6.16 where the differences between the three curves are plotted as a function of temperature.

The increase in dislocation density also affects the mechanical properties of the steel and hence an increase similar to that of coercivity was found for Vickers Hardness with plastic deformation (figure 5.12). This is also reflected in that the general linear trend of coercivity with hardness also holds for the plastically deformed samples (figure 6.04).

The covariance of initial permeability with coercivity was expressed by Jiles (1988b)in the form :

$$ln\mu'_{in} = a - bHc \ldots (6.11)$$

where a and b are constants. In this study initial differential permeability is identical to initial relative permeability and this relation was tested in figure 6.17. It was found to hold best for the higher carbon content steels with $b = -0.9 +/- 0.6$ and $a = 4.8 + / - 0.06$, but low carbon 7091 at low strains and the softer heat treated samples of 7091 with higher initial permeabilities had steeper gradients. Jiles himself found the variation to be scattered for his range of lamella pearlite samples.

Tanner et al (1988) related μ_i and Hc with the relation:

$$\frac{1}{\mu_i} = 7.95Hc + 1.23 \ldots (6.12)$$

(Converting his formula so that μ_i is dimensionless and Hc measured in kAm^{-1}.) which indicates the dominance of a domain wall pinning mechanaism for these
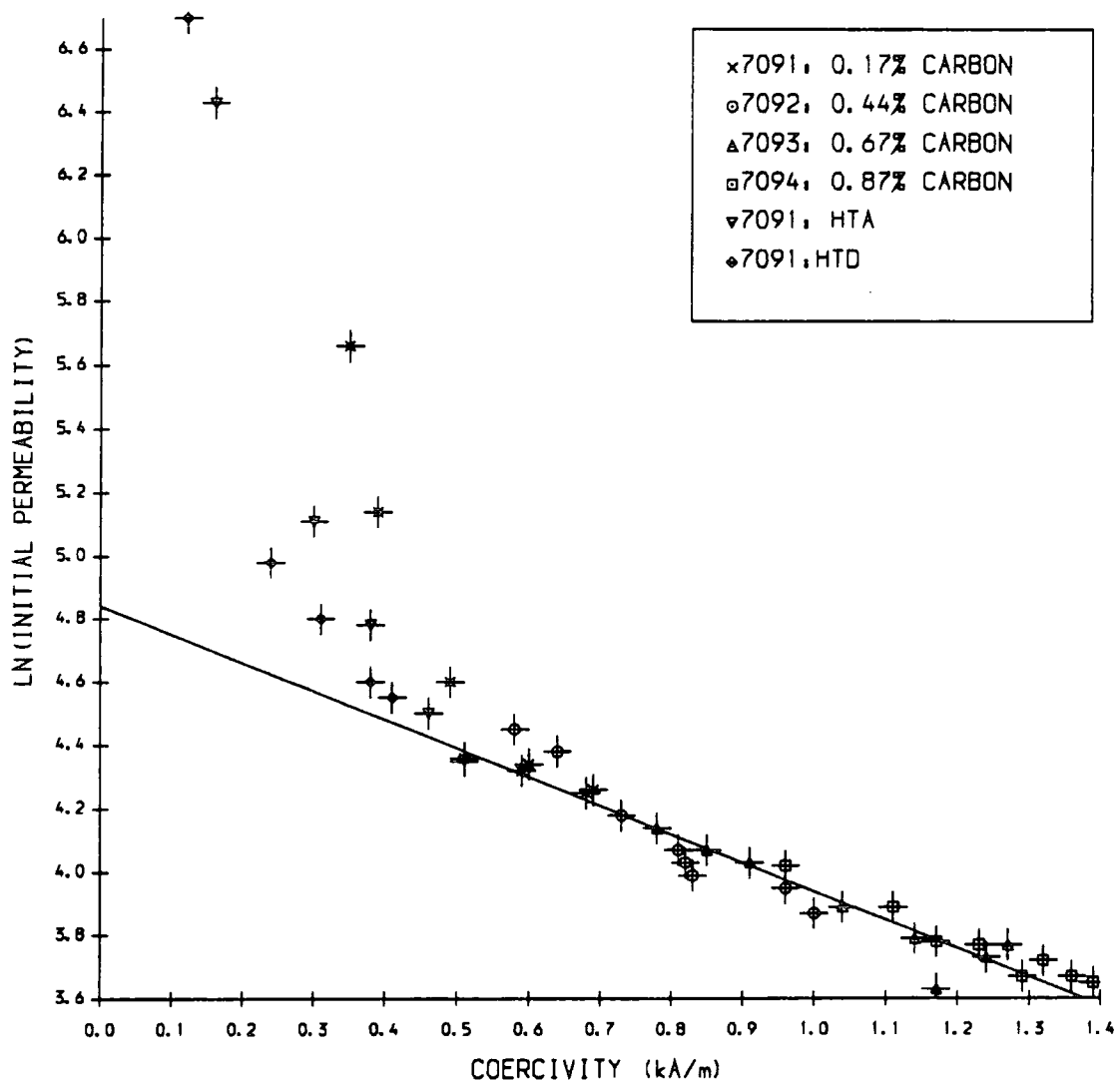
Figure 6.17 The Linear Relation of $ln\mu_{in}$ With Coercivity for the Specially Prepared Steels.

215

steels. This inverse relation was found to fit this data better than the logarithmic one in 6.11 although there was still some deviation at low carbon contents. The graph is plotted in figure 6.18 and the the relation found here to be:

$$\frac{1}{\mu_i} = 18.1 Hc + 1.63 \dots (6.13)$$

Jiles (1988d), working from his results obtained from a series of Rayleigh curves found the initial differential permeability to vary as :

$$\frac{\mu'_{in}(\varepsilon)}{\mu'_{in}(0)} = \frac{1}{\left(1 + c\varepsilon^{\frac{1}{2}}\right)} \dots (6.14)$$

where $c = 17.3$ for pure iron. The ratio of initial permeabilities as a function of $\varepsilon^{\frac{1}{2}}$ is plotted in figure 6.19. All the gradients are significantly less than the 17.3 for iron and reduce dramatically as the steel becomes harder. The curve is only found to be linear in the region below about 2.2% strain after which the gradient reduces producing a convex curve.

Using equation 6.11 for μ_{in} and Hc it is possible from 6.14 above to derive an equation relating ΔHc and ε:

$$\Delta Hc = \frac{1}{b} ln(1 + c\varepsilon^{\frac{1}{2}}) \dots (6.15)$$

It is hard to distinguish between this relation and the simpler variation of $\Delta Hc \propto \varepsilon^{\frac{1}{4}}$ evaluated earlier.

6.3.5 Anisotropy of Coercivity

Using the V.S.M. to make coercivity measurements on the pipesteel it was possible to measure the coercivity both parallel and perpendicular to the rolling and deformation direction. The undeformed steel had a higher coercivity perpendicular to the rolling direction. That this could be due to the deformation of the steel during pipe manufacture was considered but rejected as the anisotropy was also seen in the type "B" discs in which both directions of magnetisation are perpendicular to any circumferential strain existing in the pipe. In addition the samples were
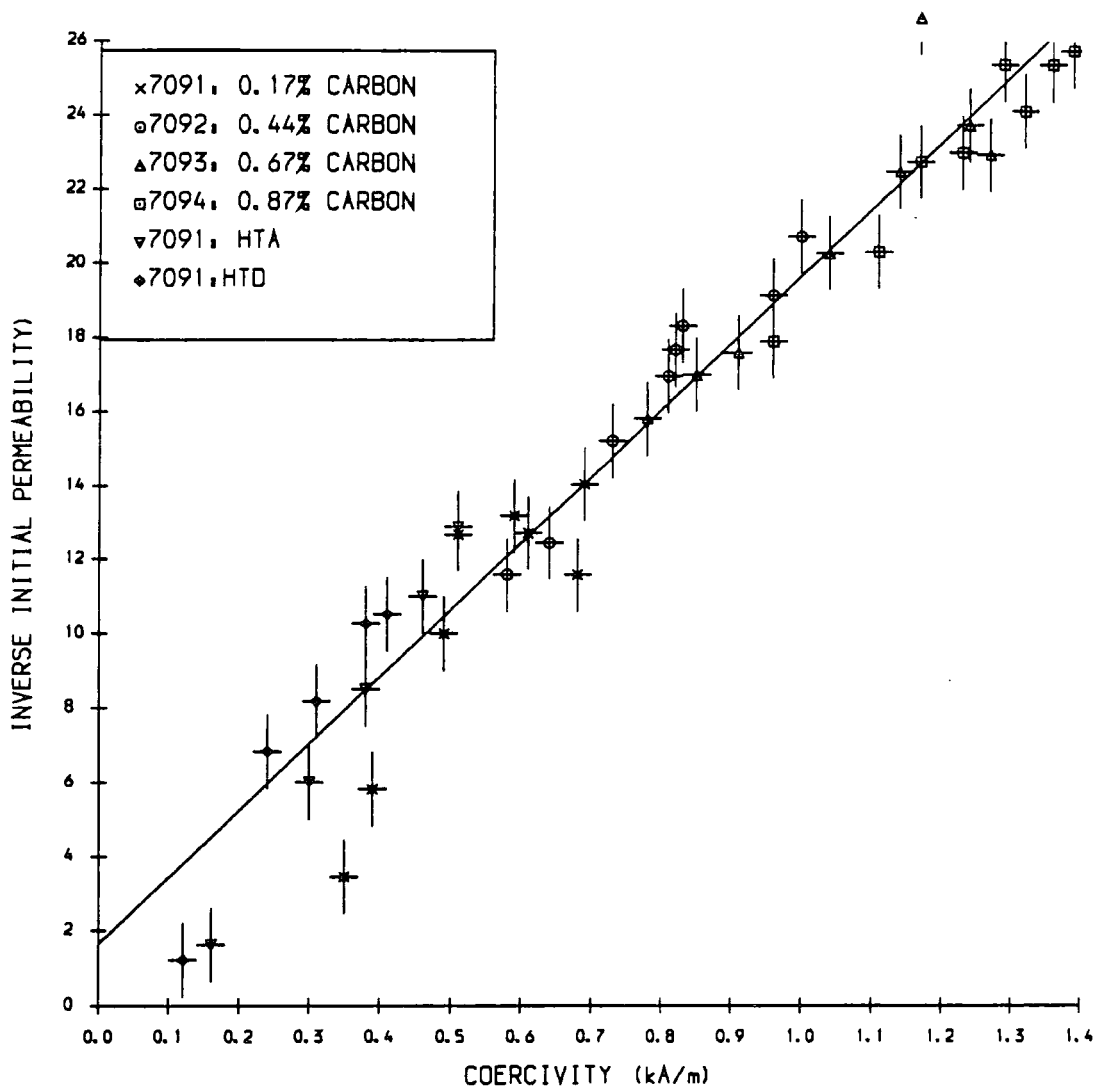
Figure 6.18 The Linear Relation of $\frac{1}{\mu_{in}}$ With Coercivity for the Specially Prepared Steels.

217
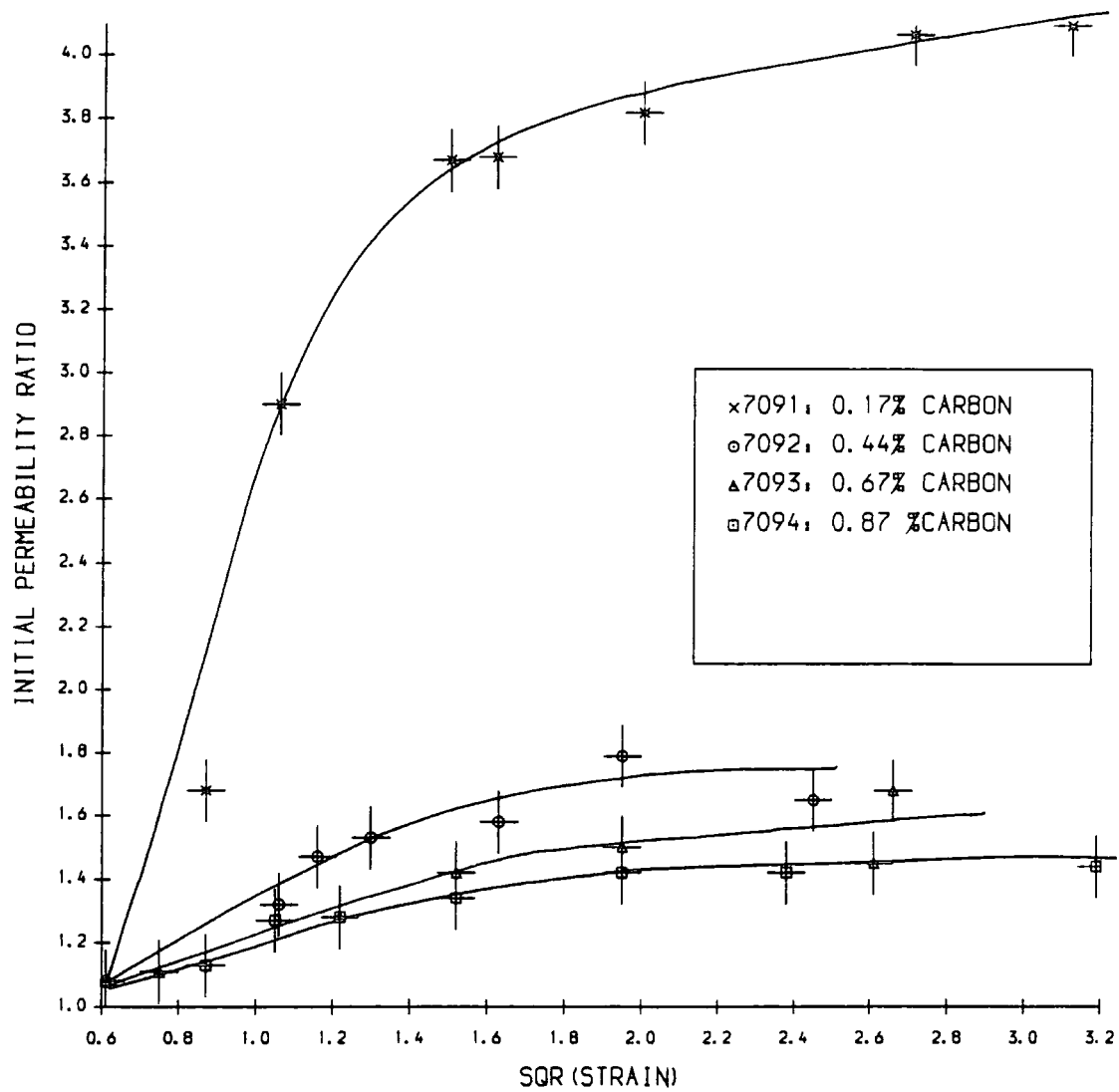
Figure 6.19 The Relation of $\frac{\mu'_{in}(\varepsilon)}{\mu'_{in}(0)}$ With $\varepsilon^{\frac{1}{2}}$ for The Specially Prepared Steels.

218

taken from the center of the pipe wall which should be undeformed in the change-over from compressive to tensile strain. Willcock (1985) also made measurements for the variation of coercivity with angle with respect to the rolling direction and found the same anisotropy with the largest variations in the controlled rolled and fully killed steels. These results indicate that it is the elongation of the grains during the rolling process that make the magnetisation more difficult perpendicular to the rolling direction. The pipesteels in this context are low carbon steels and the majority of the domain wall movement is in the ferrite grains. Parallel to the rolling direction the magnetisation will be parallel to the elongated grains and therefore the domain walls will be perpendicular to most of the ferrite-ferrite grain boundaries that they encounter along their length. Once movement has occurred in the ferrite, the walls will then extend into the pearlite grains to complete the magnetisation. However when magnetised perpendicular to the rolling direction the domain walls must lie across the elongated structure probably forming closure domains onto the pearlite grains. As the sample is magnetised the walls movement will be restricted by the parallel ferrite-ferrite grain boundaries, hence the more difficult movement is reflected in the higher coercive force. As the microstructure becomes more banded, as it does for the controlled rolled and fully killed steels, this effect will become more important hence the higher measured values of anisotropy on Hc.

A formalism has been developed by Szpunar and Tanner (1984) to describe the grain shape and grain boundary distribution in polycrystalline materials. These have shown that there is an anisotropy in the grain size of the pipesteel, especially in the pearlite (Tanner, private communication).

The anisotropy in coercivity that develops in the pipe steel with increasing plastic deformation is due to the compressive stress reducing the increase in the coercivity from the dislocation tangles perpendicular to the direction of strain and increasing it parallel to the direction of strain. The opposite anisotropy of coercivity develops with increasing plastic strain to that which existed in the undeformed state.

219

6.3.6 Higher Pearlite Content Steel.

The increase in the coercivity with plastic deformation was seen to be similar for all carbon contents and heat treatments although the increased workhardening in the 7094 100% pearlite sample was seen to reduce the rate of increase. However values of μ_{max}, μ_i, and Br decreased far more rapidly in the early stages of deformation for the softer steel. The distortion in the hysteresis curve represented by the dip in the μ'_{max} vs. Happ curve was also much more prominent for these steels. These curves are shown for the higher carbon content steels in figures 6.20 to 6.22 and should be compared to those for 7091 in figures 6.08 and 6.09. Most of the other linear relations showed most deviation at low carbon contents such as the variation of μ_i with Hc.

These differences suggest a fundamental change in the magnetisation process as the carbon content is raised. Observations of the microstructure of all the steels used showed that the increase in pearlite content from 20% to 50% results in a very different microstructure. In all the 7091 samples and the pipesteel large areas of clear ferrite were visible creating a two phase system with clearly defined ferrite and pearlite grains, whereas at higher carbon contents the pearlite is well dispersed throughout the sample resulting in a single phase system.

During the initial magnetisation curve for the low carbon samples there will be a large amount of low field domain wall movement in the ferrite grains in preference to motion in the pearlite, which does not occur until higher fields. This results in the very high values of permeability for these steels compared to the higher carbon contents in which there are no large ferrite areas for free domain wall movement and the difficult magnetisation of the pearlite is more important. This is reflected in the Barkhausen noise taken for a hysteresis loop where most of the domain wall movement occurred in initial and final peaks representative of discontinuous 90°and 180°domain wall motion in ferrite grains. Only low residual compressive stresses are necessary to suppress the 90°walls and reorientate the magnetisation perpendicular to the strain direction. Hence even for the initial stages of deformation the effect of suppressing this rapid domain wall movement will have a dramatic effect on its magnetic properties. At the higher carbon contents the pearlite is well dispersed through the microstructure and the Barkhausen plots have shown that
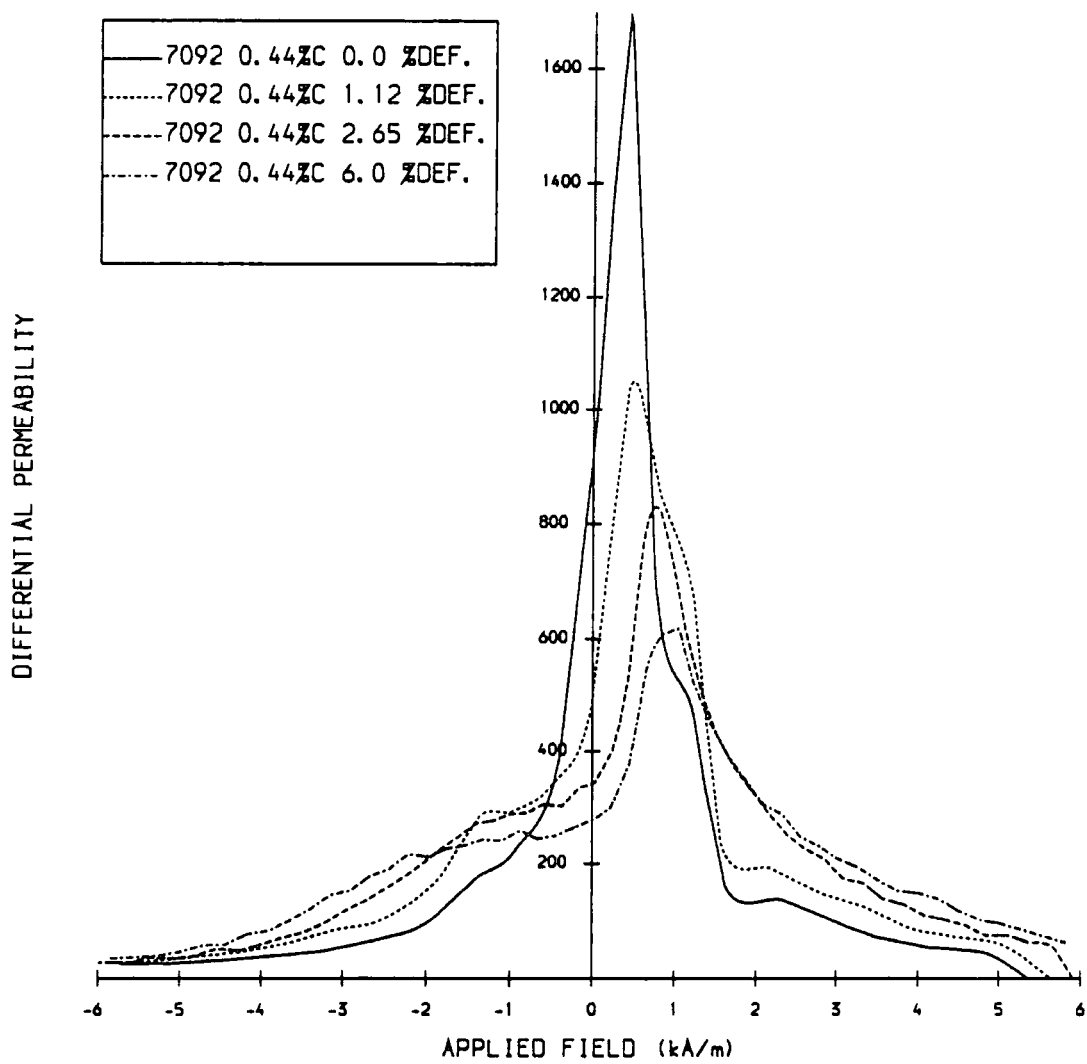
Figure 6.20 Differential Permeability as a Function of Applied Field for a Range of Plastic Deformations of Sample 7092.

221
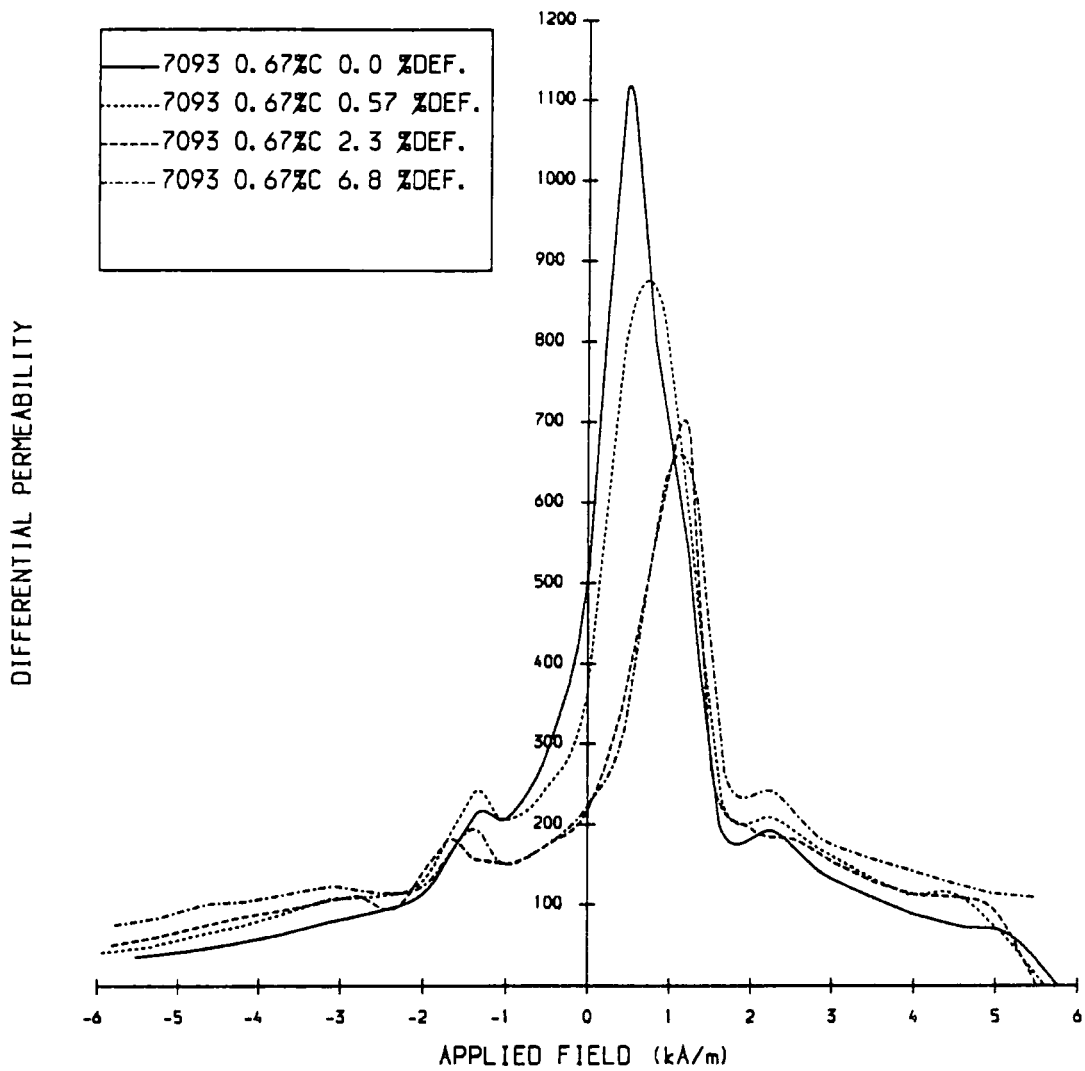
Figure 6.21 Differential Permeability as a Function of Applied Field for a Range of Plastic Deformations of Sample 7093.

222
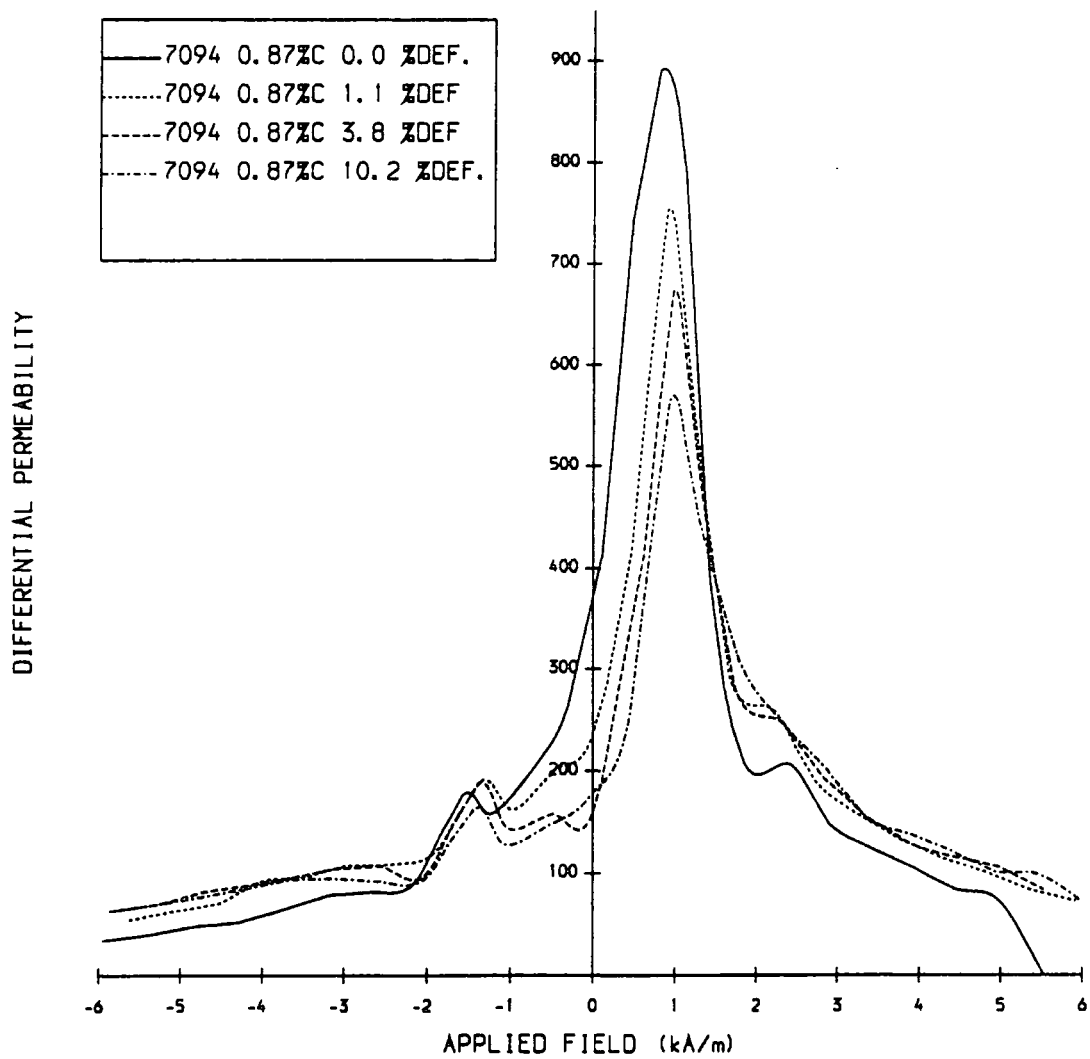
**Figure 6.22** Differential Permeability as a Function of Applied Field for a Range of Plastic Deformations of Sample 7094.

223

there is little facility for easy low field movement. Plastic deformation still reduces the domain wall movement but the effect is less dramatic as there was no easy motion in the undeformed state. As the cementite is so effective at pinning domain walls it also requires more stress to suppress the closure domains present within the pearlite reducing the stress related effects.

Jiles (1988c and d) extended his study of compressive deformation to a wide range of different heat treatments to include bainites and martensites. The former were found to follow similar trends to the lamellar samples, but the martensitic steels exhibited softer magnetic properties as they were deformed. This was attributed to the high degree of strain inherent in the undeformed martensite that may be relieved when external stress is applied.

6.4 The Kneppo Relation

An approximation to the initial magnetisation curve has been made by Kneppo (Gonda et al 1984)of the form:

$$B = A^{k-\frac{1}{H}} \dots (6.16)$$

where A and k are constants. If a good linear fit is found between lnB and 1/H for the type of steel concerned then values can be found for the constants and this formula can be employed. Willcock et al (1988) found that in general this relation held reasonably well for most pipe steels and, assuming the saturation induction to be constant for these steels, he was able to predict the whole B-H curve from the coercivity alone. However studies of welds in pipe steel (Thompson et al 1990b) showed that the Kneppo relation did not hold either for the weld material or the heat affected zone until it was renormalised. Plots of lnB against 1/H are plotted for different carbon contents in figure 6.23 and for a range of plastic deformations for 7091 prior to heat treatment in figure 6.24, heat treatment "A"in figure 6.25 and 7094 in figure 6.26.

The first portion of the initial magnetisation curve is expanded over the higher end of the 1/H x-axis, in this low induction region lnB is very sensitive to increases in B and hence there is a sharp increase in the Kneppo gradient (KP) at the field (HK) where the permeability increases and irreversible domain wall motion begins.
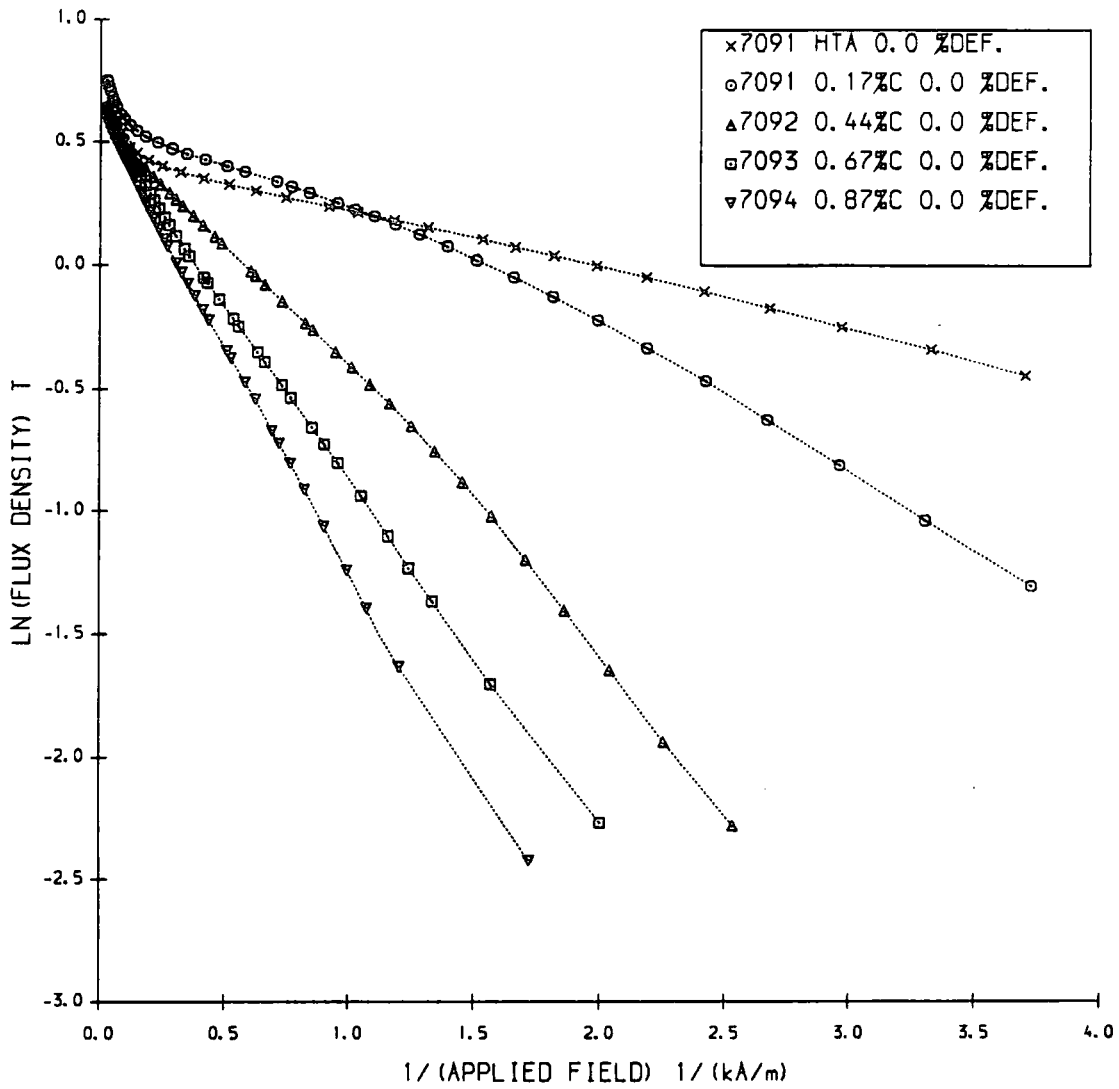
Figure 6.23 The Kneppo Relation for Undeformed Samples of Each Carbon Content.
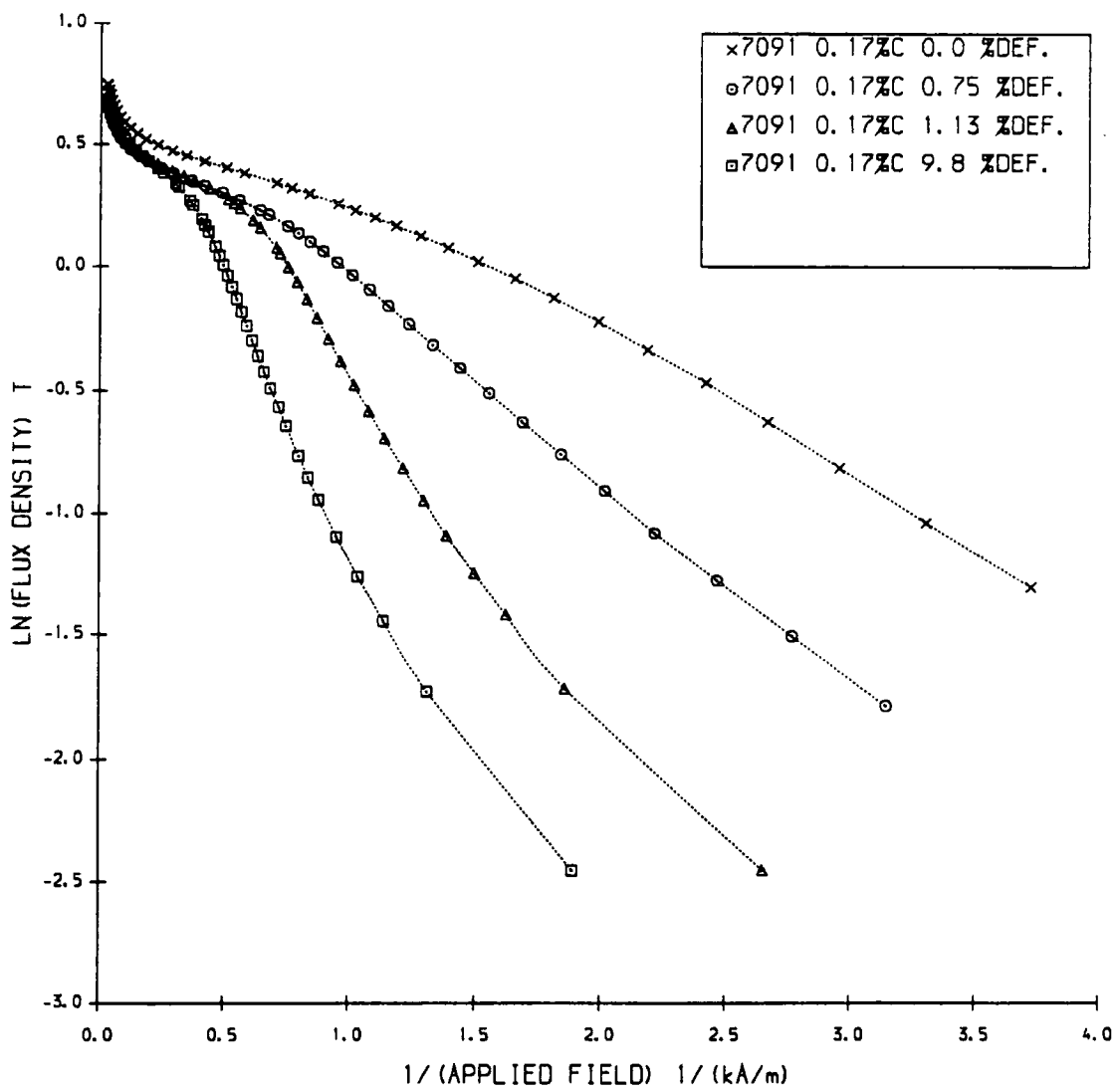
Figure 6.24 The Kneppo Relation for a Range of Plastic Deformations of Sample 7091.

226
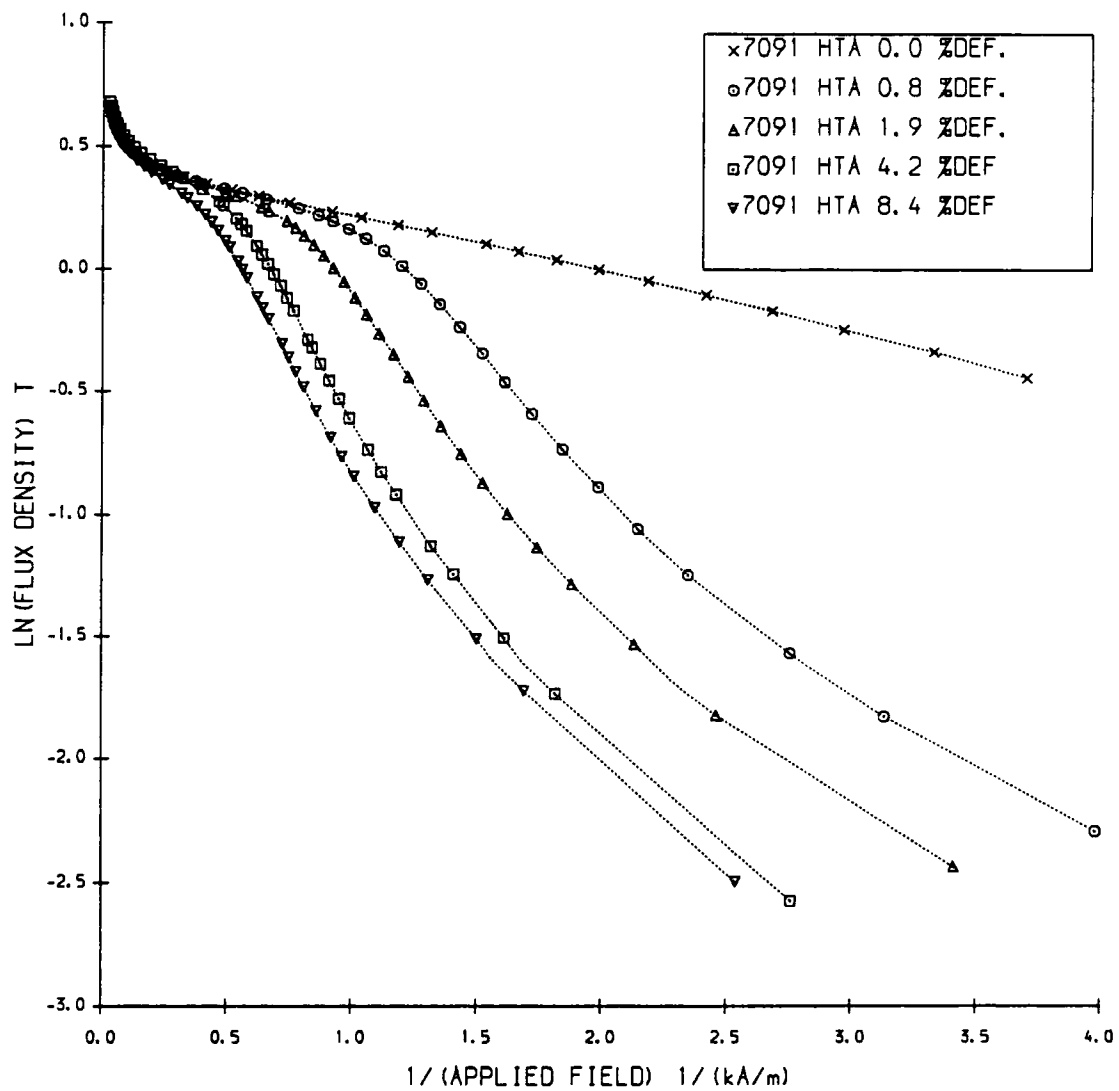
Figure 6.25 The Kneppo Relation for a Range of Plastic Deformations of Sample 7091 Heat Treatment "A".

227
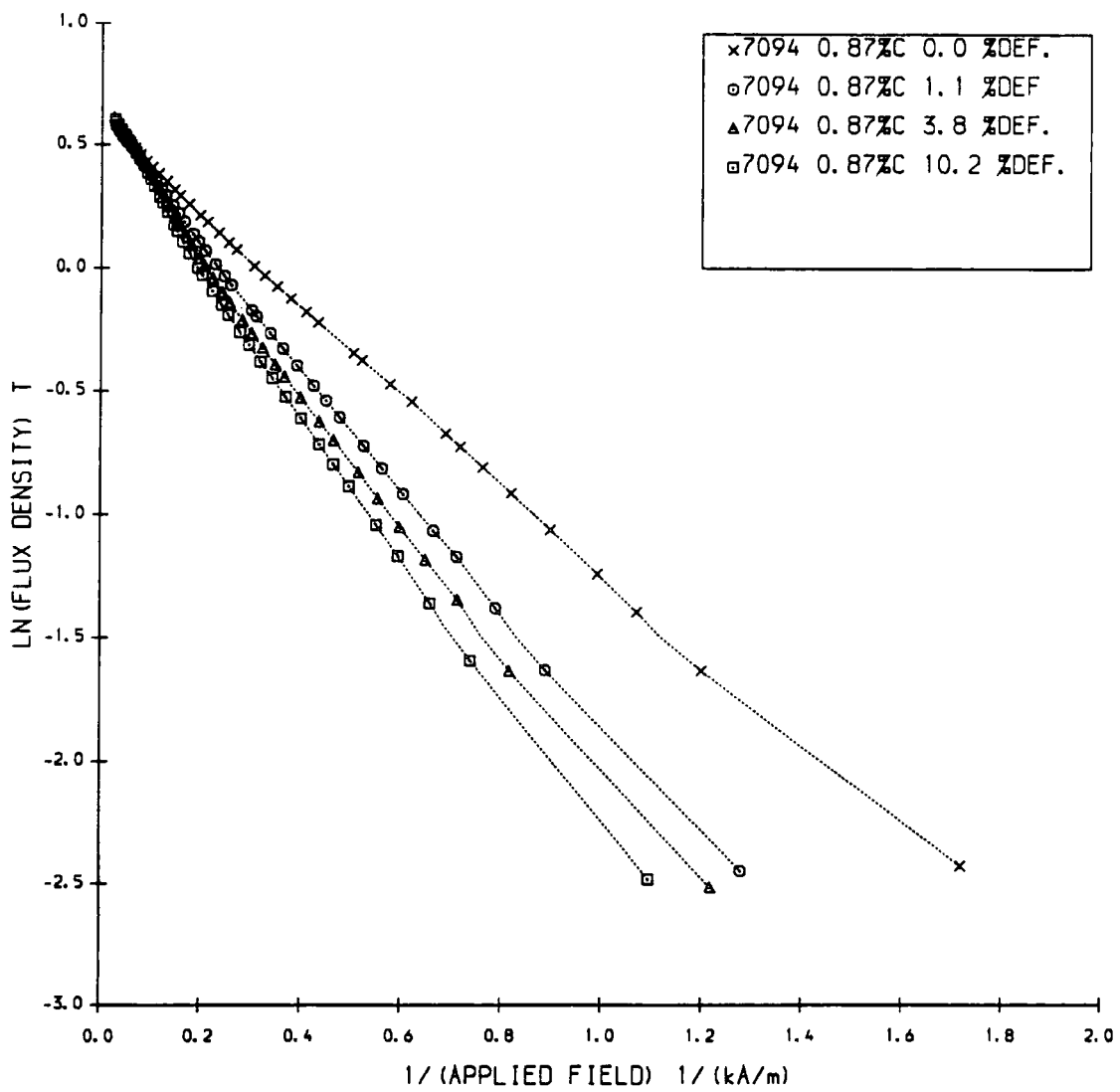
Figure 6.26 The Kneppo Relation for a Range of Plastic Deformations of Sample 7094.

A small change in HK will be reflected in a large shift along the x-axis of KP. It is in the field region above HK that the linearity of the Kneppo curve is tested and the gradient measured from which the predictions are made. As there is little change in ln(Bs) then this gradient is wholly dependent on and very sensitive to the onset of irreversible motion. This point corresponding to the field at which there is sufficient energy to overcome the pinning sites must be closely related to the coercivity and Hm. The gradient increased as a function of carbon content and of plastic deformation reflecting the measured values of coercivity. The sensitivity of the gradient is demonstrated by the very low gradient for the heat treated steel which is significantly softer than 7091 prior to heat treatment.

The approach to saturation after the knee of the magnetisation curve is very compressed near the origin of the Kneppo x-axis; after saturation the curve turns upwards towards the origin deviating from linearity, but this latter region is of no interest here. At the knee of the magnetisation curve just after the maximum relative permeability at Hm the permeability decreases. In the Kneppo curves for the softer steels this change in gradient is represented by a small peak above the generally linear curve. For these steels, as the plastic deformation increases and hence also Hm, this local maximum is further compressed as it approaches the origin and becomes more pronounced. This process can be seen in the Kneppo plots for all heat treatments of 7091.

Above Hm the Kneppo gradient is similar for all the steels, the main deviation from linearity occurring in the largest field region between HK and Hm. This concavity is present in the curves of the soft steels and increases with plastic deformation. Even for the 100% pearlite 7094 it is possible to detect the increase in concavity. For the soft steels with low values of Hm it is possible to see this detail in the Kneppo curve which represents the increasing permeability between HK and Hm. For all the steels as the degree of plastic deformation is increased the rate of increase in permeability is slower as the low field movement is restricted and the concavity of the curve increases. By studying the plots of relative permeability against applied field (figures 6.06 and 6.07) it was noted that Hm increased faster than μ_{max} decreased for increasing deformation than for increasing carbon content, another demonstration of increased shearing of the curve. The deviation from the undeformed value for this ratio will produce a concave curve.

It seems that the Kneppo relation holds best for the single phase system of the higher carbon contents due to the more uniform magnetisation process. The pipeline steels that are harder than 7091 should have a reasonable fit, as was found by Willcock (1985). Any deviations from this largely single phase process which changes the variation of permeability with applied field either by some types of heat treatment or plastic deformation will cause the curve to deviate from linearity.

Chapter VII

Conclusion.

The increase in pearlite content was found to increase both the mechanical and magnetic hardness of the steel and the effectiveness of pearlite, in particular the cementite lamellae, at pinning the domain walls was observed using Lorentz electron microscopy. Analysis of the Barkhausen traces demonstrated the increase in the magnetic force necessary to release the domain walls from these pinning sites. There was very little free ferrite even in the 50% pearlite samples severely resticting easy domain wall movement. The additional impurities in the pipe steel resulted in a harder material than the corresponding pure Fe-C samples and also exhibited an anisotropy in the coercivity, with a lower coercivity in the rolling direction. This is attributed to the elongation of the grains during the rolling process.

All the steels reacted in a similar manner to the tensile plastic deformation; the hysteresis loop shearing over as for elastic compressive stress, but also increasing the coercivity. Previous work (Jiles 1988a and b) has shown that after compressive plastic deformation the differential permeability and remanence actually increase, although the coercivity still increases. It seems that there are two mechanisms that affect the magnetic properties of the steel as it is plastically deformed. The residual stress causes the hysteresis loop to shear over for compressive residual stress resulting from tensile deformation, and to become steeper for tensile residual stress resulting from compressive plastic deformation. The coercivity of the steel is mainly affected by the pinning and subsequent bowing of the domain walls by the dislocation tangles as observed under the electron microscope, causing the coercivity to increase for both compressive and tensile deformation. In steels where the interaction of the internal stress and the domain walls is strong enough for a change in coercivity to be observed even for elastic stress, an anisotropy of coercivity will develop parallel and perpendicular to the strain direction as observed in the pipe steel. By monitoring the magnetic properties of a sample it should be

231

possible to determine whether plastic or elastic deformation has occured, whether the strain is elastic or compressive, and in which direction it is applied.

For the low carbon content steels, where prior to deformation there are large areas of free ferrite and hence easy domain wall movement, the magnetostrictive effect is greatest, rotating the magnetisation away from the easy direction. This effect produces a pronounced drop in the differential permeability at remanence and hence the characteristic bulge in the hysteresis loop. The slower increase of remanence and coercivity with maximum applied field for a deformed sample also illustrates the larger pinning forces that have to be overcome before irreversible domain wall motion can occur. The Barkhausen noise traces also showed the reduction in easy domain wall movement in the ferrite and the reduction in the low frequency intercept of the power spectrum indicated the lower probability of more than one Barkhausen jump occuring at the same time.

Inter-relationships were found between coercivity and both initial permeability and the field at which the maximum relative permeability occurs. Correlations were also found between coercivity and both Vickers Hardness and Yield Stress. These relationships held even for the deformed samples although the softer low carbon and heat treated steels had the largest deviations. The Kneppo formula was found to have a reasonable fit to all the steels, but this improved with the more uniform higher carbon content steels and deteriorated with increasing plastic deformation.

The contribution to the coercivity due to the dislocation tangles remained constant over the range 4.2K to 300K. Previous work (Schwerer et al 1978) has demonstrated a peak in the coercivity at the Curie temperature of cementite, increasing with carbon content as the pearlite becomes more important in the magnetisation process. Conducting similar experiments on the low carbon steel for a range of deformations may indicate any change in the role of the pearlite as the ferrite becomes harder to magnetise.

Although disloction density has provided a convenient parameter to relate to the increase in coercivity, the electron microscope observations show that it is in fact the dislocation tangle density that pins the domain walls. A prediction of this tangle density with plastic strain would be necessary to correctly predict the change in the dependent magnetic properties. In order to extend the model due

232

to Jiles and Atherton (1986 and Sablik et al 1988) of ferromagnetic hysteresis to include the effects of plastic strain it will be necessary not only to add a term to the pinning parameter "k" based on the density of dislocation tangles, but also to include the effects of residual stress. The additional anisotropic change in the coercivity due to the residual stress must also be taken into account.

The heat treatments used here served mainly to normalise the steel and anneal it, resulting in a softer material in which the change in magnetic properties due to the plastic deformation was more marked. Jiles (1988b) has shown that the strained martenstitic steels actually become softer as they are deformed as some of the internal strains are relieved. It is therefore imperative that any nondestructive testing techniques must be matched to the particular steel in use, and control tests be made. Provided that such care is taken, mesasurements of coercivity parallel and perpendicular to the direction of strain could be useful in the detection of deformation and on the approach of fatigue. The changes in relative permeability have implications for nondestructive testing techniques that rely on attaining a known value of flux density such as magnetic flux leakage; as compressive or tensile strain will increase or decrease the flux obtained depending on whether the strain is elastic or plastic and in what direction it is applied.

Appendix A : 2401 Pipe Steel Data

%C	%Mn	%Si	%S	%P	%Al	%Ni	%Cu	%Co	%Cr	%Mo
0.15	0.7	0.07	0.02	0.018	0.005	0.034	0.04	0.011	0.010	0.010

Table A1: Chemical Composition of 2401 Pipe Steel.

V. Hardness	U.T.S.	Y.S. (MN/m^2)	Mean ferrite diameter	Mean pearlite diameter
150	462	371	$21.88\mu m$	$7.81\mu m$

Table A2) : Mechanical Properties of 2401 Pipe Steel as Determined
by S.N.M. Willcock (1985).

Bs @ $25kAm^{-1}(T)$	μ_i	μ_{max}	Hm (kAm^{-1})	Hc (kAm^{-1})	Br (T)
2.031	300	1241	0.46	0.321	0.98

Table A3) : Magnetic Properties of 2401 Pipe Steel as Determined by
S.N.M. Willcock (1985).

%Strain +/-0.5	μ_{max} +/-60	Hm(kAm^{-1}) +/-0.1	Hc $\|^l$ (kAm^{-1}) +/-0.02	Hc $\perp^r$ (kAm^{-1}) +/-0.02	Br (T) +/-0.05	μ'_{max} +/-50
0	1186	0.33	0.31	0.40	0.79	307
2.4	820	0.27	0.38	0.39	0.59	154
6.1	613	0.92	0.44	0.41	0.54	127
7.6	557	0.97	0.44	0.40	0.54	115
7.8	613	1.07	0.53	0.38	0.53	113
11.5	565	0.83	0.47	0.42	0.54	109
11.9	501	1.16	0.48	0.43	0.50	107
20.3	-	-	0.50	0.43	0.53	-
20.4	462	1.02	0.60	0.44	0.54	100
FACTORS	⇓2.6	⇑4.2	⇑1.8	-	⇓1.5	⇓3.1

Table A3 : Magnetic Properties of 2401 Pipe Steel as a Function of Plastic Deformation.

Temperature (K)	Hc (kAm^{-1}) 0%Strain	Hc (kAm^{-1}) 7.8%Strain	Hc (kAm^{-1}) 20.4%Strain
4.2	-	0.59	0.64
20	-	0.57	0.64
40	-	0.58	0.62
60	-	0.58	0.62
80	0.4	0.56	0.62
125	0.38	-	-
130	-	0.53	0.61
175	0.36	-	-
180	-	0.52	0.58
230	0.35	0.50	0.56
290	0.33	-	-
300	-	-	0.53
330	-	0.47	-

Table A4 : Coercivity as a Function of Temperature

Appendix B: "Pure" Steel Data

%Strain	HV10	μ_i	μr_{max}	Hm (kAm^{-1})	Hc (kAm^{-1})	Br (T)	μ'_{max}
+/-0.5	+/-15	+/-20	+/-20	+/-0.05	+/-0.02	+/-0.05	+/-25
0	91	618	1892	0.27	0.16	0.94	5916
0.80	92	165	963	0.89	0.30	0.36	1761
1.90	104	116	741	1.13	0.38	0.31	1546
4.20	117	90	513	1.63	0.46	0.27	1144
8.40	127	77	442	1.86	0.51	0.26	1269

Table B1: Magnetic Properties of 7091: 0.17 wt% Carbon Content Heat Treatment "A" (Aircooled)

%Strain	HV10	μ_i	μr_{max}	Hm (kAm^{-1})	Hc (kAm^{-1})	Br (T)	μ'_{max}
+/-0.5	+/-15	+/-20	+/-20	+/-0.05	+/-0.02	+/-0.05	+/-25
0	81	816	2492	0.20	0.12	0.89	7352
1.14	88	146	899	0.83	0.24	0.27	1690
2.30	95	122	695	1.05	0.31	0.23	1148
4.90	104	97	588	1.39	0.38	0.26	1269
8.70	113	95	500	1.61	0.41	0.28	1065

Table B2: Magnetic Properties of 7091: 0.17 wt% Carbon Content Heat Treatment "D" (Furnace Cooled)

%Strain +/-0.5	HV10 +/-15	μ_i +/-20	μr_{max} +/-20	Hm (kAm^{-1}) +/-0.05	Hc (kAm^{-1}) +/-0.02	Br (T) +/-0.05	μ'_{max} +/-25
0	88	792	2155	0.20	0.13	0.73	5082
1.20	96	156	979	0.86	0.27	0.33	1919
4.24	108	112	979	1.36	0.38	0.27	1057
6.90	118	92	516	1.56	0.42	0.26	1327
10.8	130	90	450	1.67	0.44	0.28	-

Table B3: Magnetic Properties of 7091: 0.17 wt% Carbon Content Heat Treatment "B" (Held at 600°C 1 hour, Aircooled)

%Strain +/-0.5	HV10 +/-15	μ_i +/-20	μr_{max} +/-20	Hm (kAm^{-1}) +/-0.05	Hc (kAm^{-1}) +/-0.02	Br (T) +/-0.05	μ'_{max} +/-25
0	82	753	2410	0.21	0.13	0.94	7368
0.60	89	213	1118	0.74	0.23	0.34	2121
1.90	98	139	851	0.97	0.31	0.28	1416
4.34	113	99	582	1.43	0.39	0.26	1146
8340	117	77	473	1.66	0.44	0.27	1066

Table B4: Magnetic Properties of 7091: 0.17 wt% Carbon Content Heat Treatment "C" (Held at 600°C 2 hours, Aircooled)

%Strain +/-0.5	HV10 +/-15	μ_i +/-20	μr_{max} +/-20	Hm (kAm^{-1}) +/-0.05	Hc (kAm^{-1}) +/-0.02	Br (T) +/-0.05	μ'_{max} +/-25
0	107	288	1266	0.52	0.35	1.15	3625
0.75	105	171	782	0.87	0.39	0.69	2015
1.13	112	99.5	606	1.41	0.49	0.40	1228
2.25	112	78	484	1.56	0.51	0.35	983
2.63	118	78	478	1.81	0.6	0.37	1466
4.13	123	75	454	2.01	0.59	0.34	1175
7.33	132	71	383	2.31	0.69	0.34	1037
9.76	132	70	398	2.16	0.68	0.34	910

Table B5: Magnetic Properties of 7091: 0.17 wt% Carbon Content

%Strain +/-0.5	HV10 +/-15	μ_i +/-20	μr_{max} +/-20	Hm (kAm^{-1}) +/-0.05	Hc (kAm^{-1}) +/-0.02	Br (T) +/-0.05	μ'_{max} +/-25
0	121	86	535	1.01	0.58	0.85	1913
0.37	167	76	490	1.09	0.64	0.81	1774
1.12	165	65	378	1.47	0.73	0.66	1174
1.34	158	59	317	1.91	0.81	0.59	1160
1.70	178	56	300	2.29	0.82	0.58	1111
2.65	174	54	243	2.18	0.83	0.54	940
3.83	173	48	287	2.38	1.00	0.54	777
6.0	181	52	242	2.58	0.96	0.48	699

Table B6: Magnetic Properties of 7092: 0.44 wt% Carbon Content

239

%Strain +/-0.5	HV10 +/-15	μ_i +/-10	μr_{max} +/-20	Hm (kAm^{-1}) +/-0.05	Hc (kAm^{-1}) +/-0.02	Br (T) +/-0.05	μ'_{max} +/-25
0	151	63	351	1.40	0.78	0.72	1262
0.37	216	59	321	1.55	0.85	0.70	1028
0.57	217	57	298	1.77	0.91	0.67	970
1.50	205	49	248	2.09	1.04	0.61	784
2.30	216	44	217	2.22	1.14	0.57	782
3.80	225	42	199	2.53	1.24	0.56	793
6.80	228	43	199	2.50	1.27	0.57	708
7.10	228	44	224	2.07	1.17	0.55	702

Table B7: Magnetic Properties of 7093: 0.67 wt% Carbon Content

%Strain +/-0.5	HV10 +/-15	μ_i +/-10	μr_{max} +/-20	Hm (kAm^{-1}) +/-0.05	Hc (kAm^{-1}) +/-0.02	Br (T) +/-0.05	μ'_{max} +/-25
0	187	56	295	1.67	0.96	0.73	1011
0.75	217	49	252	2.03	1.11	0.64	844
1.1	242	44	210	2.55	1.17	0.61	853
1.5	251	41	213	2.38	1.23	0.61	874
2.3	261	42	208	2.38	1.32	0.59	674
3.8	257	39	188	2.72	1.29	0.57	768
5.5	263	39	180	2.62	1.36	0.57	848
10.2	267	39	174	2.92	1.39	0.58	636

Table B8: Magnetic Properties of 7094: 0.87 wt% Carbon Content

```
{******************************************************************************}
{*                                                                            *}
{* PROGRAM BH_HYS (ANALYSIS OF INITIAL MAGNETISATION AND HYSTERESIS CURVES)*}
{* S.Thompson July 1990                                                       *}
{*                                                                            *}
{******************************************************************************}


PROGRAM BH_HYS;

USES crt,graph,BH_Glob,BH_Utils,BH_graph,Num_Rec,BHDATA,HYSDATA;

PROCEDURE HYS_DATA;
BEGIN
  BH:=FALSE;
  HYS:=TRUE;
  PERM:=FALSE;
  dp_perm:=FALSE;
  KNEPP:=FALSE;
  AUTOSCALE:=FALSE;
  dr:='A:\';
  prog_head:='            HYSTERESIS CURVE ANALYSIS';
  HYS_menu;
END;


{-------------------------------------------------------------------------}


PROCEDURE BH_DATA;
BEGIN
  BH:=TRUE;
  HYS:=FALSE;
  PERM:=FALSE;
  KNEPP:=FALSE;
  AUTOSCALE:=FALSE;
  dr:='A:\';
  prog_head:='            INITIAL MAGNETISATION CURVE ANALYSIS';
  BH_menu;
END;


{-------------------------------------------------------------------------}


PROCEDURE MENU;
BEGIN
  prog_head:='        INITIAL MAGNETISATION AND HYSTERESIS CURVE ANALYSIS';
  action:='MAIN MENU';
  heading(prog_head,action,sample,pdef);
  writeln;
  writeln('1. Analyse an INITIAL magnetisation curve');
  writeln('2. Analyse a HYSTERESIS curve');
  writeln('3. EXIT');
  writeln;
  writeln('Please type the number for the option you require');
  readln(m_menu);
  CASE m_menu of
  1 : BH_data;
  2 : HYS_data;
  3 : EXIT;
  END;
  MENU;
END;
```

```
BEGIN
  MULT:=FALSE;
  sample:='_____';
  pdef:=0;
  graphset:=false;
  MENU;
END.
```

```
{*****************************************************************************}
{*                                                                          *}
{*   UNIT BHDATA   (PROCEDURES FOR INITIAL MAGNETISATION CURVE ANALYSIS)    *}
{*   S.Thompson July 1990                                                   *}
{*                                                                          *}
{*****************************************************************************}

UNIT BHDATA;

INTERFACE

USES crt,graph,BH_Glob,BH_Utils,BH_Graph,Num_Rec;

PROCEDURE perm_calc;
PROCEDURE kneppo;
PROCEDURE BH_menu;

IMPLEMENTATION

PROCEDURE perm_calc;
BEGIN
  clrscr;
  action:='Permeability Calculation';
  heading(prog_head,action,sample,pdef);
  perm_Data[1]:=(B_Data[1]/H_Data[1]*0.00125637);
  for i:=2 to npts do
  BEGIN
    perm_Data[i]:=(B_Data[i]/H_Data[i]*0.00125637);
    if perm_Data[i]>perm_Data[i-1] then
    BEGIN
      maxperm:=perm_Data[i];
      B_maxperm:=B_Data[i];
      H_maxperm:=H_Data[i];
    END;
  END;
  iniperm:=perm_Data[1];
  writeln('Maximum permeability : ',maxperm:5:1);
  writeln('Maximum permeability occured at an applied field of : ',H_maxperm:3:2,' kA
  writeln;
  writeln('Initial permeability : ',iniperm:4:1);
  writeln;
  calc_PERM:=TRUE;
  writeln('Do you want to save the permeability data ?');
  yes_no;
  if YES then
  BEGIN
    writeln(' The permeabilities will be put in a file with the extension : .pem');
    assign(f,dr+filnam+'.pem');
    rewrite(f);
    cret:=chr(13);
    space:=chr(32);
    write(f,sample,npts,pdef,cret);
    for i:=1 to npts do
    write(f,H_Data[i],perm_Data[i],cret);
    close(f);
  END;
  pause;
END;

{---------------------------------------------------------------------------}
```

243

```
PROCEDURE kneppo;
BEGIN
  clrscr;
  action:='Kneppo Calculation';
  heading(prog_head,action,sample,pdef);
  for i:=1 to npts do
  BEGIN
    xknepp[i]:=1/H_Data[i];
    yknepp[i]:=ln(B_Data[i]);
  END;
  KNEPP:=TRUE;
  writeln('Do you want to plot the data?');
  yes_no;
  if yes then P_KNEPP;
  writeln;
  writeln('Do you want to do a least squares fit to the data?');
  yes_no;
  if YES then
  BEGIN
    writeln('Over what region of 1/H ?');
    writeln('Please enter the minimim 1/H value.');
    readln(knepp_min);
    writeln('PLease enter the maximum 1/H value.');
    readln(knepp_max);
    j:=1;
    for i:=1 to npts do
    BEGIN
      if ((xknepp[i]<=knepp_max) and (xknepp[i]>=knepp_min)) then
      BEGIN
        x_knepp[j]:=xknepp[i];
        y_knepp[j]:=yknepp[i];
        j:=j+1;
      END;
    END;
    nfit:=j-1;
  mwt:=0;
  fit(x_knepp,y_knepp,nfit,sig,mwt,a,b,siga,sigb,chi2,q);
  for i:=1 to npts do
  knepp_fit[i]:=b*xknepp[i]+a;
  FIT_KNEPP:=TRUE;
  writeln('gradient : ',b:5:2,'+/-',sigb:5:2);
  writeln('constant : ',a:5:2,'+/-',siga:5:2);
  writeln('Do you want to plot the data?');
  yes_no;
  if yes then P_KNEPP;
END;
FIT_KNEPP:=FALSE;
KNEPP:=FALSE;
END;
{-----------------------------------------------------------------------}

PROCEDURE BH_menu;
BEGIN
  writeln;
  action:='Initial Magnetisation Curve Menu';
  heading(prog_head,action,sample,pdef);
  writeln('1. Load a data file.');
  writeln('2. Data Modification.');
  writeln('3. Permeability Calculation.');
```

```
writeln('4. Plot initial curve.');
writeln('5. Plot initial curve showing the permeabilities.');
writeln('6. Plot permeability vs. applied field.');
writeln('7. Plot multiple initial curves.');
writeln('8. Plot multiple permeability vs. applied field curves.');
writeln('   (CALCULATE AND SAVE PERMEABILITY DATA FIRST)');
writeln('9. KNEPPO Calculation');
writeln('10. Return to Main Menu.');
writeln;
writeln('Please Enter the code of the option that you require');
readln(m_menu);
CASE m_menu of
   1 : fileload;
   2 : data_mod;
   3 : perm_calc;
   4 : BH_HYS;
   5 : BH_PERM;
   6 : H_PERM;
   7 : mult_BH;
   8 : mult_H_PERM;
   9 : kneppo;
   10 : Exit;
END;
if i<>9 then BH_menu;
END;

{----------------------------------------------------------------------}
END.
```

```
{*******************************************************************}
{*                                                                 *}
{* UNIT HYSDATA   (PROCEDURES FOR HYSTERESIS CURVE ANALYSIS)       *}
{* S.Thompson July 1990                                            *}
{*                                                                 *}
{*******************************************************************}

UNIT HYSDATA;

INTERFACE

USES crt,graph,BH_Glob,BH_Utils,BH_graph,Num_Rec;

PROCEDURE HYS_loss_calc;
PROCEDURE Hc_calc;
PROCEDURE Br_calc;
PROCEDURE dif_perm_calc;
PROCEDURE HYS_menu;

IMPLEMENTATION

PROCEDURE HYS_loss_calc;
BEGIN
  ClrScr;
  action:='Hysteresis Loss Calculation';
  heading(prog_head,action,sample,pdef);
  hys_loss1:=0;
  for i:=2 to npts do
  hys_loss1:=hys_loss1+0.5*(B_Data[i-1]+B_Data[i])*abs(H_Data[i]-H_Data[i-1]);
  hys_loss2:=0;
  for i:=2 to npts do
  hys_loss2:=hys_loss2+0.5*(-B_Data[i-1]+(-B_Data[i]))*abs(H_Data[i]-H_Data[i-1]);
  hys_lossT:=hys_loss1-hys_loss2;
  writeln('Hysteresis Loss on the first curve : ',hys_loss1:4:2,' TkA/m');
  writeln('Hysteresis Loss on the second curve : ',hys_loss2:4:2,' TkA/m');
  writeln;
  writeln('Total Hysteresis Loss : ',hys_lossT:4:2,' TkA/m');
  pause;
END;

{-----------------------------------------------------------------------}

PROCEDURE Hc_calc;
BEGIN
  clrscr;
  action:='Coercivity Calculation';
  heading(prog_head,action,sample,pdef);
  BHc:=0.75;
  writeln('The coercivity will be calculated between B-values : +/-',BHc:3:2,' T');
  writeln('Do you want to accept this?');
  yes_no;
  if NO then
  BEGIN
    writeln('Please enter the maximum B-value to be included');
    readln(BHc);
  END;
  writeln('Field (kA/m)        Flux Density (T)');
  j:=0;
  for i:=1 to npts do
  BEGIN
```

246

```pascal
            if (abs(B_Data[i])<=BHc) then
            BEGIN
               j:=j+1;
               xHcDat[j]:=H_Data[i];
               yHcDat[j]:=B_Data[i];
               writeln(xHcDat[j],'          ',yHcDat[j]);
            END;
      END;
      writeln;
      writeln(j,'....it is recommended that no more than 6 points be used.');
      polint(yHcDat,xHcDat,j,0.0,Hc,dHc);
      writeln;
      writeln('Coercivity : ',Hc:4:2,' kA/m');
      writeln('Error on Hc : +/-',dHc:5:3);
      writeln;
      writeln('Do you want to accept this value?');
      yes_no;
      if NO then Hc_calc;
      calc_Hc:=TRUE;
END;


{-------------------------------------------------------------------------}


PROCEDURE Br_calc;
BEGIN
   clrscr;
   action:='Remanence Calculation';
   heading(prog_head,action,sample,pdef);
   HBr:=0.75;
   writeln('The remenance will be calculated between H-values : +/-',HBr:3:2,' kA/m');
   writeln('Do you want to accept this?');
   yes_no;
   if NO then
   BEGIN
      writeln('Please enter the maximum H-value to be included');
      readln(HBr);
   END;
   writeln('Field (kA/m)          Flux Density (T)');
   j:=0;
   for i:=1 to npts do
   BEGIN
      if (abs(H_Data[i])<=HBr) then
      BEGIN
         j:=j+1;
         xBrDat[j]:=H_Data[i];
         yBrDat[j]:=B_Data[i];
         writeln(xBrDat[j],'          ',yBrDat[j]);
      END;
   END;
   writeln;
   writeln(j,'....it is recommended that no more than 6 points be used.');
   polint(xBrDat,yBrDat,j,0.0,Br,dBr);
   writeln;
   writeln('Remanence : ',Br:4:2,' T');
   writeln('Error on Br : +/-',dBr:5:3);
   writeln;
   writeln('Do you want to accept this value?');
   yes_no;
   if NO then Br_calc;
   calc_Br:=TRUE;
```

```
END;

{------------------------------------------------------------------------------}

PROCEDURE dif_perm_calc;
BEGIN
  clrscr;
  action:='Differential Permeability Calculation';
  heading(prog_head,action,sample,pdef);
  dp_Data[1]:=795.77*abs((B_Data[1]-B_Data[2])/(H_Data[1]-H_Data[2]));
  dp_HData[1]:=(H_Data[1]+H_Data[2])/2;
  maxdp:=dp_Data[1];
  for i:=2 to (npts-1) do
  BEGIN
    dp_Data[i]:=797.77*abs((B_Data[i]-B_Data[i+1])/(H_Data[i]-H_Data[i+1]));
    dp_HData[i]:=(H_Data[i]+H_Data[i+1])/2;
    if (dp_Data[i]>=maxdp) then
    BEGIN
      maxdp:=dp_data[i];
      low_h:=H_Data[i];
      high_H:=H_Data[i+1];
    END;
  END;
  writeln('maximum differential permeability : ',maxdp:5:1);
  writeln('Field region : ',low_h:4:1,' kA/m,and ',high_h:4:1,' kA/m');
  writeln('Please input the coercivity .');
  readln(Hc);
  i:=1;
  repeat
    high_H:=H_Data[i];
    i:=i+1;
    until high_H>Hc;
  i:=i-1;
  low_h:=H_Data[i-1];
  dp_Hc:=795.77*abs((B_Data[i]-B_Data[i-1])/(high_H-low_h));
  writeln('differential permeability at Hc : ',dp_Hc:5:1);
  writeln('Field region : ',low_h:4:1,' kA/m,and ',high_h:4:1,' kA/m');
  writeln('Do you want to save the differential permeability data?');
  yes_no;
  if YES then
  BEGIN
    writeln('The file extension will be : .dpm');
    assign(f,dr+filnam+'.dpm');
    rewrite(f);
    cret:=chr(13);
    space:=chr(32);
    write(f,sample,npts,pdef,cret);
    for i:=1 to (npts-1) do
    write(f,H_Data[i],dp_Data[i],cret);
    close(f);
  END;
  pause;
END;

{------------------------------------------------------------------------------}

PROCEDURE HYS_menu;
BEGIN
  ClrScr;
  action:='Hysteresis Curve Menu';
```

248

```
    heading(prog_head,action,sample,pdef);
    writeln('1. Load a file.');
    writeln('2. Data Modification.');
    writeln('3. Coercivity Calculation.');
    writeln('4. Remanence Calculation.');
    writeln('5. Hysteresis Loss Calculation.');
    writeln('6. Calculate differential permeability.');
    writeln('7. Plot Hysteresis Curve.');
    writeln('8. Plot Hysteresis curve including Hc and Br.');
    writeln('9. Plot Differential permeability vs. Applied Field.');
    writeln('10. Return to Main Menu.');
    writeln;
    writeln('Pease enter the code for the option you require.');
    readln(m_menu);
    CASE m_menu of
        1 : fileload;
        2 : data_mod;
        3 : Hc_calc;
        4 : Br_calc;
        5 : hys_loss_calc;
        6 : dif_perm_calc;
        7 : BH_HYS;
        8 : HYS_Hc_Br;
        9 : H_DPERM;
        10 : Exit;
    END;
    if i<>10 then HYS_menu;
END;

{-------------------------------------------------------------------------}
END.
```

```
{***************************************************************************}
{*                                                                         *}
{* UNIT BH_Graph   (PROCEDURES USED FOR SCREEN GRAPHICS)                   *}
{*                                                                         *}
{* S.Thompson July 1990                                                    *}
{*                                                                         *}
{***************************************************************************}

UNIT BH_Graph;

INTERFACE

USES crt,graph,BH_Glob,BH_Utils;

PROCEDURE graph_mode;
PROCEDURE set_graph_var;
PROCEDURE set_plot_var;
PROCEDURE plot_calc;
PROCEDURE disp_plot_var;
PROCEDURE plot_var;
PROCEDURE ch_plot_var;
PROCEDURE HYS_ch_plot_var;
PROCEDURE DPERM_ch_plot_var;
PROCEDURE border;
PROCEDURE grid;
PROCEDURE axes_label;
FUNCTION  xconv(x:REAL):LONGINT;
FUNCTION  yconv(y:REAL):LONGINT;
PROCEDURE multload;
PROCEDURE multdata(ifile:integer);
PROCEDURE plot_mult(ifile:integer);
PROCEDURE mult_BH;
PROCEDURE mult_H_PERM;
PROCEDURE BH_HYS;
PROCEDURE BH_PERM;
PROCEDURE H_PERM;
PROCEDURE H_DPERM;
PROCEDURE P_KNEPP;
PROCEDURE HYS_Hc_Br;
PROCEDURE inscale;
PROCEDURE plot_BH_HYS;
PROCEDURE plot_BH_perm;
PROCEDURE plot_HYS_Hc_Br;
PROCEDURE plot_H_perm;
PROCEDURE plot_H_dperm;
PROCEDURE plot_knepp;

IMPLEMENTATION

PROCEDURE graph_mode;
var
  GraphDriver,ErrorCode : INTEGER;
BEGIN
  if graphset then SetGraphMode(GraphMode)
  else BEGIN
        GraphDriver:=Detect;
        InitGraph(GraphDriver,GraphMode,'');
        ErrorCode:=GraphResult;
        if ErrorCode<>grOk then
        BEGIN
```

250

```
                RestoreCrtMode;
                writeln('Graphics Error : ',GraphErrorMsg(ErrorCode));
                writeln('Program aborted');
                Halt(1);
              END;
            colour:=(GetPaletteSize=16);
            graphset:=TRUE;
            END;
    END;


{-------------------------------------------------------------------------}
PROCEDURE set_graph_var;
BEGIN
   color:=GetMaxColor;
   sc_xmax:=GetMaxX;
   sc_ymax:=GetMaxY;
   x_max:=(sc_xmax-(sc_xmax / 10));
   x_min:=(sc_xmax / 10);
   y_max:=sc_ymax-(sc_ymax / 10);
   y_min:=y_max / 10;
   x_diff:=x_max-x_min;
   y_diff:=y_max-y_min;
   if BH then x_gap:=7;
   if HYS then x_gap:=8;
   y_gap:=4;
   x_step:=(abs(x_diff)/x_gap);
   y_step:=(abs(y_diff)/y_gap);
   real_x_scale[1]:=x_min;
   for i:=2 to (x_gap+1) do
   real_x_scale[i]:=real_x_scale[i-1] + x_step;
   real_y_scale[1]:=y_min;
   for i:=2 to (y_gap+1) do
   real_y_scale[i]:=real_y_scale[i-1] + y_step;
   for i:=1 to (x_gap+1) do
   x_scale[i]:=Round(real_x_scale[i]);
   for i:=1 to (y_gap+1) do
   y_scale[i]:=Round(real_y_scale[i]);
   i_sc_xmax:=Round(sc_xmax);
   i_sc_ymax:=Round(sc_ymax);
   END;


{-------------------------------------------------------------------------}

PROCEDURE set_plot_var;
BEGIN
   if BH then
   BEGIN
      field_max:=42;
      field_min:=0;
      flux_max:=2.0;
      flux_min:=0;
      x_label:='Field H(kA/m)';
      y_label:='Flux density B(T)';
      gph_head:='Initial Magnetisation curve for : '+sample+' Plastic Def. : '+rtostr(p
      if MULT then gph_head:='Initial Magnetisation curves for : '+msample;
   END;

   if HYS then
   BEGIN
      field_max:=32;
```
251

```
      field_min:=-32;
      flux_max:=2.2;
      flux_min:=-2.2;
      x_label:='Field H(kA/m)';
      y_label:='Flux density B(T)';
      gph_head:='Hysteresis curve for : '+sample+' Plastic Def. : '+rtostr(pdef)+'%';
   END;


   if PERM then
   BEGIN
      field_max:=42;
      field_min:=0;
      flux_max:=1000;
      perm_max:=flux_max;
      flux_min:=0;
      perm_min:=flux_min;
      x_label:='Field H(kA/m)';
      y_label:='Permeability ';
      gph_head:='Permeability vs Field for : '+sample+' Plastic Def. : '+rtostr(pdef)+'
      if MULT then gph_head:='Permeability vs Field for samples :'+msample;
   END;


   if dp_perm then
   BEGIN
      field_max:=6;
      field_min:=-6;
      flux_max:=4600;
      perm_max:=flux_max;
      flux_min:=-10.0;
      perm_min:=flux_min;
      x_label:='Field H(kA/m)';
      y_label:='Diff. Permeability ';
      gph_head:='Diff Perm vs Field for : '+sample+' Plastic Def. : '+rtostr(pdef)+'%';
      if MULT then gph_head:='Permeability vs Field for samples :'+msample;
   END;


   if KNEPP then
   BEGIN
      field_max:=15;
      field_min:=0.0;
      flux_max:=1.0;
      flux_min:=-5.0;
      x_label:='1/H  1/(kA/m)';
      y_label:='lnB (T) ';
      gph_head:='ln(B) vs 1/H : KNEPPO for : '+sample+' Plastic Def. : '+rtostr(pdef)+'
      if MULT then gph_head:='Permeability vs Field for samples :'+msample;
   END;


   plot_calc;
END;


{-----------------------------------------------------------------------------}


PROCEDURE plot_calc;
BEGIN
    field_diff:=abs(field_max-field_min);
    flux_diff:=abs(flux_max-flux_min);
    perm_diff:=perm_max-perm_min;
    field_step:=field_diff/x_gap;
    flux_step:=flux_diff/y_gap;
```
252

```
        perm_step:=perm_diff/y_gap;
END;


{------------------------------------------------------------------------}


PROCEDURE disp_plot_var;
BEGIN
   clrscr;
   if AUTOSCALE then writeln('AUTOSCALE is in operation....');
   writeln('The plotting variables are currently set to the following:');
   writeln;
   writeln('1. Maximum field : ',field_max:3:1,' kA/m');
   writeln('2. Minimum field : ',field_min:2:1,' kA/m');
   if (NOT PERM) then
   BEGIN
   writeln('3. Maximum flux : ',flux_max:3:2,' T');
   writeln('4. Minimum flux : ',flux_min:2:1,' T')
   END;
   if PERM then
   BEGIN
     writeln('3. Maximum permeability : ',perm_max:4:1);
     writeln('4. Minimum permeability : ',perm_min:4:1)
   END;
END;


{------------------------------------------------------------------------}


PROCEDURE plot_var;
BEGIN
   action:='Plotting variables';
   heading(prog_head,action,sample,pdef);
   disp_plot_var;
   writeln;
   writeln('Do you want to accept these variables?');
   yes_no;
   if (NO and BH) then ch_plot_var;
   if (NO and dp_perm) then DPERM_ch_plot_var;
   if ((NO and HYS) and (not dp_perm)) then HYS_ch_plot_var;
   plot_calc;
END;


{------------------------------------------------------------------------}


PROCEDURE ch_plot_var;
   BEGIN
     disp_plot_var;
     if (NOT MULT) then writeln('5. AUTOSCALE');
     writeln('6. Default values');
     writeln;
     writeln('Please chose an option? (1-6)');
     writeln('If you have finished making alterations type : 0.');
     readln(i);
     if i=1 then
     BEGIN
       writeln('Please enter the new maximum field.');
       readln(field_max);
     END;
     if i=2 then
     BEGIN
       writeln('Please enter the new minimum field.');
```

```
       readln(field_min);
     END;
     if ((i=3) and (NOT PERM)) then
     BEGIN
       writeln('Please enter the new maximum flux.');
       readln(flux_max);
     END;
     if ((i=4) and (NOT PERM)) then
     BEGIN
       writeln('Please enter the new minimum flux.');
       readln(flux_min);
     END;
     if ((i=3) and PERM) then
     BEGIN
       writeln('Please enter the new maximum permeability.');
       readln(flux_max);
       perm_max:=flux_max;
     END;
     if ((i=4) and PERM) then
     BEGIN
       writeln('Please enter the new minimum permeability.');
       readln(flux_min);
       perm_min:=flux_min;
     END;
     if i=5 then
     BEGIN
       AUTOSCALE:=TRUE;
       field_max:=H_Data[1];
       field_min:=H_Data[1];
       flux_max:=B_Data[1];
       flux_min:=B_Data[1];
       if PERM then
       BEGIN
         perm_max:=perm_Data[1];
         perm_min:=perm_Data[1];
       END;
       for k:=2 to npts do
       BEGIN
         if H_Data[k]>H_Data[k-1] then field_max:=1+H_Data[k];
         if H_Data[k]<H_Data[k-1] then field_min:=H_Data[k]-1;
         if B_Data[k]>B_Data[k-1] then flux_max:=B_Data[k]+0.1;
         if B_Data[k]<B_Data[k-1] then flux_min:=B_Data[k]-0.1;
         if PERM then
         BEGIN
           if perm_Data[k]>perm_Data[k-1] then perm_max:=perm_Data[k]+5;
           flux_max:=perm_max;
           if perm_Data[k]<perm_Data[k-1] then perm_min:=perm_Data[k]-5;
           flux_min:=perm_min;
         END;
       END;
     END;
     if i=6 then
     BEGIN
     set_plot_var;
     END;
     if i<>5 then AUTOSCALE:=FALSE;
     if i=0 then exit
     else ch_plot_var;
   END;
```

254

```
{----------------------------------------------------------------------}

PROCEDURE HYS_ch_plot_var;
  BEGIN
    clrscr;
    if AUTOSCALE then writeln('AUTOSCALE is in operation....');
    writeln('The plotting variables are currently set to the following:');
    writeln('1. Absolute Maximum field : ',field_max:3:1,'kA/m');
    writeln('2. Absolute Maximum flux : ',flux_max:3:2,'T');
    writeln('3. AUTOSCALE');
    writeln('4. Default values');
    writeln;
    writeln('Please chose an option? (1-4)');
    writeln('THE VALUES WILL BE MADE SYMMETRIC');
    writeln('If you have finished making alterations type : 0.');
    readln(i);
    if i=1 then
    BEGIN
      writeln('Please enter the new maximum field.');
      readln(field_max);
    END;
    field_min:=-field_max;
    if i=2 then
    BEGIN
      writeln('Please enter the new maximum flux.');
      readln(flux_max);
    END;
    flux_min:=-flux_max;
    if i=3 then
    BEGIN
      AUTOSCALE:=TRUE;
      field_max:=abs(H_Data[1]);
      flux_max:=abs(B_Data[1]);
      for k:=2 to npts do
      BEGIN
        if abs(H_Data[k])>abs(H_Data[k-1]) then field_max:=1+abs(H_Data[k]);
        if abs(B_Data[k])>abs(B_Data[k-1]) then flux_max:=abs(B_Data[k])+0.1;
      END;
      field_min:=-field_max;
      flux_min:=-flux_max;
    END;
    if i=4 then
    BEGIN
    set_plot_var;
    END;
    if i<>3 then AUTOSCALE:=FALSE;
    if i=0 then exit
    else HYS_ch_plot_var;
END;



{----------------------------------------------------------------------}


PROCEDURE DPERM_ch_plot_var;
  BEGIN
    clrscr;
    if AUTOSCALE then writeln('AUTOSCALE is in operation....');
    writeln('The plotting variables are currently set to the following:');
    writeln('1. Absolute Maximum field : ',field_max:3:1,'kA/m');
    writeln('2. Absolute Maximum diff perm. : ',flux_max:3:2,'T');
```

255

```
      writeln('3. AUTOSCALE');
      writeln('4. Default values');
      writeln;
      writeln('Please chose an option? (1-4)');
      writeln('THE FIELD VALUES WILL BE MADE SYMMETRIC');
      writeln('If you have finished making alterations type : 0.');
      readln(i);
      if i=1 then
      BEGIN
        writeln('Please enter the new maximum field.');
        readln(field_max);
      END;
      field_min:=-field_max;
      if i=2 then
      BEGIN
        writeln('Please enter the new maximum diff perm.');
        readln(flux_max);
        writeln('Please enter the new minimum diff perm.');
        readln(flux_min);
      END;

      if i=3 then
      BEGIN
        AUTOSCALE:=TRUE;
        field_max:=abs(dp_HData[1]);
        flux_max:=abs(dp_Data[1]);
        for k:=2 to npts do
        BEGIN
          if abs(dp_HData[k])>abs(dp_HData[k-1]) then field_max:=1+abs(dp_HData[k]);
          if abs(dp_Data[k])>flux_max then flux_max:=abs(dp_Data[k])+0.1;
          if abs(dp_Data[k])<flux_min then flux_min:=abs(dp_Data[k])-0.1;
        END;
        field_min:=-field_max;

      END;
      if i=4 then
      BEGIN
      set_plot_var;
      END;
      if i<>3 then AUTOSCALE:=FALSE;
      if i=0 then exit
      else DPERM_ch_plot_var;
END;
{-------------------------------------------------------------------------------}


PROCEDURE plot_menu;
BEGIN
  heading(prog_head,action,sample,pdef);
  writeln('1. Display and alter plotting variables');
  writeln('2. Plot curve');
  writeln('3. Return to the main menu.');
  readln(p_menu);
  if p_menu=1 then plot_var;
  if p_menu=2 then
  BEGIN
    if BH then
    BEGIN
      CASE m_menu of
      4 : plot_BH_HYS;
```

256

```
          5 : plot_BH_PERM;
          6 : plot_H_PERM;
          7 : plot_mult(ifile);
          8 : plot_mult(ifile);
          9 : plot_knepp;
          END;
      END;
      if HYS then
      BEGIN
        CASE m_menu of
           7 : plot_BH_HYS;
           8 : plot_HYS_Hc_Br;
           9 : plot_H_dperm
        END;
      END;
   END;
   if p_menu=3 then exit;
   plot_menu;
END;


{------------------------------------------------------------------------}


PROCEDURE border;
BEGIN
  MoveTo(0,0);
  LineTo(i_sc_xmax,0);
  LineTo(i_sc_xmax,i_sc_ymax);
  LineTo(0,i_sc_ymax);
  LineTo(0,0);
END;


{------------------------------------------------------------------------}


PROCEDURE grid;
BEGIN
  border;
  for i:=1 to (x_gap+1) do
  Line(x_scale[i],y_scale[1],x_scale[i],y_scale[y_gap+1]);
  for i:=1 to (y_gap+1) do
  Line(x_scale[1],y_scale[i],x_scale[x_gap+1],y_scale[i]);
END;


{------------------------------------------------------------------------}


PROCEDURE axes_label;
BEGIN
  SetTextJustify(centertext,centertext);
  for i:=1 to x_gap +1 do
  OutTextXY(x_scale[i],(y_scale[y_gap+1]+Round(y_min/3)),rtostr(field_min+(i-1)*field
  for i:=y_gap+1 downto 1 do
  OutTextXY((x_scale[1]-Round(x_min/3)),y_scale[i],rtostr(flux_min+(y_gap+1-i)*flux_s

  OutTextXY(Round(sc_xmax/2),(y_scale[y_gap+1]+Round(y_min*2/3)),x_label);
  SetTextStyle(defaultfont,vertDir,1);
  OutTextXY((x_scale[1]-round(x_min*3/4)),Round(sc_ymax/2),y_label);

  SetTextStyle(defaultfont,HorizDir,1);
  OutTextXY(Round(sc_xmax/2),round(y_min/2),gph_head);
  SetTextJustify(LeftText,TopText);
END;
```

257

```
{--------------------------------------------------------------------------------------}

FUNCTION xconv(x:REAL):LONGINT;
BEGIN
   if (BH or PERM) then
   xconv:=Round((x_diff/field_diff)*x+x_min);
   if HYS then
   xconv:=Round((x_diff/field_diff)*(x+field_diff/2)+x_min);
END;


{--------------------------------------------------------------------------------------}

FUNCTION yconv(y:REAL):LONGINT;
BEGIN
 { if BH  then}
  yconv:=Round(sc_ymax-(y_diff/flux_diff)*(y-flux_min)-y_min);
 {   if PERM then
  yconv:=Round(sc_ymax-(y_diff/perm_diff)*y-y_min);
   if (HYS and (not dp_perm)) then
  yconv:=Round(sc_ymax-(y_diff/flux_diff)*(y+flux_diff/2)-y_min);
   if dp_perm then
  yconv:=Round(sc_ymax-(y_diff/perm_diff)*y-y_min);    }

END;


{--------------------------------------------------------------------------------------}

PROCEDURE BH_HYS;
BEGIN
   graph_mode;
   set_graph_var;
   set_plot_var;
   RestoreCRTMode;
   action:='Magnetisation Curve Plot';
   plot_menu;
END;


{--------------------------------------------------------------------------------------}

PROCEDURE BH_PERM;
BEGIN
   if (NOT calc_PERM) then
   BEGIN
     writeln('You have not calculated the permeability yet');
     pause;
     exit;
   END;
   graph_mode;
   set_graph_var;
   set_plot_var;
   RestoreCRTMode;
   action:='Initial Magnetisation Curve Plot with permeabilities';
   plot_menu;
END;


{--------------------------------------------------------------------------------------}

PROCEDURE H_PERM;
BEGIN
```

258

```pascal
    if (NOT calc_PERM) then
    BEGIN
      writeln('You have not calculated the permeability yet');
      pause;
      exit;
    END;
    PERM:=TRUE;
    graph_mode;
    set_graph_var;
    set_plot_var;
    RestoreCRTMode;
    action:='Permeability vs. Applied Field Plot';
    plot_menu;
    PERM:=FALSE;
END;

{----------------------------------------------------------------------}

PROCEDURE H_DPERM;
BEGIN
  dp_perm:=true;
  graph_mode;
  set_graph_var;
  set_plot_var;
  RestoreCRTMode;
  action:='Diff Per vs. Applied Field plot';
  plot_menu;
  dp_perm:=FALSE;
END;

{----------------------------------------------------------------------}

PROCEDURE P_KNEPP;
BEGIN
  KNEPP:=TRUE;
  graph_mode;
  set_graph_var;
  set_plot_var;
  RestoreCRTMode;
  action:='KNEPPO plot';
  plot_menu;
  KNEPP:=FALSE;
END;

{----------------------------------------------------------------------}

PROCEDURE HYS_Hc_Br;
BEGIN
  if (NOT calc_Hc) then
  BEGIN
    writeln('You have not calculated  Hc yet');
    pause;
    exit;
  END;
  if (NOT calc_Br) then
  BEGIN
    writeln('You have not calculated  Br yet');
    pause;
    exit;
  END;
```

259

```
   graph_mode;
   set_graph_var;
   set_plot_var;
   RestoreCRTMode;
   action:='Hysteresis Curve Plot with Hc and Br.';
   plot_menu;
END;


{--------------------------------------------------------------------------}

PROCEDURE multload;
BEGIN
   writeln('How many files do you want to plot ? (maximum 10)');
   readln(nofiles);
   for ifile:=1 to nofiles do
   BEGIN
     if (NOT PERM) then
     BEGIN
       fileload;
       multdata(ifile);
     END;
     if PERM then
     BEGIN
       permload;
       multdata(ifile);
     END;
   END;
END;


{--------------------------------------------------------------------------}

PROCEDURE multdata;
BEGIN
   if ifile=1 then
   BEGIN
     for j:=1 to npts do
     BEGIN
       Hdata1[j]:=H_Data[j];
       if (NOT PERM) then Bdata1[j]:=B_Data[j];
       if (PERM) then Pdata1[j]:=Pdata[j];
     END;
   END;

   if ifile=2 then
   BEGIN
     for j:=1 to npts do
     BEGIN
       Hdata2[j]:=H_Data[j];
       if (NOT PERM) then Bdata2[j]:=B_Data[j];
       if (PERM) then Pdata2[j]:=Pdata[j];
     END;
   END;

   if ifile=3 then
   BEGIN
     for j:=1 to npts do
     BEGIN
       Hdata3[j]:=H_Data[j];
       if (NOT PERM) then Bdata3[j]:=B_Data[j];
```
260

```
      if (PERM) then Pdata3[j]:=Pdata[j];
    END;
END;


  if ifile=4 then
BEGIN
   for j:=1 to npts do
   BEGIN
     Hdata4[j]:=H_Data[j];
     if (NOT PERM) then Bdata4[j]:=B_Data[j];
     if (PERM) then Pdata4[j]:=Pdata[j];
   END;
END;


  if ifile=5 then
BEGIN
   for j:=1 to npts do
   BEGIN
     Hdata5[j]:=H_Data[j];
     if (NOT PERM) then Bdata5[j]:=B_Data[j];
     if (PERM) then Pdata5[j]:=Pdata[j];
   END;
END;


  if ifile=6 then
BEGIN
   for j:=1 to npts do
   BEGIN
     Hdata6[j]:=H_Data[j];
     if (NOT PERM) then Bdata6[j]:=B_Data[j];
     if (PERM) then Pdata6[j]:=Pdata[j];
   END;
END;


  if ifile=7 then
BEGIN
   for j:=1 to npts do
   BEGIN
     Hdata7[j]:=H_Data[j];
     if (NOT PERM) then Bdata7[j]:=B_Data[j];
     if (PERM) then Pdata7[j]:=Pdata[j];
   END;
END;


  if ifile=8 then
BEGIN
   for j:=1 to npts do
   BEGIN
     Hdata8[j]:=H_Data[j];
     if (NOT PERM) then Bdata8[j]:=B_Data[j];
     if (PERM) then Pdata8[j]:=Pdata[j];
   END;
END;


  if ifile=9 then
BEGIN
   for j:=1 to npts do
   BEGIN
     Hdata9[j]:=H_Data[j];
     if (NOT PERM) then Bdata9[j]:=B_Data[j];
```

```
          if (PERM) then Pdata9[j]:=Pdata[j];
        END;
     END;

      if ifile=10 then
    BEGIN
      for j:=1 to npts do
      BEGIN
         Hdata10[j]:=H_Data[j];
         if (NOT PERM) then Bdata10[j]:=B_Data[j];
         if (PERM) then Pdata10[j]:=Pdata[j];
      END;
    END;

  END;

{--------------------------------------------------------------------}


PROCEDURE mult_BH;
BEGIN
  MULT:=TRUE;
  PERM:=FALSE;
  writeln('Please enter the sample for the title');
  readln(msample);
  multload;
  graph_mode;
  set_graph_var;
  set_plot_var;
  plot_calc;
  RestoreCRTMode;
  action:='Plotting Multiple BH Curves';
  plot_menu;
  MULT:=FALSE;
END;

{--------------------------------------------------------------------}

PROCEDURE mult_H_PERM;
BEGIN
  MULT:=TRUE;
  PERM:=TRUE;
  writeln('Please enter the sample for the heading');
  readln(msample);
  multload;
  graph_mode;
  set_graph_var;
  set_plot_var;
  plot_calc;
  RestoreCRTMode;
  action:='Plotting Multiple H vs. Permeability Curves';
  plot_menu;
  MULT:=FALSE;
  PERM:=FALSE;
END;

{--------------------------------------------------------------------}

PROCEDURE inscale;
BEGIN
```

262

```
  if NOT PERM then
    if (((H_Data[i]<field_max) and (H_Data[i]>field_min)) and ((B_Data[i]<flux_max) a
    then SCALE:=TRUE else SCALE:=FALSE;
  if PERM then
    if (((H_Data[i]<field_max) and(H_Data[i]>field_min)) and ((perm_Data[i]<perm_max)
    then SCALE:=TRUE else SCALE:=FALSE;
END;


{---------------------------------------------------------------------}

PROCEDURE  plot_BH_HYS;
BEGIN
  graph_mode;
  ClearDevice;
  grid;
  axes_label;
  SetColor(4);
  for i:=1 to npts do
  BEGIN
    inscale;
    if SCALE then
    PutPixel(xconv(H_Data[i]),yconv(B_Data[i]),color);
  END;
  if HYS then
  BEGIN
    for i:=1 to npts do
    BEGIN
      inscale;
      if SCALE then
      PutPixel(xconv(-H_Data[i]),yconv(-B_Data[i]),color)
    END;
  END;
  gpause;
  RestoreCRTMode;
END;




{---------------------------------------------------------------------}

PROCEDURE  plot_BH_PERM;
BEGIN
  graph_mode;
  ClearDevice;
  grid;
  axes_label;
  for i:=1 to npts do
  BEGIN
    inscale;
    if SCALE then
    PutPixel(xconv(H_Data[i]),yconv(B_Data[i]),color);
  END;
  Line(xconv(field_min),yconv(flux_min),xconv(1000*flux_max/maxperm),yconv(flux_max))
  Line(xconv(field_min),yconv(flux_min),xconv(1000*flux_max/iniperm),yconv(flux_max))
  Line(xconv(H_maxperm),y_scale[y_gap+1],xconv(H_maxperm),yconv(B_maxperm));
  OutTextXY(xconv(1000*(2*flux_max/(3*maxperm))+field_step/4),yconv(2*flux_max/3),'ma
  OutTextXY(xconv(1000*(1*flux_max/(3*iniperm))+field_step/4),yconv(1*flux_max/3),'in
  OutTextXY(xconv(H_maxperm+field_step/4),yconv(flux_min+flux_step/4),'H at max perm:
  gpause;
  RestoreCRTMode;
END;
```

263

```
{-------------------------------------------------------------------------}

PROCEDURE  plot_HYS_Hc_Br;
BEGIN
  graph_mode;
  ClearDevice;
  grid;
  axes_label;
  for i:=1 to npts do
  BEGIN
    inscale;
    if SCALE then
    PutPixel(xconv(H_Data[i]),yconv(B_Data[i]),color);
    PutPixel(xconv(-H_Data[i]),yconv(-B_Data[i]),color)
  END;
  Line(xconv(Hc),yconv(0-flux_diff/20),xconv(Hc),yconv(0+flux_diff/20));
  Line(xconv(0-field_diff/20),yconv(Br),xconv(0+field_diff/20),yconv(Br));
  OutTextXY(xconv(Hc+field_step/4),yconv(0+flux_step/4),'Hc:'+rtostr(Hc)+'kA/m');
  OutTextXY(xconv(0+field_step/4),yconv(Br+flux_step/4),'Br:'+rtostr(Br)+'T');
  gpause;
  RestoreCRTMode;
END;


{-------------------------------------------------------------------------}

PROCEDURE  plot_H_PERM;
BEGIN
  graph_mode;
  ClearDevice;
  grid;
  axes_label;
  for i:=1 to npts do
  BEGIN
    inscale;
    if SCALE then
  PutPixel(xconv(H_Data[i]),yconv(perm_Data[i]),color);
  END;
  gpause;
  RestoreCRTMode;
END;


{-------------------------------------------------------------------------}

PROCEDURE plot_H_dperm;
BEGIN
  graph_mode;
  ClearDevice;
  grid;
  axes_label;
  MoveTo(xconv(dp_HData[1]),yconv(dp_Data[i]));
  for i:=2 to (npts-1) do
  BEGIN
    inscale;
    if SCALE then
    LineTo(xconv(dp_HData[i]),yconv(dp_Data[i]));
  END;
  Line(xconv(Hc),yconv(flux_min),xconv(Hc),yconv(flux_max));
  OutTextXY(xconv(field_min+field_step/10),yconv(flux_max-flux_step/3),'diff perm. ma
  OutTextXY(xconv(field_min+field_step/10),yconv(flux_max-2*flux_step/3),'diff perm.
```

```
    OutTextXY(xconv(field_min+field_step/10),yconv(flux_max-4*flux_step/3),'Hc : '+rtos
    gpause;
    RestoreCRTMode;
END;


{----------------------------------------------------------------------}

PROCEDURE plot_knepp;
BEGIN
  graph_mode;
  ClearDevice;
  grid;
  axes_label;
  for i:=1 to (npts-1) do
  BEGIN
{   inscale;
    if SCALE then}
    PutPixel(xconv(xknepp[i]),yconv(yknepp[i]),color);
    Line(xconv(xknepp[i]),yconv(yknepp[i]),xconv(xknepp[i+1]),yconv(yknepp[i+1]));
  END;
  PutPixel(xconv(xknepp[npts]),yconv(yknepp[npts]),color);
  if FIT_KNEPP then
  BEGIN
    for i:=1 to (npts-1) do
    Line(xconv(xknepp[i]),yconv(knepp_fit[i]),xconv(xknepp[i+1]),yconv(knepp_fit[i+1]
    OutTextXY(xconv(field_max-3*field_step),yconv(flux_max-flux_step/3),'gradient : '
    OutTextXY(xconv(field_max-3*field_step),yconv(flux_max-2*flux_step/3),'constant :
  END;
  gpause;
  RestoreCRTMode;
END;


{----------------------------------------------------------------------}

PROCEDURE plot_mult;
BEGIN
  graph_mode;
  ClearDevice;
  grid;
  axes_label;
  SetColor(4);
  for ifile:=1 to nofiles do
  BEGIN
    if ifile=1 then
    BEGIN
      for i:=1 to npts do
        BEGIN
          inscale;
          if SCALE then
          if (NOT PERM) then PutPixel(xconv(Hdatal[i]),yconv(Bdatal[i]),color);
          if PERM then PutPixel(xconv(HData1[i]),yconv(Pdatal[i]),color);
        END;
    END;

    if ifile=2 then
    BEGIN
      for i:=1 to npts do
        BEGIN
          inscale;
          if SCALE then
```

265

```
           if (NOT PERM) then PutPixel(xconv(Hdata2[i]),yconv(Bdata2[i]),color);
           if PERM then PutPixel(xconv(HData2[i]),yconv(Pdata2[i]),color);
         END;
     END;


     if ifile=3 then
     BEGIN
       for i:=1 to npts do
         BEGIN
           inscale;
           if SCALE then
           if (NOT PERM) then PutPixel(xconv(Hdata3[i]),yconv(Bdata3[i]),color);
           if PERM then PutPixel(xconv(HData3[i]),yconv(Pdata3[i]),color);
         END;
     END;


     if ifile=4 then
     BEGIN
       for i:=1 to npts do
         BEGIN
           inscale;
           if SCALE then
           if (NOT PERM) then PutPixel(xconv(Hdata4[i]),yconv(Bdata4[i]),color);
           if PERM then PutPixel(xconv(HData4[i]),yconv(Pdata4[i]),color);
         END;
     END;


     if ifile=5 then
     BEGIN
       for i:=1 to npts do
         BEGIN
           inscale;
           if SCALE then
           if (NOT PERM) then PutPixel(xconv(Hdata5[i]),yconv(Bdata5[i]),color);
           if PERM then PutPixel(xconv(HData5[i]),yconv(Pdata5[i]),color);
         END;
     END;


     if ifile=6 then
     BEGIN
       for i:=1 to npts do
         BEGIN
           inscale;
           if SCALE then
           if (NOT PERM) then PutPixel(xconv(Hdata6[i]),yconv(Bdata6[i]),color);
           if PERM then PutPixel(xconv(HData6[i]),yconv(Pdata6[i]),color);
         END;
     END;


     if ifile=7 then
     BEGIN
       for i:=1 to npts do
         BEGIN
           inscale;
           if SCALE then
           if (NOT PERM) then PutPixel(xconv(Hdata7[i]),yconv(Bdata7[i]),color);
           if PERM then PutPixel(xconv(HData7[i]),yconv(Pdata7[i]),color);
         END;
     END;
```

```
      if ifile=8 then
      BEGIN
        for i:=1 to npts do
          BEGIN
            inscale;
            if SCALE then
            if (NOT PERM) then PutPixel(xconv(Hdata8[i]),yconv(Bdata8[i]),color);
            if PERM then PutPixel(xconv(HData8[i]),yconv(Pdata8[i]),color);
          END;
      END;

      if ifile=9 then
      BEGIN
        for i:=1 to npts do
          BEGIN
            inscale;
            if SCALE then
            if (NOT PERM) then PutPixel(xconv(Hdata9[i]),yconv(Bdata9[i]),color);
            if PERM then PutPixel(xconv(HData9[i]),yconv(Pdata9[i]),color);
          END;
      END;


      if ifile=10 then
      BEGIN
        for i:=1 to npts do
          BEGIN
            inscale;
            if SCALE then
            if (NOT PERM) then PutPixel(xconv(Hdata10[i]),yconv(Bdata10[i]),color);
            if PERM then PutPixel(xconv(HData10[i]),yconv(Pdata10[i]),color);
          END;
      END;
    END;
  gpause;
  RestoreCRTMode;
END;
{ ---------------------------------------------------------------------- }
END.
```

```
{*****************************************************************************}
{*                                                                         *}
{* UNIT BH_Utils (UTILITY PROCEDURES USED IN BH ANALYSIS)                  *}
{*                                                                         *}
{* S.Thompson July 1990                                                    *}
{*                                                                         *}
{*****************************************************************************}

UNIT BH_Utils;

INTERFACE

USES Crt,BH_Glob;

FUNCTION rtostr(r:REAL):STRING;
PROCEDURE pause;
PROCEDURE gpause;
PROCEDURE yes_no;
PROCEDURE heading(prog_head,action:string;sample:string;pdef:real);
PROCEDURE fileload;
PROCEDURE permload;
PROCEDURE data_mod;
PROCEDURE int_constant;
PROCEDURE sam_dim;
PROCEDURE H_mod;
PROCEDURE B_mod;
PROCEDURE ch_file;

IMPLEMENTATION

FUNCTION rtostr(r:REAL):STRING;
var
  s:STRING[15];
BEGIN
  Str(r:4:2,s);
  rtostr:=s;
END;

{---------------------------------------------------------------------------}

PROCEDURE pause;
BEGIN
  writeln;
  writeln('Please press any key to continue......');
  BEGIN
    repeat until keypressed;
    ch:=readkey;
  END;
END;

{---------------------------------------------------------------------------}

PROCEDURE gpause;
BEGIN
  BEGIN
    repeat until keypressed;
    ch:=readkey;
  END;
END;
```

268

```
{ ----------------------------------------------------------------------------- }

PROCEDURE yes_no;
BEGIN
  ANS:=FALSE;
  while NOT ANS do
  BEGIN
    writeln('Please answer Y or N');
    readln(ch);
    if ((ch='Y') or (ch='y')) then
    BEGIN
      YES:=TRUE;
      NO:=FALSE;
      ANS:=TRUE
    END;
    if ((ch='N') or (ch='n')) then
    BEGIN
      NO:=TRUE;
      YES:=FALSE;
      ANS:=TRUE
    END;                                    1
  END;
END;


{ ----------------------------------------------------------------------------- }

PROCEDURE heading;
BEGIN
  Window(1,1,80,8);
  TextBackground(4);
  TextColor(7);
  ClrScr;
  writeln;
  writeln(prog_head);
  writeln;
  writeln('Sample : ',sample);
  writeln('Plastic Deformation : ',pdef:3:1,'%');
  writeln;
  writeln(action);
  Window(1,9,80,25);
  TextBackground(7);
  TextColor(1);
  ClrScr;
  writeln;
  END;


{ ----------------------------------------------------------------------------- }

PROCEDURE fileload;
BEGIN
  calc_PERM:=FALSE;
  calc_Hc:=FALSE;
  calc_Br:=FALSE;
  action:='Loading in a datafile';
  heading(prog_head,action,sample,pdef);
  if BH then
  BEGIN
    filnam:='psh2cl';
    ext:='.bh'
  END;
```

269

```pascal
    if HYS then
    BEGIN
      filnam:='psh2c2';
      ext:='.hys'
    END;
    writeln('Default file to be loaded is : ',filnam+ext);
    writeln('Do you want to accept the default?');
    yes_no;
    if NO then
    BEGIN
      writeln('Please enter the file to be loaded (without the extension)');
      readln(filnam)
    END;
    assign(f,dr+filnam+ext);
    reset(f);
    readln(f,sample,npts,pdef);
    for i:=1 to npts do
    read(f,H_Data[i],B_Data[i]);
    writeln(filnam+ext,' has been loaded.');
    writeln;
    writeln('This is the data for sample : ',sample);
    writeln('Plastic deformation : ',pdef:3:1,'%');
    writeln('Number of points : ',npts);
    close(f);
    pause;
END;

{------------------------------------------------------------------------}

PROCEDURE permload;
BEGIN
  action:='Loading in a permeability datafiles';
  heading(prog_head,action,sample,pdef);
    filnam:='psh2c1';
    ext:='.pem';
  writeln('Default file to be loaded is : ',filnam+ext);
  writeln('Do you want to accept the default?');
  yes_no;
  if NO then
  BEGIN
    writeln('Please enter the file to be loaded (without the extension)');
    readln(filnam)
  END;
  assign(f,dr+filnam+ext);
  reset(f);
  readln(f,sample,npts,pdef);
  for i:=1 to npts do
  read(f,H_Data[i],Pdata[i]);
  writeln(filnam+ext,' has been loaded.');
  writeln;
  writeln('This is the data for sample : ',sample);
  writeln('Plastic deformation : ',pdef:3:1,'%');
  writeln('Number of points : ',npts);
  close(f);
  pause;
END;

{------------------------------------------------------------------------}

PROCEDURE ch_file;
```

```
BEGIN
  writeln;
  writeln('What extension would you like on the modified file?');
  readln(ext);
  ext:='.'+ext;
  assign(f,dr+filnam+ext);
  rewrite(f);
  space:=chr(32);
  cret:=chr(13);
  write(f,sample,npts,pdef,cret);
  for i:=1 to npts do
  write(f,H_Data[i],space,B_Data[i],cret);
  close(f);
END;


{-------------------------------------------------------------------------}


PROCEDURE  int_constant;
BEGIN
  action:='Data mod: Integrator Constant';
  heading(prog_head,action,sample,pdef);
  writeln('Please enter the existing integrator constant');
  readln(old_int_const);
  writeln('Please enter the new integrator constant.');
  readln(new_int_const);
  int_factor:=old_int_const/new_int_const;
  for i:=1 to npts do
  B_Data[i]:=B_Data[i]*int_factor;
  pause;
END;


{-------------------------------------------------------------------------}


PROCEDURE sam_dim;
BEGIN
  action:='Data mod: Sample Dimensions';
  heading(prog_head,action,sample,pdef);
  writeln('Please enter the existing bar width (cm)');
  readln(old_bar_width);
  writeln('Please enter the existing bar thickness (cm)');
  readln(old_bar_thick);
  old_X_area:=old_bar_width/old_bar_thick;
  writeln('Please enter the new bar width (cm)');
  readln(new_bar_width);
  writeln('Please enter the new bar thickness (cm)');
  readln(new_bar_thick);
  new_X_area:=new_bar_width/new_bar_thick;
  dim_factor:=old_X_area/new_X_area;
  for i:=1 to npts do
  B_Data[i]:=B_Data[i]*dim_factor;
  pause;
END;


{-------------------------------------------------------------------------}


PROCEDURE H_mod;
BEGIN
  action:='Data mod: Field Data';
  heading(prog_head,action,sample,pdef);
  writeln('Please enter the factor you wish to multiply the field data with');
```

```
      readln(H_factor);
      for i:=1 to npts do
      H_Data[i]:=H_Data[i]*H_factor;
      pause;
END;


{---------------------------------------------------------------------}


PROCEDURE B_mod;
BEGIN
   action:='Data mod: Flux Data';
   heading(prog_head,action,sample,pdef);
   writeln('Please enter the factor you wish to multiply the flux data with');
   readln(B_factor);
   for i:=1 to npts do
   B_Data[i]:=B_Data[i]*B_factor;
   pause;
END;


{---------------------------------------------------------------------}


PROCEDURE data_mod;
BEGIN
   action:='Data modification';
   heading(prog_head,action,sample,pdef);
   writeln('1. Change the integrator constant');
   writeln('2. Change the sample dimensions');
   writeln('3. Multiply the field data by a factor');
   writeln('4. Multiply the flux data by a factor');
   writeln('5. Save the changes');
   writeln('6. Return to the main menu');
   writeln;
   writeln;
   writeln('Please enter the code for the option you require.');
   readln(i);
   case i of
     1 : int_constant;
     2 : sam_dim;
     3 : H_mod;
     4 : B_mod;
     5 : ch_file;
     6 : Exit;
   END;
   data_mod;
END;


{---------------------------------------------------------------------}

END.
```

```
{*******************************************************************************}
{*                                                                           *}
{* UNIT num_rec                                                              *}
{*                                                                           *}
{* from 'Numerical Recipes in Pascal'                                       *}
{*                                                                           *}
{*******************************************************************************}


UNIT num_rec;

interface

USES BH_Glob;


PROCEDURE polint(VAR xa,ya: RealArrayNP;
                          n: integer;
                          x: real;
                  VAR y,dy: real);

PROCEDURE fit(VAR x,y: RealArrayNDATA;
                ndata: integer;
            VAR sig: RealArrayNDATA;
                  mwt: integer;
         VAR a,b,siga: real;
      VAR sigb,chi2,q: real);

implementation

PROCEDURE polint;
VAR
   ns,m,i: integer;
   w,hp,ho,dift,dif,den: real;
   c,d: ^RealArrayNP;
BEGIN
   new(c);
   new(d);
   ns := 1;
   dif := abs(x-xa[1]);
   FOR i := 1 TO n DO BEGIN
      dift := abs(x-xa[i]);
      IF dift < dif THEN BEGIN
         ns := i;
         dif := dift
      END;
      c^[i] := ya[i];
      d^[i] := ya[i]
   END;
   y := ya[ns];
   ns := ns-1;
   FOR m := 1 TO n-1 DO BEGIN
      FOR i := 1 TO n-m DO BEGIN
         ho := xa[i]-x;
         hp := xa[i+m]-x;
         w := c^[i+1]-d^[i];
         den := ho-hp;
         IF den = 0.0 THEN BEGIN
            writeln ('pause in routine POLINT');
            readln
         END;
```
273

```
                        den := w/den;
                        d^[i] := hp*den;
                        c^[i] := ho*den
                END;
                IF 2*ns < n-m THEN
                        dy := c^[ns+1]
                ELSE BEGIN
                        dy := d^[ns];
                        ns := ns-1
                END;
                y := y+dy
        END;
        dispose(d);
        dispose(c)
END;


{-------------------------------------------------------------------------}


PROCEDURE fit;
VAR
        i: integer;
        wt,t,sy,sxoss,sx,st2,ss,sigdat: real;
BEGIN
        sx := 0.0;
        sy := 0.0;
        st2 := 0.0;
        b := 0.0;
        IF mwt <> 0 THEN BEGIN
                ss := 0.0;
                FOR i := 1 TO ndata DO BEGIN
                        wt := 1.0/sqr(sig[i]);
                        ss := ss+wt;
                        sx := sx+x[i]*wt;
                        sy := sy+y[i]*wt
                END
        END
        ELSE BEGIN
                FOR i := 1 TO ndata DO BEGIN
                        sx := sx+x[i];
                        sy := sy+y[i]
                END;
                ss := ndata
        END;
        sxoss := sx/ss;
        IF mwt <> 0 THEN BEGIN
                FOR i := 1 TO ndata DO BEGIN
                        t := (x[i]-sxoss)/sig[i];
                        st2 := st2+t*t;
                        b := b+t*y[i]/sig[i]
                END
        END
        ELSE BEGIN
                FOR i := 1 TO ndata DO BEGIN
                        t := x[i]-sxoss;
                        st2 := st2+t*t;
                        b := b+t*y[i]
                END
        END;
        b := b/st2;
        a := (sy-sx*b)/ss;
```

274

```
    siga := sqrt((1.0+sx*sx/(ss*st2))/ss);
    sigb := sqrt(1.0/st2);
    chi2 := 0.0;
    {IF mwt = 0 THEN BEGIN}
        FOR i := 1 TO ndata DO
            chi2 := chi2+sqr(y[i]-a-b*x[i]);
        q := 1.0;
        sigdat := sqrt(chi2/(ndata-2));
        siga := siga*sigdat;
        sigb := sigb*sigdat
    { END
    ELSE BEGIN
        FOR i := 1 TO ndata DO
            chi2 := chi2+sqr((y[i]-a-b*x[i])/sig[i]);
        q := gammq(0.5*(ndata-2),0.5*chi2)
    END;}
END;

END.
```

```
{****************************************************************************}
{*                                                                          *}
{*   UNIT BH_Glob (VARIABLES FOR BH ANALYSIS PROGRAM)                       *}
{*                                                                          *}
{*   S.Thompson July 1990                                                   *}
{*                                                                          *}
{****************************************************************************}

UNIT BH_Glob;

INTERFACE

CONST
   np=50;
   ndatap=100;

TYPE
   RealArrayNP=Array[1..np] of REAL;
   RealArrayNDATA=Array[1..ndatap] of REAL;

VAR
color:word;
f:text;
ch,cret,space:STRING[1];
ext:STRING[4];
dr,filnam,lfilnam,msample,sample:STRING[10];
x_label,y_label:STRING[20];
action,prog_head,gph_head:STRING[100];

calc_PERM,calc_Hc,calc_Br,dp_perm,MULT,SCALE,AUTOSCALE:BOOLEAN;
colour,graphset,BH,HYS,PERM,KNEPP,FIT_KNEPP,YES,NO,ANS:BOOLEAN;
i,j,k,ifile,nofiles,p_menu,m_menu,GraphMode,npts,nfit,mwt:INTEGER;
x_diff,y_diff:REAL;
sc_xmax,sc_ymax,x_max,y_max,x_min,y_min,x_step,y_step:REAL;
i_sc_xmax,i_sc_ymax,x_gap,y_gap:INTEGER;

real_x_scale,real_y_scale:ARRAY [1..20] OF REAL;
x_scale,y_scale:ARRAY [1..20] OF LONGINT;

pdef,r,x,y:REAL;
old_int_const,new_int_const,int_factor,H_factor,B_factor:REAL;
old_bar_width,old_bar_thick,old_X_area:REAL;
new_bar_width,new_bar_thick,new_X_area,dim_factor:REAL;
maxperm,H_maxperm,B_maxperm,iniperm,maxdp,dp_Hc,low_h,high_h:REAL;
a,b,siga,sigb,chi2,q,knepp_min,knepp_max:REAL;
hys_loss1,hys_loss2,hys_lossT,BHc,Hc,dHc,HBr,Br,dBr:REAL;
field_step,field_max,field_min,field_diff:REAL;
flux_step,flux_max,flux_min,flux_diff:REAL;
perm_step,perm_max,perm_min,perm_diff:REAL;

B_Data,H_Data,Perm_Data,dp_Data,dp_HData,knepp_fit:ARRAY [1..100] OF REAL;
Bdata1,Bdata2,Bdata3,Bdata4,Bdata5:ARRAY [1...100] OF REAL;
Bdata6,Bdata7,Bdata8,Bdata9,Bdata10:ARRAY [1..100] OF REAL;
Hdata1,Hdata2,Hdata3,Hdata4,Hdata5:ARRAY [1...100] OF REAL;
Hdata6,Hdata7,Hdata8,Hdata9,Hdata10:ARRAY [1...100] OF REAL;
Pdata1,Pdata2,Pdata3,Pdata4,Pdata5:ARRAY [1...100] OF REAL;
Pdata6,Pdata7,Pdata8,Pdata9,Pdata10:ARRAY [1...100] OF REAL;

xHcDat,yHcDat,xBrDat,yBrDat:RealArrayNP;
xknepp,yknepp,x_knepp,y_knepp,sig:RealArrayNDATA;
```

IMPLEMENTATION
END.

```
{******************************************************************************
*                                                                            *
*     PROGRAM BARK - Collection of Barkhausen data.                          *
*     21/05/90 S.M.Thompson                                                  *
*                                                                            *
*****************************************************************************}

{This program leads the operator through setting up the apparatus and in
particular adjusting the settings on the waveform analyser (wfa) through
the IEEE interface. Once the operator is satisfied with the trace obtained
on the wfa then the program will record the data in the required format
for the analysis and GHOST plotting programs to be found on NUMAC.        }


program bark;

uses crt,ieee,smtglob,vsmglob,se2250,wsetup;

{crt:
smtglob : global variables for use with bark.pas
se2250  : routines for the waveform analser
ieee    : IEEE routines (D.B.Lambrick)
wsetup  : procedures for setting up the waveform analyser}

begin
  textbackground(4);
  textcolor(14);
  clrscr;
  writeln('***************************************************************************************
  for i:=1 to 9 do
  writeln('*
  writeln('*                        WELCOME TO THE BARKHAUSEN PROGRAM
  writeln('*
  writeln('*                               by S.M.Thompson
  for i:=1 to 9 do
  writeln('*
  writeln('***************************************************************************************
  writeln('Please press any key to continue');
  repeat
    until keypressed;
  ch:= readkey;
  clrscr;
  writeln;
  writeln('              SETTING UP THE WAVEFORM ANALYSER : SE2550');
  writeln('              ----------------------------------------');
  writeln;
  writeln;
  writeln('Initialising the waveform analyser.....');
  wfa_init;
  writeln('Setting the waveform analyser to predetermined settings....');
  preset;
  writeln;
  varset;
  writeln;
  writeln('Please press any key to continue');
  repeat
    until keypressed;
  ch:= readkey;
  writeln('Reading all the settings from the waveform analyser......');
  readset;
```
278

```
clrscr;
disprset;   {Displays the predetermined settings}
writeln('Please press any key to continue.');
repeat
  until keypressed;
ch:=readkey;
clrscr;
setup;    {Displays the settings that can be altered (disvars) and
          uses setup to alter settings and test the signal}
clrscr;
writeln('The apparatus is now set up and ready to collect the data');
writeln;
Writeln('What do you want the datafile to be called?');
readln(filnam);
writeln(filnam);
writeln('Which section of the recording is this?');
readln(sectn);
writeln('What is the maximum current (positive)');
readln(imax);
writeln('Please press any key when you are ready to start data collection.');
repeat
until keypressed;
clrscr;
for i:=1 to 6 do
writeln;
writeln('              DATA COLLECTION');

str_write('!20,CD5');
read_setup(devnum);
str_search('!27');              {Reads in the number of the first sample}
str_search('FS');
repeat
  byt_read;
until data<>'0';
str_marker(',');
val(mkstr,fstsam,cd);

str_search('LS');              {Reads in the number of the last sample}
repeat
  byt_read;
until data<>'0';
str_marker(',');
val(mkstr,lstsam,cd);

nosam:=lstsam-fstsam+1;        {Calculates the number of samples}
str(nosam,nos);


assign(datout,filnam);         {Open the data file}
rewrite(datout);
cret:=chr(13);

                               { Writes details of recording to the file}
file_string(sectn ,filnam);
file_string(nos,filnam);
file_string(sdl,filnam);
file_string(imax,filnam);
file_string(ssp2,filnam);
write(datout,cret);
```

```pascal
    writeln;
    writeln('                DATA TRANSFER');

    atst:='+';                                {Reads in data and writes to the}
    btst:='-';                                {file in rows of 10}
    for i:=1 to nosam div 10 do
    begin
      for j:=1 to 10 do
      begin
        repeat
        byt_read;
        until (data=atst) or (data=btst);
        byt_read;
        str_marker(',');
        file_string(mkstr,filnam);
      end;
      write(datout,cret);
    end;

    for i:=1 to (nosam mod 10) do             {Reads in last line of data if}
    begin                                     {the number of samples is not a }
      repeat byt_read                         {multiple of 10}
      until (data=atst) or (data=btst);
      byt_read;
      str_marker(',');
      file_string(mkstr,filnam);
    end;

    read_end;
    close(datout);

    clrscr;
    for i:=1 to 10 do writeln;
    writeln('                DATA TRANSFER  HAS FINISHED');
    for i:=1 to 10 do writeln;

    sound(220);
    delay(1000);
    nosound;

end.
```

```
{*****************************************************************************
*                                                                          *
*     PROGRAM RECORD - Collection of Barkhausen data.                      *
*     21/05/90 S.M.Thompson                                                *
*                                                                          *
*****************************************************************************}


{This program assumes the operator has already set up the apparatus in
particular adjusting the settings on the waveform analyser (wfa).
Once the operator is satisfied with the trace obtained
on the wfa then the program will record the data in the required format
for the analysis and GHOST plotting programs to be found on NUMAC.          }



program bark;

uses crt,ieee,smtglob,vsmglob,se2250,wsetup;

{crt:
smtglob : global variables for use with bark.pas
se2250   : routines for the waveform analser
ieee     : IEEE routines (D.B.Lambrick)
wsetup   : procedures for setting up the waveform analyser}

begin
  textbackground(4);
  textcolor(14);
  clrscr;
  writeln('*********************************************************************************
  for i:=1 to 9 do
  writeln('*
  writeln('*                        WELCOME TO THE BARKHAUSEN DATA
  writeln('*                        TRANSFER PROGRAM.
  writeln('*                            by S.M.Thompson
  for i:=1 to 9 do
  writeln('*
  writeln('*********************************************************************************
  writeln('Please press any key to continue');
  repeat
    until keypressed;
  ch:= readkey;
  clrscr;
  writeln;
  writeln('          ENSURE THE WAVEFORM ANALYSER IS SET UP');
  writeln('          ----------------------------------------');
  writeln;
  writeln;
  writeln('Please press any key to continue');
  repeat
    until keypressed;
  ch:= readkey;
  writeln;
  writeln('Initialising the waveform analyser.....');
  wfa_init;
  readset;
  clrscr;
  writeln('The apparatus is now set up and ready to collect the data');
  writeln;
  Writeln('What do you want the datafile to be called?');
  readln(filnam);
```

```pascal
writeln(filnam);
writeln('Which section of the recording is this?');
readln(sectn);
writeln('What is the maximum current (positive)');
readln(imax);
writeln('What is the delay in microseconds?');
readln(sdl);
writeln('What is the time period between samples in microseconds?');
readln(ssp2);
writeln('Please press any key when you are ready to start data collection.');
repeat
until keypressed;
clrscr;
for i:=1 to 6 do
writeln;
writeln('                DATA COLLECTION');

str_write('!20,CD5');
read_setup(devnum);
str_search('!27');               {Reads in the number of the first sample}
str_search('FS');
repeat
  byt_read;
until data<>'0';
str_marker(',');
val(mkstr,fstsam,cd);

str_search('LS');                {Reads in the number of the last sample}
repeat
  byt_read;
until data<>'0';
str_marker(',');
val(mkstr,lstsam,cd);

nosam:=lstsam-fstsam+1;          {Calculates the number of samples}
str(nosam,nos);


assign(datout,filnam);           {Open the data file}
rewrite(datout);
cret:=chr(13);

                                 { Writes details of recording to the file}
file_string(sectn ,filnam);
file_string(nos,filnam);
file_string(sdl,filnam);
file_string(imax,filnam);
file_string(ssp2,filnam);
write(datout,cret);

writeln;
writeln('             DATA TRANSFER');

atst:='+';                                 {Reads in data and writes to the}
btst:='-';                                 {file in rows of 10}
for i:=1 to nosam div 10 do
begin
  for j:=1 to 10 do
  begin
    repeat
```

282

```
        byt_read;
        until (data=atst) or (data=btst);
        byt_read;
        str_marker(',');
        file_string(mkstr,filnam);
    end;
    write(datout,cret);
end;

for i:=1 to (nosam mod 10) do           {Reads in last line of data if}
begin                                    {the number of samples is not a }
    repeat byt_read                      {multiple of 10}
    until (data=atst) or (data=btst);
    byt_read;
    str_marker(',');
    file_string(mkstr,filnam);
end;

read_end;
close(datout);

clrscr;
for i:=1 to 10 do writeln;
writeln('                DATA TRANSFER  HAS FINISHED');
for i:=1 to 10 do writeln;

sound(220);
delay(1000);
nosound;

end.
```

```
{*****************************************************************************
 *                                                                          *
 *       UNIT WSETUP - procedures for setting up the waveform analyser      *
 *       22/5/90 S.M.Thompson                                               *
 *                                                                          *
 *****************************************************************************}

unit wsetup;

interface

uses smtglob,ieee,crt,se2250;

procedure preset; {Sets the waveform analyser to predetermined settings.}
procedure varset; {Sets up the values that may be altered}
procedure readset; {Reads the settings from the waveform analyser}
procedure start_read(sttst:string); {Ensures correct string is read in}
procedure discodset; {Displays the codes read in from the waveform Analyser}
procedure disprset; {Display the preset settings}
procedure nextfunc(nf:string); {Conversion of code to next function}
procedure disvars; {Display the variable settings}
procedure fftable(iff:string); {Conversion of code to frequency}
procedure setup; {Organises alteration of the variable settings & testing}
procedure test; {Tests the Barkhausen noie}
procedure display; {displays graphics page}
procedure choice;  {Option to change, retest or transfer data}
procedure channel; {To change the channel number}
procedure iaffreq; {Filter frequency}
procedure iamps; {To change the input amplifier setting}
procedure trigdelay; {Trigger delay}
procedure seg1; {Segment settings}
procedure seg2;
procedure seg3;
procedure seg4;
procedure seg5;
procedure seg6;
procedure seg7;
procedure seg8;
procedure seg9;
procedure seg10;
procedure fsample; {Set first sample}
procedure lsample; {Set last sample}
procedure iochann; {Set no. channels for input/output}


{---------------------------------------------------------------------------}

implementation

procedure preset;
begin

  writeln('Service Requests:-');
  str_write('!19,SR1,SO1,SV1,!17,SS1');
  writeln;

  writeln('Input Amplifiers:-');
  str_write('!21,CH1,FM1,FL1,OF50,PI1,NI0,TM3,PL55,NL45,NF0,!17,SS1');
  writeln;

  writeln('Analog Input:-');
```

284

```pascal
      str_write('!22,IN0,TB0,ET1,NF6,!17,SS1');
      writeln;

      writeln('Digital Input Output:-');
      str_write('!25,MO2,IO0,BN1,NF0,!17,SS1');
      writeln;

      end; {preset}

{------------------------------------------------------------------------}

procedure varset;
begin

   writeln('Input Amplifiers:-');
   str_write('!21,CH1,FF08,AM120,!17,SS1');
   writeln;

   writeln('Analog Input:-');
   str_write('!22,CH1,DL5500000,SE01,SNO00008,SP00000010,');
   str_write('SE02,SN032760,SP00000031,');
   str_write('SE03,SN000000.SP00000000,');
   str_write('SE04,SN000000.SP00000000,');
   str_write('SE05,SN000000.SP00000000,');
   str_write('SE06,SN000000.SP00000000,');
   str_write('SE07,SN000000.SP00000000,');
   str_write('SE08,SN000000.SP00000000,');
   str_write('SE09,SN000000.SP00000000,');
   str_write('SE10,SN000000.SP00000000,!17,SS1');
   writeln;

   writeln('Digital Input/Output:-');
   str_write('!25,CH11,FS000009,LS32768,!17,SS1');
   writeln;

end; {varset}

{------------------------------------------------------------------------}

procedure readset;
begin
   start_read('SR');

{  repeat
      writeln('!17,RS1');
      writeln('Reading the Service Registers...');
      str_write('?19');
      writeln(' sent');
      read_setup(devnum);
      chr_test('S');
      str_test('SR');
      read_end
   until datastring='SR';
   read_setup(devnum);     }
   writeln('about to byt_read');
   byt_read;
   sr:=datastring+data;
   writeln(sr);
   str_marker(',');
   for i:=1 to 2 do
```

```
begin
  byt_read;
  str_marker(',');
  case i of
     1 : so:=mkstr;
     2 : sv:=mkstr;
  end;
end;
writeln(so);
writeln(sv);
delay(100);
read_end;


writeln('Reading the Input Amplifiers....');
str_write('?21');
read_setup(devnum);
for i:=1 to 12 do
begin
  byt_read;
  str_marker(',');
  case i of
     1 : fm:=mkstr;
     2 : ianf:=mkstr;
     3 : ff:=mkstr;
     4 : iach:=mkstr;
     5 : am:=mkstr;
     6 : ofs:=mkstr;
     7 : pi:=mkstr;
     8 : ni:=mkstr;
     9 : tm:=mkstr;
    10 : pl:=mkstr;
    11 : negl:=mkstr;
    12 : fl:=mkstr;
  end;
end;
for i:=1 to 10 do
str_marker(',');
read_end;

writeln('Reading the Analog Input settings....');
str_write('?22');
read_setup(devnum);
for i:=1 to 36 do
begin
  byt_read;
  str_marker(',');
  case i of
     1 : ain:=mkstr;
     2 : tb:=mkstr;
     3 : et:=mkstr;
     4 : bl:=mkstr;
     5 : dl:=mkstr;
     6 : ainf:=mkstr;
     7 : sel:=mkstr;
     8 : snl:=mkstr;
     9 : spl:=mkstr;
    10 : se2:=mkstr;
    11 : sn2:=mkstr;
    12 : sp2:=mkstr;
```

```
           13 : se3:=mkstr;
           14 : sn3:=mkstr;
           15 : sp3:=mkstr;
           16 : se4:=mkstr;
           17 : sn4:=mkstr;
           18 : sp4:=mkstr;
           19 : se5:=mkstr;
           20 : sn5:=mkstr;
           21 : sp5:=mkstr;
           22 : se6:=mkstr;
           23 : sn6:=mkstr;
           24 : sp6:=mkstr;
           25 : se7:=mkstr;
           26 : sn7:=mkstr;
           27 : sp7:=mkstr;
           28 : se8:=mkstr;
           29 : sn8:=mkstr;
           30 : sp8:=mkstr;
           31 : se9:=mkstr;
           32 : sn9:=mkstr;
           33 : sp9:=mkstr;
           34 : se10:=mkstr;
           35 : sn10:=mkstr;
           36 : sp10:=mkstr;
        end;
     end;
     read_end;

     writeln('Reading Digital Input/Output Settings....');
     str_write('?25');
     read_setup(devnum);
     for i:= 1 to 7 do
     begin
        byt_read;
        str_marker(',');
        case i of
           1 : mo:=mkstr;
           2 : io:=mkstr;
           3 : bn:=mkstr;
           4 : ioch:=mkstr;
           5 : fs:=mkstr;
           6 : ls:=mkstr;
           7 : ionf:=mkstr;
        end; {case}
     end;
     writeln('Junk');
     str_marker(',');
     str_marker(',');
     writeln('About to read_end');
     read_end;
     writeln('Read end');
end; {readset}

{ ----------------------------------------------------------------------- }
procedure start_read;
label 100;
var schar:string;
begin
   str_write('!17,RS1');    {Recalling the settings}
   str_write('?19');
```

287

```pascal
  read_setup(devnum);
  schar:=copy (sttst,1,1);
  chr_test(schar[1]);
  writeln('chr_test finished');
  str_test(sttst);
  if datastring='SR' then goto 100
  else
  read_end;
  start_read(SR);
  100:
end;
```

{---}

```pascal
procedure discodset;
begin
  writeln('PREDETERMINED  SETTINGS (CODES)');
  writeln('-----------------------');
  writeln;
  writeln('Service Requests:-');
  writeln('------------------');
  writeln(sr,so,sv);
  writeln;
  writeln('Input Amplifiers:-');
  writeln('------------------');
  writeln(fm,fl,ofs,pi,ni,tm,pl,negl,ianf);
  writeln;
  writeln('Analog Input:-');
  writeln('--------------');
  writeln(ain,tb,et,ainf);
  writeln;
  writeln('Digital Input/Output');
  writeln('--------------------');
  writeln(mo,io,bn,ionf);
  writeln('Please press any key to continue');
  repeat
  until keypressed;
  ch:=readkey;
  writeln('Variable Settings');
  writeln('-----------------');
  writeln(ff,am,dl);
  write(sel,snl,spl);
  write(se2,sn2,sp2);
  write(se3,sn3,sp3);
  write(se4,sn4,sp4);
  write(se5,sn5,sp5);
  write(se6,sn6,sp6);
  write(se7,sn7,sp7);
  write(se8,sn8,sp8);
  write(se9,sn9,sp9);
  writeln(se10,sn10,sp10);
  writeln(fs,ls);
  writeln(iach,ioch);

end;  {discodset}
```

{---}

```pascal
procedure disprset;
begin
```

```
textcolor(3);
writeln('PREDETERMINED SETTINGS');
writeln('----------------------');
writeln('Service Requests (SRQ) :-');
textcolor(14);
if sr='SR0' then ssr:='No'
else ssr:='';
writeln(ssr,' SRQ at the end of the recording');

if so='SO0' then sso:='No'
else sso:='';
writeln(sso,' SRQ at the end of output');

if sv='SV0' then ssv:='No'
else ssv:='';
writeln(ssv,' SRQ at input overload');

textcolor(3);
writeln('Input Amplifiers :-    (Uses Channel 1)');
textcolor(14);
if fm='FM0' then sfm:='automatic'
else sfm:='manual';
writeln('Filter mode : ',sfm);

if fl='FL0' then sfl:='off'
else sfl:='on';
writeln('Anti-alias filters ',sfl);

sofs:=copy(ofs,3,2);
writeln('Offset is ',sofs,' %');

ipi:=copy(pi,3,1);
val(ipi,i,cd);
case i of
  0 : spi:='ground';
  1 : spi:='AC';
  2 : spi:='DC';
end;
writeln('Positive Input is ',spi);

ini:=copy(ni,3,1);
val(ini,i,cd);
case i of
  0 : sni:='ground';
  1 : sni:='AC';
  2 : sni:='DC';
end;
writeln('Negative Input is ',sni);

itm:=copy(tm,3,1);
val(itm,i,cd);
case i of
  0 : stm:='off';
  1 : stm:='negative after positive';
  2 : stm:='positive after negative';
  3 : stm:='positive or negative';
end;
writeln('Slope triggering : ',stm);

iianf:=copy(ianf,3,1);
```

```
if ans='y' then setup;
writeln;
writeln('Amplitude Ranges:-');
writeln('1 : 0.1 - 0.99 V');
writeln('2 : 1 - 9.9 V');
writeln('3 : 10 - 99 V');
writeln;
writeln('Please enter which range of amplitudes you require : ');
readln(v1);
writeln;
writeln('Please enter two digits for the numerical value : ');
readln(v2);
am:='AM'+v1+v2;
str_write('!21,');
str_write(iach);
str_write(',');
str_write(am);
str_write(',!17,SS1');
readset;
setup;
end;

{--------------------------------------------------------------------------}

procedure trigdelay;
begin
clrscr;
writeln('The present trigger delay is ',sdl,' microseconds');
writeln('Type: y if this is O.K. or: n to change the setting');
readln(ans);
if ans='y' then setup;
writeln;
writeln('Please enter the delay in microseconds you require : ');
readln(v1);
dl:='DL'+v1;
str_write('!22,');
str_write(dl);
str_write(',!17,SS1');
readset;
setup;
end;

{--------------------------------------------------------------------------}

procedure seg1;
begin
clrscr;
writeln('Segment 1 : sample number : ',ssn1,', sample period : ',ssp1);
writeln('Type: y if this is O.K. or: n to change the setting');
readln(ans);
if ans='y' then setup;
writeln;
writeln('Please enter the new sample number of segment 1 : ');
readln(v1);
sn1:='SN'+v1;
writeln('and the new sample period (in microseconds) : ');
readln(v2);
sp1:='SP'+v2;
str_write('!22,SE01,');
str_write(sn1);
```

296

```
str_write(',');
str_write(sp1);
str_write(',!17,SS1');
readset;
setup;
end;
```

{---}

```
procedure seg2;
begin
clrscr;
writeln('Segment 2 : sample number : ',ssn2,', sample period : ',ssp2);
writeln('Type: y if this is O.K. or: n to change the setting');
readln(ans);
if ans='y' then setup;
writeln;
writeln('Please enter the new sample number of segment 2 : ');
readln(v1);
sn2:='SN'+v1;
writeln('and the new sample period (in microseconds) : ');
readln(v2);
sp2:='SP'+v2;
str_write('!22,SE02,');
str_write(sn2);
str_write(',');
str_write(sp2);
str_write(',!17,SS1');
readset;
setup;
end;
```

{---}

```
procedure seg3;
begin
clrscr;
writeln('Segment 3 : sample number : ',ssn3,', sample period : ',ssp3);
writeln('Type: y if this is O.K. or: n to change the setting');
readln(ans);
if ans='y' then setup;
writeln;
writeln('Please enter the new sample number of segment 3 : ');
readln(v1);
sn3:='SN'+v1;
writeln('and the new sample period (in microseconds) : ');
readln(v2);
sp3:='SP'+v2;
str_write('!22,SE03,');
str_write(sn3);
str_write(',');
str_write(sp3);
str_write(',!17,SS1');
readset;
setup;
end;
```

{---}

```
procedure seg4;
```

297

```
begin
clrscr;
writeln('Segment 4 : sample number : ',ssn4,', sample period : ',ssp4);
writeln('Type: y if this is O.K. or: n to change the setting');
readln(ans);
if ans='y' then setup;
writeln;
writeln('Please enter the new sample number of segment 4 : ');
readln(v1);
sn4:='SN'+v1;
writeln('and the new sample period (in microseconds) : ');
readln(v2);
sp4:='SP'+v2;
str_write('!22,SE04,');
str_write(sn4);
str_write(',');
str_write(sp4);
str_write(',!17,SS1');
readset;
setup;
end;


{-------------------------------------------------------------------------}


procedure seg5;
begin
clrscr;
writeln('Segment 5 : sample number : ',ssn5,', sample period : ',ssp5);
writeln('Type: y if this is O.K. or: n to change the setting');
readln(ans);
if ans='y' then setup;
writeln;
writeln('Please enter the new sample number of segment 5 : ');
readln(v1);
sn5:='SN'+v1;
writeln('and the new sample period (in microseconds) : ');
readln(v2);
sp5:='SP'+v2;
str_write('!22,SE05,');
str_write(sn5);
str_write(',');
str_write(sp5);
str_write(',!17,SS1');
readset;
setup;
end;


{-------------------------------------------------------------------------}


procedure seg6;
begin
clrscr;
writeln('Segment 6 : sample number : ',ssn6,', sample period : ',ssp6);
writeln('Type: y if this is O.K. or: n to change the setting');
readln(ans);
if ans='y' then setup;
writeln;
writeln('Please enter the new sample number of segment 6 : ');
readln(v1);
sn6:='SN'+v1;
```

```
writeln('and the new sample period (in microseconds) : ');
readln(v2);
sp6:='SP'+v2;
str_write('!22,SE06,');
str_write(sn6);
str_write(',');
str_write(sp6);
str_write(',!17,SS1');
readset;
setup;
end;


{---------------------------------------------------------------------------}


procedure seg7;
begin
clrscr;
writeln('Segment 7 : sample number : ',ssn7,', sample period : ',ssp7);
writeln('Type: y if this is O.K. or: n to change the setting');
readln(ans);
if ans='y' then setup;
writeln;
writeln('Please enter the new sample number of segment 7 : ');
readln(v1);
sn7:='SN'+v1;
writeln('and the new sample period (in microseconds) : ');
readln(v2);
sp7:='SP'+v2;
str_write('!22,SE07,');
str_write(sn7);
str_write(',');
str_write(sp7);
str_write(',!17,SS1');
readset;
setup;
end;


{---------------------------------------------------------------------------}


procedure seg8;
begin
clrscr;
writeln('Segment 8 : sample number : ',ssn8,', sample period : ',ssp8);
writeln('Type: y if this is O.K. or: n to change the setting');
readln(ans);
if ans='y' then setup;
writeln;
writeln('Please enter the new sample number of segment 8 : ');
readln(v1);
sn8:='SN'+v1;
writeln('and the new sample period (in microseconds) : ');
readln(v2);
sp8:='SP'+v2;
str_write('!22,SE08,');
str_write(sn8);
str_write(',');
str_write(sp8);
str_write(',!17,SS1');
readset;
setup;
```

```pascal
end;

{------------------------------------------------------------------------}

procedure seg9;
begin
clrscr;
writeln('Segment 9 : sample number : ',ssn9,', sample period : ',ssp9);
writeln('Type: y if this is O.K. or: n to change the setting');
readln(ans);
if ans='y' then setup;
writeln;
writeln('Please enter the new sample number of segment 9 : ');
readln(v1);
sn9:='SN'+v1;
writeln('and the new sample period (in microseconds) : ');
readln(v2);
sp9:='SP'+v2;
str_write('!22,SE09,');
str_write(sn9);
str_write(',');
str_write(sp9);
str_write(',!17,SS1');
readset;
setup;
end;

{------------------------------------------------------------------------}

procedure seg10;
begin
clrscr;
writeln('Segment 10 : sample number : ',ssn10,', sample period : ',ssp10);
writeln('Type: y if this is O.K. or: n to change the setting');
readln(ans);
if ans='y' then setup;
writeln;
writeln('Please enter the new sample number of segment 10 : ');
readln(v1);
sn10:='SN'+v1;
writeln('and the new sample period (in microseconds) : ');
readln(v2);
sp10:='SP'+v2;
str_write('!22,SE10,');
str_write(sn10);
str_write(',');
str_write(sp10);
str_write(',!17,SS1');
readset;
setup;
end;

{------------------------------------------------------------------------}

procedure fsample;
begin
clrscr;
writeln('The first sample number is ',sfs);
writeln('Type: y if this is O.K. or: n to change the setting');
readln(ans);
```

```
if ans='y' then setup;
writeln;
writeln('Please enter the first sample number you require : ');
readln(vl);
fs:='FS'+vl;
str_write('!25,');
str_write(fs);
str_write(',!17,SS1');
readset;
setup;
end;

{----------------------------------------------------------------------}

procedure lsample;
begin
clrscr;
writeln('The last sample number is ',sls);
writeln('Type: y if this is O.K. or: n to change the setting');
readln(ans);
if ans='y' then setup;
writeln;
writeln('Please enter the last sample number you require : ');
readln(vl);
ls:='LS'+vl;
str_write('!25,');
str_write(ls);
str_write(',!17,SS1');
readset;
setup;
end;

{----------------------------------------------------------------------}

procedure iochann;
begin
clrscr;
writeln('The current setting is to send or receive ',siocha);
writeln('Type: y if this is O.K. or: n to change the setting');
readln(ans);
if ans='y' then setup;
writeln;
writeln('Please enter :0 to use all channel memories or');
writeln('              1 to use just a single channel');
readln(vl);
writeln;
writeln('Please enter the channel number required : ');
readln(v2);
ioch:='CH'+vl+v2;
str_write('!25,');
str_write(ioch);
str_write(',!17,SS1');
readset;
setup;
end;

{----------------------------------------------------------------------}
end.
```

301

```
   nextfunc(iianf);
   sianf:=snf;
   writeln('Next function is ',sianf);

   writeln('Analog Input:-');
   if ain='IN0' then sain:='pretrigger'
   else sain:='block';
   writeln('The set mode is ',sain);

   if tb='TB0' then stb:='internal'
   else stb:='external';
   writeln('The timebase is set to ',stb);

   if et='ET0' then nset:='off'
   else nset:='on';
   writeln('The external trigger is switched ',nset);

   iainf:=copy(ainf,3,1);
   nextfunc(iainf);
   sainf:=snf;
   writeln('The next function is ',sainf);

   textcolor(3);
   writeln('Digital Input/Output:-');
   textcolor(14);
   imo:=copy(mo,3,1);
   val(imo,i,cd);
   case i of
     0 : smo:='parallel';
     1 : smo:='serial';
     2 : smo:='IEEE';
   end;
   writeln('The mode is ',smo);

   if io='IO0' then sio:='output'
   else sio:='input';
   writeln('Communication direction : ',sio);

   ibn:=copy(bn,3,1);
   if ibn='0' then   sbna:='all blocks'
   else sbna:='a single block';
   writeln('Transmitting ',sbna);
   sbnb:=copy(bn,4,4);
   writeln('Block number : ',sbnb);

   iionf:=copy(ionf,3,1);
   nextfunc(iionf);
   sionf:=snf;
   writeln('The next function is ',sionf);

   end;
{--------------------------------------------------------------------------}

procedure nextfunc;
begin
   val(nf,i,cd);
   case i of
     0 : snf:='off';
     1 : snf:='Analog Input';
     2 : snf:='Recycle mode';
```
290

```pascal
    3 : snf:='Analog Output';
    4 : snf:='Timer';
    5 : snf:='Digital Input/Output';
    6 : snf:='Display';
  end;
end;
```

```
{----------------------------------------------------------------------}
```

```pascal
procedure disvars;
begin
  clrscr;
  textcolor(3);
  writeln('VARIABLE SETTINGS OF THE WAVEFORM ANALYSER');
  writeln('-------------------------------------------');
  writeln('Input Amplifiers:-');
  textcolor(14);
  siach:=copy(iach,5,1);
  writeln('Channel : ',siach);

  iff:=copy(ff,3,2);
  fftable(iff);
  writeln(' 1 : Filter Frequency : ',sff,'kHz');

  iam:=copy(am,4,2);
  val(iam,riam,cd);
  irange:=copy(am,3,1);
  val(irange,i,cd);
  case i of
    1 : arange:=0.01;
    2 : arange:=0.1;
    3 : arange:=1;
  end; {case}
  rsam:=riam*arange;
  writeln(' 2 : Peak Voltage : ',rsam,'V');

  textcolor(3);
  writeln('Analog Input:-');
  textcolor(14);
  sdl:=copy(dl,3,8);
  writeln(' 3 : Trigger Delay : ',sdl,' microseconds');

  sse1:=copy(se1,5,2);
  ssn1:=copy(sn1,3,6);
  ssp1:=copy(sp1,3,8);
  writeln(' 4 : Segment: ',sse1,' Sample Number: ',ssn1,' Sample Period: ',ssp1);

  sse2:=copy(se2,5,2);
  ssn2:=copy(sn2,3,6);
  ssp2:=copy(sp2,3,8);
  writeln(' 5 : Segment: ',sse2,' Sample Number: ',ssn2,' Sample Period: ',ssp2);

  sse3:=copy(se3,5,2);
  ssn3:=copy(sn3,3,6);
  ssp3:=copy(sp3,3,8);
  writeln(' 6 : Segment: ',sse3,' Sample Number: ',ssn3,' Sample Period: ',ssp3);

  sse4:=copy(se4,5,2);
  ssn4:=copy(sn4,3,6);
  ssp4:=copy(sp4,3,8);
```

291

```
      writeln(' 7 : Segment: ',sse4,' Sample Number: ',ssn4,' Sample Period: ',ssp4);

    sse5:=copy(se5,5,2);
    ssn5:=copy(sn5,3,6);
    ssp5:=copy(sp5,3,8);
    writeln(' 8 : Segment: ',sse5,' Sample Number: ',ssn5,' Sample Period: ',ssp5);

    sse6:=copy(se6,5,2);
    ssn6:=copy(sn6,3,6);
    ssp6:=copy(sp6,3,8);
    writeln(' 9 : Segment: ',sse6,' Sample Number: ',ssn6,' Sample Period: ',ssp6);

    sse7:=copy(se7,5,2);
    ssn7:=copy(sn7,3,6);
    ssp7:=copy(sp7,3,8);
    writeln('10 : Segment: ',sse7,' Sample Number: ',ssn7,' Sample Period: ',ssp7);

    sse8:=copy(se8,5,2);
    ssn8:=copy(sn8,3,6);
    ssp8:=copy(sp8,3,8);
    writeln('11 : Segment: ',sse8,' Sample Number: ',ssn8,' Sample Period: ',ssp8);

    sse9:=copy(se9,5,2);
    ssn9:=copy(sn9,3,6);
    ssp9:=copy(sp9,3,8);
    writeln('12 : Segment: ',sse9,' Sample Number: ',ssn9,' Sample Period: ',ssp9);

    sse10:=copy(se10,5,2);
    ssn10:=copy(sn10,3,6);
    ssp10:=copy(sp10,3,8);
    writeln('13 : Segment: ',sse10,' Sample Number: ',ssn10,' Sample Period: ',ssp10);

    textcolor(3);
    writeln('Digital Input/Output');
    textcolor(14);
    sfs:=copy(fs,3,6);
    writeln('14 : First Sample: ',sfs);

    sls:=copy(ls,3,6);
    writeln('15 : Last Sample: ',sls);

    iioch:=copy(ioch,3,1);
    if iioch='0' then siocha:='all memory channels'
    else siocha:='a single  memory channel';
    writeln('16 : Set to send or receive ',siocha);
    siochb:=copy(ioch,4,1);
    writeln('Channel number : ',siochb);
end;

{--------------------------------------------------------------------------}

procedure fftable;
begin
  val(iff,i,cd);
  case i of
    01 : sff:='100';
    02 : sff:='66.4';
    03 : sff:='44.3';
    04 : sff:='32.3';
    05 : sff:='26.7';
```

292

```
      06 : sff:='19.9';
      07 : sff:='17.5';
      08 : sff:='14.5';
      09 : sff:='12.0';
      10 : sff:='9.19';
      11 : sff:='6.93';
      12 : sff:='5.54';
      13 : sff:='4.18';
      14 : sff:='3.65';
      15 : sff:='3.04';
      16 : sff:='1.89';
      17 : sff:='1.69';
      18 : sff:='1.45';
      19 : sff:='1.14';
      20 : sff:='0.84';
      21 : sff:='0.760';
      22 : sff:='0.595';
      23 : sff:='0.515';
      24 : sff:='0.322';
      25 : sff:='0.305';
      26 : sff:='0.243';
      27 : sff:='0.185';
      28 : sff:='0.140';
      29 : sff:='0.106';
      30 : sff:='0.079';
      31 : sff:='0.061';
      32 : sff:='0.046';
    else writeln('ERROR IN FILTER FREQUENCY STATEMENT : RUN PROGRAM AGAIN');
    end;
end;
{--------------------------------------------------------------------------}

procedure setup;
begin;
disvars;
   writeln('Type :- 0 : to test, 20 : to abort ,1-16 : to change the  setting');
   readln(i);
   case i of
        0 : test;
        1 : iaffreq;
        2 : iamps;
        3 : trigdelay;
        4 : seg1;
        5 : seg2;
        6 : seg3;
        7 : seg4;
        8 : seg5;
        9 : seg6;
       10 : seg7;
       11 : seg8;
       12 : seg9;
       13 : seg10;
       14 : fsample;
       15 : lsample;
       16 : iochann;
       20 : halt;
     else setup;
     end; {case}

end;
```

293

```
{----------------------------------------------------------------------}

procedure test;
begin
clrscr;
writeln('Recalling settings.........');
str_write('!17,RS1');
writeln;
writeln('Analog recording started........');
str_write('!20,CD1');
writeln;
writeln('Watch for "ARMED..TRIGGERED"');
choice;
end;


{----------------------------------------------------------------------}

procedure display;
begin
clrscr;
str_write('!20,DI5');
writeln('When you have finished looking at the display');
writeln('press any key to return to the menu');
repeat
until keypressed;
ch:=readkey;
str_write('!20,CD6');
choice;
end;



{----------------------------------------------------------------------}
procedure choice;
begin
writeln('Examine the trace and then type:');
writeln('      1 : to retest without changing the settings');
writeln('      2 : to change some of the settings');
writeln('      3 : to abort the program');
writeln('      4 : to display information on the wfa');

writeln('ANY-THING ELSE WILL TRANSFER THE DATA TO THE P.C.');
readln(ans);
val (ans,i,cd);
case i of
  1 : test;
  2 : setup;
  3 : halt;
  4 : display;
else end;
end;

{----------------------------------------------------------------------}

procedure channel;
begin
clrscr;
writeln('The present channel number is ',siach);
writeln('Type: y if this is O.K. or: n to change the setting');
readln(ans);
```

```
if ans='y' then setup;
writeln;
writeln('Please enter the number of the channel you require : ');
readln(v1);
iach:='CH'+v1;
str_write('!21,');
str_write(iach);
str_write(',!17,SS1');
delay(1000);
readset;
setup;
end;


{-----------------------------------------------------------------------}


procedure iaffreq;
begin
clrscr;
writeln('The present filter frequency is ',sff,' kHz');
writeln('Type: y if this is O.K. or: n to change the setting');
readln(ans);
if ans='y' then setup;
writeln('Here are the available filter frequencies:-');
writeln('    CODE    FREQUENCY (kHZ)         CODE    FREQUENCY (kHZ)');
writeln('    ----    ---------------         ----    ---------------');
writeln('    01     100                     17      1.69');
writeln('    02     66.4                    18      1.45');
writeln('    03     44.3                    19      1.14');
writeln('    04     32.3                    20      0.84');
writeln('    05     26.7                    21      0.760');
writeln('    06     19.9                    22      0.595');
writeln('    07     17.5                    23      0.515');
writeln('    08     14.5                    24      0.322');
writeln('    09     12.0                    25      0.305');
writeln('    10     9.19                    26      0.243');
writeln('    11     6.93                    27      0.185');
writeln('    12     5.54                    28      0.140');
writeln('    13     4.18                    29      0.106');
writeln('    14     3.65                    30      0.079');
writeln('    15     3.04                    31      0.061');
writeln('    16     1.89                    32      0.046');
writeln;
writeln('Please enter the code of the frequency you require : ');
readln(v1);
ff:='FF'+v1;
str_write('!21,');
str_write(ff);
str_write(',!17,SS1');
readset;
setup;
end;


{-----------------------------------------------------------------------}


procedure iamps;
begin
clrscr;
writeln('The present peak voltage is set to : ',rsam,' V');
writeln('Type: y if this is O.K. or: n to change the setting');
readln(ans);
```

```
{*****************************************************************************}
{*                                                                          *}
{*     UNIT SE2250 - routines for use with the waveform analyser            *}
{*     11/04/90 S.M.Thompson                                                *}
{*                                                                          *}
{*****************************************************************************}

unit se2250;

interface

uses smtglob,vsmglob,ieee,crt;

procedure wfa_init; {initialises the waveform analyser}
procedure byt_read; {reads character achar must be preceeded by read_setup }
procedure str_write(datastring:string); {writes datastring to wfa}
procedure chr_test(chtst:char);    {searches for the specified character chtst}
procedure str_test(sttst:string);{reads datastring same length as sttst}
procedure str_search(sttst:string);  {searches for the string sttst}
procedure str_marker(marker:char);   {reads string:mkstr until reaches marker}
procedure file_write(filnam:namfil;devnum:integer);
procedure file_string(mkstr:string;filnam:namfil);{writes string to file}


{---------------------------------------------------------------------------}

implementation

procedure wfa_init;
begin
  zero_add;
  cntrllr:=true;
  my_flag:=false;
  my_addr:=1;
  int1stat:=0;
  devla[1].prim:=12;
  devta[1].prim:=12;
  eois:=chr(10);
  iors:='i';
  devnum:=1;
  init;
end;


{---------------------------------------------------------------------------}

procedure byt_read;
var iobyt:integer;
begin
  repeat
    int1stat:=port[Bdadd+1];
    until ((int1stat and 1)<>0);
  iobyt:=Port[Bdadd+0];
  data:=chr(iobyt);
end;


{---------------------------------------------------------------------------}

procedure str_write;
var iobyt,strcnt:integer;
    schar:string[1];
    achar:char;
```

302

```pascal
begin
  write_setup(devnum);
    for strcnt:=1 to length(datastring) do
    begin
      schar:=copy(datastring,strcnt,1);
      achar:=schar[1];
      iobyt:=ord(achar);
      wr_byte(iobyt);
    end;
  dat:=13;
  Port[Bdadd+5]:=$6;
  Port[Bdadd+0]:=dat;
  Port[Bdadd+0]:=ord(eois);
  lastint1:=int1stat;
  if cntrllr then tcsy;
end;

{----------------------------------------------------------------------}

procedure chr_test;
begin
  repeat
    byt_read;
  until data=chtst;
end;

{----------------------------------------------------------------------}

procedure str_test;
var leng:integer;
begin
writeln('testing for string',sttst);
 datastring:='';
 datastring:=data;
    for leng:=1 to length(sttst)-1 do
    begin
      byt_read;
      datastring:=datastring+data;
    end;
writeln('string read in is:',datastring);
delay(2000);
end;

{----------------------------------------------------------------------}

procedure str_search;
var schar:string[1];
begin
  schar:=copy(sttst,1,1);
  repeat
    chr_test(schar[1]);
    str_test(sttst);
  until datastring=sttst;
end;

{----------------------------------------------------------------------}

procedure str_marker;
{var data:char;}
begin
```
303

```pascal
  mkstr:='';
  repeat
    mkstr:=mkstr+data;
    byt_read;
  until data=marker ;
end;
```

{---}

```pascal
procedure file_write;
var datout : file of char;
    i,j,iobyt : integer;
    achar : char;
begin
  assign(datout,filnam);
  rewrite(datout);
  read_setup(devnum);
  {int1stat:=Port[Bdadd+1];
  while ((int1stat and 1)=1) do
  begin}
    for i:=1 to (nosam div 70) do
    begin
      for j:=1 to 70 do
      begin
        iobyt:=Port[Bdadd+0];
        achar:=chr(iobyt);
        write(datout,achar);
       { write(achar);}
        int1stat:=Port[Bdadd+1];
      end;
    write(achar);
    achar:=chr(13);
    write(datout,achar);
    end;
 { end;}
  read_end;
  close(datout);
  end;
```

{---}

```pascal
procedure file_string;
var strcnt:integer;
    schar:string[1];
    achar:char;
begin
  for strcnt:=1 to length(mkstr) do
  begin
    schar:=copy(mkstr,strcnt,1);
    achar:=schar[1];
    write(datout,achar);
  end;
  achar:=chr(32);
  write(datout,achar);
end;
```

{---}

```pascal
end.
```

```
{******************************************************************
*                                                                *
*    SMTGLOB-global variables for use with Barkhausen programs   *
*    12/04/90 S.M.Thompson                                       *
*                                                                *
******************************************************************}

unit smtglob;

interface

const Bdadd:integer=$310;    {Address of the IEEE board}

var i,j,cd,devnum,gset,iaset,nosam : integer;
    fstsam,lstsam:longint;
    atst,btst,ch,chst,cret,data,marker:char;
    v1,v2,ans:string[10];

    sr,so,sv,fm,ff,fl,iach,am,ofs,pi,ni,tm,pl,negl,ianf:string[15];
    ain,tb,et,bl,dl,ainf:string[15];
    se1,se2,se3,se4,se5,se6,se7,se8,se9,se10:string[15];
    sn1,sn2,sn3,sn4,sn5,sn6,sn7,sn8,sn9,sn10:string[15];
    sp1,sp2,sp3,sp4,sp5,sp6,sp7,sp8,sp9,sp10:string[15];
    mo,io,bn,ioch,fs,ls,ionf,nf:string[15];

    ssr,sso,ssv,sfm,sff,sfl,siach,sam,sofs,spi,sni,stm,spl,snegl,sianf:string[25];
    sain,stb,nset,sbl,sdl,sainf:string[25];
    sse1,sse2,sse3,sse4,sse5,sse6,sse7,sse8,sse9,sse10:string[25];
    ssn1,ssn2,ssn3,ssn4,ssn5,ssn6,ssn7,ssn8,ssn9,ssn10:string[25];
    ssp1,ssp2,ssp3,ssp4,ssp5,ssp6,ssp7,ssp8,ssp9,ssp10:string[25];
    smo,sio,sbna,sbnb,siocha,siochb,sfs,sls,sionf,snf:string[25];
    iam,irange,ibn,iff,ipi,ini,itm,iianf,iainf,imo,iionf,iioch:string[25];
    riam,arange,rsam:real;

    imax,nos,nosec,sectn,st,sttst,trigl:string[25];
    as,datastring,mkstr:string[255];
    datout:file of char;

{Description of the variables:-

Integers:-
i,j : counting integers
cd :
devnum : the number of the device to be adressed
gset,iaset : case selector
nosam : the number of samples to be recorded
nosec : the number of sections that will be recorded for this bar sample
sectn : the number of the section to be recorded
trigl : the delay set in microseconds after the trigger point
Long integers:-
fstsam : the number of the first sample to be recorded
lstsam : the number of the last sample to be recorded
Characters:-
atst,btst : test characters
Strings:-
as,st : used in set-up procedure
sr,so,sv,fm,ff,fl,iach,am,ofs,pi,ni,tm,pl,negl,ianf : input amplifier
ain,tb,et,bl,se,dl,sn,sp,ainf : analog input
mo,io,bn,ioch,fs,ls,ionf,tr : digital input/output & status}
```

```
implementation

end.
```

```
(**************************************************************************)
(*                                                                        *)
(*    UNIT vsmglob - Global variables for VSM programs                    *)
(*    12/04/89 D.B.Lambrick : NECESSARY FOR THE IEEE ROUTINES             *)
(*                                                                        *)
(**************************************************************************)

unit vsmglob;

{------------------------------------------------------------------------}

interface
   type
       namfil = string[12];
        str2   = string[2];
        str3   = string[3];
        str4   = string[4];
        str5   = string[5];
        str6   = string[6];
        str8   = string[8];
        str10  = string[10];
        str12  = string[12];
        str14  = string[14];
        str16  = string[16];
        str20  = string[20];
        str25  = string[25];
        str80  = string[80];
        str255 = string[255];

     var
       bdeal,flke : integer;
{------------------------------------------------------------------------}

implementation
{------------------------------------------------------------------------}
end.
```

Bibliography: Chapter I

Alcock J. Ph.D Thesis, University of Leeds (1988)

Bates L.F. *Modern Magnetism* Cambridge University Press(1963)

Bittel H. *Noise of Ferromagnetic materials* IEEE Trans. Mag. MAG-5 No. 3, 359 (1969)

Bozorth R.M. *Ferromagnetism* Van Nostrand (1951)

Brailsford F. *Physical Principles of Magnetism* D. Van Nostrand (1966)

Buttle D.J., Briggs G.A.D., Jakubovics J.P., Little E.A. and Scruby C.B. *Magneto-acoustic and Barkhausen Emission in Ferromagnetic Materials* Phil. Trans. R. Roc. London A (GB) **320**, No. 1554, 367 (1986)

Celasco M., Fiorillo F. and Mazzetti P. *Time-amplitude Correlation Effect between Large Barkhausen Discontinuities (in the Magnetisation Noise)* Il Nuovo Cimento **23** N0.2, 376 (1974a)

Celasco M. and Fiorillo F. *The Effect of Surface on the Power Spectrum of the Barkhausen Noise in Ferromagnetic Materials* IEEE Trans. Mag. MAG-10 No. 2, 115 (1974b)

Chapman J.N. *Review article: The Investigations of Magnetic Domain Structures in Thin Foils by Electron Microscopy* J. Phys. D: Appl. Phys. **17**, 623 (1984)

Chikazumi S. *Physics of Magnetism* Wiley, New York (1964)

Crangle J. *The Magnetic Properties of Solids* Arnold (1977)

Craig D.J., Tebble R.S. *Ferromagnetism, and Ferromagnetic Domains* Wiley (1965)

Cullity B.D. *Introduction to Magnetic Materials* Addison Wesley (1972)

Fuller H.W. and Hale M.E. *Determination of Magnetisation Distribution in Thin Films Using Electron Microscopy* J. Appl. Phys. (U.S.A.) **31**, 238 (1960a)

Fuller H.W. and Hale M.E. *Domains in Thin Magnetic Films Observed by Electron Microscopy* J. Appl. Phys. (U.S.A.) **31**, 1699 (1960a)

Gong H. and Chapman J.N. *On the Use of Divergent Wall Images in the Fresnel Mode of Lorentz Micrscopy For the Measurement of the Widths of Very Narrow Domain Walls* J. Magn. Magn. Mat. **67**, 4 (1987)

Grundy P.J. and Tebble R.S. *Lorentz Electron Microscopy* Adv. in Phys. **17**, 153 (1968)

Grundy P.J. and Jones G.A. *Electron Microscopy in the Study of Materials* Edward Arnold (1976)

Hirsch P.B., Howie A., Nicholson R.B., Pashley D.W. and Whelan M.J. *Electron Microscopy of Thin Crystals* Butterworths (1965)

Jakubovics J.P. D.Phil Thesis University of Cambridge (1965)

Jakubovics J.P. *Lorentz Microscopy and Applications (TEM and SEM)* Electron Microscopy in Materials Science, Part IV, Ed. U. Valdre and E. Ruedl, 1303 (1975)

Jakubovics J.P. *Magnetism and Magnetic Materials* The Institute of Metals (1977)

Jones G.A. *Magnetic Contrast in the Scanning Electron Microscope: An Appraisal of Techniques and their Applications* J. Magn. Magn. Mat. **8**, 263 (1978)

Kittel C. *Introduction to Solid-State Physics* 5th (and further) editions, Wiley New York, (1976)

Manson G. and Hoffman de Visme G. *The Frequency Spectrum of Barkhausen Noise* J. Phys. D: Appl. Phys. **5**, 1389 (1972)

Mazzetti P. and Montalenti G. *Power Spectrum of the Barkhausen Noise of Various Magnetic Materials* J. Appl. Phys. **34**, No. 11, 3223 (1963)

Mazzetti P. *Correlation Function and Power Spectrum of a Train of Nonindependent Overlapping Pulses Having Random Shape and Amplitude* Il Nuovo Cimento **XXXI** No.1, 88 1964

Mazzetti P. and Montalenti G. *The Theory of the Power Spectrum of Barkhausen Noise* Proceedings of the International Conference on Magnetism, Nottingham, 701 (1964b)

Morrish A.H. *The Physical Principles of Magnetism* Wiley New York, (1965)

Reimar L. *Transmission Electron Microscopy* Springer Series in Optical Sciences, Springer Verlag (1984)

Säynäjäkangas S. *A New Surface Transducer for Generating and Detecting Magnetic Field Transients in Ferromagnetics* IEEE Trans. Mag. **MAG-10** No.1, 44 (1974a)

Säynäjäkangas S. *Statistical Properties of Magnetisation Discontinuities in Technical Steels* IEEE Trans. Mag. **MAG-10** No.1, 39 (1974b)

Tebble R.S., Skidmore I.C. and Corner W.D. *The Barkhausen Effect* proc. Phys. Soc. London, Section A, **A63** 739 (1950)

Tiitto S. and Säynäjäkangas S. *Spectral Damping in Barkhausen Noise* IEEE Trans. Mag. **MAG-11** No,6. 1666 (1975)

Tiitto S., Säynäjäkangas S. and Rulka R. *High Frequency Investigations of Magnetic Noise Characteristics* IEEE Trans. Mag. **MAG-12** No.4, 406 (1976)

Tiitto S. *On the Magnetic Transitions in Steel* Acta Polytechnica Scandinavica Appl. Phys. Series **119**, (1977)

Tiitto S. *On the Mechanism of Magnetisation Transitions in Steel* IEEE Trans. Mag. MAG-14 **5**, 527 (1978)

Tiitto *Depth of Measurement in Barkhausen Noise Testing* American Stress Technologies Report **171** (1988)

Bibliography: Chapter II

Anderson M.R. *Magnetic Properties of Structural Steel* A.E.R.E. Harwell Report, OT/R/8034 (1980)

Atherton D.L. and Teitsma A. *Detection of Anomalous Stresses in Gas Pipelines by Magnetometer Survey* J. Appl. Phys. **53** (11), 8130 (1982)

Atherton D.L., Coathup L.W., Jiles D.C., Longo L., Welbourn C. and Teitsma A. *Stress Induced Magnetiaation changes of Steel pipes: Laboratory Tests* IEEE Trans. Mag. **MAG-19** No. 4, 1564 (1983)

Bailey F.W. *Fundamentals of Engineering Metallurgy and Materials* Cassel (1972)

Biggs W.D. *The Mechanical Behaviour of Engineering Materials* Pergamon Press (1965)

Buttle D.J., Little E.A., Scruby C.B., Briggs G.A.D. and Jakubovics J.P. *A study of Neutron Irradiation Damage in α-iron using magnetoacoustic and Barkhausen Emission* A.E.R.E. Harwell Report 12332 (1987)

Cottrell A. H. *Dislocations and Plastic Flow in Crystals* Oxford and the Clarendon Press (1953)

Edwards C. and Palmer S.B. *The Magnetic Leakage Field of Surface Breaking Cracks* J. Phys. D: Appl. Phys. **19**, 657 (1986)

Förster *Nondestructive Inspection by the Method of Magnetic Leakage Fields. Theoretical and Experimental Foundations of the Detection of Surface Cracks of Infinite and Finite Depth.* Magnetic and Electromagnetic Methods, Plenum Publishing Corp., 841 (1983)

Friedel J. *Dislocations* Pergamon Press (1964)

Hetherington M.G., Jakubovics J.P., Szpunar J.A. and Tanner B.K. *High Voltage Electron Microscopy Studies of Domain Structures and Magnetisation Processes in Pearlitic Steels* Phil. Mag. B. **56**, No.5, 561 (1987)

Higgins R.A. *Engineering Metallurgy (Part I)* The English Universities Press Ltd., London (1965)

Honeycombe R.W.K. *The Plastic Deformation of Metals* Edward Arnold (1970)

Honeycombe R.W.K. *Steels Microstructure and Properties* Edward Arnold (1981)

Jiles D.C. *Review of Magnetic Methods for Nondestructive Evaluation* N.D.T. Int. (G.B.) **21**, No. 5, 311 (1988a)

Jiles D.C. *The Influence of Size and Morphology of Eutectoid Carbides on the Magnetic Properties of Carbon Steels* J.Appl. Phys.(U.S.A.) **63**, 2980 (1988b)

Jiles D.C. *Magnetic Properties and Microstructure of A.I.S.I. 1000 Series Carbon Steels* J. Phys. D: Appl. Phys. **61**, 1186 (1988c)

Jiles D.C., Harihan S. and Devine M.K. *Magnescope: A Portable Magnetic Inspection System for Evaluation of Steel Structures and Components* IEEE Trans Mag. **26**, No. 5 (1990)

Jiles D.C. and Verhoeven J.D. *Investigation of the Microstructural Dependence of the Magnetic Properties of 4130 Alloy Steels and Carbon Steels for Nondestructive Evaluation* Review of the Progress in Quantitative N.D.E., Ed. D. Thompson and D.Chinenti, 1681 (1988)

Johnson C.S. and Weeks W.R. *Metallurgy* The Technical Press Ltd., London (1964)

Langman R. *Some Comparisons Between the Measurements of Stress in Mild Steel by Means of Barkhausen Noise or Rotation of Magnetisation.* N.D.T. Int. (G.B.) **20** part2, 93 (1987)

Kottrell A.H. *An Introduction to Metallurgy* Arnold (1967)

Lubahn J.D. and Felgar R.P. *Plasticity and Creep of Metals* J. Wiley and Sons (1961)

McCoy J.M. *The Physical Properties of Magnetic Inks* Ph.D. Thesis, University of Durham (1988)

McCoy J.M. and Tanner B.K. *Simulation of Particle Trajectories in Magnetic Paricle Inspection* IEEE Trans. Mag. MAG-24, 1665 (1988)

McCoy J.M. and Tanner B.K. *Magnetisation of Inks for Magnetic Particle Inspection* J. Phys. D: Appl. Phys. **22**, 1366 (1989)

Morgan L.L., B.K.Tanner and Willcock S.N.M. *Magnetic Characteristics of Constructional Steels* Proc. 21st Annual British Conference on N.D.T.: N.D.T.86 (1986)

Nabarro F.R.N. *Dislocations in a Simple Lattice* Proc Phys. Soc. **59**, 256 (1947)

Pierls R. *The Size of a Dislocation* Proc. Phys. Soc. **52**, 34 (1940)

Rollason F.C. *Metallurgy for Engineers* Arnold, London (1964)

Rudd C.O. *A Review of Nondestructive Methods for Residual Stress Measurement* N.D.T. Int. **15**, 15 (1982)

Sundström O. and Törröen K. *The Use of Barkhausen Noise Analysis in Nondestructive Testing* Materials Evaluation 51 Feb. (1979)

Tanner B.K., McCoy J.M., Willcock S.N.M., Hetherington M.G. and Jakubovics J.P. *The Structure and Behaviour of inks for magnetic particle inspection* J. Mater. Sci. Letts. **5**, 296 (1986)

Tanner B.K. *The Magnetic Properties of High Strength Steels* J. Nondestr. Eval., **5**, 2 (1989)

Tanner B.K., Szpunar J.A., Willcock S.N.M., Morgan L.L. and Mundell P.A. *The Magnetic and Metallurgical Properties of High Tensile Steels* J. Mater. Sci. **23**, 4534 (1988)

Taylor G.I. *The Mechanics of Plasyic Deformation of Crystals, Part I: Theoretical, Part II: Comparison with Observations* Proc R. Soc. **A145**, 362 (1934)

Theiner W.A. and Altpeter I. *Determination of Residual Stresses Using Micromagnetic Parameters* New Proceedures in Nondestructive Testing, ed. P. Höller, Springer Verlag, 575 (1983)

Tiitto K. *Using Barkhausen Noise in Nondestructive Evaluation of Residual Stress, Material Defects and Texture* (1988)

Tiitto K. *Use of Barkhausen Noise in Fatigue* J. Nondestr. Eval., 5, 27 (1989)

Willcock S.N.M. *An Investigation of the Magnetic Properties of High Tensile Steels* Ph.D. Thesis, University of Durham (1985)

Willcock S.N.M. and Tanner B.K. *Harmonic Analysis of B-H Loops of Constructional Steel* IEEE Trans. Mag. **MAG-19** No.5, 2145 (1983)

Willcock S.N.M. and Tanner B.K. *The Application of Harmonic Analysis to the Magnetic Properties of High-Tensile Steels* Mat. Letters 4, 307 (1986)

Willcock S.N.M., Tanner B.K. and Mundell P.A. *The Magnetic Properties of Seamless Steel Pipe* J. Magn. Magn. Mat. **66**,153 (1987)

Bibliography : Chapter III

Birkett A.J. *Barkhausen Noise in Steels* Ph.D. Thesis University of Durham (1988)

Brailsford F. *Physical Principles of Magnetism* D. Van Nostrand Company Ltd. 8-12 (1966)

British Standards Institution *Determination of d.c. Magnetic Measurements of Magnetic Materials* BS5884 (1980)

British Standards Institution *Magnetic Materials : Methods of Measurements of the d.c. Magnetic Properties of Solid Steels* BS6404 Part 4 (1986)

Brown S.T. *Optomised Magnetic Particle Inspection Techniques for Welded Joints. Part 5: Magnetic Properties* Welding Institute report 5542/19/85 (1985)

Chescoe D. and Goodhew P.J. *The Operation of the Transmission Electron Microscope* R. Microscopy Soc., Microscopy Handbooks 02, O.U.P. (1984)

Cullity B.D. *Introduction to Magnetic Materials* Addison Wesley (1972)

Edington J.W. *The Operation and Calibration of the Electron Microscope* Practical Electron Microscopy in Materials Science: Monograph One, The Macmillan Press: Phillips Technical Library (1974)

Edington J.W. *Electron Diffraction in the Electron Microscope* Practical Electron Microscopy in Materials Science: Monograph Two, The Macmillan Press: Phillips Technical Library (1975)

Edington J.W. *Interpretation of Transmission Electron Micrographs* Practical Electron Microscopy in Materials Science: Monograph Three, The Macmillan Press: Phillips Technical Library (1975)

Edington J.W. *Typical Electron Microscope Investigations* Practical Electron Microscopy in Materials Science: Monograph One, The Macmillan Press: Phillips Technical Library (1974)

Foner S. *Vibrating Sample Magnetometer* Rev. Sci. Instrum. **27**, 548 (1956)

Goodhew P.J. *Specimen Preparation for Transmission Electron Microscopy* R. Microscopy Soc., Microscopy Handbooks 03, O.U.P. (1984)

Hetherington M.G. *Coercivity Mechanisms in some Ferromagnetic Materials* D.Phil Thesis University of Oxford (1985)

Hoon S.R. *An Inexpensive, Sensitive Vibrating Sample Magnetometer* Eur. J. Phys. **4**, 61 (1983)

Hoon S.R. and Willcock S.N.M. *The Design and Operation of an Automated Double-crank Vibrating Sample Magnetometer* J.Phys. E: Sci. Instrum. **21**, 772 (1988)

Mallinson J. *Magnetometer Coils and Reciprocity* J. Appl. Phys. (U.S.A.) **37**, 2514 (1966)

McCoy J.M. *The Physical Properties of Magnetic Inks* Ph.D. Thesis University of Durham (1988)

Petzow G. *Metallographic Etching: Metallographic and Ceramographic Methods for Revealing Microstructure* translated from German: R.Koch and J.A. Nelson, Metals Park A.S.M. (1978)

Press W.H., Flannery B.P., Teukolsky S.A. and Vetterling W.T. *Numerical Recipes in Pascal–The Art of Scientific Computing* C.U.P. (1989)

Richarson R.C. and Smith E.T. *Experimental Techniques in Low Temperature Physics* Addison Wesley (1988)

Rulka R. *A New laboratory Apparatus for Investigating the Magnetic Properties of Magnetic Materials* University of Oulu Rep. **T29** (1975)

Taylor R.A. *Top Entry Stage for the A.E.I. EM7 Electron Microscope* E.M. 1980: Proceedings of the 6th International Conference on High Voltage E.M. Antwerp **4**, 38 (1980)

Willcock S.N.M. *An Investigation of the Magnetic Properties of High Tensile Steels* Ph.D Thesis, University of Durham (1985)

316

Zijlstra H. *Experimental Methods in Magnetism I, Generation and Computation of Magnetic Fields*, Selected topics in Solid State Physics **VOL IX** Ed. E.P. Wohlfarth, North Holland Pub. Co. (1967)

Bibliography: Chapter IV

Birkett A.J. *Barkhausen Noise in Steels* Ph.D Thesis, University of Durham (1988)

Willcock S.N.M. *An Investigation of the Magnetic Properties of High Tensile Steels* Ph.D Thesis, University of Durham (1985)

Bibliography: Chapter VI

Abuku S. *Magnetic Studies of Residual Stress in Iron and Steel Induced by Uniaxial Deformation* Jap. J. Appl. Phys. **16** No. 7, 1161 (1977)

Abuku S. and Takizawa C. *Magnetic Measurement of Residual Stress Induced in Carbon Steel by Uniaxial Plastic Deformation* Proceedings of the 17th Japanese Congress on Materials Research 50 (1973)

Alcock J. Ph.D. Thesis University of Leeds (1988)

Altpeter I. Höller P. *Influence of Cementite Specific Residual Sresses of the Second Kind on Dynamic Magnetic and Magnetoelastic Measuring Quantities* Proceedings of 9th International Conference on Experimental Mechanics (1990), ISBN: 87-7740-035-6

Anderson M.R. *Magnetic Properties of Structural Steel* A.E.R.E. Harwell Report OT/R/8034 (1980)

Astié B., Degauque J., Portseil J.L. and Vergn R. *Influence of the Dislocation Structures on the Magnetic and Magnetomechanical Properties of High Purity Iron* IEEE Trans. Mag. **MAG-17** No.6, 2929 (1981)

Atherton D.L. and Jiles D.C. *Effects of Stress on the Magnetisation of Steel* IEEE Trans. Mag. **MAG-19** No. 5,2020 (1983)

Bagchi D.K. and Cullity B.D. *Effects of Applied and Residual Stress on the Magnetoresistance of Nickel* J. Appl. Phys. **38** No. 3., 999 (1967)

Bertotti G. and Montorsi A. *Dependence of Barkhausen Noise on Grain Size in Ferromagnetic Materials* J. Magn. Mag. Mat. **83** , 214 (1990)

Birkett A.J., Corner W.D., Tanner B.K. and Thompson S.M. *Influence of Plastic Deformation on Barkhausen Power Spectra in Steels* J. Phys. D: Appl. Phys. **22**, 1240 (1989)

Buttle D.J., Briggs, G.A.D., Jakubovics J.P., Little E.A. and Scruby C.B. *Magnetoacoustic and Barkhausen Emission in Ferromagnetic Materials* Phil. Trans. R. Soc. Lond. **A320**, 363 (1986)

Buttle D.J., Scruby C.B., Briggs, G.A.D. and Jakubovics J.P. *The Measurement of Stress in Steels of Varying Microstructure by Barkhausen and Magnetoacostic Emission* A.E.R.E. Harwell Report 12387 HL87/1108(C14) (1987)

Cullity B.D. *Sources of Error in X-Ray Measurements of Residual Stress* J. Appl. Phys. **35** No. 6, 1915 (1964)

Cullity B.D. *Introduction to Magnetic Materials* Addison Wesley (1972)

Degauque J. and Astié B. *Evolution of Magnetic Domains Interacting with Structural Defects in High Purity Iron* Phys. Stat. Sol. (a) **74** , 201 (1982)

Dobranski L.G., Jiles D.C. and Atherton D.L. *Dependence of the Anhysteretic Magnetisation on Uniaxial Stress in Steel* J. Appl. Phys. **57** (1), 4229 (1985)

English A.T. *Influence of Temperature and Microstructure on Coercive Force of 0.8%C Steel* Acta Metallurgica **15** , 1573 (1967)

Friedburg R. and Paul D. *New Theory of Coercive Force of Ferromagnetic Materials* Physical Review Letters **34** , No. 19, 1234 (1975), and Erratum: **34** No. 22, 1415 (1975)

Garikepati, Chang T.T. and Jiles D.C. *Theory of Ferromagnetic Hysteresis: Evaluation of Stress from Hysteresis Curves* IEEE Trans. Mag. **24** No. 6, 2922 (1988)

Gonda P., Marcely P., Macko J. and Pavlovič *Computerised Evaluation of Magnetic Properties* J. Magn. Mag. Mat. **41** , 241 (1984)

Hetherington M.G. *Coercivity Mechanisms in Some Ferromagnetic Materials* D.Phil Thesis, University of Oxford (1985)

Hetherington M.G., Jakubovics J.P., Szpunar J.A. and Tanner B.K. *High Voltage Lorentz Electron Microscopy Studies of Domain Structures and Magnetisation Processes in Pearlitic Steels* Phil. Mag. B. **56** No. 5, 561 (1987)

Hwang D.G. and Kim H.C. *The Influence of Plastic Deformation on Barkhausen Effects and Magnetic Properties in Mild Steel* J. Phys. D: Appl. Phys.

21 , 1807 (1988)

Jagadish C., Clapham L. and Atherton D.L. *Influence of Uniaxial Elastic Stress on Power Spectrum and Pulse Height Distribution of Surface Barkhausen Noise in Pipeline Steel* IEEE Trans. Mag. **26** No. 3, 1160 (1990)

Jiles D.C. *The Influence of Size and Morphology of Eutectoid Carbides on the Magnetic Properties of Carbon Steels* J. Appl. Phys. (U.S.A.) **63** (8), 2980 (1988a)

Jiles D.C. *Magnetic Properties and Microstructure of AISI 1000 Series Carbon Steels* J. Phys. D: Appl. Phys. **21** ,1186 (1988b)

Jiles D.C. *The Effect of Compressive Deformation on the Magnetic Properties of AISI 4130 Steels with Various Microstructures* J. Phys. D: Appl. Phys. **21** , 1196 (1988c)

Jiles D.C. *Variation of the Magnetic Properties of AISI 4140 Steels with Plastic Strain* Phys. Stat. Sol. a) **108**, 417 (1988d)

Jiles D.C. and Atherton D.L. *Ferromagnetic Hysteresis* IEEE Trans. Mag. MAG-19 No. 5, 2183 (1983)

Jiles D.C. and Atherton D.L. *Theory of the Magnetisation Process in Ferromagnets and its Application to the Magnetomechanical Effect* J. Phys. D: Appl. Phys. **17**, 1265 (1984)

Jiles D.C. and Atherton D.L. *Theory of Ferromagnetic Hysteresis* J. Magn. Mag. Mat. **61**, 48 (1986)

Karjalainen L.P. and Moilanen M. *Detection of Plastic Deformation During Fatigue of Mild Steel by the Measurement of Barkhausen Noise* N.D.T. Int. (G.B.) 51 (1979)

Karjalainen L.P. and Moilanen M. *Fatigue Softening and Hardening in Mild Steel Detected from Barkhausen Noise* IEEE Trans. Mag. MAG-16 No. 3, 514 (1980)

Kwun H. *Investigation of the Dependence of the Barkhausen Noise on Stress and the Angle Between the Stress and Magnetsation Directions* J. Magn. Mag. Mat. **49**, 235 (1985)

Kwun H. and Burkhardt G.L. *Effects of Grain Size and Stress on the Magnetic Hysteresis Loops of Ferromagnetic Steels* J. Appl. Phys. (U.S.A.) **61**, 1576 (1987)

Langman R. *Prediction and Measurement of Rotation of Magnetisation in an Anisotropic Polycrystalline Ferromagnetic Material* IEEE Trans. Mag. **MAG-17** No. 1, 1159 (1981)

Langman R. *Measurement of the Mechanical Stress in Mild Steel by Means of Rotation of Magnetic Field Strength* N.D.T. Int. (G.B.) **14** Part 5, 255 (1981)

Langman R. *Measurement of the Mechanical Stress in Mild Steel by Means of Rotation of Magnetic Field Strength: II Axial Stress* N.D.T. Int. (G.B.) **15** Part 2, 91 (1982)

Langman R. *Measurement of the Mechanical Stress in Mild Steel by Means of Rotation of Magnetic Field Strength: III Practical Applications* N.D.T. Int. (G.B.) **16** Part2, 59 (1983)

Langman R. *The Effect of Stress on the Magnetisation of Mild Steel at Moderate Field Strengths* IEEE Trans. Mag. **MAG-21** No. 4, 1314 (1985)

Lieneweg U. *Barkhausen Noise of 3% Si-Fe Strips after Plastic Deformation* IEEE Trans. Mag. **MAG-10** N0. 2, 118 (1974)

Paul D. *The Coercive Force and the Theory of Ferromagnetic Domain Wall Pinning* A.I.P. Conference Proceedings **129**, 545 (1976)

Paul D. *Domain Wall Pinning in the Hard Permanent Magnet* $Sm_2Co_{10}Cu_{1.48}Fe_{3.16}Zn_{0.194}$ IEEE Trans. Mag. **MAG-16**, No. 51 1003 (1980)

Paul D. *General Theory of the Coercive Force due to Domain Wall Pinning* J. Appl. Phys. (U.S.A.) **53**, 1649 (1982a)

Paul D. *Extended Theory of the Coercive Force due to Domain Wall Pinning* J. Appl. Phys. (U.S.A.) **53**, 2362 (1982b)

Pitman K.C. *The Influence of Stress on Ferromagnetic Hysteresis* IEEE Trans. Mag. **26** No. 5. (1990)

Qureshi A.H. and Chaudhary L.N. *Influence of Platic Deformation on Coercive Field and Initial Susceptibility of Fe-3.25% Si Alloys* J. Phys. D. **41** No. 3, 1042 (1970)

Rauthioaho R., Karjalainen P. and Moilanen M. *Coercivity and Power Spectrum of Barkhausen Noise in Structural Steels* J. Magn. Mag. Mat. **61** , 183 (1986)

Rusnak R.M. and Cullity B.D. *Correlation of Magnetic Permeability and X-Ray Diffraction Line Broadening in Cold-Worked Iron* J. Appl. Phys. **40** No. 3, 1581 (1969)

Sablik M.J., Kwun H., Burkhardt G.L. and Jiles D.C. *Model for the Effect of Tensile and Compressive Stress on Ferromagnetic Hysteresis* J. Appl. Phys. (U.S.A.) **61** (8), 3799 (1987)

Sablik M.J., Burkhardt G.L., Kwun H. and Jiles D.C. *A Model for the Effect of Stress on the Low Frequncy Harmonic Content of the Magnetic Induction in Ferromagnetic Materials* J. Appl. Phys. (U.S.A.) **63** (8), 3930 (1988)

Schwerer F.C., Spangler C.E.,Jr., and Kelly J.F. *Temperature Dependence of the Magnetic Coercivity of Pearlite* Acta Metallurgica **26** , 579 (1978)

Seeger A., Kronmüller H., Rieger H. and Traüble *Effect of Lattice Defects on the Magnetisation Curve of Ferromagnets* J. Appl. Phys. **35** No.3 (Part 2), 740 (1964)

Szpunar B. and Szpunar J.A. *Influence of Stresses on the Hysteresis Curve in Condtructional Steel* IEEE Trans. Mag. **MAG-20** No. 5, 1882 (1984)

Szpunar B. and Tanner B.K. *Grain Shape and Distribution of the Grain Boundary Density in Polycrstalline Materials* J. Mat. Sci. **19**, 3249 (1984)

Tanner B.K., Szpunar J.A., Willcock, Morgan L.L. and Mundell P.A. *The Magnetic and Metallurgical Properties of High Tensile Steels* J. Mat. Sci. **23** , 4534 (1988)

Taylor R.A., Jakubovics J.P., Astié B. and Degauque J. *Direct Observation of the Interaction Between Magnetic Domain Walls and Dislocations in Iron* J. Magn. Mag. Mat. **31-34**, 970 (1983)

Taylor R.A. *Quantitative Study of the Magnetisation Processes in Thin Ferromagnetic Foils Conaining Non-Magnetic Precipitates.* J. Magn. Mag. Mat. **31-34**, 999 (1983)

Thompson S.M., Allen P.J. and Tanner B.K. *Magnetic Properties of Welds in High-Strength Pearlitic Steels* IEEE Trans. Mag. **26** no. 5 (1990)

Thompson S.M., Tanner B.K. *The Magnetic Properties of Plastically Deformed Steels* J. Magn. Mat. **83**, 221 (1990)

Tiitto S.I. *Influence of Elastic and Plastic Strain on the Magnetisation Process in Fe-3,5%Si* IEEE Trans. Mag. **MAG-12** No. 6, 855 (1976)

Tiitto S. *On the Influence of Microstructure on Magnetisation Transitions in Steel* Acta Polytechnica Scandinavica, Applied Physics Series No. 119 (1977)

Tiitto S. *On the Mechanism of Magnetisation Transitions in Steel* IEEE Trans. Mag. **MAG-14** No. 5, 527 (1978)

Willcock S.N.M. *An Investigation of the Magnetic Properties of High Tensile Steels* Ph.D. Thesis, University of Durham (1985)

Willcock S.N.M. and Tanner B.K. *Harmonic Analysis of B-H Loops of Constructional Steel* IEEE Trans. Mag. **MAG-19** No. 5, 2145 (1983)

Willcock S.N.M., Tanner B.K. and Mundell P.A. *The Parameterization of Virgin B-H Curves of High Strength Steels* J. Magn. Mag. Mat. **72**, 45 (1988)

Bibliography: Chapter VII

Jiles D.C. *The Effect of Compressive Deformation on the Magnetic Properties of AISI 4130 Steels with Various Microstructures* J. Phys. D: Appl. Phys. **21** , 1196 (1988a)

Jiles D.C. *Variation of the Magnetic Properties of AISI 4140 Steels with Plastic Strain* Phys. Stat. Sol. a) **108**, 417 (1988b)

Jiles D.C. and Atherton D.L. *Theory of Ferromagnetic Hysteresis* J. Magn. Mag. Mat. **61**, 48 (1986)

Sablik M.J., Kwun H., Burkhardt G.L. and Jiles D.C. *Model for the Effect of Tensile and Compressive Stress on Ferromagnetic Hysteresis* J. Appl. Phys. (U.S.A.) **61** (8), 3799 (1987)

Schwerer F.C., Spangler C.E.,Jr., and Kelly J.F. *Temperature Dependence of the Magnetic Coercivity of Pearlite* Acta Metallurgica **26** , 579 (1978)